LABORATORY MODELING OF HYDRAULIC DREDGES AND DESIGN OF DREDGE CARRIAGE FOR LABORATORY FACILITY

A Thesis

by

GORDON JASON GLOVER

Submitted to the Office of Graduate Studies of
Texas A&M University
in partial fulfillment of the requirements for the degree of

MASTER OF SCIENCE

December 2002

Major Subject: Ocean Engineering

LABORATORY MODELING OF HYDRAULIC DREDGES AND DESIGN OF DREDGE CARRIAGE FOR LABORATORY FACILITY

A Thesis

by

GORDON JASON GLOVER

Submitted to the Office of Graduate Studies of
Texas A&M University
in partial fulfillment of the requirements for the degree of

MASTER OF SCIENCE

December 2002

Major Subject: Ocean Engineering

LABORATORY MODELING OF HYDRAULIC DREDGES AND DESIGN OF DREDGE CARRIAGE FOR LABORATORY FACILITY

A Thesis

by

GORDON JASON GLOVER

Submitted to Texas A&M University
in partial fulfillment of the requirements
For the degree of

MASTER OF SCIENCE

Approved as to style and content by:

Robert E. Randall (Committee Chair)	Billy L. Edge (Member)
Gerald L. Morrison (Member)	John M. Niedzwecki (Head of Department)

December 2002

Major Subject: Ocean Engineering

ABSTRACT

Laboratory Modeling of Hydraulic Dredges and Design of Dredge Carriage
for Laboratory Facility. (December 2002)
Gordon Jason Glover, B.S., The University of Texas at Austin
Chair of Advisory Committee: Dr. Robert Randall

The deepening and maintenance of the world's ports and navigable waterways has been an integral part of the world economy for centuries. In recent years, cutterhead and draghead hydraulic suction dredges have performed a majority of the dredging work. The ongoing design and testing of hydraulic dredges is important for maintaining efficient dredging operations within the limits set by increasing environmental regulations.

The high cost of building and operating a hydraulic dredge makes field testing of full-scale prototypes very expensive and time consuming. Moreover, the testing conditions are generally difficult to control, and the natural unpredictability of the sea can render experimental results inconclusive. These factors substantiate the need for laboratory model testing of hydraulic dredging operations.

The usefulness of any hydraulic model depends on the degree of geometric, kinematic, and dynamic similarity between the model and its prototype. The primary challenge in establishing useful similitude criteria for model dredge studies is proper kinematic scaling of the suction inlet velocity, average particle settling velocity, dredge swing velocity, and cutter rotational speed. Despite the inherent challenges, model studies of hydraulic dredge equipment have proven useful for obtaining qualitative results.

The new Coastal Engineering Laboratory at Texas A&M University is equipped with model dredge testing facilities ideal for performing such experiments. The tow/dredge carriage has a fully adjustable dredge ladder, a 14.9 kW (20 hp) cutter drive, and a 2.54 cm (3 in) dredge pump. A Programmable Logic Controller (PLC) provides computer numerical control and real-time data collection and analysis during model dredging operations.

The purpose of this thesis is to investigate scaling relationships for hydraulic dredge model studies and to design a model dredge carriage for the new laboratory facilities recently constructed at the Texas A&M University College Station campus. Pursuant to the design of the new dredge modeling facilities, a rationale for scaling the model dredge operating parameters based on previous model studies is put forward. Examples of model studies that could be performed with the proposed facilities are discussed as well as how the scaling methodology is applied to each experiment to allow the quantitative interpretation of experimental data.

ACKNOWLEDGEMENTS

The author would like to acknowledge all those who contributed to the completion of this thesis. The author is very thankful to Dr. Robert E. Randall, his committee chair, for his support, direction, and overall guidance not only for this research but also for the 18 months spent at Texas A&M University pursuing the Master of Science degree in Ocean Engineering. The author is also grateful to Dr. Billy L. Edge and Dr. Gerald L. Morrison for serving as committee members. The author expresses his gratitude to Pete deJong for his assistance in estimating the dredge production and side winch forces for a model cutterhead dredge.

The author would like to acknowledge the U.S. Navy Civil Engineer Corps, specifically the Ocean Facilities Program and the Naval Postgraduate School, for their assistance during graduate studies. The author is also thankful to his wife Kathryn, and three children: Dabney, Truitt, and Bryn, for their general support and for enduring the odd hours and unpredictable schedule that accompanies such a project.

TABLE OF CONTENTS

CHAPTER Page

Page

LIST OF FIGURES

FIGURE Page

FIGURE Page

LIST OF TABLES

NOMENCLATURE

$\overline{A}$	= Average Axial Cutterhead Force	lb
b_c	= Cutting Force per Unit Layer Thickness	lb/ft
b_n	= Normal Force per Unit Layer Thickness	lb/ft
BHP	= Brake Horsepower	hp
c_1	= Cutting Force Coefficient (non-cavitating)	-
d_1	= Cutting Force Coefficient (cavitating)	-
d_{50}	= Mean grain diameter	mm
D_c	= Depth of Cut	in
D_{cutter}	= Diameter of cutterhead	in
e	= Volume Strain	%
ϕ_c	= Cavitation Transition Angle	rad
$F_{cutting}$	= Cutterhead forces	lb
Fr	= Froude Number	-
g	= Gravitational constant	ft/s^2
Γ	= Torque	ft-lb (in-lb)
Γ_{cutter}	= Cutterhead torque	ft-lb (in-lb)
$\overline{H}$	= Average Horizontal Cutterhead Force	lb
H	= Hydrostatic Head	ft
$H_{velocity}$	= Velocity head	ft
J	= Area Moment of Inertia	in^4
φ	= Angular Position of Cutterhead Blade	rad
φ_{IN}	= Angular Positionof Cutterhead Blade Through Entire Cut	rad
φ_o	= Angular Position of Cutterhead Blade at Start of Cut	rad
κ	= Cutterhead Profile Angle	rad
k_m	= Average Permeability	ft/s
l	= Length of Cutterhead along Axis	in
λ_c	= Hydrostatic Pressure Factor	-
m	= Ratio of Cutterhead Tangential Velocity to Swing Speed	-
$\overline{N}$	= Average Normal Cutterhead Force	lb

ν	= Kinematic viscosity	ft^2/s
N_{cutter}	= Cutterhead rotational speed (rpm)	rpm
P	= Power	hp
p	= Cutterhead Blade Pitch	-
$p_{cavitation}$	= Cavitation Pore Pressure	psi
r	= Cutterhead Radius	in
Re	= Reynolds Number	-
ρ_{water}	= Water Density	lb/ft^3
SG	= Specific Gravity	-
$\overline{T}$	= Average Tangential Cutterhead Force	lb
t_{layer}	= Layer Thickness	in
$U_{suction}$	= Average suction pipe flow velocity	ft/s
$\overline{V}$	= Average Vertical Cutterhead Force	lb
V_c	= Critical Velocity	ft/s
$V_{settling}$	= Settling velocity	mm/s
V_{swing}	= Cutterhead swing velocity	in/s (ft/min)
WHP	= Water Horsepower	hp
ω_{cutter}	= Cutterhead angular velocity	rad/s
θ_o	= Angle Between Cutting Force and X-Axis at Start of Cut	rad
θ_{IN}	= Angle Between Cutting Force and X-Axis Through Entire Cut	rad
$Q_{suction}$	= Volumetric flow rate through suction/discharge pipe	GPM (ft^3/s)
z	= Water Depth	ft

CHAPTER I

INTRODUCTION

1.1 Hydraulic Dredging

Dredging of the world's ports and navigable waterways has been an integral part of the world economy for centuries. In recent years, hydraulic cutterhead and hopper dredges have performed a majority of the dredging work. Figures 1.1 and 1.2 are examples of modern cutterhead and hopper dredges respectively.

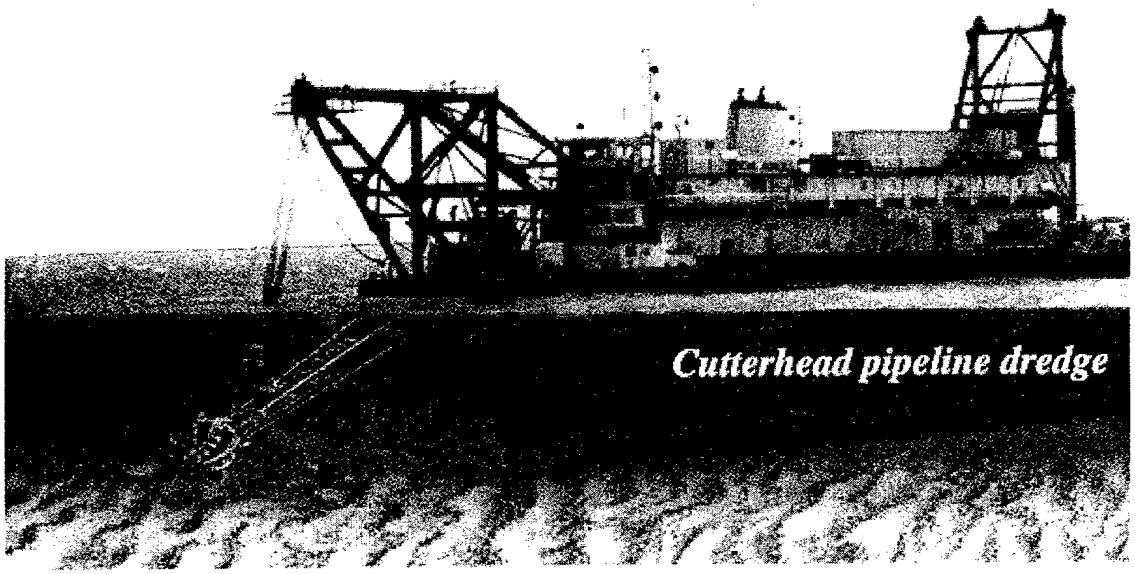

Figure 1.1: A Modern Cutterhead Dredge
(Army Corps of Engineers 2000)

These machines remove large volumes of clay, mud, silt, sand, and shells from the seabed. The design of hydraulic dredges has traditionally been aimed at maximizing solids production and operating efficiency. However, the sediment in some ports and harbors has become increasingly contaminated and recent environmental considerations are limiting the amount of resuspended solids from dredging operations that could potentially contaminate navigable waterways. Most of the turbidity created by hydraulic dredges originates in the vicinity of the cutter or drag head

This thesis follows the style and format of the Journal of Dredging Engineering.

(Herbich and Brahme 1983). Any material removed from the seafloor that does not enter the suction pipe increases the level of turbidity during a dredging operation. This has added the emphasis of reducing turbidity generated by cutterheads and dragheads while maximizing solids production to the design of hydraulic dredge equipment.

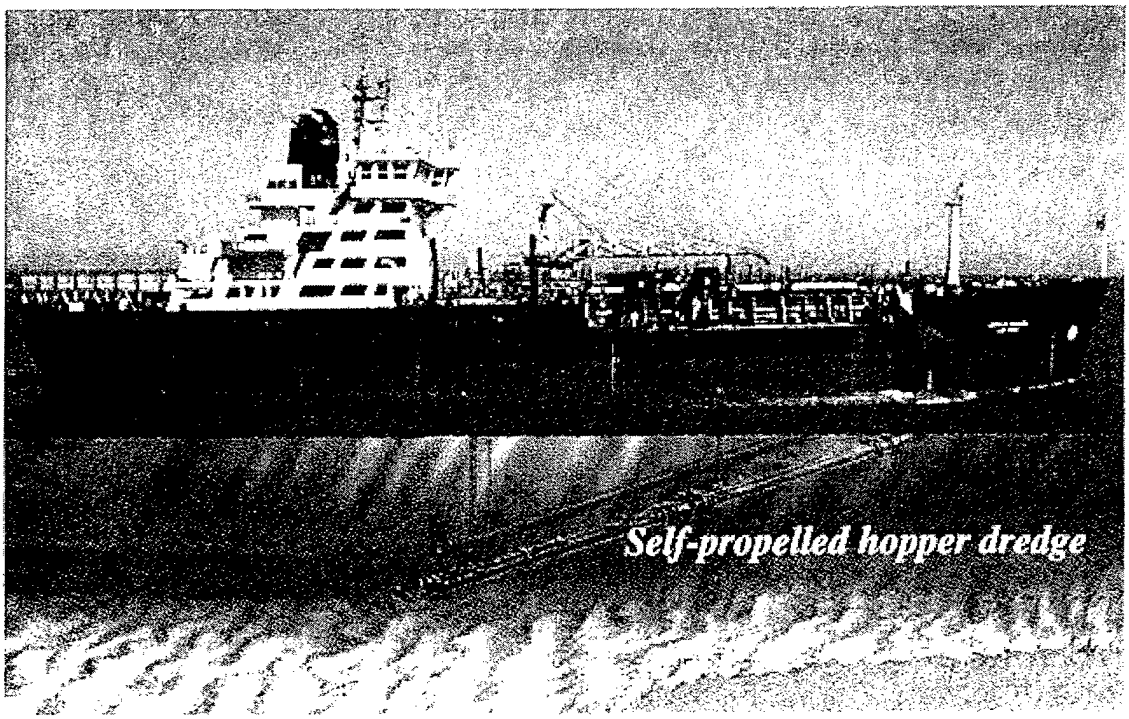

Figure 1.2: A Modern Hopper Dredge
(Army Corps of Engineers 2000)

Other environmental considerations, such as the preservation of marine life, are placing new constraints on the design of hydraulic dredges. For example, new hydraulic draghead designs may be equipped with biological exclusion devices that may reduce solids production rates. Environmental constraints can be expected to become more restrictive and requirements for new and innovative hydraulic dredge designs will become more important.

The purpose of this thesis is to investigate model scaling relationships for hydraulic dredge model studies and to design a hydraulic dredge carriage for the new laboratory facilities currently under construction at the Texas A&M University College Station campus. Pursuant to the design of the new dredge modeling facilities, a rationale for scaling the model dredge

parameters based on previous model studies is put forward. Examples of new model studies that could be performed with the proposed facilities are discussed as well as how the scaling methodology could be applied to each case.

1.2 Need and Purpose for Model Studies

The design of hydraulic dredges has traditionally been by trial-and-error with testing of full-scale prototypes (Brahme and Herbich 1986). The high cost of operating a hydraulic dredge makes field testing of full-scale prototypes very expensive. Moreover, it is very difficult to filter out and/or control environmental effects such as current, wind, bed topography, sediment properties, and surface waves so that experimental results can be properly evaluated for the effects that are being studied. Evaluating turbidity generation of full-scale prototypes has been done, but with great cost and difficulty (Huston 1976). Complete flow visualization in the vicinity of the cutterhead or draghead is practically impossible due to the limited visibility of most navigable waterways. In the past, researchers have resorted to dangerous techniques such as sending divers to make physical observations of flows in the vicinity of a rotating full-scale cutterhead (Slotta 1968). Results obtained from prototype tests are subject to errors that could render them inconclusive and unreliable (Franco 1967). For these reasons, scaled model testing of hydraulic dredging equipment can save time and money in the design process.

Because of the complex nature of the solid-fluid interaction between the cutterhead and the suction pipe, prototype to model similitude relationships have been difficult to define and establish. Moreover, relating quantities such as suction flow rate, swing speed, cutterhead rpm, bank height, and depth of cut to solids production requires a useful hydraulic model. Empirical data are needed to develop such models. The need for laboratory facilities capable of conducting controlled experiments to establish and verify theoretical models has been established by Randall et al. (1998).

1.3 Achieving Model Similitude

The usefulness of any hydraulic model depends on the degree of geometric, kinematic, and

dynamic similarity between the model and its prototype (Franco 1967). In general, it is very difficult to obtain complete similitude between a hydraulic model and its prototype. Even if similitude based on a limited number of parameters can be achieved, it can still be difficult to physically satisfy all of the scaled operating conditions for the model studies. Thus, the complex nature of the solid-fluid interactions that take place during a dredging operation tend to produce numerous scale effects that make it difficult to correlate data from hydraulic dredge models to the full-scale prototypes.

There are several different physical phenomena that take place during a hydraulic dredging operation. For the sake of convenience, these factors have been categorized into two different processes (Brahme and Herbich 1986, Joanknecht 1976). First, there is the mechanical process of the cutterhead or draghead to remove in-situ material and create a mixture of sediment and water commonly referred to as slurry. If the sand is loosely packed, then the hydraulic action of the suction pipe may also contribute to sediment removal (Joanknecht 1976). There are many factors that affect the rate at which material is removed by the cutter and put into suspension (Herbich and Brahme 1983). The cutterhead angular velocity, the depth of cut, whether over-cutting or under-cutting, the lateral (swing) speed of cutterhead along the arc of cut, the mechanics and geometry of the cutterhead itself such as blade angle, and the properties and type of material being cut all affect the amount of suspended material, or slurry, supplied to the suction pipe.

There is then the hydrodynamic process of slurry flow through and around the cutterhead or draghead while being drawn towards the suction inlet. This can be influenced by the geometry and kinematics of the cutter, the presence of currents and or waves, the settling velocity of the bed material, the velocity field created by the suction, and the horizontal swing velocity of the cutterhead along the seabed (Slotta 1968). The purpose of the suction pipe is to remove as much of the slurry as possible and transport it to a disposal site. The suction creates a velocity field in the vicinity of the rotating cutterhead. The magnitude of the velocity field is determined by the volumetric flow rate through the suction inlet (Brahme and Herbich 1986). The placement and orientation of the inlet and the geometry and kinematics of the cutter or draghead determine the shape of the velocity field. Suspended sediment particles, or slurry, created by the cutting action enters the suction pipe if the individual settling velocities are less than the velocity field at the

space that they occupy. Otherwise, they settle out or remain suspended, increasing the turbidity generated by the operation.

It is generally accepted that each of these two processes cannot be accurately scaled with the same model using a consistent set of similitude relationships (Joanknecht 1976, Slotta 1968). For example, Froude scaling requires model velocities to decrease and Reynolds scaling requires model velocities to increase. As a result, successful models must be able to at least correlate model and prototype data for one or more of the processes mentioned above. Moreover, how to scale the median grain diameter of the bed material and how the ensuing reduction in particle settling velocity affects the model has been an issue from the earliest studies (Army Corps of Engineers 1947, Franco 1967). The following similitude example demonstrates some of the issues that must be considered when modeling hydraulic suction dredges.

1.4 Similitude Example

In most fluid models, geometric similitude is obtained by simply scaling the linear dimensions of the model to the prototype. However, in dredge modeling the mean grain diameter of the in-situ material must also be linearly scaled down to maintain geometric similitude of the entire cutter-sediment system (Anonymous 1947, Franco 1967). This presents unique challenges, as very fine sediments, such as microbeads, must be used to achieve proper scaling. Moreover, 1:10 to 1:15 scale reductions in the median grain diameter for medium to fine sands can cause the settling velocity of the scaled material to approach its limit of near zero in water. This can affect the ability of the model to accurately predict the amount of slurry picked up by the suction pipe and/or degree of turbidity generated by the cutter if flow rates and velocity field at the suction inlet are not appropriately scaled. On the other hand, if mean particle diameter of the sediment material is not linearly scaled and the settling velocity is not changed, then correlating the mechanical cutting action of the model cutter to the prototype may be compromised because the grain size relative to the cutter has effectively increased.

To quantify these dilemmas, consider a 1:10 scale model of a 76.2 cm (30 in) cutter-suction dredge with a cutterhead diameter of 254 cm (100 in) operating in coarse material with a median grain diameter of 0.5 mm. Linearly scaling the model dimensions by a factor of 10 would

require a 7.62 cm (3 in) dredge with a model cutterhead diameter of 25.4 cm (10 in) operating in fine material with a median grain diameter of 0.05 mm. Thus complete geometric scaling of the cutter/sediment system is possible. However, consider Reynolds scaling (Equation 1.1): if water is used as the working model fluid, then model velocities must increase by a factor of 10 for the Reynolds number (Re) to remain constant,

$$\mathrm{Re} = \frac{uD}{\nu} \tag{1.1}$$

where u is the model/prototype velocity, D is the model/prototype linear dimension, ν is the viscosity of water.

Already there is serious discrepancy. If the model median grain diameter is scaled down by a factor of 10, the resulting model particle settling velocity is scaled down by a factor of 40 using the Schiller equation (Equation 1.2) for sand particle settling velocities (Herbich 2000). The calculated velocities are shown in Table 1.1.

$$V_{settling} = 134.14\left(d_{50} - 0.039\right)^{0.972} \tag{1.2}$$

Table 1.1: Settling Velocity versus Median Grain Diameter for 1:10 Scale Similitude Example

	Particle Median Grain Diameter	**Particle Settling Velocity**
Prototype	0.5 mm	63.2 mm/s
Model	0.05 mm	1.7 mm/s

The result is that the particle settling velocities do not follow the Reynolds scaling parameter. If the model suction velocity is increased by a factor of 10 while model settling velocities are decreased by a factor of 40, the model suction has the potential to pick up 400 times more suspended sediment than the prototype. The only way to reconcile these quantities is to select a bed material with a density sufficient so that a 0.05 mm diameter particle achieves a settling velocity of 632 mm/s. Even if this were physically possible, how would the inertia of such weighty sediment affect the ability of the model to perform?

If model tests are performed using Froude (Fr) scaling on earth where the gravitation constant is held constant, then velocities must decrease by a factor of $10^{½}$ according to Equation 1.3,

$$\mathrm{Fr} = \frac{u}{\sqrt{Dg}} \tag{1.3}$$

where u is the model/prototype velocity, D is the model/prototype linear dimension, g is the gravitational constant.

Again there are serious discrepancies. If the model median grain diameter is scaled down by a factor of 10, the resulting model particle settling velocity is scaled down by a factor of 40 as shown in Table 1.1. The result is that the particle settling velocities do not follow the Froude scaling parameter. If the model suction velocity is decrease by a factor of $10^{½}$ while model settling velocities are decreased by a factor of 40, the model suction has the potential to pick up 13 times more suspended sediment than the prototype. Not as disproportionate as the Reynolds example but still outside the bounds of a successful model. These quantities could be reconciled by selecting a bed material with a density sufficient so that a 0.05 mm diameter particle achieves a settling velocity of 20 mm/s. While there are materials, namely metals, that have sufficient density to achieve this, using them as bed material would not be practical. Moreover, previous hydraulic model studies by Slotta (1968) have shown that the data for sediment pick-up behavior shows a slight correlation to the Reynolds number while no correlation to the Froude number has been observed.

As this simple example shows, satisfying all of the conditions for geometric, kinematic, and dynamic similitude is very unlikely using sand and water for hydraulic model tests. There are many other operating parameters, other than sediment grain size, that require scaling and each have similar difficulties. However, research suggests that meaningful hydraulic model studies can still be conducted if the limits of the model are clearly understood. During the last 60 years, there have been a handful of studies and model experiments published that have attempted to establish valid similitude relationships for hydraulic suction dredge models.

CHAPTER II

PREVIOUS HYDRAULIC MODEL STUDIES

2.1 The Role of Previous Hydraulic Model Studies

Before new laboratory facilities for hydraulic dredge modeling can be proposed, a rationale for scaling down the operating parameters must first be developed. The first step in this process is to examine previous model studies. While the modeling of hydraulic dredges has been studied now for over 60 years, a handful of relevant studies have been published. In fact, few laboratories exist with the facilities capable of performing model studies on hydraulic dredges.

2.2 Army Corps of Engineers Model Dredge Studies

From 1942 to 1944 the Army Corps of Engineers Waterways Experiment Station conducted a model study of the suction head for the Dredge Jadwin (Army Corps of Engineers 1947). The purpose of this study was to investigate the performance characteristics of a newly designed dustpan-type suction head by testing different 1:10 scale models. Data from the model tests were used to determine how changes in the suction head design parameters would affect solids output, soil removal rate, and efficiency. Consequently, no attempt was made to use the model test data to quantitatively predict prototype performance. Figures 2.1 and 2.2 illustrate the model test facilities used to test hydraulic dredge dragheads.

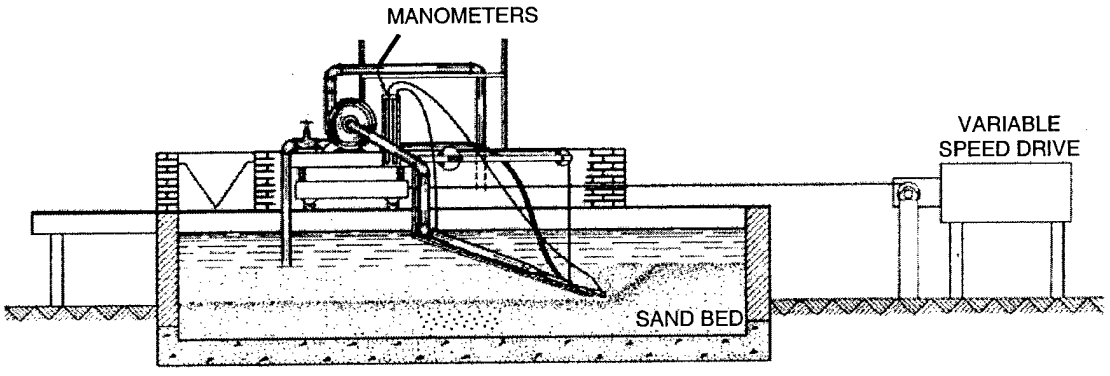

Figure 2.1: Side View of USACE WES Hydraulic Dredge Modeling Facility
(Army Corps of Engineers 1947)

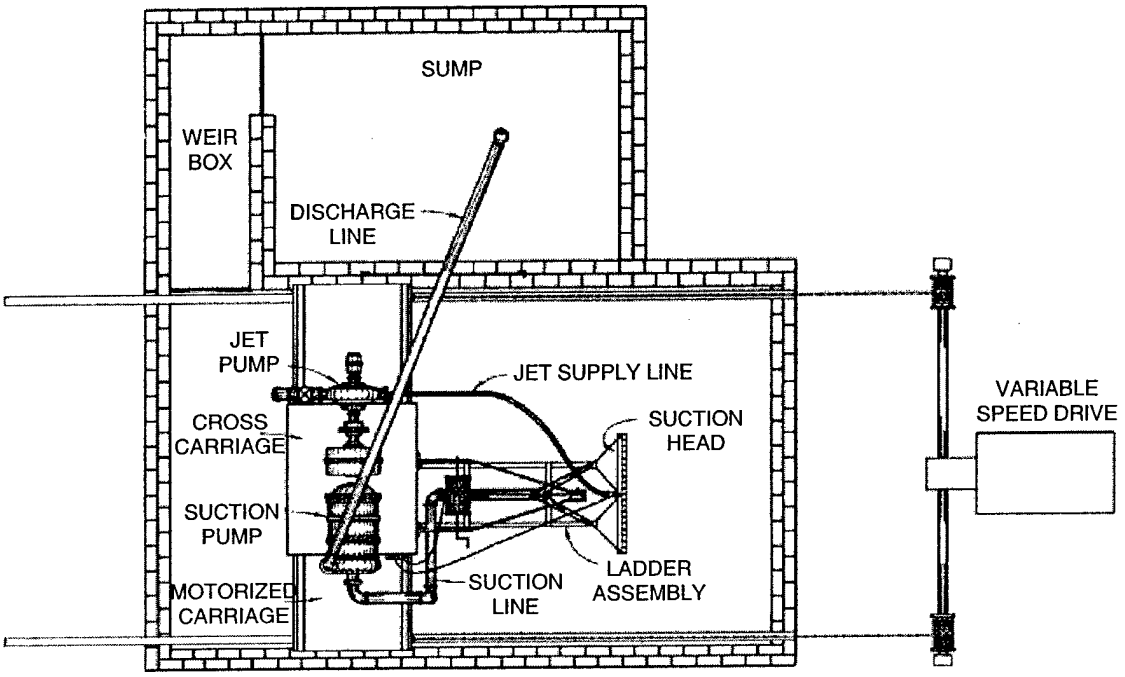

Figure 2.2: Overhead View of USACE WES Hydraulic Dredge Modeling Facility (Army Corps of Engineers 1947)

While the objectives of these tests were not to establish a set of similitude criteria between the model and the prototype, several useful observations were made during the study. Most importantly, the grain diameter of the sand that was used for the bed material was not linearly scaled to the model leading the researchers to conclude:

> *...exact similarity was not established for those tests in which the suction head operated in the sand bed. Thus, the results of the latter tests are only qualitative in nature, and cannot be translated to absolute prototype terms; this notwithstanding, the results of these tests may be used as a satisfactory basis for comparison between the relative efficiencies and performances of the various designs tested* (Army Corps of Engineers 1947).

From 1959 to 1963, the Army Corps of Engineers Waterways Experiment Station conducted another hydraulic model investigation to improve the design of dredge dragheads (Franco 1967). Like the previous hydraulic model study, the purpose of this study was to make qualitative

observations on model performance under various operating conditions in order to improve performance of the full-scale prototype. Once again, the median grain diameter of the bed material used was full-scale for the model tests. As a result of the sand not being proportionately scaled to the model, it was determined that a linear 1:6 scale for the drag-head model and suction line was the smallest possible without adverse scale effects. Ideally, a set of useful similitude relationships for dredge modeling should be scalable on the order of 1:10 geometric scale ratio without any adverse scale effects.

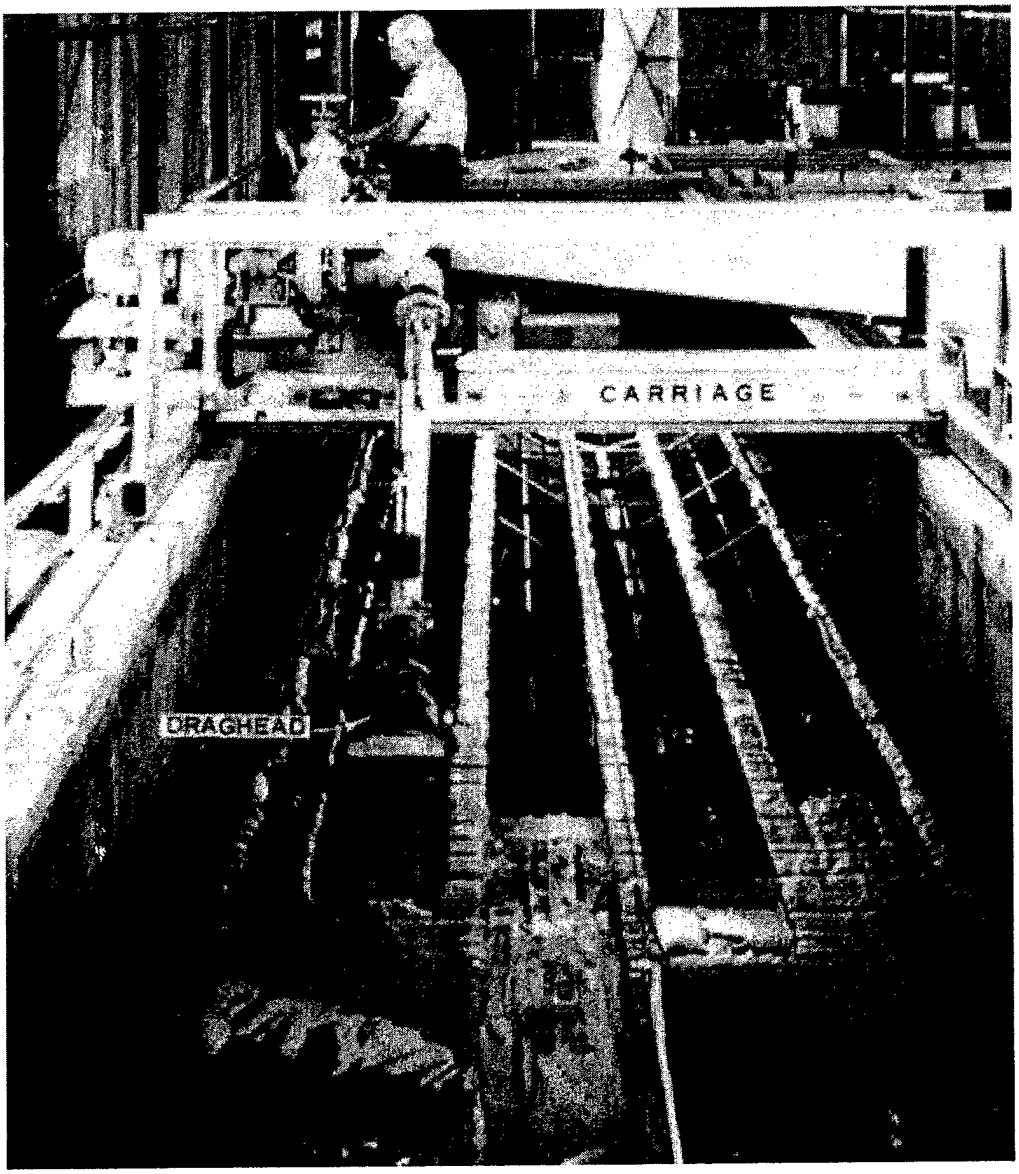

Figure 2.3: Experimental Set-Up for Testing Hydraulic Dredge Dragheads (Franco 1967)

In this case, physical limitations of the testing facilities prevented the water depth, suction line length, pump elevation above the water level, and median grain size of bed material from being appropriately scaled. As a result, data collected from the model runs could not be directly used to calculate the analogous quantities for the prototype. Figure 2.3 illustrates the testing facility used to conduct the hydraulic model tests.

The model bed material used had a median grain diameter of 0.23 mm, which corresponds to the prototype bed material having a median grain diameter of 1.38 mm. Clearly, the system head, flow rate, solids production, and turbidity generated would differ greatly if material with such a large particle size were to be dredged by the prototype. Attempts to correct the model data for the differences in similarity related to the median grain diameter of the bed material were unsuccessful. As a result, the adjusted model data did not accurately reflect the data eventually obtained from the prototype. The study concludes:

> *Because of the limitations and dissimilarities between model and prototype mentioned above, the results of this study cannot be considered strictly quantitative when applied to the prototype. However, the results do provide reasonable indications of the comparative effectiveness of the various dragheads and modifications* (Franco 1967).

2.3 Flow Visualization Studies

Results of a cutterhead flow visualization study using scaled models were presented at the 1968 World Dredging Conference in the Netherlands (Slotta 1968). The purpose of this model study was to study the flow in and around the cutterhead under different operating conditions and how the flow affects turbidity and solids production. An attempt was also made to establish similitude criteria for hydraulic suction dredge models so that data taken from the model studies could be used to quantitatively predict full-scale effects.

The experiments were performed with a 1:15 scale cutterhead using clear water in a Plexiglas tank. Hydrogen bubbles created by electrolysis provided visualization of the streamlines that were recorded onto film for further observation and analysis. In this study, the test conditions

attempted to satisfy the similitude criteria for the Reynolds number (Equation 2.1), the Froude number (Equation 2.2), a kinematic scale of velocities (Equation 2.3), and the specific speed of the rotating cutterhead (Equation 2.4).

$$\left[\frac{U_{suction} D_{cutter}}{\nu}\right]_{model} = \left[\frac{U_{suction} D_{cutter}}{\nu}\right]_{prototype} \tag{2.1}$$

$$\left[\frac{(U_{suction})^2}{g D_{cutter}}\right]_{model} = \left[\frac{(U_{suction})^2}{g D_{cutter}}\right]_{prototype} \tag{2.2}$$

$$\left[\frac{\omega_{cutter} D_{cutter}}{U_{suction}}\right]_{model} = \left[\frac{\omega_{cutter} D_{cutter}}{U_{suction}}\right]_{prototype} \tag{2.3}$$

$$\left[\frac{\omega_{cutter} \sqrt{Q_{Suction}}}{(H_{velocity})^{3/4}}\right]_{model} = \left[\frac{\omega_{cutter} \sqrt{Q_{suction}}}{(H_{velocity})^{3/4}}\right]_{prototype} \tag{2.4}$$

Where: $H_{velocity} = \frac{(U_{suction})^2}{2g}$

These relationships were developed by a dimensional analysis on the cutterhead and suction pipe parameters. Equations 2.3 and 2.4 were found to accurately correlate the data for suction velocity, cutterhead speed, and volumetric flow rate. Since the tests were done without any swing or haulage velocity, this quantity was omitted from the dimensional analysis. Moreover, no attempt was made to scale cutting forces, production, or cutter power, only the fluid behavior.

Satisfying Equations 2.1 and 2.2 simultaneously was found to be physically impossible for reasons previously stated in the similitude example. Separate but related studies on sand pick-up behavior showed that a quasi-Reynolds relationship could more accurately predict the suction of sand particles into the line under scaled test conditions than Froude scaling. However, neither

parameter produced an adequate correlation of model-prototype data. Later studies will show that neither the Reynolds nor the Froude numbers are particularly useful in scaling the sand pick-up behavior by the suction inlet. These difficulties led the researchers to make the following statement:

> *A rationale for projecting the results from model tests is at present not available, except on a qualitative basis. Dimensional analysis offers a guide to experimentation and forms a rational basis for proper analysis of results...*(Slotta 1968).

2.4 Model Cutterhead Studies at Delft University

Results of another suction cutterhead model study were presented at the 1976 World Dredging Conference in California (Joanknecht 1976). Unlike the previous studies described, the sole purpose of this study was to establish similitude relationships between model and prototype that would allow quantitative analysis of full-scale effects based on the model data. The cutterheads used in this study were 1:3 and 1:4 scales, and the sand used had a median grain diameter of 0.2 mm. Several test runs were performed in a towing tank while numerous data were recorded. Figure 2.4 depicts the model dredge testing facility at the Delft Hydraulics Laboratory.

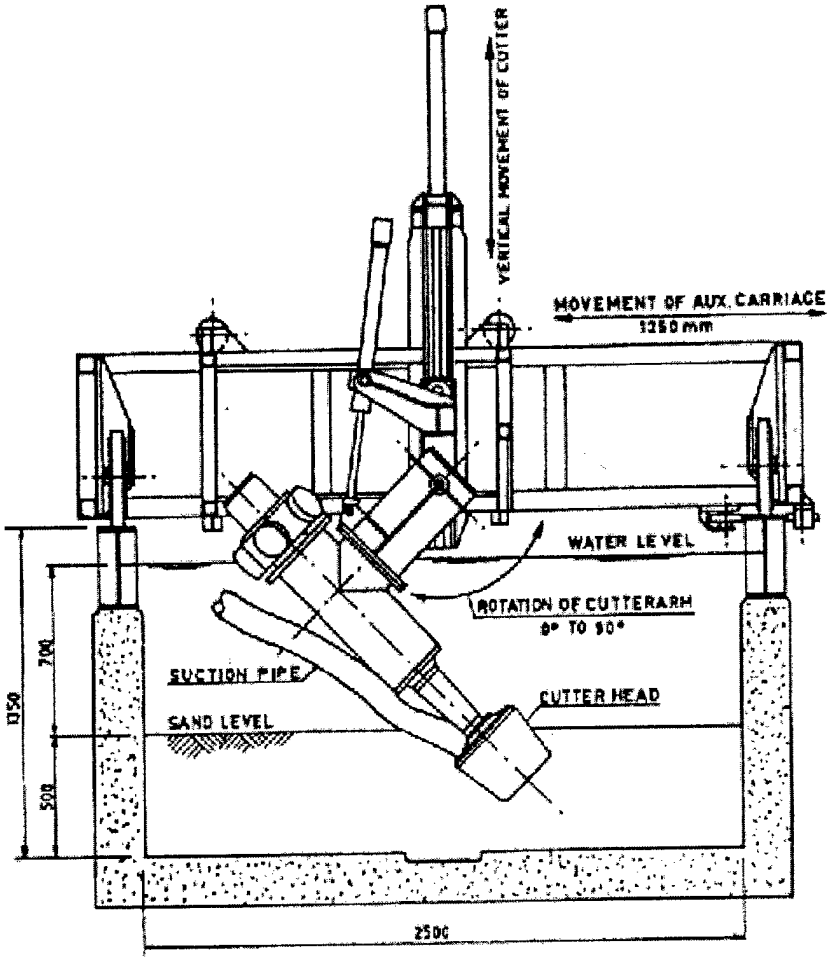

Figure 2.4: Side View of the Dredge Modeling Facility at the Delft Hydraulics Laboratory (Joanknecht 1976)

In this study, the dominant parameter for overall dynamic and kinematic similarity was assumed to be the Froude number. However, rather than using the intake velocities at the suction inlet and the cutterhead diameters as was the common practice, the Froude relationship was applied using the particle settling velocities ($V_{settling}$) and the median grain diameters (d_{50}) (Equation 2.5) of the model and prototype bed materials.

$$\left[\frac{V_{settling}}{\sqrt{gd_{50}}}\right]_{\text{model}} = \left[\frac{V_{settling}}{\sqrt{gd_{50}}}\right]_{\text{prototype}} \tag{2.5}$$

Since the same bed material was used for both model and prototype in these experiments, this condition was automatically satisfied. However, given that settling velocity is strictly a function of grain diameter for a given material density, it would be difficult to satisfy this relationship using sand if the model median grain diameter differed from the prototype median grain diameter. For example, if particle size were to be scaled at a 1:10 ratio, particle density would have to be increased by an order of magnitude to satisfy this parameter. The same situation was encountered in the similitude example (Section 1.4) when using Froude and geometric scaling. Froude scaling was also used to develop the kinematic similitude relationships for cutterhead swing velocity (Equation 2.6) and cutterhead rpm (Equation 2.7). The relationships were developed on the basis of scaling the forces only, without concern for any similarity of the production or sediment pick-up behavior.

$$\left[\frac{V_{swing}}{\sqrt{gD_{cutter}}}\right]_{\text{model}} = \left[\frac{V_{swing}}{\sqrt{gD_{cutter}}}\right]_{\text{prototype}} \tag{2.6}$$

$$\left[N_{cutter}\sqrt{\frac{D_{cutter}}{g}}\right]_{\text{model}} = \left[N_{cutter}\sqrt{\frac{D_{cutter}}{g}}\right]_{\text{prototype}} \tag{2.7}$$

Kinematic similarity for fluid/particle interaction was achieved by keeping the ratio of particle settling velocity to the velocity at the suction pipe inlet identical for both model and prototype (Equation 2.8).

$$\left[\frac{V_{settling}}{U_{suction}}\right]_{\text{model}} = \left[\frac{V_{settling}}{U_{suction}}\right]_{\text{prototype}} \tag{2.8}$$

This relationship attempts to ensure proper scaling of the velocity field relative to the settling velocity of the bed material. Since the same bed material was used for both model tests, the suction velocity was also made to be identical for both model tests. While satisfying Equation 2.8 acts to properly scale the velocity field magnitude relative to the particle settling velocity, it does not take into consideration the geometry of the velocity field, which is determined by the

volumetric flow rate. This can be more easily illustrated if a 1:10 scale model were used as an example. If a prototype were 10 times the size of a model, and the suction inlet diameters, velocities, and sediment settling velocities were all identical in both model and prototype, then the size and magnitude of the model velocity field would be identical to the size and magnitude of the prototype velocity field. Clearly, in this case the model sediment pick-up behavior would not be similar to the prototype in that the relative size of the model velocity field is 10 times that of the prototype velocity field. Since the size of the velocity field is a function of volumetric flow rate, the suction inlet diameter of the model would have to be scaled down in order to properly scale the model velocity field size. Because of this, simply scaling the intake velocity to the particle settling velocity as shown in Equation 2.8 will not guarantee proper velocity field scaling with respect to field geometry. However, at the small scale of 3:4 tested during this study, the resulting scale effects were not detrimental.

Providing that Equations 2.5-2.8 are satisfied, other similitude relationships based on the Froude relationship were developed that accurately correlated test data between the two models for volumetric flow rate (Equation 2.9), cutting force (Equation 2.10), and shaft torque (Equation 2.11).

$$\left[\frac{Q_{suction}}{(D_{cutter})^{5/2}}\right]_{model} = \left[\frac{Q_{suction}}{(D_{cutter})^{5/2}}\right]_{prototype} \tag{2.9}$$

$$\left[\frac{F_{cutting}}{(D_{cutter})^{3}}\right]_{model} = \left[\frac{F_{cutting}}{(D_{cutter})^{3}}\right]_{prototype} \tag{2.10}$$

$$\left[\frac{\Gamma_{shaft}}{(D_{cutterhead})^{4}}\right]_{model} = \left[\frac{\Gamma_{shaft}}{(D_{cutterhead})^{4}}\right]_{prototype} \tag{2.11}$$

Again, these relationships were based on the Froude scaling of the forces and do not attempt to correlate production data between model and prototype. A full-scale prototype was being built and was to be tested at a future date and was therefore not included in this paper (Joanknecht

1976). Unfortunately, results of this study cannot be found in the available literature so it is uncertain if the subsequent study ever took place.

Noting that the two models tested were 1:3 scale and 1:4 scale, their relative scale to each other would only be 3:4. For these similitude relationships to be useful, they would need to be tested for scale ratios on the order of 1:5 to 1:10 so that any possible scale effects can be more easily seen.

2.5 Flow Field Studies and Sediment Pick-up Behavior

Brahme and Herbich (1986) described a series of studies conducted to examine the velocity flow field around the suction inlet and the influence of the velocity field on sediment pick-up behavior. A dimensionless parameter (Equation 2.12) was developed while creating dimensionless velocity field plots around suction inlets of various orientations. It was found that by using these dimensionless plots, the velocity (V) at any point in the field could be determined with reasonable accuracy if the volumetric flow rate (Q) and the radial distance (R) of the point from the suction inlet are known. This was found to hold true regardless of the geometric scale of the velocity field.

$$\frac{Q_{suction}}{R^2 V} = \text{Dimensionless velocity field} \tag{2.12}$$

One very important observation is the fact that the magnitude of the velocity field was not found to depend on intake velocity or intake diameter if the volumetric flow rate through the suction pipe was held constant. In fact, the magnitude of the velocity field was found to depend solely on volumetric flow rate through the suction pipe, regardless of pipe geometry or intake velocity.

CHAPTER III

SCALING LAWS FOR MODELING HYDRAULIC DREDGING OPERATIONS

3.1 Basis of Design for Laboratory Modeling Facility

As was stated at the beginning of Chapter II, a rationale for scaling down the operating parameters must first be developed before new laboratory facilities for hydraulic dredge modeling can be proposed. However, previous studies were inconclusive and to the author's knowledge, a complete and experimentally verified set of similitude criteria has not been published. The kinematic scale of velocities by Slotta (1968), the velocity scale by Joanknect (1976), and the dimensionless velocity field parameter by Brahme and Herbich (1986) have been shown to accurately correlate the test data, but they are not enough to provide a rationale for complete model scaling. Recommendations based on dimensional analysis and cutting theory have also been made by many including Slotta (1968), Joanknect (1976), Burger (1997), and Miedema (1987). However, many of these recommendations are incongruent with one another as will be demonstrated in this Chapter. Ironically, new laboratory facilities capable of performing such model tests are just what is needed before such criteria can be adequately developed and tested. Despite this obvious paradox, the author believes that a sufficient rationale for developing such facilities can be derived from the current body of knowledge.

In order for a laboratory modeling facility to be workable, a perfect set of similitude criteria need not be known. In fact, if the stated goal of the facility is to develop such relationships, then some sort of approximation will have to be made in the outset. The proposed facilities must be able to successfully model, at a geometric scale of 1:10, large commercial suction cutterhead dredges. An example of a large dredge could have a 76.2 cm (30 in) diameter discharge line, a 254 cm (100 in) diameter cutter head rotating at an average speed of 30 rpm, pump up to 189,270 LPM (50,000 GPM) of slurry at a specific gravity of 1.3, have a haulage, or swing, velocity of up to 30.5 cm/s (60 ft/min), and operate in bed material ranging from fine sand (0.1 mm) to coarse sand (1 mm). This hypothetical dredge will hereafter be referred to as the "prototype dredge." These parameters are summarized in Table 3.1.

Table 3.1: Prototype and Model Dredge Maximum Operating Parameters

Operating Parameter	Prototype Dredge	Model Dredge
Geometric Scale	1:1	1:10
Discharge Line	76.2 cm (30 in)	7.62 cm (3 in)
Cutterhead Diameter	254 cm (100 in)	25.4 cm (10 in)
Cutterhead rpm	30 rpm	Need to Determine
Cutterhead Power	4476 kW (6000 hp)	Need to Determine
Suction Flow Rate	189,270 LPM (50,000 GPM)	Need to Determine
Slurry Specific Gravity	1.3	Need to Determine
Pump Power	7460 kW (10,000 hp)	Need to Determine
Haulage Velocity	30.5 cm/s (60 ft/min)	Need to Determine
Side Winch Power	560 kW (750 hp)	Need to Determine
Digging Depth	13.72 m (45 ft)	3.05 – 4.27 m (10-14 ft)
Bed Material	0.1 mm – 1.0 mm	Need to Determine

Therefore, a 1:10 scale laboratory modeling facility should have at least a 7.62 cm (3 in) diameter suction/discharge line and model cutterheads up to 25.4 cm (10 in) in diameter. The challenge is how to properly scale the cutterhead power, side winch power, haulage velocity, pump power, bed material, and volumetric flow rate so that the selection of equipment can be made. The minimum model dredge digging depth will be determined by the water level in the towing tank, which is 3.05 m (10 ft). The maximum model dredge digging depth will be determined by the depth of the sediment pit, which is 4.56 m (15 ft), minus 0.305 m (1 ft) for the cutterhead to safely clear the tank bottom while cutting. Therefore, the model dredge digging depth range will be 3.05 m (10 ft) to 4.27 m (14 ft) as shown in Table 3.1.

There are several other quantities that must be properly scaled. Earlier studies from the 1940's through the 1960's seemed to be focused primarily on the Reynolds/Froude paradox and how to properly scale the median grain size of the bed material to achieve similitude. During the late 1970's through the middle 1980's, the research began to look at the individual processes being modeled. For the mechanical process of cutting, rotating, and swinging, similitude criteria developed from Froude scaling showed a fair correlation of the data (Joanknecht 1976). These relationships are expressed in Equations 2.6, 2.7, 2.9, 2.10, and 2.11. For the hydraulic sediment pick-up process, the classic Reynolds vs. Froude argument may not be relevant for reasons discussed in the previous similitude example (Section 1.4). Dimensional analysis of the

cutterhead and fluid flow has led to the development of similitude relationships as expressed in Equations 2.3, 2.4, and 2.8.

Rather than attempt to develop an exact set of similitude criteria that applies to every type of dredge in every type of situation, the author proposes to determine the upper operating limits of the key parameters. This will ensure that many different dredging scenarios can be modeled successfully and meaningful data can be collected without being limited by model dredge performance. Therefore, cutter drive power, suction pump power and swing winch power must all be sufficient so that the largest commercial dredges, such as the aforementioned "prototype dredge" can be successfully modeled. Once such facilities are in place, perhaps more detailed model studies could be performed to determine the exact scaling between the model and prototype quantities.

3.2 Sediment Pick-up Behavior

If a model dredge is to be successful, the model suction must be properly scaled such that the sediment pick-up behavior is similar to the prototype suction. The flow of water through the suction inlet creates a velocity field around the inlet (Burger 1997). Before any amount of sediment can be drawn towards the suction inlet via the velocity field, it must first be removed, or excavated, by the cutter. Assuming that the model cutter has been geometrically, kinematically, and dynamically scaled to the prototype (this will be looked at later), then the model cutter is removing a geometrically similar volume of material as the prototype. Given this, the model suction needs to pick up a geometrically similar volume of material as the prototype suction. Consider the following example illustrated in Figure 3.1: suction A and suction B are both geometrically similar suction inlets with a 1:2 geometric scale ratio. Each suction inlet has a flow rate (Q) that creates a velocity field around the inlet with a similar geometry and magnitude. The lines of constant velocity potential are shown. The heavy line represents the range (R) at which the magnitude of the velocity field (V) is equal to the median grain diameter settling velocity.

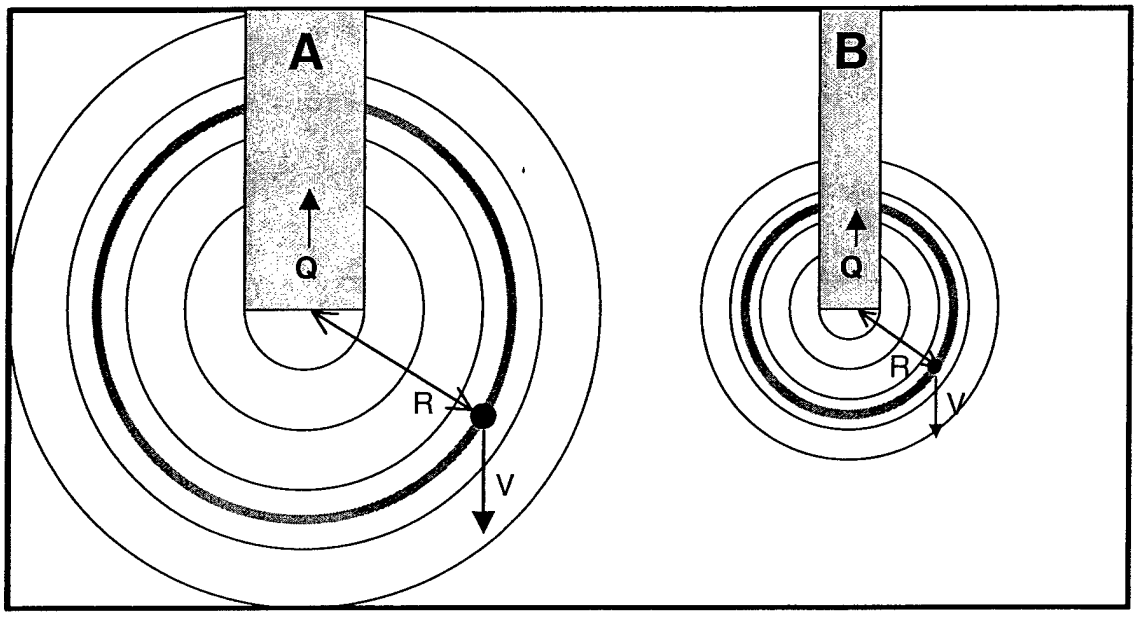

Figure 3.1: Velocity Field Similitude Example

Theoretically, all particles within the heavy line are captured by the velocity field and drawn towards the suction inlet. Conversely, all particles outside the heavy line will either settle out or remain in suspension. For suction A and suction B to be geometrically similar with respect to sediment pick-up, the range for A must be twice that of B, in accordance with the 1:2 geometric scale ratio. The range (R) of the heavy line is a function of both velocity field magnitude and particle settling velocity. For instance, for a given median grain size, the range will move closer or further from the inlet as the magnitude of the velocity filed is changed. Higher field velocities will pick up more material (move the range out), and lower field velocities will pick up less material (move the range in). Likewise, for a given velocity field magnitude, the range will move closer or further from the inlet as the particle settling velocity is changed. Higher settling velocities will cause less material to be picked up (move the range in) and lower settling velocities will cause more material to be picked up (move the range out).

The rotating cutterhead also creates a velocity field around the suction inlet (Burger 1997), as do the cutterhead swing and any currents passing through the area. These velocity fields also have an impact on sediment pick-up behavior. As a result, they too must be similarly scaled if similarity with respect to sediment pick-up is to be maintained between model and prototype.

To summarize, for two suctions to achieve similarity with regard to sediment pick up behavior, the range of each velocity field must be scaled in accordance with the geometric scale ratio. This is accomplished by the scaling of two quantities: the velocity field geometry and the velocity field magnitude. For a cutterhead dredge, the ratio of velocity field geometry to cutter diameter must be identical for both model and prototype, and the ratio of velocity filed magnitude to particle selling velocity must be identical for model and prototype. For a hopper dredge, the ratio of velocity field geometry to draghead size must be identical for both model and prototype, and the ratio of velocity filed magnitude to particle selling velocity must be identical for model and prototype.

3.2.1 The Role of the Dimensionless Velocity Field Parameter

Research at Delft University highlighted the importance of properly scaling the velocity field at the suction inlet to the settling velocity of the bed material (Joanknect 1976). However, subsequent studies with dimensionless velocity field plots showed that the magnitude of the velocity field was found to be more a function of the volumetric flow rate through the suction pipe than the suction inlet velocity (Brahme and Herbich 1986). More importantly, outside the immediate vicinity of the suction inlet, suction pipe velocity and diameter have a negligible effect on the velocity field. Since the velocity in the immediate vicinity of the suction inlet is several orders of magnitude greater than the particle settling velocity, proper scaling of the velocity field for the purposes of sediment pick-up similitude is only critical at distances from the suction inlet where field velocities are similar to particle settling velocities. Therefore, proper scaling of the velocity field shape and magnitude created by the suction pipe is dependent only on the volumetric flow rate through the suction pipe. As a result, accurate velocity field scaling can be achieved for any given median grain diameter, geometric scale ratio, and pipe diameter simply by scaling the volumetric model flow rate in accordance with Equation 3.1.

$$\left[\frac{Q_{suction}}{(D_{cutter})^2 V_{settling}}\right]_{model} = \left[\frac{Q_{suction}}{(D_{cutter})^2 V_{settling}}\right]_{prototype} \tag{3.1}$$

The dimensionless parameter developed by Brahme and Herbich (1986) to plot dimensionless velocity fields for different intakes can be used to non-dimensionalize the velocity field around any suction inlet. By replacing the sediment pick up range with the cutterhead diameter and the field velocity with the settling velocity, the velocity field is "normalized" to the geometric scale of the dredge and the settling velocity of the sediment. Unlike Equation 2.8, this relationship takes into consideration geometric scaling of the velocity field as well as scaling the velocity field magnitude relative to the particle settling velocity. Moreover, stronger or weaker prototype velocity fields, larger or smaller prototype cutterheads, and different prototype sediment sizes can be modeled without changing the model suction pipe geometry or the model bed material. Only the model volumetric flow rate need be adjusted. Accurate scaling of the velocity field shape and magnitude for sediment pick-up is critical when modeling hydraulic dredges for the purpose of studying turbidity and the effects of re-suspension, as well as sediment pick-up and solids production.

It is important to note the relationship between Equation 3.1 and Equation 2.8. While the magnitude of the velocity field created by the suction is not dependant on the velocity at the suction inlet as expressed by Equation 3.1, Equation 2.8 is still a valid relationship under the right circumstances. If the prototype and model suction inlet diameters do not follow the geometric scale ratio, then certainly Equation 2.8 will not be valid as model suction inlet velocity will be determined by model suction inlet diameter. However, if the prototype and model suction inlet diameters do follow the geometric scale ratio, then Equation 3.1 reduces to Equation 2.8. Therefore, Equation 2.8 is a special case of the dimensionless velocity field parameter in which the prototype and model suction inlet diameters exactly follow the geometric scale ratio.

3.2.2 Other Challenges for Sediment Scaling

Even if perfect kinematic and geometric scaling of the velocity field around a model cutterhead can be achieved via Equation 3.1, there are several other factors that require experimentation to determine. For instance, the effect of geometrically scaling the median grain diameter of the model bed material on cutterhead dynamics has not been tested. It appears that proper geometric scaling of the model bed material in this way is practically impossible to achieve without

adversely affecting the settling velocity of the model sediment particles and creating unintended scale effects with increased material density. Perhaps proper scaling of the sediment material entails more than simply geometric scaling of the median grain diameters and dynamic scaling of the particle settling velocities. Bed sediment compactness, void ratio, material density, and cohesive/adhesive properties will all contribute to dynamic scaling of the cutting forces. While consideration of these other factors is beyond the scope of this thesis, the author believes that the rationale presented represents a good starting point for the stated purpose of model dredge pump selection.

3.3 Mixture Forming in a Cutterhead

Studies have shown that the kinematic scale of suction and cutterhead velocities by Slotta (1968) (Equation 2.3) is useful in scaling the flow in and around the cutterhead (Burger 1997). The purpose of the cutterhead is twofold, to remove the sediment from the seabed, and to form a slurry that is captured by and moves into the velocity field created by the suction. The rotation of the cutterhead can create a velocity field that interacts with the velocity field created by the suction. This may cause some of the material that would have been captured by the suction velocity field had the cutterhead been stationary to "spill" outside of the range of influence of the suction. This portion of the mixture, known as spillage, creates turbidity in the water as these particles either slowly settle to the bottom or remain suspended.

If the spillage of slurry outside the cutterhead between model and prototype is to be similar, then Equation 2.3 can be used to normalize the cutterhead angular velocity to the magnitude of the suction velocity (Burger 1997). Model tests conducted at the Delft Hydraulics Laboratory have shown there is a threshold for the cutterhead rpm above which spillage occurs (Mol 1977a, Mol 1977b). The kinematic scale of velocities for geometrically similar models can be used to determine that point. Equation 3.2 demonstrates how the model cutterhead rpm can be scaled if the suction velocities and the prototype rpm are known.

$$\left(N_{cutter}\right)_{\text{model}} = \left(N_{cutter}\right)_{\text{prototype}} \left[\frac{\left(U_{suction}\right)_{\text{model}}}{\left(U_{suction}\right)_{\text{prototype}}}\right]\left[\frac{\left(D_{cutter}\right)_{\text{prototype}}}{\left(D_{cutter}\right)_{\text{model}}}\right] \tag{3.2}$$

Section 3.2 gives a rationale for scaling the volumetric flow rate according to the geometry of the cutter and the settling velocity. If the model and prototype suction inlet diameters are known, then the pipe velocities in the suction inlets can be calculated from the flow rates, and thus the model cutterhead rpm can be scaled down from the prototype rpm.

It should be noted that the scale laws developed by Slotta (1968) and Burger (1997) scale the model cutterhead rotation to the model suction inlet velocity. However, Brahme and Herbich (1986) proved that velocity field scaling was dependant on the volumetric flow rate through the suction and not the velocity at the suction inlet. Therefore, since scaling the velocity field created by the suction inlet to the velocity at the suction inlet is a special case of the dimensionless velocity field parameter, Equations 2.3 and 3.2 must assume that the model and prototype suction inlet diameters follow the geometric scale, which may not always be the case. In order to avoid confusion, Equation 3.2 is rewritten based on the volumetric flow rate. Equation 3.3 is a more general application of the scale laws by Slotta (1968) and Burger (1997) in light of the dimensionless velocity field parameter developed by Brahme and Herbich (1986).

$$(N_{cutter})_{\text{model}} = (N_{cutter})_{\text{prototype}} \left[\frac{(D_{cutter})_{\text{prototype}}}{(D_{cutter})_{\text{model}}} \right]^3 \left[\frac{(Q_{suction})_{\text{model}}}{(Q_{suction})_{\text{prototype}}} \right] \tag{3.3}$$

The distinction between the velocity field created by the suction and the suction inlet velocity may seem academic. However, the difference becomes clear if one considers two identical suction pipes with identical flow rates. Each suction creates an identical velocity field around each suction inlet. Each suction also creates an identical suction inlet velocity. Placing a fitting over one of the suction inlets to reduce the suction inlet diameter will change the velocity at the suction inlet. However, the velocity field created by the suction will not change, being dependent on the volumetric flow rate only. Therefore, Equation 3.2 is considered a special case of Equation 3.3 that assume the suction inlet diameters follow the geometric scale ratio.

Following this same rationale for cutterhead swing as for cutterhead rpm, the swing speed of the cutterhead also creates a velocity field relative to the cutterhead that interacts with the velocity

fields created by the suction and cutterhead rotation. Equation 3.2 can be rewritten to include cutterhead swing speed in the place of the suction velocity as shown in Equation 3.4.

$$\left(V_{swing}\right)_{\text{model}} = \left(V_{swing}\right)_{\text{prototype}} \left[\frac{\left(N_{cutter} D_{cutter}\right)_{\text{model}}}{\left(N_{cutter} D_{cutter}\right)_{\text{prototype}}} \right] \tag{3.4}$$

It must be noted that the computer simulations run by Burger (1997) did not account for the swing speed. While Equation 3.4 follows the same rationale for the swing speed as followed for the suction velocity, neither physical modeling nor mathematical simulation has confirmed its usefulness. It is, however, included in this thesis as one of several means by which the swing speed of a model dredge can be appropriately scaled.

3.4 Cutterhead Dynamics

Equation 3.3 is a similitude relationship based on hydraulic similarity and is therefore different than Equation 2.7, which is based on the Froude similarity. Both of these will be considered in sizing the cutterhead drive, but there are other considerations as well. The cutting forces acting on the cutterhead must also be properly scaled since this directly affects the power required by the cutter. According to Miedema (1987) the cutting process is characterized by two quantities: the geometry of the layer being cut and whether a cavitating or non-cavitation cutting process is occurring. Moreover, if cavitation does occur during cutting in both model and prototype, then the angle of the cutterhead blade at the start of cavitation (φ_c) must also be similar between model and prototype.

3.4.1 Layer Geometry

When the rotating cutterhead is being translated over the seabed via the swing motion of the ladder, each tooth takes a specified path through the sediment based on the swing speed, the cutterhead rpm, the pitch of the blades or teeth (p), and the profile angle (κ) (Miedema 1987). The path of each cutting edge through the sediment cuts individual layers with a thickness as a

function of the angular position of the blade (φ) as defined by Equation 3.5. Figure 3.2 illustrates the relationship of the layer thickness to the other parameters.

$$t_{layer} = \frac{V_{swing} 60}{N_{cutter} p} \cos(\varphi)\cos(\kappa) \tag{3.5}$$

Where κ is defined in Figure 5.6.

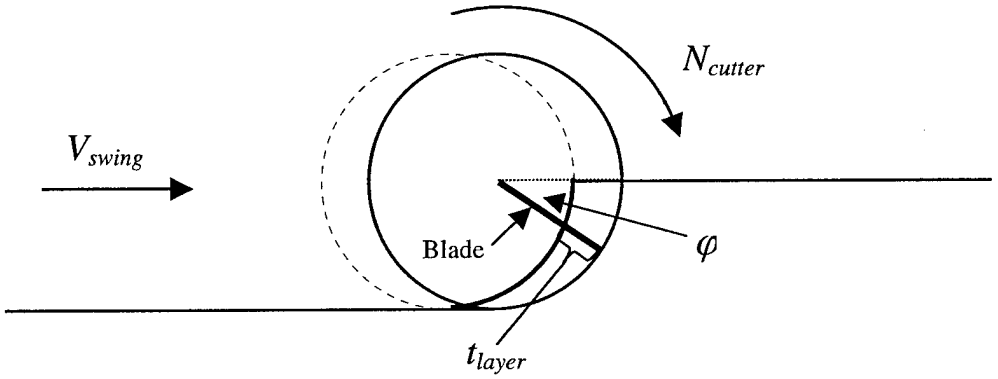

Figure 3.2: The Layer Thickness in Relation to Cutterhead Geometry and Kinematics

The model layer thickness must follow the same geometric scale ratio applied to the rest of the model. This is accomplished when the ratio of cutterhead blade velocity to swing speed is identical for model and prototype according to Equation 3.6.

$$\left[\frac{N_{cutter} D_{cutter}}{V_{swing}}\right]_{\text{model}} = \left[\frac{N_{cutter} D_{cutter}}{V_{swing}}\right]_{\text{prototype}} \tag{3.6}$$

It is noted that Equation 3.6 is identical to Equation 3.4. This provides a rationale for scaling the swing speed once the cutterhead rpm has been scaled. However, there are conflicting methods of scaling the cutterhead rpm: one based on hydraulic similarity (Equation 3.3) and one based on Froude similarity (Equation 2.7). In addition to this, there are now two conflicting methods of scaling the swing speed, one based on geometric and hydraulic similarity (Equation 3.6 and

Equation 3.4 respectively), and one based on Froude similarity (Equation 2.6). Both of these will need to be considered in sizing the model swing winch power and required pull force.

3.4.2 Cavitating versus non-Cavitating Sediment Cutting

The effect of cavitation in the sediment during cutting has a significant impact on the cutting forces developed by the cutter (Miedema 1989). If no cavitation occurs during the cutting process, the cutting forces increase as the cutting velocity increases. As the cutting velocity continues to increase, the pressure in the voids of the sediment continues to decrease. When the pore pressure in the sediment drops below the vapor pressure of the water during the cutting process, cavitation occurs. Once cavitation has begun, continuing to increase the cutting velocity doesn't drop the pore pressure any further and the cutting forces become primarily a function only of digging depth rather than cutting velocity. The effects of inertia, gravity, cohesion and adhesion still affect the cutting forces developed as the cutting velocity increases, but they are relatively insignificant and not included in Miedema's analysis (the same reasons were stated in Section 3.2.2).

If and when cavitation occurs is a function of the digging depth, the cutterhead rpm, and the layer thickness as well as the sediment properties and blade angle. Equation 3.7 shows the condition that has to be met for cavitation to occur (Miedema 1995),

$$\left(\frac{d_1}{c_1}\right)\left(\frac{k_m}{e}\right)\frac{z+33}{V_{cutter}t_{layer}}<1 \tag{3.7}$$

where V_{cutter} is equal to $N_{cutter}\pi D_{cutter}/60$.

The ratio of d_1/c_1 is a function of the given blade angle and the ratio k_m/e is a function of the sediment mechanical properties. Since the layer thickness is a function of the blade position as it moves through the sediment for any given swing speed and cutterhead rpm (Equation 3.3), cavitation usually occurs at a certain cutting angle as each blade progresses through the layer.

Figure 3.3 illustrates the relationship between the cavitation transition angle (φ_c) and the other operating parameters.

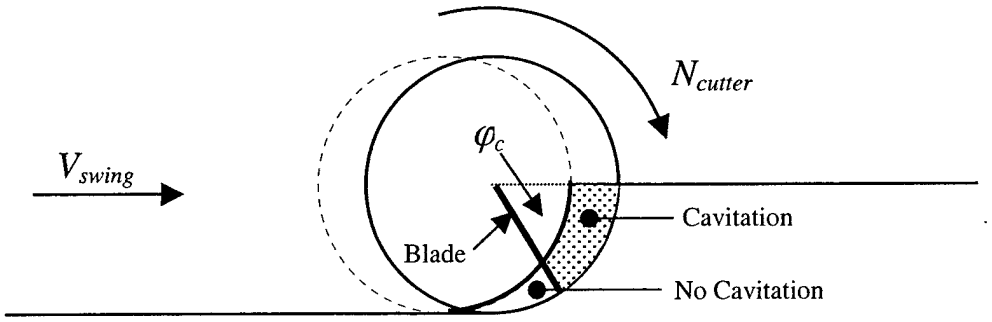

Figure 3.3: The Cavitation Transition Angle

The onset of cavitation in the prototype occurs when the absolute pore pressure reaches the limit described by Equation 3.8 (Miedema 1987). This will also occur in the model dredge according to Equation 3.9 (Miedema 1987). The ratio of the prototype to model cavitation pressures is known as the cavitation scale factor, or hydrostatic pressure factor λ_c, and is defined by Equation 3.10 (Miedema 1987). It is important to note that Equation 3.10 assumes that the model soil mechanics (i.e. volume strain, e, and average permeability, k_m) are identical to the prototype soil mechanics.

$$[p_{cavitation}]_{\text{prototype}} = [\rho_{water} g(z+33)]_{\text{prototype}} \tag{3.8}$$

$$[p_{cavitation}]_{\text{model}} = [\rho_{water} g(z+33)]_{\text{model}} \tag{3.9}$$

$$\frac{z_{\text{prototype}} + 33}{z_{\text{model}} + 33} = \lambda_c \tag{3.10}$$

To achieve similarity between model and prototype with respect to the *degree* of cavitation during the cutting process, the prototype/model pore pressure ratio must be equal to the cavitation scale factor. Since the pore pressure for the non-cavitating case is proportional to the

product of the layer thickness and the cutterhead rpm, this leads to another rationale for scaling the model cutterhead rpm according to Equation 3.11.

$$\left(N_{cutter}\right)_{\text{model}} = \left(N_{cutter}\right)_{\text{prototype}} \left[\frac{\left(D_{cutter}\right)_{\text{prototype}}}{\left(D_{cutter}\right)_{\text{model}}}\right]^2 \frac{1}{\lambda_c} \tag{3.11}$$

Recall that Equation 3.3 is a similitude relationship for model cutterhead rpm based on the hydraulics, or fluid/particle interaction in an around the cutterhead. Also recall that Equation 2.7 is a similitude relationship for model cutterhead rpm based on the Froude number. There is also Equation 3.11, which is a similitude relationship for model cutterhead rpm based on the dynamics, or cutting forces developed during the dredging process with respect to cavitation. These will all have to be considered in Chapter IV when the laboratory set-up is outlined.

To achieve similarity between model and prototype with respect to the *geometry* of cavitation during the cutting process, the cavitation transition angle as shown in Figure 3.3 needs to be identical between model and prototype. This involves solving Equations 3.7 and 3.5 in terms of the angular position of the blade, φ, and setting the two quantities equal to each other. This leads to another rationale for scaling the model cutterhead swing speed according to Equation 3.12.

$$\left(V_{swing}\right)_{\text{model}} = \left(V_{swing}\right)_{\text{prototype}} \left[\frac{\left(D_{cutter}\right)_{\text{prototype}}}{\left(D_{cutter}\right)_{\text{model}}}\right] \frac{1}{\lambda_c} \tag{3.12}$$

Recall that Equation 3.6 is a similitude relationship for model swing speed based on hydraulic and geometric similarity. Also recall that Equation 2.6 is a similitude relationship for model cutterhead swing speed based on the Froude number. There is also Equation 3.12, which is a similitude relationship for model cutterhead swing speed based on the dynamics, or cutting forces developed during the dredging process with respect to cavitation. Whether or not Equations 3.6, 3.11, and 3.12 can be consistently solved with a given model digging depth will have to be considered in Chapter IV when the laboratory set-up is outlined.

3.5 Summary of Scaling Laws

While there are still many unresolved issues and incongruent scale laws, the author believes that the analysis presented in Chapter III provides an adequate basis for experimentation and will be used in the design and development of the proposed modeling facilities. The application of these scale laws to hopper dredges is much less involved and only includes the proper scaling of the velocity field via the suction (Equation 3.1), and the draghead speed. The draghead velocity scale is identical to the settling velocity scale. The following is a summary of the scale laws that have been examined thus far.

3.5.1 Hydraulic Scaling Based on Sediment Pick-up Behavior

In order to achieve similarity with respect to sediment pick-up behavior and fluid flow in and around the cutterhead the following scale laws have been proposed:

For the suction flow rate in terms of geometry and settling velocity:

$$\left(Q_{suction}\right)_{\text{model}} = \left(Q_{suction}\right)_{\text{prototype}} \left[\frac{\left(D_{cutter}\right)_{\text{model}}}{\left(D_{cutter}\right)_{\text{prototype}}}\right]^2 \left[\frac{\left(V_{settling}\right)_{\text{model}}}{\left(V_{settling}\right)_{\text{prototype}}}\right] \tag{3.13}$$

For the cutterhead rpm in terms of geometry and suction flow rate:

$$\left(N_{cutter}\right)_{\text{model}} = \left(N_{cutter}\right)_{\text{prototype}} \left[\frac{\left(D_{cutter}\right)_{\text{prototype}}}{\left(D_{cutter}\right)_{\text{model}}}\right]^3 \left[\frac{\left(Q_{suction}\right)_{\text{model}}}{\left(Q_{suction}\right)_{\text{prototype}}}\right] \tag{3.14}$$

For the cutterhead swing speed in terms of geometry and cutterhead rpm:

$$\left(V_{swing}\right)_{\text{model}} = \left(V_{swing}\right)_{\text{prototype}} \left[\frac{\left(N_{cutter} D_{cutter}\right)_{\text{model}}}{\left(N_{cutter} D_{cutter}\right)_{\text{prototype}}}\right] \tag{3.15}$$

3.5.2 Kinematic Scaling Based on the Froude Number

In order to achieve similarity with respect to the Froude number and the scaling of velocities based on inertial forces, the following scale laws have been proposed:

For the suction flow rate in terms of geometry (Equation 2.9):

$$(Q_{suction})_{\text{model}} = (Q_{suction})_{\text{prototype}} \left[\frac{(D_{cutter})_{\text{model}}}{(D_{cutter})_{\text{prototype}}} \right]^{\frac{5}{2}} \tag{3.16}$$

For the cutterhead rpm in terms of geometry (Equation 2.7):

$$(N_{cutter})_{\text{model}} = (N_{cutter})_{\text{prototype}} \left[\frac{(D_{cutter})_{\text{prototype}}}{(D_{cutter})_{\text{model}}} \right]^{\frac{1}{2}} \tag{3.17}$$

For the cutterhead swing speed in terms of geometry (Equation 2.6):

$$(V_{swing})_{\text{model}} = (V_{swing})_{\text{prototype}} \left[\frac{(D_{cutter})_{\text{model}}}{(D_{cutter})_{\text{prototype}}} \right]^{\frac{1}{2}} \tag{3.18}$$

3.5.3 Dynamic Scaling Based on the Cutting Forces with Respect to Cavitation

In order to achieve similarity with respect to the cutting forces based on cavitation and layer geometry, the following scale laws have been proposed:

For the cutterhead swing speed in terms of geometry and cutterhead rpm:

$$\left(V_{swing}\right)_{\text{model}} = \left(V_{swing}\right)_{\text{prototype}} \left[\frac{\left(N_{cutter} D_{cutter}\right)_{\text{model}}}{\left(N_{cutter} D_{cutter}\right)_{\text{prototype}}}\right] \tag{3.19}$$

For the cutterhead rpm in terms of geometry and the cavitation coefficient:

$$\left(N_{cutter}\right)_{\text{model}} = \left(N_{cutter}\right)_{\text{prototype}} \left[\frac{\left(D_{cutter}\right)_{\text{prototype}}}{\left(D_{cutter}\right)_{\text{model}}}\right]^2 \frac{1}{\lambda_c} \tag{3.20}$$

For the cutterhead swing speed in terms of geometry and the cavitation coefficient:

$$\left(V_{swing}\right)_{\text{model}} = \left(V_{swing}\right)_{\text{prototype}} \left[\frac{\left(D_{cutter}\right)_{\text{prototype}}}{\left(D_{cutter}\right)_{\text{model}}}\right] \frac{1}{\lambda_c} \tag{3.21}$$

In order to satisfy Equations 3.19, 3.20, and 3.21, a cavitation coefficient will have to be chosen that allows the conditions to be satisfied. With large scales on the order of 1:10, this would require that model dredging be conducted in a vacuum so that cavitation can be achieved without excessive rpm and haulage velocities. Since this is impossible to achieve with the proposed facilities, some of these conditions may not be able to be fulfilled. These issues are revisited in greater detail in Chapter IV.

3.6 Rationale for Using Scaling Laws for Dredge Experiments

Three sets of scaling laws have been proposed. One is based on similarity with respect to sediment pick-up behavior, one is based on similarity with respect to the Froude number, and one is based on similarity with respect to cavitation during the cutting process. These criteria can not all be satisfied with one set of model operating parameters. Laboratory data collected by Slotta (1968), Joanknect (1976), Brahme and Herbich (1986), and Burger (1997), suggest that similarity with respect to sediment pick-up is the most important similitude criterion when modeling hydraulic dredges. This set of scale laws is used in Chapter IV to develop the operating characteristics of the model dredge.

CHAPTER IV

LABORATORY SET-UP FOR DREDGE MODEL TESTING

4.1 Requirements of a Model Dredge

Despite the inherent challenges of scalability, hydraulic model testing of dredge equipment can be useful if the limitations of the similitude relationships are clearly understood. The complex nature of these relationships warrants further development of the similitude criteria and testing of proposed relationships under controlled conditions. The new laboratory constructed at Texas A&M University will provide the ideal type of experimental setup needed to conduct further hydraulic model studies. The stated purpose of this thesis is to design a model dredging apparatus, hereby referred to as the "model dredge" and to develop a rationale for scaling the operating parameters of a full-scale prototype dredge to fit the model dredge. In this Chapter, the model dredge concept of operation is developed and specifications for hardware and operation are recommended.

There are certain elements that a model cutterhead dredge must have to function. These are primarily the cutterhead, the suction, and the haulage or "swing" velocity. A hopper dredge needs only the suction, a draghead or suctionhead, and the means to advance along the seabed. The mechanics of how the cutterhead or suctionhead is manipulated inside the sediment pit will be discussed in Chapter V. The basic questions one must ask are how much suction, how much cutter power, and how much side winch power are necessary? The goal of this design is to provide a model testing facility that has the ability and flexibility to model many different size dredges at different scales operating in different sizes of bed material. The basis for a proposed design was discussed in Section 3.1.

4.2 Scaling the Suction

A large 76.2 cm (30 in) dredge is capable of pumping 189,270 LPM (50,000 GPM) of slurry from the seabed (Herbich 2000). The dredge pump creates a velocity field around the cutterhead that draws water and sediment to the suction pipe inlet. In order for the model dredge pump

suction to behave similarly, the model velocity field must be properly scaled as discussed in Sections 3.2 and 3.3. Equations 3.13 and 3.16 present two different rationales for scaling the flow through the suction. However, the arguments presented in Sections 3.2 and 3.6 strongly suggest that the magnitude and geometry of the velocity field created by the suction inlet must be scaled such that similarity of the sediment pick-up behavior, the primary function of the dredge pump, is achieved. Therefore, model flow rates depend on the grain size of the model and prototype bed material in accordance with Equation 3.1. A single model bed material that allows many different types of prototype bed materials to be modeled without extremely large or small model flow rates to compensate for the difference in settling velocities is recommended. This prevents having to manage different lots of sediment for different experiments and the difficulty inherent in changing the sediment material between experiments. If a model test needs to be performed that requires a different model bed material in order to achieve similitude, then it is not impossible to change sediment lots. However, the ideal situation is to select a model bed material that is versatile enough to handle most any scaling scenario. This avoids the complicated logistics of removing, storing, and replacing the 50 m^3 (65.4 cy) of model sediment.

Large suction flow rates may cause excessive flow velocities in the discharge pipe and limit the duration of model tests by moving too large a volume of slurry too quickly. Small flow rates may cause the pipe flow velocities to drop and material to settle out in the discharge line. The dimensionless velocity field parameter is calculated for the prototype dredge operating in different bed material ranging from fine sand to coarse gravel. Model flow rates are calculated based on the dimensionless velocity field parameter of the prototype dredge. Table 4.1 shows the relationship between model grain diameter (*Model* d_{50}), prototype grain diameter (*Prototype* d_{50}), model pipe velocity (*Model* $V_{suction}$), prototype pipe velocity (*Prototype* $V_{suction}$) and model flow rate (*Model* $Q_{suction}$) for a 1:10 model and a prototype flow of 189,270 LPM (50,000 GPM). Settling velocities for sand are calculated based on the model by Schiller (Herbich 2000) as shown in Equation 4.1.

$$V_{settling} = 134.14\left(d_{50} - 0.039\right)^{0.972} \tag{4.1}$$

Table 4.1: Relationship between Model Grain Diameter, Prototype Grain Diameter, Model Flow Rate, and Model Pipe Velocity

Prototype d_{50} (mm)	**0.1**	**0.2**	**0.5**	**1.0**	0.1	0.2	0.5	1.0	0.1	0.2	0.5	1.0
Prototype $V_{settling}$ (mm/s)	**8.8**	**22.7**	**63.2**	**129**	8.8	22.7	63.2	129	8.8	22.7	63.2	129
Model d_{50} (mm)	**0.1**	**0.1**	**0.1**	**0.1**	0.2	0.2	0.2	0.2	0.5	0.5	0.5	0.5
Model $V_{settling}$ (mm/s)	**8.8**	**8.8**	**8.8**	**8.8**	22.7	22.7	22.7	22.7	63.2	63.2	63.2	63.2
Model $Q_{suction}$ (LPM)	**1893**	**738**	**265**	**129**	4860	1893	681	333	13518	5262	1893	927
(GPM)	***500***	***195***	***70***	***34***	*1284*	*500*	*180*	*88*	*3571*	*1390*	*500*	*245*
Model $U_{suction}$ (m/s)	**6.92**	**2.68**	**0.98**	**0.49**	17.8	6.54	2.5	1.22	49.4	19.2	6.54	3.38
(ft/s)	***22.7***	***8.8***	***3.2***	***1.6***	*58.3*	*22.7*	*8.2*	*4.0*	*162*	*63.1*	*22.7*	*11.1*

As Table 4.1 shows, selecting a model bed material of fine sand (d_{50} = 0.1 mm) allows many different prototype bed materials from fine to coarse sand to be modeled without excessive model flow rates and pipe velocities. In general, prototype sand that is finer than the model sand cannot be accurately tested under extreme prototype operating conditions. In order to properly scale the velocity field to ensure that fine sediment pick-up behavior is accurately modeled, model flow rates would need to be increased to unacceptable levels. However, model flow rates can easily be decreased to accurately model sediment pick-up behavior of larger prototype grain size.

4.2.1 Discharge Pipe Velocity and Slurry Transport

Whenever slurry is being pumped through a pipeline, care must be taken to ensure that transport velocities must not drop below the critical velocity. Equation 4.2 can be used to determine the critical velocity for pipeline transport (Wilson et al. 1997),

$$V_c = \frac{8.8\left[\frac{\mu_s\left(SG_{solid} - SG_{fluid}\right)}{0.66}\right]^{0.55}(D_{suction})^{0.7}(d_{50})^{1.75}}{(d_{50})^2 + 0.11(D_{suction})^{0.7}} \quad (4.2)$$

where μ_s is the mechanical friction coefficient (approx. = 0.44), SG_{solid} is the specific gravity of the solid, SG_{fluid} is the specific gravity of the fluid, $D_{suction}$ is the transport pipe diameter in meters, and d_{50} is the particle median grain diameter (0.1 mm for the model).

Given the above operating parameters, the critical velocity for the model dredge discharge pipe is 0.734 m/s (2.41 ft/s). Most of the model discharge pipe will be oriented vertically and settling should not be an issue even if the transport velocity drops below the critical velocity. However, care must be taken when modeling coarse sand and gravel (d_{50} = 1.0 mm) because according to Table 4.1, transport velocities will drop below the critical velocity. Selecting a smaller diameter discharge pipe would raise the transport velocities but would have adverse effects when modeling fine sand (d_{50} = 0.1 mm). For example, flow rates for a 7.62 cm (3 in) diameter pipe should not exceed 2271 LPM (600 GPM) or the friction losses become too great (Glover 1999). This still allows the modeling of fine sand according to Table 4.1. However, if the pipe diameter were reduced to 6.35 cm (2.5 in), maximum flow rates would be limited to 1136 LPM (300 GPM) and prototype flow rates greater than 113,550 LPM (30,000 GPM) could not be modeled if fine sand were the prototype bed material (Table 4.1). Therefore, the 7.62 cm (3 in) diameter suction and discharge line is deemed to be ideal for the range of sediments and flow rates being considered for modeling.

4.2.2 Selecting a Pump Drive

A pump motor must be selected that has sufficient power and speed to drive the 7.62 cm (3 in) pump at its maximum operating condition. If a model bed material of d_{50} = 0.1 mm is used, then the maximum model flow rate would be 1893 LPM (500 GPM) if the prototype sand being modeled were also fine sand with d_{50} = 0.1 mm. In other words, the velocity field is only scaled geometrically based on the square of the length scale so that the magnitude of the velocity field between model and prototype is identical. This represents the case of maximum model suction

flow according to Equation 3.13 assuming a maximum prototype flow rate of 189,270 LPM (50,000 GPM) as shown in Table 4.1. If actual prototype flow rates being modeled are less, then the model flow would be reduced accordingly. If a maximum model slurry specific gravity of 1.3 and an operating head of 15.24 m (50 ft) including minor and frictional losses is assumed, a pump operating at 80% efficiency (η) would require a motor drive of no more than 10 hp based on Equations 4.3.

$$\frac{Q_{suction} H \rho_{water} SG_{slurry}}{550\eta} = \text{BHP} \tag{4.3}$$

The operating head used is the estimated elevation from suction inlet to the discharge line (maximum 5.5 m or 18 ft) with an estimated 6 m (20 ft) of friction loss for 7.6 m (25 ft) of 7.62 cm (3 in) pipe at 1893 LPM (500 GPM), and another 3.7 m (12 ft) of friction loss for three 90 degree elbow fittings (Glover 1999).

The rationale for assuming a model slurry specific gravity of 1.3 is based on average slurry densities of dredges as outlined in the prototype dredge in Table 3.1. If the model sediment pick-up behavior is properly scaled according to the rationale presented in Section 3.2, then the model suction should be picking up the same ratio of solids to fluid as the prototype dredge. This would lead to similar specific gravities between model and prototype. The fact that the specific gravity is already a dimensionless quantity makes this a valid assumption. More importantly, there is no other reasonable way to estimate what the density of the slurry would be for a 7.62 cm (3 in) dredge operating under scaled model conditions other than the ratio of solids to fluid (slurry density) be similar. An assumption about slurry density must be made if model dredge equipment is to be selected. On this basis, it is reasonable to assume a model slurry specific gravity identical to the prototype.

4.3 Scaling the Cutter Drive

Sizing of the cutter drive is based on maximum test conditions so that enough power is present to conduct model tests under the most extreme prototype conditions. For example, a large 76.2 cm (30 in) dredge could employ a 254 cm (100 in) diameter cutter. The model cutter is 25.4 cm (10

in) in diameter based on a 1:10 geometric scale ratio. A prototype dredge of such size can have cutter drives over 4476 kW (6000 hp) for cutting through hard rock at significant depths (Vlasblom 1998). To determine the power required to remove a given amount of sediment, the specific energy method (Miedema 1985) is used.

4.3.1 The Specific Energy Method

Specific energy is the amount of work required to remove a unit of sediment from the seabed. This depends on many factors including the soil mechanical properties and the geometry and kinematics of the cutterhead. The theory also assumes that all material excavated by the cutterhead enters the suction pipe and therefore does not account for spillage. If details about the cutter geometry and operating characteristics are not known, an estimate can be made based on the Standard Penetration Test (SPT) data. Using the specific energy method in this way serves as an "upper limit" for the cutting forces and required cutterhead power and a "lower limit" for the estimate of production. Since the model dredge must have sufficient power to operate various 1:10 scale cutterhead designs under the most extreme prototype conditions, using the SPT test data with the specific energy method is consistent with the design methodology stated in Section 3.1.

In the laboratory testing facility, a 25.4 cm (10 in) model cutterhead is expected to cut fine sand (d_{50} = 0.1 mm) compacted to a maximum SPT value of 50 blowcounts at depths of 10 to 14 feet (deJong 2002). This represents about 95% compaction and is the most that can be expected in the laboratory (Miedema 1995) as shown in Figure 4.1. Different methods of sediment compaction are described in Section 5.5.3.

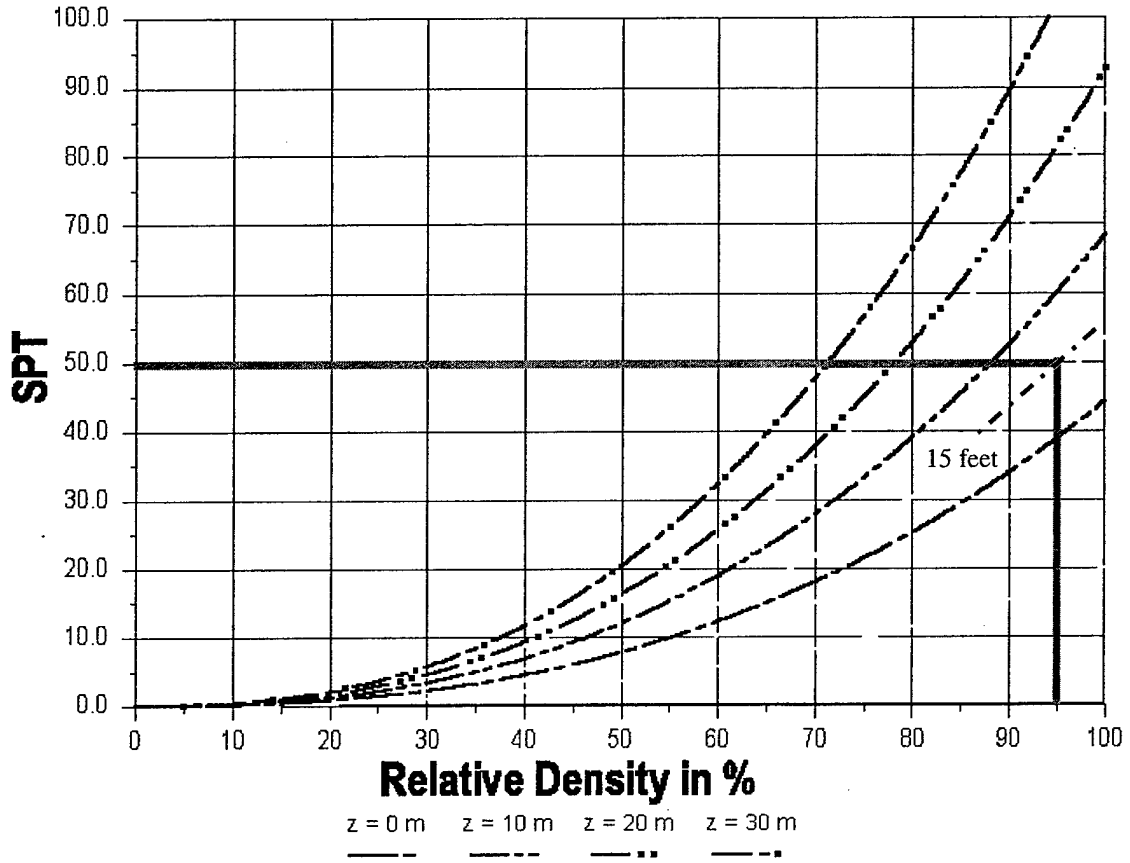

Figure 4.1: SPT Values versus Relative Density
(Miedema 1987)

The specific energy method is used to estimate the maximum cutterhead power required for blade angles of 30, 45, and 60 degrees based on measured SPT values reduced to 10 m (33 ft), or 1 atm of hydrostatic pressure. Figure 4.2 shows that the reduced SPT value is 60, identical to 95% compaction measured at 10 m according to Figure 4.1.

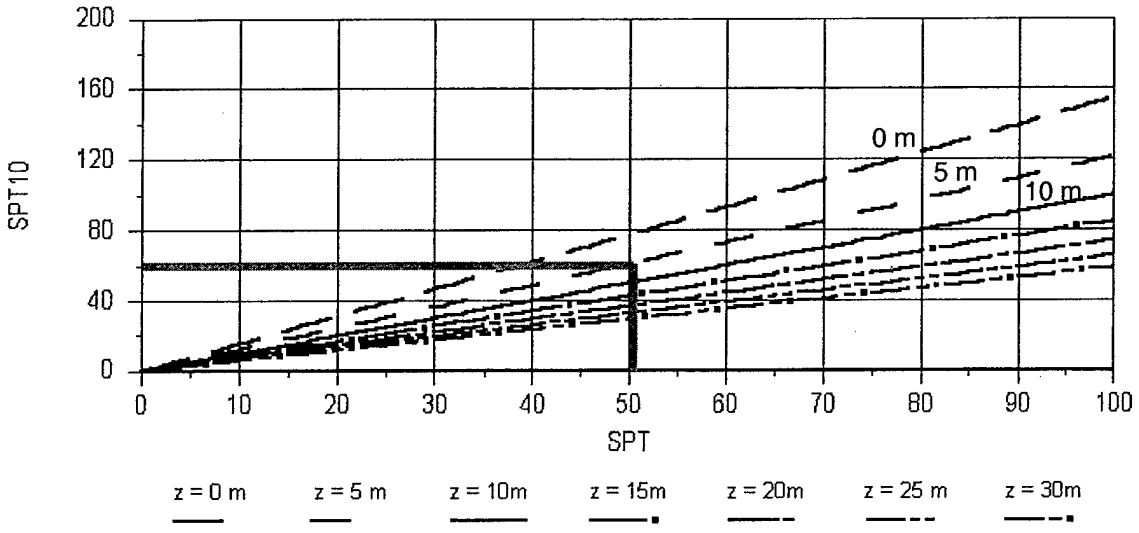

Figure 4.2: Measured SPT Values Reduced to 1 atm Hydrostatic Pressure (Miedema 1987)

Figure 4.3 shows that for a compaction of 60 blowcounts and a water depth of just less than 5 m (16.4 ft), a production rate of 440 m^3/hr (575 cy/hr) per 100 kW (134 hp) of cutterhead power is possible for a 30 degree blade angle.

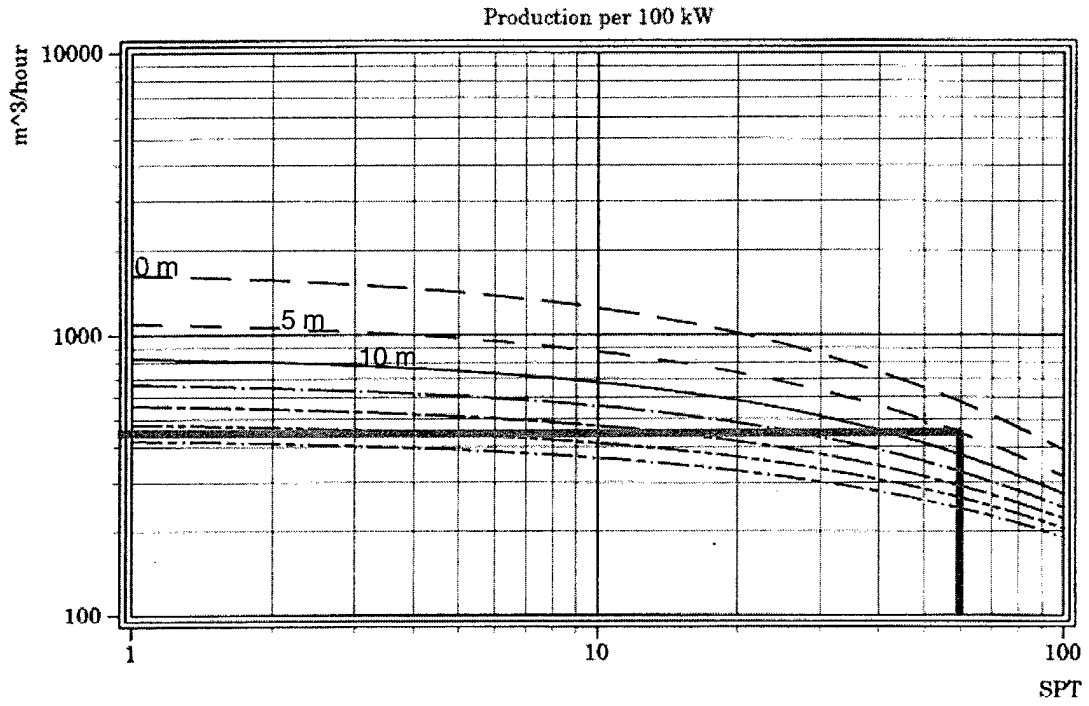

Figure 4.3: Specific Energy for a 30 Degree Blade Angle in Sand (Miedema 1987)

In Section 4.2 a maximum estimated model flow rate of 1893 LPM (500 GPM) was calculated, which equates to 114 m^3/hr (149 cy/hr) of slurry. Assuming again that the slurry has a maximum possible specific gravity of 1.3, which yields a maximum estimated production of 31.3 m^3/hr (41.2 cy/hr) according to Equation 4.4.

$$Q_{suction}\frac{SG_{mix}-SG_{water}}{SG_{sand}-SG_{water}}=149\text{ cy/hr}\frac{1.3-1}{2.08-1}=41.2\text{ cy/hr} \tag{4.4}$$

Therefore, for a blade angle of 30 degrees, 7.16 kW (9.6 hp) of cutter power is required. The same procedure is performed using blade angles of 45 and 60 degrees according to Figures 4.4 and 4.5.

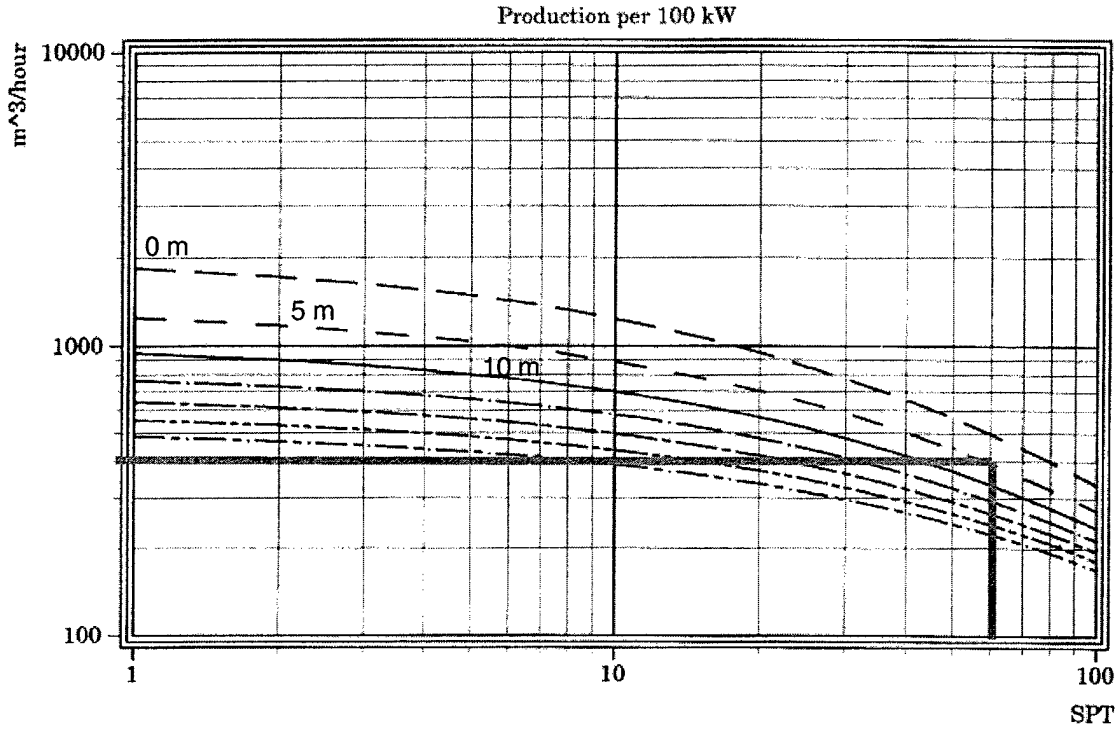

Figure 4.4: Specific Energy for a 45 Degree Blade Angle in Sand
(Miedema 1987)

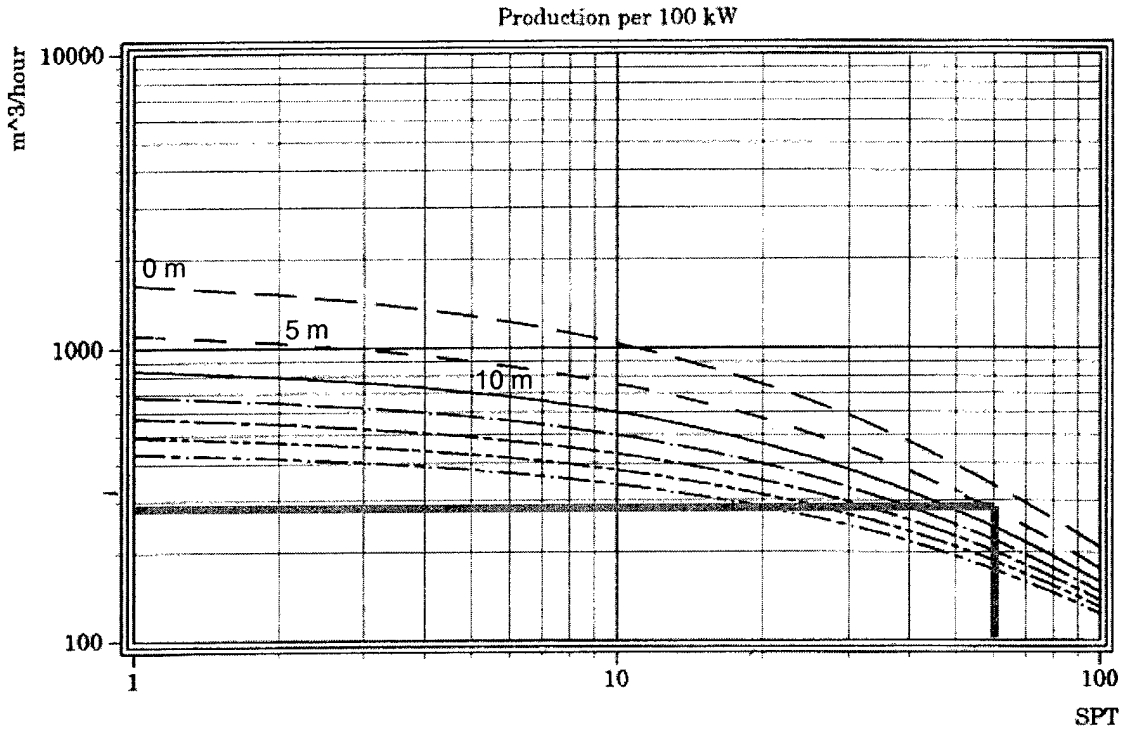

Figure 4.5: Specific Energy for a 60 Degree Blade Angle in Sand
(Miedema 1987)

Table 4.2 summarizes the results. Based on the analysis above, 11.7 kW (15.7 hp) is predicted to be the maximum power required by a 25.4 cm (10 in) cutter. Assuming the transmission from the cutter drive through the gearbox and universal joints is 80%, a cutter drive of at least 14.9 kW (20 hp) is recommended for the model dredge.

Table 4.2: Blade angle versus Required Cutter Power

Blade angle	Theoretical production per 134 hp	Theoretical required cutter power
30 degrees	440 m^3/hr (575 cy/hr)	9.6 hp
45 degrees	400 m^3/hr (523 cy/hr)	10.6 hp
60 degrees	270 m^3/hr (353 cy/hr)	15.7 hp

4.3.2 Scaling the Cutterhead Rotation

Section 3.5.5 outlined three different rationales for cutterhead rpm similitude based on hydraulic, Froude, and dynamic similarity. If a prototype rotation of 30 rpm is assumed, then model speeds can be estimated. Hydraulic scaling (Equation 3.14) gives a model rpm range from 21 to 300 based on the suction velocities achieved by the 7.62 cm (3 in) diameter suction inlet as shown in Table 4.1. Froude scaling (Equation 3.17) gives a constant model rpm of 95. For dynamic scaling (Equation 3.20), an average model digging depth of 3.66 m (12 ft) and an average prototype digging depth of 13.7 m (45 ft) are assumed. This gives a maximum model rpm of 1731, not easily achievable to say the least.

Ideally, operating parameters would be chosen such that each of these three equations could be simultaneously fulfilled. Of the three equations, only the Froude relationship is based solely on the geometric scale ratio. The other two equations have other parameters that could conceivably be adjusted to make the model work. If Equation 3.14 is solved in terms of Equation 3.17 for the maximum prototype flow rate of 189,270 LPM (50,000 GPM), then a maximum model flow rate of 598 LPM (158 GPM) must be achieved. This can not be accomplished with sacrificing proper scaling of the velocity field created by the suction required by Equation 3.13. If Equation 3.20 is solved in terms of Equation 3.17, then a model digging depth of -9.81 m (-32.3 ft) is required. Solving Equation 3.20 in terms of Equation 3.14 requires a model digging depth of -7.68 m (-25.2 ft). The only way to achieve negative model digging depths is to operate the model dredge in a near vacuum, facilitating a similar degree of cavitation.

Since all of the similitude relationships for scaling the cutterhead rpm cannot be satisfied, one or more of them may have to be relaxed or ignored. Other than satisfying the Froude number, Equation 3.17 has little physical meaning when it comes to scaling the model cutterhead rpm. If special care has been taken to properly scale the velocity flow field created by the suction inlet for similar sediment pick-up behavior, it stands to reason that the effect of the cutterhead rotation on the velocity field should also be appropriately scaled according to Equation 3.14 so that similar sediment pick-up behavior is maintained. Moreover, the higher model cutterhead rpm required by hydraulic scaling is closer to the quantity required by dynamic scaling. A higher model cutterhead rpm will minimize the scale effects caused by not being able to operate the

model dredge in a low-pressure environment as required by Equation 3.20. Therefore, a maximum model cutterhead rpm of 300 will be selected. Since this number is calculated from the maximum suction inlet velocity shown in Table 4.1, modeling larger prototype sediment grain diameters will require lower cutterhead rpms to maintain similar sediment pick-up behavior.

4.3.3 Scaling the Swing Speed

Section 3.5.6 outlined four different rationales for scaling the cutterhead swing speed based on geometric, hydraulic, Froude, and dynamic similarity. The geometric and hydraulic scale laws were found to be identical. If a maximum prototype swing speed of 30.5 cm/s (12 in/s) is assumed, then maximum model swing speeds can be estimated. Geometric and hydraulic scaling (Equations 3.15 and 3.19) both give a maximum model swing speed of 30.5 cm/s (12 in/s) based on the maximum model cutterhead rpm estimated in Section 4.3.1. The fact that these two scale laws are identical is significant since one similitude relationship satisfies the requirements for both geometric (size and shape of the layer being cut) and hydraulic (flow and suction velocities in and around the cutterhead relative to the particle settling velocity) scaling. Froude scaling (Equation 3.18) gives a model swing speed of 9.7 cm/s (3.8 in/s) and is independent of cutterhead rpm or intake velocity. For dynamic scaling (Equation 3.21), an average model digging depth of 3.66 m (12 ft) and an average prototype digging depth of 13.7 m (45 ft) are assumed. This gives a maximum model swing speed of 175 cm/s (69 in/s), which is extremely fast and will not likely be achieved. As with the cutterhead rpm in Section 4.3.1, the cutting velocities required to achieve similarity with respect to the degree and onset of cavitation cannot be physically obtained. The impact of the resulting scale effects has yet to be determined. Nevertheless, a maximum model cutterhead swing speed of 30.5 cm/s (12 in/s) is considered when sizing the model side winch drives.

While the model cutterhead swing speed may be predicted by the similitude relationships, in practice the upper limit of the model swing speed may be based on the maximum production achievable with a 11.7 kW (15.7 hp) cutter as predicted by the specific energy theory. This production was calculated by Equation 4.4 to be 31.5 m^3/hr (41.2 cy/hr). To maintain this rate of production with a 25.4 cm (10 in) diameter by 20.3 m (8 in) long cutterhead, the maximum

swing speed will be a function of the depth of cut, not of any similitude relationships. So while the similitude relationships may be useful in analyzing data, they may not be practical for sizing the model side winch drives. Table 4.3 illustrates the swing speed versus depth of cut for a constant 31.5 m^3/hr (41.2 cy/hr) production. This assumes that the cutterhead is operating at maximum power. During an actual model test where the swings speeds are determined by the similitude relationships, the cutterhead is most likely not fully loaded. However, a fully loaded condition will be assumed for the purpose of sizing the side winch drives.

Table 4.3: Swing Speed versus Depth of Cut for a 41.2 cy/hr Production

Digging Depth cm (in)	Swing Speed cm/s (in/sec)
25.4 (10)	18.4 (7.24)
22.9 (9)	20.4 (8.05)
20.3 (8)	23.0 (9.05)
17.8 (7)	26.3 (10.34)
15.2 (6)	30.7 (12.07)
12.7 (5)	36.8 (14.48)
10.2 (4)	46.0 (18.10)
7.62 (3)	61.3 (24.14)
5.08 (2)	92.0 (36.21)
2.54 (1)	184 (72.41)

For the purpose of selecting a side winch with sufficient power to pull the cutter at the speeds listed in Table 4.3, an analysis of the cutting forces must be performed. There is no point in exceeding the limits in Table 4.3 regardless of the scaling laws outlined in Section 3.5.6 because there would not be sufficient cutterhead power available to remove more than 31.5 m^3/hr (41.2 cy/hr) of sediment based on the specific energy theory.

4.4 Cutting Force Analysis

To design an apparatus capable of maneuvering the cutter through model dredging operations, the loads on the cutterhead must be predicted. There are at least two ways to go about this. Enough data on the relationship between cutter drive power and side winch power for large dredges exists to estimate the power required to pull the cutterhead against the bank during a cut.

Also, numerical cutting force equations can be applied to the cutterhead so horizontal pull forces can be calculated.

4.4.1 Swing Winch to Cutter Power Ratios for Prototype Dredges

On a large cutterhead dredge, swing winch power is typically 12% of the cutter power when cutting hard materials such as rock (Vlasblom 1998). However, that ratio may be lower for laboratory modeling facilities cutting fine sand. On a large cutterhead dredge, side winch forces are not only pulling the cutter against the bed material, but they must work to pull the entire dredge over the surface of the water. Laboratory facilities may not be required to overcome the drag forces typically seen on a prototype dredge. Prototype side winch pull force must also be sufficient to pull a dredge out of the corner, which can be twice the normal pull force (deJong 2002). On this basis alone, it would seem reasonable that side winch power for a model dredge could be roughly 6% of the cutter drive power (½ of the 12% common on large dredges). This gives a model side winch power of 0.90 kW (1.2 hp), or 6% of 15.3 kW (20 hp).

There are other factors to consider when sizing the side winches for the model dredge. When large dredges are cutting hard rock, side winch power is the limiting factor in dredge production and these dredges typically have a side winch power to cutter power ratio as high as 20%. On the other hand, the ratio of side winch power to cutter power in soft material such as sand and clay can be as low as 3% if the cutter teeth are kept sharp (Vlasblom 1998). On this basis, having the side winch power be 3% of the cutter power seems reasonable for a model dredge operating in fine sand. This gives a swing winch power of 0.46 kW (0.6 hp) or 3% of 15.3 kW (20 hp).

If the side winch power can be reasonably estimated, then horizontal cutting forces can be calculated if the swing speed is known. Table 4.4 shows the calculated pull forces based on the estimated swing winch power and swing speeds listed in Table 4.3. The data assume that the side winches are fully loaded at each digging depth, which may not be true in practice.

Table 4.4: Pull Forces versus Swing Winch Power and Speeds

Digging Depth *cm (in)*	**Swing Speed** *cm/s (in/s)*	**Force @ 0.45 kW (0.6 hp)** *N (lb)*	**Force @ 0.90 kW (1.2 hp)** *N (lb)*
25.4 (10)	18.4 (7.24)	2433 (547)	4866 (1094)
22.9 (9)	20.4 (8.05)	2189 (492)	4377 (984)
20.3 (8)	23.0 (9.05)	1944 (437)	3892 (875)
17.8 (7)	26.3 (10.3)	1704 (383)	3407 (766)
15.2 (6)	30.7 (12.1)	1459 (328)	2918 (656)
12.7 (5)	36.8 (14.5)	1214 (273)	2433 (547)
10.2 (4)	46.0 (18.1)	974 (219)	1944 (437)
7.62 (3)	61.3 (24.1)	730 (164)	1459 (328)
5.08 (2)	92.0 (36.2)	485 (109)	974 (219)
2.54 (1)	184 (72.4)	245 (55)	485 (109)

4.4.2 Numerical Models for Predicting the Cutting Forces on a Rotating Cutterhead

The previous analysis represents a simplified method of roughly sizing the pulling forces required to swing a dredge. It is not known whether the ratio of cutter power to winch power on a small 1:10 scale model dredge is similar to that of a large prototype dredge. Fortunately, there are also mathematical models for cutting sand that relate horizontal and vertical cutting forces to the tangential force on the cutterhead. This is valuable since the tangential force is directly related to the available torque of the cutterhead, and since there is an estimate of maximum cutterhead power and rpm, the maximum possible cutting forces can be calculated.

In Section 4.3.2 the model cutterhead rotation (N_{cutter}) is expected to be in the range of 21 to 300 rpm depending on the settling velocity of the prototype bed material. Since coarser grains larger than d_{50} = 0.4 mm are not as likely to be modeled as the finer grains, the normal operating range should be from about 150 to 300 rpm. If the cutterhead is rotating under its maximum power (P_{cutter}) of 11.7 kW (15.7 hp), the torque (Γ_{cutter}) and average tangential force ($\overline{T}$) can be calculated according Equations 4.5 and 4.6 respectfully.

$$\frac{P_{cutter}}{N_{cutter}} 63025 = \Gamma_{cutter} \text{ (in-lb)} \tag{4.5}$$

$$\frac{\Gamma_{cutter}}{D_{cutter}/2} = \overline{T} \tag{4.6}$$

The theoretical average tangential force for a 25.4 cm (10 in) diameter by 20.3 cm (8 in) long cylindrical cutterhead is calculated according to Equations 4.7, 4.8, 4.9, 4.10, and 4.11 as follows (Vlasblom 1998):

$$\varphi_0 = \arcsin(\frac{D_c}{r} - 1) \tag{4.7}$$

Where D_c is the depth of cut and r is the cutterhead radius.

$$\theta_0 = \arctan\left[\frac{\cos\varphi_0}{m - \sin\varphi_0}\right] \tag{4.8}$$

Where m is the swing speed/cutter speed.

$$\theta_{IN} = \frac{\theta_0\cos\theta_0 - \sin\theta_0}{\cos\theta_0 - 1} \tag{4.9}$$

$$\varphi_{IN} = \theta_{IN} - \arccos(m\sin\theta_{IN}) \tag{4.10}$$

$$\overline{T} = \overline{N}\left[\frac{b_c}{b_n}\sin(\theta_{IN} - \varphi_{IN}) - \cos\kappa\cos(\theta_{IN} - \varphi_{IN})\right] \tag{4.11}$$

Where κ is the cutterhead profile angle and defined in Section 5.2.2. For calculations performed in this chapter, κ is assumed to be 30 degrees.

The ratio of b_c/b_n (cutting force to normal force) is assumed to be 8 for a cutter with sharp teeth operating in cavitating sand (Miedema 1987). Since the average tangential force on the model cutterhead can be calculated based on Equations 4.7 and 4.8, Equation 4.11 can be used to back-

calculate the average normal force on the cutterhead, at different swing speeds, cutting depths, and rpms. Once the average normal force on the cutterhead is known, the average horizontal, vertical, and axial forces can be calculated according to Equations 4.12, 4.13, and 4.14 respectively (Vlasblom 1998).

$$\overline{H} = \overline{N}\left[\frac{b_c}{b_n}\cos\theta_{IN} - \cos\kappa\cos\theta_{IN}\right] \tag{4.12}$$

$$\overline{V} = \overline{N}\left[\frac{b_c}{b_n}\sin\theta_{IN} - \cos\kappa\cos\theta_{IN}\right] \tag{4.13}$$

$$\overline{A} = \overline{N}\sin\kappa \tag{4.14}$$

Table 4.5 lists the calculated values of the cutting forces for a fully loaded cutterhead operating at its maximum power of 11.7 kW (15.7 hp). The maximum swing speeds chosen for each depth of cut are based on the maximum required to maintain a model production of 31.5 m^3/hr (41.2 cy/hr) at each cutting depth (Table 4.3). Once again, this is based on the specific energy theory of cutting sand which predicts a maximum of 11.7 kW (15.7 hp) is required to remove 31.5 m^3/hr (41.2 cy/hr) of sand compacted to a SPT value of 50 blowcounts at a cutting depth of 4.6 m (15 feet) (Section 4.3.1). In reality, undercutting at depths of less than 13 cm (5 in) may not use all of the 11.7 kW (15.7 hp) available to the cutter as the sand tends to break free more easily when undercutting thin layers. In these cases, the average tangential force will be considerably less than the indicated value, making all of the calculated forces less as well. Moreover, the cutting force analysis based on the SPT data assumes a cavitating cutting process. If similarity with respect to cavitation is not achieved in the model dredge (i.e. cannot operate in a vacuum as per Section 4.3.2 and 4.3.3), then the cutter power required to maintain maximum production will be less than 11.7 kW (15.7 hp). As a result, the average torque on the cutterhead will be lower and thus the remaining cutting forces will be significantly less than what is shown in Table 4.5 as well. However, for the purposes of the model dredge design the maximum theoretical cutting forces are considered.

Table 4.5: Cutterhead Forces versus Cutting Depth and Swing Speeds at 300 RPM

Depth *cm (in)*	**Swing** *cm/s (in/s)*	**Production** *m^3/hr (cy/hr)*	**Power** *kW (hp)*	**V** *N (lb)*	**H** *N (lb)*	**A** *N (lb)*
25 (10)	2.5 (1)	4.6 (6)	1.5 (2)	44 (10)	396 (89)	27 (6)
25 (10)	5.1 (2)	9.2 (12)	3.0 (4)	85 (19)	796 (179)	49 (11)
25 (10)	7.7 (3)	15 (19)	4.5 (6)	129 (29)	1192 (268)	76 (17)
25 (10)	10 (4)	19 (25)	6.7 (9)	173 (39)	1588 (357)	98 (22)
25 (10)	13 (5)	24 (31)	8.2 (11)	214 (48)	1988 (447)	125 (28)
25 (10)	15 (6)	28 (37)	10 (13)	258 (58)	2384 (536)	151 (34)
25 (10)	18 (7)	32 (42)	11 (15)	302 (68)	2780 (625)	173 (39)
19 (7.5)	2.5 (1)	2.3 (3)	1.5 (2)	214 (48)	209 (47)	18 (4)
19 (7.5)	5.1 (2)	4.6 (6)	2.2 (3)	431 (97)	418 (94)	36 (8)
19 (7.5)	7.7 (3)	6.9 (9)	3.7 (5)	645 (145)	623 (140)	58 (13)
19 (7.5)	10 (4)	9.2 (12)	4.5 (6)	863 (194)	827 (186)	76 (17)
19 (7.5)	13 (5)	11 (15)	6.0 (8)	1085 (244)	1032 (232)	93 (21)
19 (7.5)	15 (6)	15 (19)	7.5 (10)	1303 (293)	1232 (277)	111 (25)
19 (7.5)	18 (7)	17 (22)	8.2 (11)	1526 (343)	1432 (322)	129 (29)
19 (7.5)	20 (8)	19 (25)	10 (13)	1748 (393)	1628 (366)	147 (33)
19 (7.5)	23 (9)	21 (28)	11 (15)	1975 (444)	1824 (410)	169 (38)
13 (5.0)	2.5 (1)	24 (31)	0.7 (1)	156 (35)	125 (28)	13 (3)
13 (5.0)	5.1 (2)	26 (34)	1.5 (2)	311 (70)	254 (57)	27 (6)
13 (5.0)	7.7 (3)	28 (37)	2.2 (3)	463 (104)	383 (86)	36 (8)
13 (5.0)	10 (4)	31 (40)	3.0 (4)	618 (139)	512 (115)	49 (11)
13 (5.0)	13 (5)	33 (43)	3.7 (5)	770 (173)	645 (145)	62 (14)
13 (5.0)	15 (6)	1.5 (2)	4.5 (6)	921 (207)	774 (174)	76 (17)
13 (5.0)	18 (7)	2.3 (3)	5.2 (7)	1072 (241)	912 (205)	89 (20)
13 (5.0)	20 (8)	3.8 (5)	6.7 (9)	1223 (275)	1045 (235)	98 (22)
13 (5.0)	23 (9)	4.6 (6)	7.5 (10)	1370 (308)	1183 (266)	111 (25)
13 (5.0)	25 (10)	6.1 (8)	8.2 (11)	1521 (342)	1321 (297)	125 (28)
13 (5.0)	28 (11)	6.9 (9)	9.0 (12)	1668 (375)	1459 (328)	138 (31)
13 (5.0)	30 (12)	8.4 (11)	10 (13)	1815 (408)	1601 (360)	151 (34)
13 (5.0)	33 (13)	9.2 (12)	10 (14)	1962 (441)	1744 (392)	165 (37)
13 (5.0)	36 (14)	11 (14)	11 (15)	2108 (474)	1886 (424)	173 (39)
6 (2.5)	2.5 (1)	11 (15)	0.7 (1)	53 (12)	85 (19)	4 (1)
6 (2.5)	5.1 (2)	13 (17)	0.7 (1)	107 (24)	169 (38)	13 (3)
6 (2.5)	7.7 (3)	32 (42)	1.5 (2)	160 (36)	254 (57)	18 (4)
6 (2.5)	10 (4)	2.3 (3)	1.5 (2)	214 (48)	338 (76)	27 (6)
6 (2.5)	13 (5)	4.6 (6)	2.2 (3)	267 (60)	423 (95)	31 (7)
6 (2.5)	15 (6)	6.9 (9)	2.2 (3)	316 (71)	512 (115)	36 (8)
6 (2.5)	18 (7)	9.2 (12)	3.0 (4)	369 (83)	596 (134)	44 (10)
6 (2.5)	20 (8)	11 (15)	3.0 (4)	418 (94)	685 (154)	49 (11)
6 (2.5)	23 (9)	15 (19)	3.7 (5)	472 (106)	770 (173)	58 (13)
6 (2.5)	25 (10)	17 (22)	3.7 (5)	520 (117)	859 (193)	62 (14)
6 (2.5)	28 (11)	19 (25)	4.5 (6)	569 (128)	947 (213)	67 (15)
6 (2.5)	30 (12)	19 (25)	4.5 (6)	618 (139)	1036 (233)	76 (17)

Table 4.5: Continued

Depth *cm (in)*	**Swing** *cm/s (in/s)*	**Production** *m^3/hr (cy/hr)*	**Power** *kW (hp)*	**V** *N (lb)*	**H** *N (lb)*	**A** *N (lb)*
6 (2.5)	33 (13)	15 (20)	5.2 (7)	667 (150)	1125 (253)	80 (18)
6 (2.5)	36 (14)	17 (22)	5.2 (7)	712 (160)	1214 (273)	89 (20)
6 (2.5)	38 (15)	18 (23)	6.0 (8)	761 (171)	1303 (293)	93 (21)
6 (2.5)	41 (16)	19 (25)	6.7 (9)	805 (181)	1397 (314)	102 (23)
6 (2.5)	43 (17)	20 (26)	6.7 (9)	854 (192)	1486 (334)	107 (24)
6 (2.5)	46 (18)	21 (28)	7.5 (10)	899 (202)	1579 (355)	111 (25)
6 (2.5)	48 (19)	22 (29)	7.5 (10)	943 (212)	1668 (375)	120 (27)
6 (2.5)	51 (20)	24 (31)	8.2 (11)	988 (222)	1761 (396)	125 (28)
6 (2.5)	53 (21)	24 (32)	8.2 (11)	1032 (232)	1855 (417)	133 (30)
6 (2.5)	56 (22)	26 (34)	9.0 (12)	1076 (242)	1948 (438)	138 (31)
6 (2.5)	58 (23)	27 (35)	9.0 (12)	1121 (252)	2042 (459)	147 (33)
6 (2.5)	61 (24)	28 (37)	10 (13)	1165 (262)	2135 (480)	151 (34)
6 (2.5)	64 (25)	30 (39)	10 (13)	1205 (271)	2229 (501)	156 (35)
6 (2.5)	66 (26)	31 (40)	10 (14)	1250 (281)	2322 (522)	165 (37)
6 (2.5)	69 (27)	32 (42)	11 (15)	1290 (290)	2415 (543)	169 (38)
6 (2.5)	71 (28)	33 (43)	11 (15)	1334 (300)	2513 (565)	178 (40)
6 (2.5)	74 (29)	34 (45)	11 (15)	1374 (309)	2607 (586)	182 (41)

The geometry of the proposed model dredge is such that the horizontal forces acting on the cutterhead are identical to the swing, or pull force, required by the side winch. The maximum pull force when the cutterhead is rotating at 300 rpm is about 2780 N (625 lb) at 18 cm/s (7 in/s) (Table 4.5). This requires a side winch power of 0.49 kW (0.66 hp), consistent with the amounts proposed in Table 4.4. The maximum swing speed is about 74 cm/s (29 in/s) at a pull force of 2607 N (586 lb). Despite the lower pull force, this scenario requires a side winch power of 1.9 kW (2.8 hp) because of the high speed. It is unlikely that the haulage velocity will exceed 30 cm/s (12 in/s) for reasons already covered in Section 4.3.2.

The average vertical forces acting on the cutterhead can act in an upward or downward direction, depending on the type of cut being made. When the cutterhead is undercutting the cutter teeth are impacting the seabed in an upward motion causing the average vertical cutterhead force to act in a downward direction. When the cutterhead is overcutting the cutter teeth are impacting the seabed in a downward motion causing the average vertical cutterhead force to act in an upward direction. Figure 4.6 shows the physical significance of overcutting and undercutting with a rotating cutterhead.

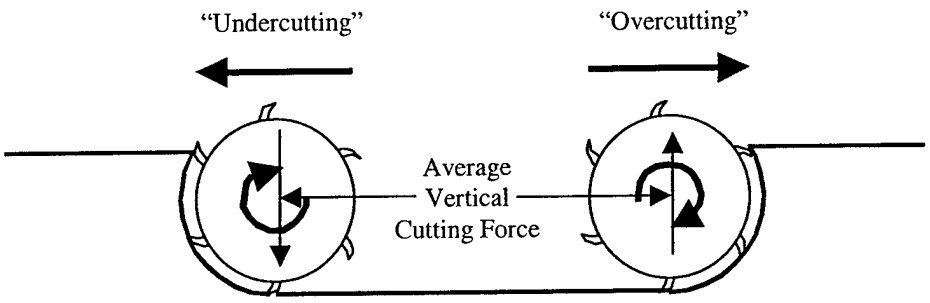

Figure 4.6: The Relationship between Overcutting, Undercutting, and the Direction of the Average Vertical Cutting Force

The model cutterhead speed could be as low as 21 rpm to maintain proper hydraulic scaling with respect to spillage due to cutterhead rotation and the velocity field created by the suction. If a large prototype bed material were being modeled such as gravel or very coarse sand (d_{50} = 1.0 mm), flow rates would have to be lowered in order to achieve proper velocity field scaling. With a fixed suction inlet diameter of 3 inches, the suction velocity will decrease and the cutterhead rpm would have to be lowered such that Equation 3.14 is satisfied. Table 4.6 lists the cutting forces based on a cutterhead rotating at 21 rpm. All other parameters are identical to Table 4.5.

Table 4.6: Cutterhead Forces versus Cutting Depth and Swing Speeds at 21 RPM

Depth *cm (in)*	**Swing** *cm/s (in/s)*	**Production** *m^3/hr (cy/hr)*	**Power** *kW (hp)*	**V** *kN (lb)*	**H** *kN (lb)*	**A** *kN (lb)*
25 (10)	2.5 (1)	5 (6)	1.5 (2)	0.61 (138)	5.68 (1276)	0.36 (80)
25 (10)	5.1 (2)	9 (12)	3.0 (4)	1.23 (276)	11.4 (2552)	0.71 (160)
25 (10)	7.6 (3)	15 (19)	4.5 (6)	1.84 (414)	17.0 (3829)	1.06 (239)
25 (10)	10 (4)	19 (25)	6.7 (9)	2.46 (553)	22.7 (5105)	1.42 (319)
25 (10)	13 (5)	24 (31)	8.2 (11)	3.07 (691)	28.4 (6381)	1.77 (399)
25 (10)	15 (6)	28 (37)	9.7 (13)	3.69 (829)	34.1 (7657)	2.13 (479)
25 (10)	18 (7)	33 (43)	11 (15)	4.30 (967)	39.7 (8934)	2.48 (558)
19 (7.5)	2.5 (1)	4 (5)	1.5 (2)	3.18 (716)	2.83 (637)	0.27 (60)
19 (7.5)	5.1 (2)	7 (9)	2.2 (3)	6.67 (1499)	5.30 (1192)	0.53 (119)
19 (7.5)	7.6 (3)	11 (14)	3.7 (5)	10.5 (2359)	7.39 (1662)	0.80 (179)
19 (7.5)	10 (4)	15 (19)	4.5 (6)	14.7 (3312)	9.11 (2047)	1.08 (242)
19 (7.5)	13 (5)	18 (23)	6.0 (8)	19.5 (4383)	10.5 (2354)	1.37 (309)
19 (7.5)	15 (6)	21 (28)	7.5 (10)	23.1 (5194)	19.8 (4454)	1.89 (425)
19 (7.5)	18 (7)	24 (32)	8.2 (11)	26.6 (5973)	25.7 (5787)	2.30 (517)
19 (7.5)	20 (8)	28 (37)	10 (13)	29.7 (6679)	32.5 (7297)	2.74 (615)
19 (7.5)	23 (9)	32 (42)	11 (15)	32.4 (7292)	39.8 (8958)	3.19 (718)

Table 4.6: Continued

Depth *cm (in)*	**Swing** *cm/s (in/s)*	**Production** *m^3/hr (cy/hr)*	**Power** *kW (hp)*	**V** *kN (lb)*	**H** *kN (lb)*	**A** *kN (lb)*
13 (5)	2.5 (1)	2 (3)	0.7 (1)	2.15 (483)	1.93 (433)	0.18 (40)
13 (5)	5.1 (2)	5 (6)	1.5 (2)	4.15 (933)	4.14 (930)	0.36 (82)
13 (5)	7.6 (3)	7 (9)	2.2 (3)	6.01 (1350)	6.64 (1492)	0.56 (125)
13 (5)	10 (4)	9 (12)	3.0 (4)	7.71 (1733)	9.43 (2120)	0.76 (170)
13 (5)	13 (5)	11 (15)	3.7 (5)	9.26 (2081)	12.5 (2810)	0.97 (217)
13 (5)	15 (6)	15 (19)	4.5 (6)	10.6 (2393)	15.8 (3558)	1.18 (266)
13 (5)	18 (7)	17 (22)	5.2 (7)	11.9 (2670)	19.4 (4358)	1.41 (318)
13 (5)	20 (8)	19 (25)	6.7 (9)	13.0 (2913)	23.1 (5203)	1.65 (371)
13 (5)	23 (9)	21 (28)	7.5 (10)	13.9 (3124)	27.1 (6087)	1.89 (425)
13 (5)	25 (10)	24 (31)	8.2 (11)	14.7 (3303)	31.1 (7002)	2.14 (481)
13 (5)	28 (11)	26 (34)	9.0 (12)	15.4 (3454)	35.3 (7944)	2.39 (538)
13 (5)	30 (12)	28 (37)	10 (13)	15.9 (3578)	39.6 (8906)	2.65 (596)
13 (5)	33 (13)	31 (40)	10 (14)	16.4 (3679)	44.0 (9884)	2.91 (655)
13 (5)	36 (14)	33 (43)	11 (15)	16.7 (3757)	48.4 (10875)	3.18 (715)
6.4 (2.5)	5.1 (2)	2 (3)	0.7 (1)	1.36 (305)	2.57 (577)	0.18 (41)
6.4 (2.5)	7.6 (3)	4 (5)	1.5 (2)	1.90 (427)	3.96 (891)	0.27 (61)
6.4 (2.5)	10 (4)	5 (6)	1.5 (2)	2.37 (532)	5.43 (1221)	0.37 (83)
6.4 (2.5)	13 (5)	6 (8)	2.2 (3)	2.77 (622)	6.95 (1563)	0.47 (105)
6.4 (2.5)	15 (6)	7 (9)	2.2 (3)	3.10 (698)	8.52 (1916)	0.56 (127)
6.4 (2.5)	18 (7)	8 (11)	3.0 (4)	3.39 (763)	10.1 (2278)	0.66 (149)
6.4 (2.5)	20 (8)	9 (12)	3.0 (4)	3.63 (817)	11.8 (2648)	0.77 (172)
6.4 (2.5)	23 (9)	11 (14)	3.7 (5)	3.83 (861)	13.5 (3025)	0.87 (195)
6.4 (2.5)	25 (10)	11 (15)	3.7 (5)	3.99 (898)	15.2 (3408)	0.97 (219)
6.4 (2.5)	28 (11)	13 (17)	4.5 (6)	4.12 (927)	16.9 (3796)	1.08 (243)
6.4 (2.5)	30 (12)	15 (19)	4.5 (6)	4.23 (950)	18.6 (4189)	1.19 (267)
6.4 (2.5)	33 (13)	15 (20)	5.2 (7)	4.30 (967)	20.4 (4584)	1.29 (291)
6.4 (2.5)	36 (14)	17 (22)	5.2 (7)	4.35 (979)	22.2 (4984)	1.41 (316)
6.4 (2.5)	38 (15)	18 (23)	6.0 (8)	4.39 (987)	24.0 (5385)	1.51 (340)
6.4 (2.5)	41 (16)	19 (25)	6.7 (9)	4.40 (990)	25.8 (5790)	1.62 (365)
6.4 (2.5)	43 (17)	20 (26)	6.7 (9)	4.40 (990)	27.6 (6196)	1.73 (390)
6.4 (2.5)	46 (18)	21 (28)	7.5 (10)	4.39 (986)	29.4 (6604)	1.85 (415)
6.4 (2.5)	48 (19)	22 (29)	7.5 (10)	4.35 (979)	31.2 (7014)	1.96 (440)
6.4 (2.5)	51 (20)	24 (31)	8.2 (11)	4.31 (970)	33.0 (7425)	2.07 (465)
6.4 (2.5)	53 (21)	24 (32)	8.2 (11)	4.27 (959)	34.9 (7837)	2.18 (491)
6.4 (2.5)	56 (22)	26 (34)	9.0 (12)	4.20 (945)	36.7 (8250)	2.30 (516)
6.4 (2.5)	58 (23)	27 (35)	9.0 (12)	4.13 (929)	38.5 (8664)	2.41 (541)
6.4 (2.5)	61 (24)	28 (37)	10 (13)	4.05 (911)	40.4 (9079)	2.52 (567)
6.4 (2.5)	64 (25)	30 (39)	10 (13)	3.97 (892)	42.2 (9495)	2.64 (593)
6.4 (2.5)	66 (26)	31 (40)	10 (14)	3.87 (871)	44.1 (9911)	2.75 (618)
6.4 (2.5)	69 (27)	32 (42)	10 (14)	3.77 (848)	45.9 (10329)	2.86 (644)
6.4 (2.5)	71 (28)	33 (43)	11 (15)	3.67 (824)	47.8 (10746)	2.98 (670)
6.4 (2.5)	74 (29)	34 (45)	11 (15)	3.56 (800)	49.7 (11164)	3.09 (695)

The maximum pull force when the cutterhead is rotating at its lower limit of 21 rpm is about 49.7 kN (11,164 lb) at 74 cm/s (29 in/s). This requires a side winch power of almost 37 kW (50 hp), more than 2.5 times the power required to drive the cutter. For any given side winch power, it is clear that if coarser sand is to be modeled and thus smaller volumetric flow rates are used to satisfy Equation 3.13, care must be taken in selecting the geometric scale so that the model cutterhead rpms do not drop too low. It may seem counter-intuitive that the cutting forces on the cutterhead would increase as the cutterhead speed is decreased. However, the specific energy method is based on a given cutter power required to achieve a given production while cutting sediment compacted to a given SPT value. Therefore, when the cutterhead rpms are reduced, the cutting forces, and thus the developed torque, must increase to achieve the same production with the available power. As a result, the cutterhead speed used in the model test should be kept close to the design value of 300 rpm. This may limit the ability of the model dredge to simulate a prototype dredge operating in coarse sand at certain scales.

4.4.3 Practical Considerations for Estimating Maximum Allowable Pull Force

When determining the side winch power necessary to pull the cutterhead through the sediment pit at different cutterhead rpms, excess power should be allowed such that side winch power is not a limiting factor in any scale model test. Therefore, the maximum side winch force can also be determined by practical considerations other than the similitude relationships, which are used primarily in interpreting data. One such practical limit would be to allow as much side winch force as possible without tipping the carriage.

The static load analysis presented in Appendix B shows that, for the estimated weights listed in Appendix A and a maximum vertical cutting force of 9452 N (2125 lb), a side winch force in excess of 15,026 N (3378 lb) could cause the net force on one side of the dredge to go to zero if no vertical or axial cutting forces acted on the cutterhead and the ladder angle was 90 degrees relative to the seabed cutting at a maximum depth of 4.27 m (14 ft). In this case, the minimum normal force on two of the four wheels becomes negative and the carriage becomes unstable and is in danger of tipping. This is more than 5 times greater than the maximum average horizontal cutting force predicted by the calculations in Table 4.5.

Another practical limit is to allow as much side winch force as possible without exceeding the load capacity of any of the structural members or bearings. The weakest members of the proposed dredge carriage design are the vertical and horizontal guide rods. This will be explained in greater detail in Chapter V. As a result, it makes little sense to have more side winch power than can be structurally tolerated. It is also unwise to limit the side winch power to the predicted cutting forces required by the model dredge as listed in Table 4.5. Therefore, side winch power is limited by the structural integrity of the dredge carriage to ensure maximum available power without causing a structural failure of the dredge.

The analysis of Appendix B shows that well before the dredge becomes unstable, bending stresses in the vertical and horizontal guide rods exceed their yield strength. For the predicted cutting forces listed in Table 4.5, the maximum bending moment in the vertical guide rods is well below the structural limit. This is important to note since the forces calculated by the specific energy method represent the upper limit of the predicted cutting forces. It is critical that the dredge be structurally sound under the greatest predicted loading. It should also be noted that there are several other simplifications made to the guide rod bending moment analysis that will cause the predicted stresses to be greater the actual stresses. These are explained in detail in Appendix B. The reason for the simplification is that the additional effort required to calculate the actual stresses is not worth the extra precision gained. Moreover, the simplified analysis has a "built-in" safety factor that will help to ensure the integrity of the dredge carriage. In addition, the stainless steel used in the calculation has a yield strength of 300,000 kPa (43,000 psi). There are stainless steels available that have 6 times the yield strength as this. These could be used to increase the load bearing capacity of the guides if the loads presented in Table 4.5 need to be drastically exceeded. The only other way to strengthen the guides is to increase their diameter. However, as will be explained in Appendix A and Chapter V, the dredge assembly must remain below 26,689 N (6000 lb) to be removed by the overhead crane.

The Structural analysis performed in Appendix B shows that a side winch force in excess of 3559 N (800 lb) could cause failure of the dredge carriage at certain digging depths and ladder angles if no other forces act on the cutter. If vertical and axial loads are present, the combined loading could cause failure even if the pull force is less than the maximum. The functional design of the dredge carriage and the role of the vertical and horizontal guide rods are explained

in Chapter V. However, for the purposes of scaling the model dredge side winches, the structural features that limit the pull force and side winch power must be discussed. In summary, a 1.1 kW (1.5 hp) side winch power on each side of the dredge carriage should be sufficient to operate the model dredge up to its structural limit at the maximum predicted swing speed of 30.5 cm/s (12 in/s).

Some of the swing speeds required to maintain maximum production as listed in Table 4.5 are greater than the maximum predicted model swing speed of 30.5 cm/s (12 in/s). Some model tests may require swings speed greater than what is predicted by the similitude relationships. As a result, the recommended side winch power is increased to allow the maximum pull force of 3559 N (800 lb) to act in conjunction with swing speeds up to 61 cm/s (24 in/s). This gives a 2.2 kW (3 hp) side winch. At swing speeds less than 61 cm/s (24 in/s), the side winches will have enough power to damage the dredge carriage under certain conditions. The combined loading on the horizontal and vertical guide rods will be monitored such that the yield strength in any of these members is not exceeded and damage to the dredge carriage does not occur. However, even under the most extreme scaled operating conditions represented by the predicted cutterhead forces listed in Table 4.5, there is still a safety factor of up to 5 (depending on the steel used to fabricate the guide rods) in terms of possible structural failure of the model dredge. The excess power in the recommended side winches is simply to ensure that side winch pull force is never a limiting factor during a model dredging operation. Table 4.7 is a summary of the recommended power needed by the model pump, cutter, and side winches.

Table 4.7: Summary of Recommended Power for Cutter Drive, Pump Drive, and Side Winches

Drive	**Power kW (hp)**
Pump	7.5 (10)
Cutter	15 (20)
Side Winch	2.2 (3)

CHAPTER V

DESIGN OF TOW/DREDGE CARRIAGE FOR LABORATORY FACILITY

5.1 The Coastal Engineering Laboratory

The new Coastal Engineering Laboratory at Texas A&M University College Station is equipped with a shallow water wave basin and a towing tank. The towing tank serves as a facility for conducting model studies of hydraulic dredging operations. This includes testing of model cutterheads, suctionheads, dragheads, modeling of open water disposal, and disposal site monitoring. Figure 5.1 shows the Coastal Engineering Laboratory under construction.

Figure 5.1: Texas A&M University Coastal Engineering Laboratory as of May 2002

5.2 The Towing Tank

The towing tank is 45.7 m (150 ft) long with a maximum water depth of 3.05 m (10 ft) and a width of 3.66 m (12 ft). At one end of the tank is a 9.14 m (30 ft) long by 1.54 m (5 ft) deep sediment pit. This sediment will remain covered during model towing operations but will be

uncovered, using the overhead crane to lift the cover plates and expose the bed material, for dredging operations. In the tank wall directly above the sediment there are several viewing and instrument windows. Figure 5.2 shows the sediment pit during construction with the instrument windows clearly visible.

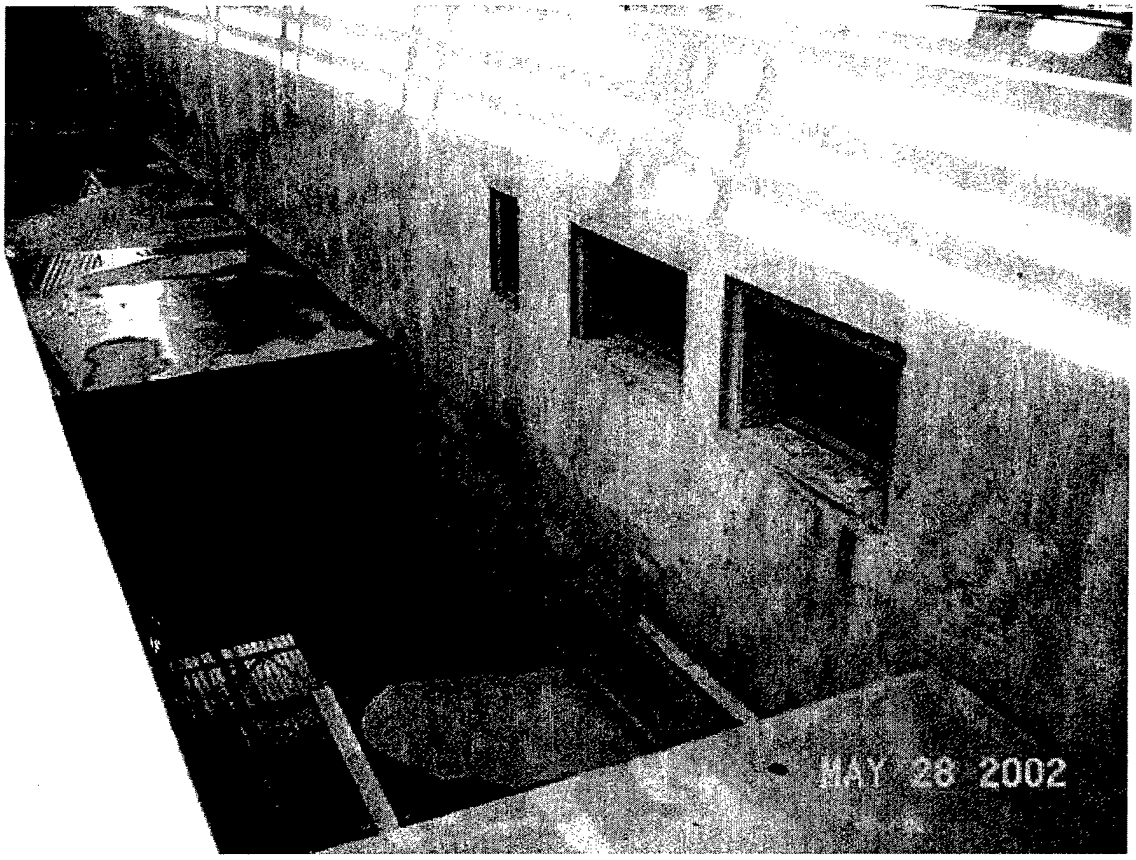

Figure 5.2: The Sediment Pit During Construction

The windows are particularly useful in flow visualization studies around the cutter or suction head, or to simply monitor testing operations. The capability to produce currents is available via a current manifold at the far end of the tank and a wavemaker is to be added at a later date. Figure 5.3 shows the tank layout.

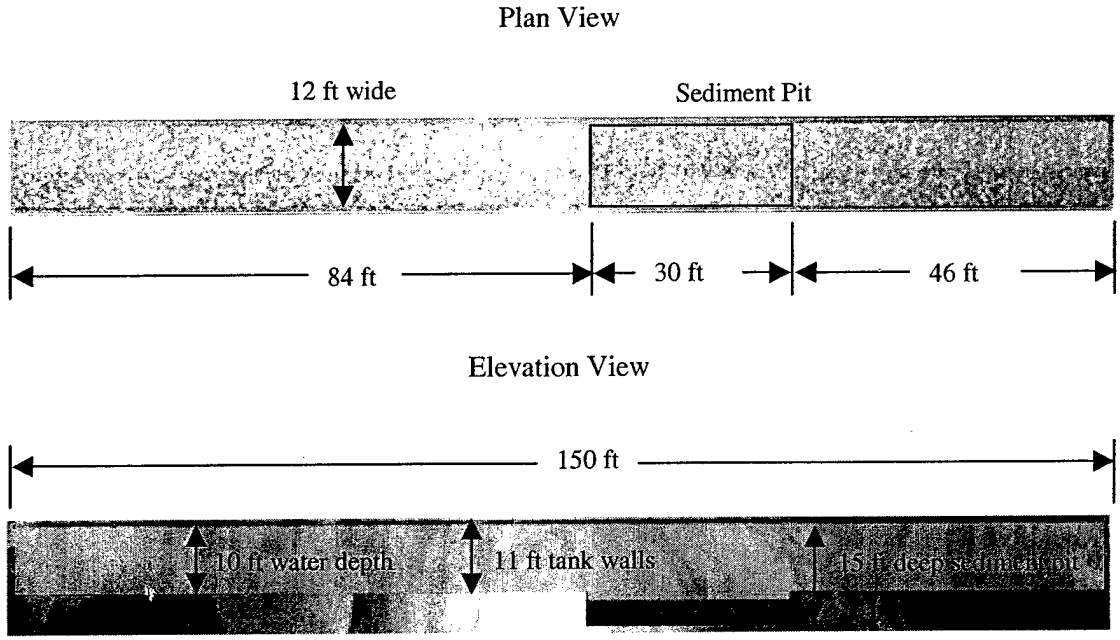

Figure 5.3: Layout of the Towing Tank

The tank walls rise 30.5 cm (1 ft) above the maximum water line and are 91 cm (3 ft) above the laboratory floor. Steel rails are to be installed on the tops of the tank walls for a towing carriage. The towing carriage itself rides atop the tank in the +/- *X* direction and incorporates a model dredge. The model dredge, as designed, consists of a frame and carriage to move the cutterhead side-to-side in the tank, or in the +/- *Y* direction to simulate the swinging motion of a cutterhead dredge. The model dredge can be removed from the tow carriage via the 2721 kg (3 ton) overhead crane and placed in a cradle in the work area adjacent to the tank. This will allow the towing carriage to be used for model towing without the model dredge getting in the way. The model dredge carriage incorporates a ladder arm that provides vertical translation of the model dredge ladder in the +/- *Z* direction. The ladder at the end of the ladder arm contains the cutter and suction pipe and has an adjustable angle. Figure 5.4 depicts the towing carriage with the model dredge atop the tank. Table 5.1 lists the design requirements for the tow and dredge carriages.

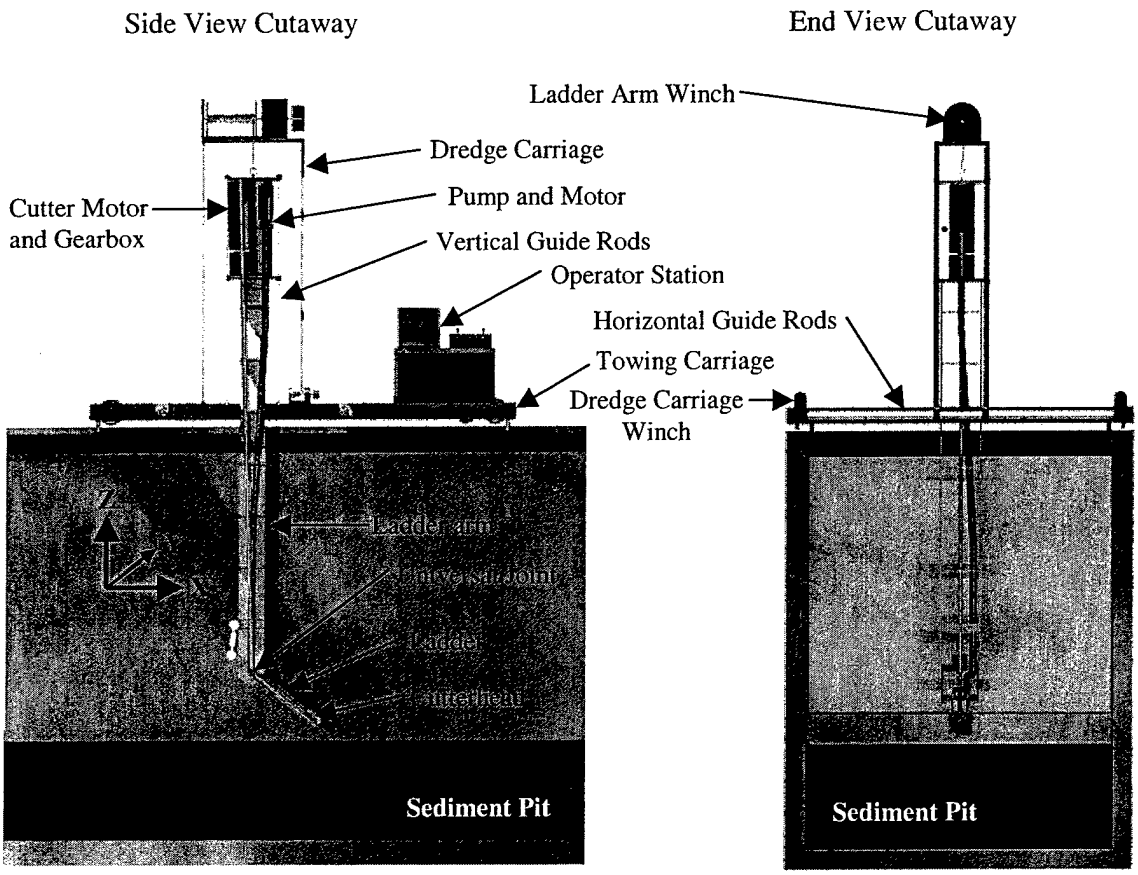

Figure 5.4: Towing Carriage with Dredge Carriage Sitting atop Towing Tank

Table 5.1: Design Requirements for Towing Carriage and Model Dredge Carriage

Category	Design Requirement
Velocity	Tow carriage must achieve 1.2 m/s (4 ft/s) during towing operation
Acceleration	Tow carriage must accelerate from 0 to 1.2 m/s (4 ft/s) over 12 m (40 ft)
Weight	Removable dredge carriage limited to 2721 kg (6000 lb)
Weight	tow carriage and dredge carriage not to exceed 4534 kg (10,000 lb) total
Force	Max side-winch pull force not to exceed 3559 N (800 lb)
Cutter Power	14.9 kW (20 hp)
Pump Power	7.46 kW (10 hp)
Side Winch Power	2.24 kW (3 hp) each side
Flow Rate	Maximum 1893 LPM (500 GPM) from 7.62 cm (3 in) pump
Control System	Automated and manual operation
Data Acquisition	Real-time display and data storage
Digging Depth	3.05 - 4.27 m (10 - 14 ft) measured from the cutterhead axis leaving 178 mm (7 in) clearance to tank bottom
Swing Travel	1.6 m (63 in) on either side of center measured from the cutterhead axis leaving 229 mm (9 in) clearance to each side of tank
Ladder Angle	0 to 90 degrees from horizontal
Discharge	Not to interfere with dredging operation

5.3 The Towing Carriage

The towing carriage is designed to ride on the steel tank rails using rubber rimmed steel wheels. A motor/gearbox drives two of the four carriage wheels to provide translation in the +/- *X* direction. A direct on-board drive was chosen over a system of winches to translate the towing carriage along the length of the tank. This was done to eliminate the amount of cable dangling over the tank during a dredging or towing operation. Moreover, the large weight of the fully assembled carriage provides the traction necessary to drive the carriage from the wheels. Positive control of carriage position can also be more easily obtained without a system of opposing winches pulling the carriage across the tank. The operator area contains a space for an on-board operator and a personal computer, as well as the control system and instrumentation.

The proposed towing carriage has a length of 5.08 m (200 in) and a width of 4.01 m (158 in) which is equal to the width of the tank plus the 254 mm (10 in) thick walls. It is estimated that the fully assembled tow carriage with the dredge carriage weighs up to 4534 kg (10,000 lb) as shown in Appendix A. The tow carriage operating by itself is estimated to weigh 1814 kg (4000

lb) with the dredge carriage removed. Figure 5.5 shows a conceptual view of the tow carriage without the model dredge on top of the tank.

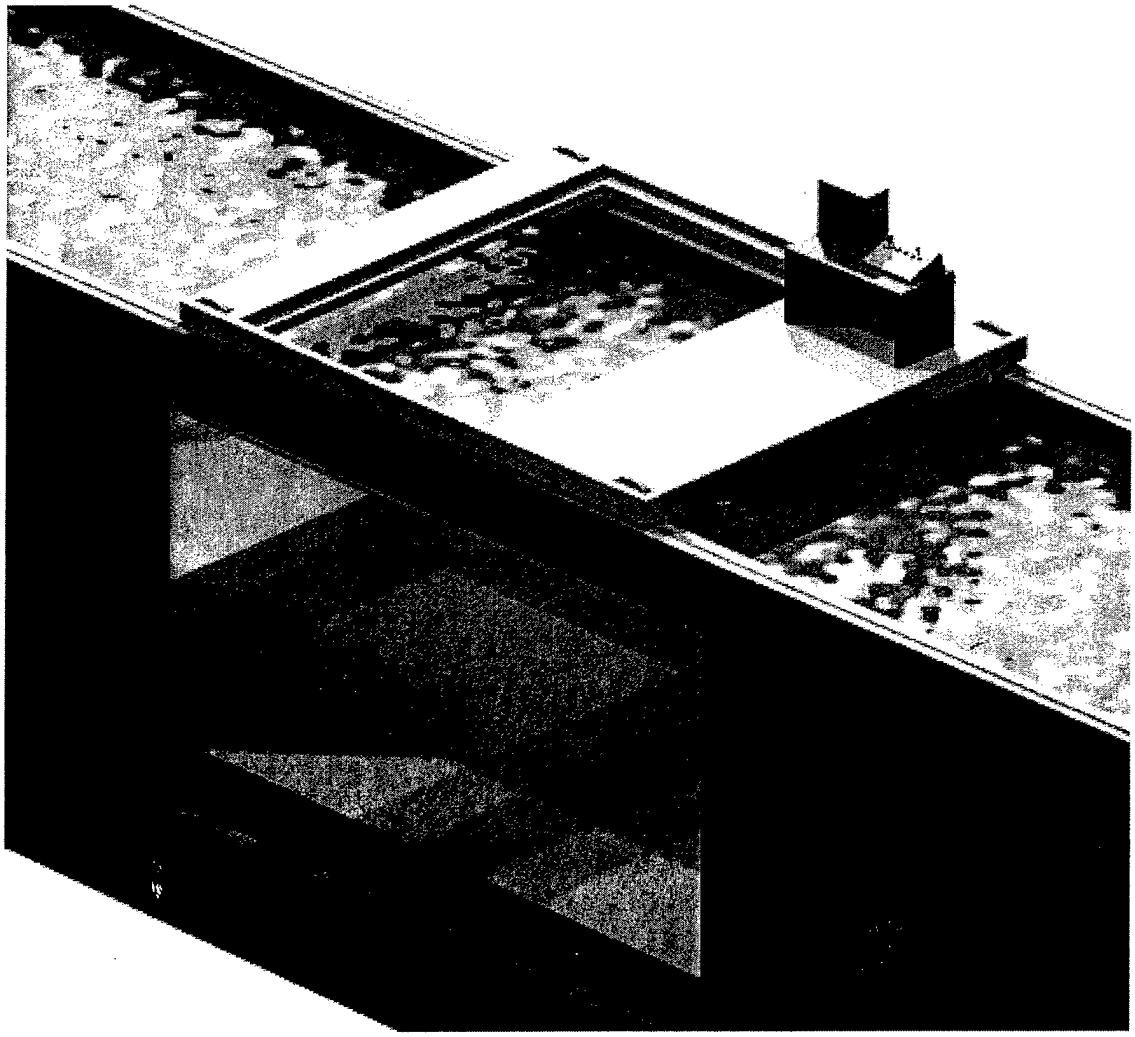

Figure 5.5: Conceptual View of the Tow Carriage without the Model Dredge on Top of the Tank

5.3.1 Towing Carriage Drive System

The speed and acceleration requirements of the tow carriage are restated from Table 5.1 as follows: a maximum speed of 1.2 m/s (4 ft/s) is required for towing operations (dredge carriage removed) with a maximum acceleration of 0 to 1.2 m/s (4 ft/s) over a 12.2 m (40 ft) distance.

This equates to an acceleration of 0.06 m/s^2 (0.2 ft/s^2). To accelerate a 1814 kg (4000 lb) body at this rate, 111 N (25 lb) of lateral force is required. At 1.2 m/s (4 ft/s), only 0.13 kW (0.18 hp) is needed to achieve this. However, there is an unknown quantity of rolling resistance due to friction that must also be overcome, plus the drag forces on the towed payload. Therefore, the amount of total lateral force needed for a towing operation is unknown. Rather than underestimate the rolling resistance for a towing operation and miscalculate the carriage drive or chose an arbitrarily high value, an alternate method is used.

During dredging operations, the tow carriage drive acts to advance the model cutter axially through the sediment analogous to the motion created by spud carriage motion on a prototype dredge. The resistance to forward motion resulting from the axial cutting forces is assumed to be far greater than the rolling resistance and model drag of the tow carriage. Given that the model cutterhead is 20.3 cm (8 in) long, each step of advance should not be longer than this distance when simulating a cutter suction dredge. Estimated axial loads on a model cutterhead under various dredging scenarios were calculated in the cutting force analysis of Section 4.4.2 (Table 4.5). The axial force developed is a function of the profile angle κ that the cutting edge of the employed cutterhead makes with the axis and the normal force on the cutting edge (Vlasblom 1998) as shown in Figure 5.6.

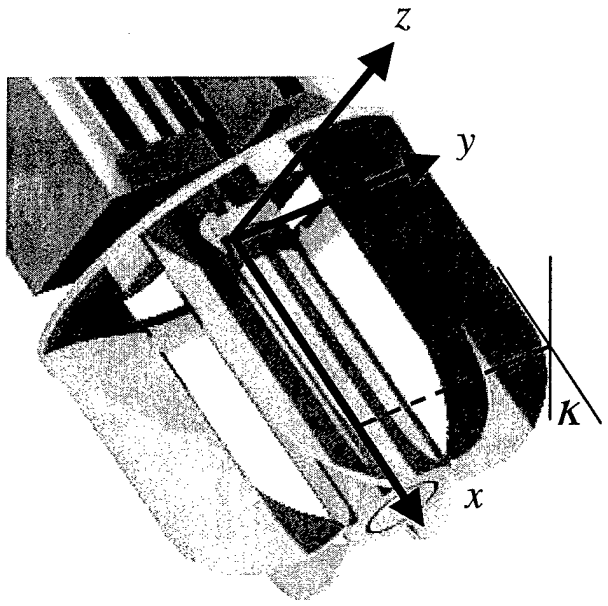

Figure 5.6: The Profile Angle κ of a Cutterhead along the x-Axis

On a large cutterhead, there are typically several rows of teeth as you move along the axis of the cutterhead. Each row along the cutterhead profile has a discrete profile angle κ. Total forces are calculated for each row based on that row's discrete profile angle. On a model cutterhead such as shown in Figure 5.6, the blades could be continuous along the axis and the profile angle would therefore be a function of x such that the profile angle can be described by $f(x)$. In this case, $f(x)$ could be integrated along the axis so that an average or "equivalent" profile angle is found as shown in Equation 5.1,

$$\bar{\kappa} = \frac{1}{l}\int_0^l f(x)dx \tag{5.1}$$

where l is the length of the cutterhead along the x axis.

The maximum average axial force calculated in Section 4.4.2 is 182 N (41 lb) for κ = 30 degrees. However, this is the force developed during lateral or swing motion and would be far greater if the cutterhead were advancing axially. Unfortunately, the cutting theory presented in Section 4.4.2 does not address the average axial cutting force when the cutterhead is advancing that direction. Therefore, in the case where the ladder angle is 0 degrees (horizontal), the axial load remains undetermined. In the case where the ladder angle is 90 degrees (vertical), the average horizontal cutting force becomes the cutting force in the X direction, the average axial cutting force becomes the cutting force acting in the Z direction, and the average vertical cutting force becomes the cutting force acting in the Y direction. Figure 5.7 shows how a vertical ladder angle and a forward carriage motion transform the coordinate system of the cutting forces as defined in Section 4.4.2.

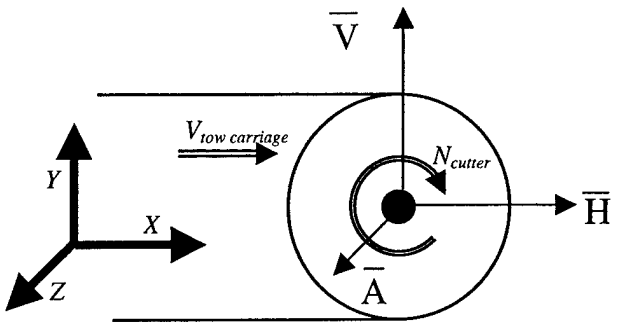

Figure 5.7: The Average Cutting Forces for a Vertical Ladder

In the case of a vertical ladder, the maximum cutting force in the *X* direction is equal to the maximum horizontal (*Y*-direction) cutting force for a horizontal ladder, which is calculated to be 2780 N (625 lb) at 17.8 cm/s (7 in/s) for the model dredge according to Table 4.5. The 90 degree ladder angle, however, is a rare case and there are still many unknowns. Even if the average axial cutting force is assumed to also be about 2780 N (625 lb) at 17.8 cm/s (7 in/s) for more acute ladder angles, it is still not known with any degree of certainty what acceleration or velocity the dredge will be required to advance during axial cutting. Therefore, the dynamic forces and thus the horsepower required by the tow carriage drive can still not be estimated in this way.

When a suctionhead is being modeled, the carriage drive advances the dredge analogous to the forward motion of a hopper dredge. During this scenario, there is also resistance against the direction of motion from dragging the suctionhead over the sediment surface. The magnitude of this resistance cannot be easily calculated or estimated, although it is estimated to be much less than with the cutterhead.

All of these unknowns put a large degree of uncertainty in sizing a carriage drive system that is powerful enough to perform 1:10 scale model studies of large hydraulic dredges. Rather than incorrectly under estimate what this power might be, the most powerful drive that is practical should be specified so that ample power is available to perform any task that may be required. The fully loaded tow carriage with the model dredge carriage attached is estimated to weigh 44,482 N (10,000 lb) as detailed in Appendix A. The static load analysis performed in Appendix B shows 24,910 N (5600 lb) of this weight acts through the front wheels when advancing

without resistance. When advancing against an estimated resistance of 2780 N (625 lb), the percentage of the load shifted to the front wheels in increased to 27,414 N (6163 lb). The greater the cutterhead resistance to the forward motion of the carriage, the greater the normal force acting on the front wheels.

Following the same logic of Section 4.4.3 and using the structural analysis in Appendix B, a maximum axial cutting force of 4226 N (950 lb) will cause the bending stress in the vertical guide rods to reach their yield strength for a horizontal ladder and a 3.81 m (12.5 ft) digging depth. The normal force acting on the front wheels under this maximum load is 28,718 N (6456 lb). The coefficient of static friction between hard rubber and smooth steel is between 0.7 and 0.9 depending on the temperature and the presence of water. Given these facts, no more than 25,800 N (5800 lb) of lateral force can act through the front wheels under ideal conditions or slippage between the wheel and rail will occur. Without loading the cutterhead, at least 17,437 N (3920 lb) of lateral force can act through the front wheels before slippage may occur. These two quantities represent the minimum and maximum practical limits of available power to the drive system depending on how the cutterhead is loaded while advancing in the X direction based solely on wheel traction. However, given that the only resistance to motion in the X direction is axial cutting force, there is no reason for the drive system to push the carriage with more than 4226 N (950 lb) of force. Anything beyond this could damage the vertical guide rods as detailed in Appendix B.

At the maximum dredging speed of 30.5 cm/s (12 in/s), an electric motor of approximately 1.5 kW (2 hp) is required to drive the carriage under the maximum permissible loading. This is more than enough power to tow a model in the tank at the required speed of 1.2 m/s (4 ft/s) with the model dredge removed. At the maximum towing speed of 1.2 m/s (4 ft/s), a 1.5 kW (2 hp) motor can overcome a combined resistance (drag + rolling resistance) of 1223 N (275 lb). The 1814 kg (4000 lb) tow carriage can accelerate over 0.61 m/s^2 (2 ft/s^2), 10 times more than what is required by Table 5.1. A gear reduction system is coupled with the motor so that a maximum of 80 rpm is achieved from the 5.1 cm (2 in) diameter drive shaft at the maximum carriage speed of 1.2 m/s (4 ft/s). However, to ensure that the maximum amount of power is available at carriage speeds of 0 to 1.2 m/s (4 ft/s), a variable speed drive or motion controller is used with the motor. Alternatively, a more powerful motor capable of delivering greater horsepower at lower rpms

may be substituted for the constant power, variable speed motor controller. A brake motor is specified to ensure that the tow carriage can be quickly stopped from its maximum speed of 1.2 m/s (4 ft/s).

A stainless steel shaft has a tensile yield strength of at least 296,475 kPa (43,000 psi), 148,237 kPa (21,500 psi) in shear. If the model dredge advances at a speed of 30.5 cm/s (12 in/s), the drive shaft will rotate at 19 rpm. According to Equations 5.2 and 5.3, a 3.8 cm (1.5 in) diameter shaft is sufficient to transmit 1.5 kW (2 hp) at 19 rpm with a maximum shear stress of 69,024 kPa (10,011 psi). Appendix B predicts a maximum vertical shear load of V_{shear} = 28,673 N (6446 lb) on the shaft causing an additional 56,585 kPa (8207 psi) of shear stress as calculated by Equation 5.4. The combined maximum shear stress is estimated to be 125,609 N (18,218 psi), well below the materials' yield strength. If maximum power is required during a towing operation, the shaft will be required to deliver 1.5 kW (2 hp) at 80 rpm with less than 25% of the shear stress determined in the previous case. If a greater margin of safety is desired, a larger or stronger drive shaft can be substituted.

$$\frac{P*63025}{RPM} = \Gamma \text{ (torque in-lbs)} \tag{5.2}$$

$$\tau_{\max} = \frac{\Gamma}{J} r \tag{5.3}$$

$$\tau = \frac{V_{shear}}{\pi r^2} \tag{5.4}$$

Where r is the shaft radius and J is the area moment of inertia for a cylinder ($\frac{1}{2}\pi r^4$).

5.3.2 Electrification of the Towing Carriage

Electrification of the towing carriage is accomplished using a cable spool, which pays out cable to the carriage as it moves across the tank. Figure 5.8 shows various spools available from

Industrial Power and Control Inc. The spool will keep tension in the line to avoid loose cable dangling atop the test rig.

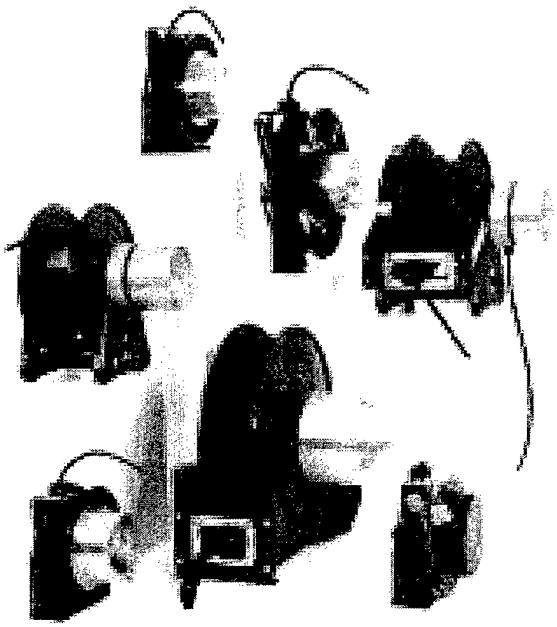

Figure 5.8: Cable Spools from Industrial Power and Control

A cable spool is recommended over electrified rails for several reasons. Electrified rails are used primarily for large, high-power equipment such as cranes and shuttle cars because a steady source of power is not required. The tiny fluctuations caused by imperfections, moisture, or wear in the sliding contacts can disrupt sensitive instrumentation and computer equipment. Also, ensuring the safety of the operator while exposed electrical contacts operate in a marine environment would be a greater challenge with an energized rail system. Lastly, an energized rail system would require more infrastructure such as a suspended beam that the energized rails could be mounted under. This beam would have to span the length of the tank and be elevated enough to ensure safety of those on the ground. It would also need to be high enough to ensure clearance with the ladder arm and not interfere with the movement of the overhead crane.

5.3.3 Towing Carriage Equipment and Instrumentation

The tow carriage includes the user/operator station that consists of a Personal Computer wired to a Programmable Logic Controller or PLC. The function of the PLC as it pertains to the automation and control of the apparatus is further explained in Section 5.7. The tow and model dredge carriages are fitted with instrumentation to detect and record data during operation. Among the tow carriage equipment is a load cell capable of detecting the drag forces of a towed payload along three axes of motion. A cable extension linear position sensor (LPS) is recommended so that absolute position of the towing carriage along the *X*-axis can be known. These devices function by paying out a small cable from a spool attached to the carriage. The end of the cable would be attached to one end of the tank. An encoder is attached to the spool and the device transmits an analog signal that once calibrated can continuously determine the exact position of the carriage. A limit switch for the carriage drive with adjustable set points and a "hard disconnect" is recommended to prevent the tow carriage from running off the end of the tank. To ensure that the tow carriage remains centered over the tank and is not derailed by strong lateral forces during a dredging operation, each corner of the carriage should have a 5 - 8 cm (2 - 3 in) diameter bearing contacting the inner surface as shown in Figure 5.9.

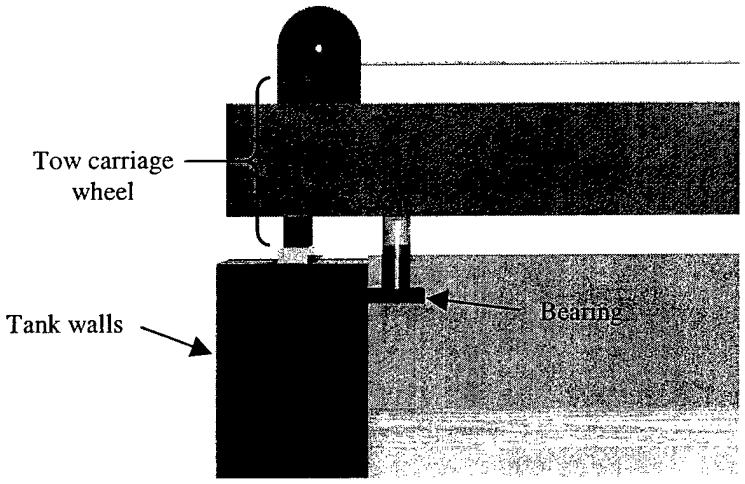

Figure 5.9: Small Bearing Inside the Tank Wall to Prevent Tow Carriage Derailment

According to the static load analysis of Appendix B, the radial load never exceeds 2900 N (652 lb) under the maximum possible loading allowed by the chosen drives. This should be considered the design criteria when selecting the wheel shaft and bearing.

5.4 Model Dredge

The model dredge frame rests securely inside the towing carriage as shown in Figure 5.10. The model dredge can be removed from the towing carriage via the overhead crane and set in a separate cradle located in the work area adjacent to the towing tank. The dredge carriage holds the ladder arm over the sediment pit and can adjust the vertical position of the cutterhead by raising and lowing the ladder arm in the +/- *Z* direction by a winch located atop the dredge carriage.

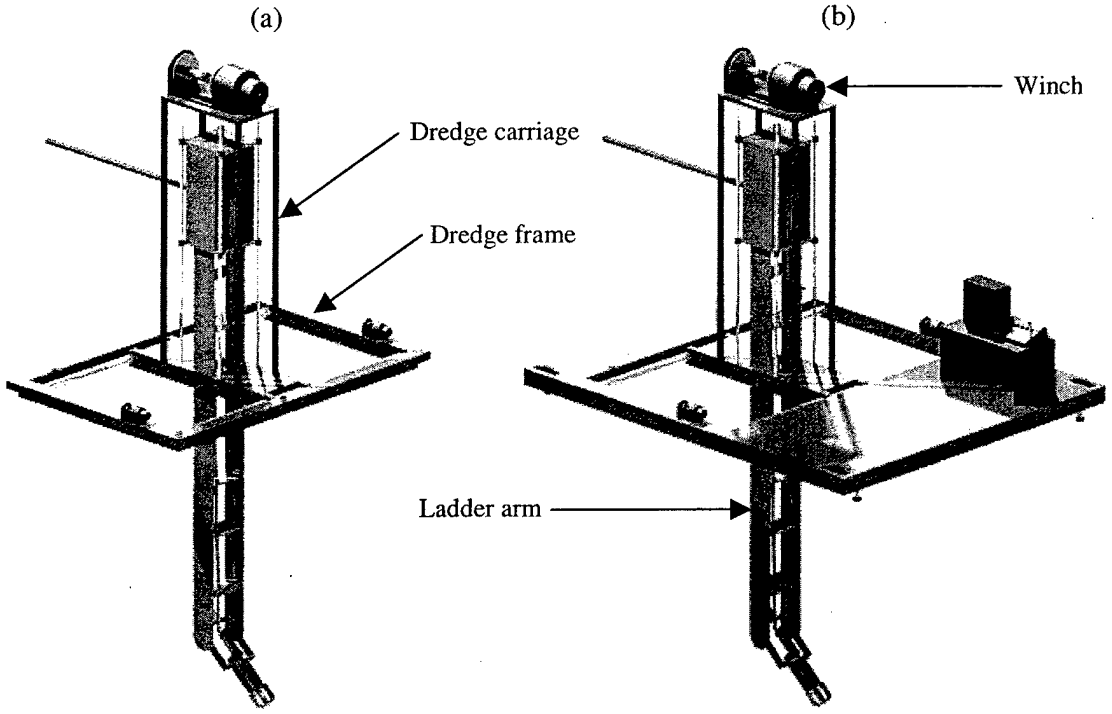

Figure 5.10: The Model Dredge by Itself (a) and Secured in the Towing Carriage (b)

5.4.1 Model Dredge Carriage

Four 51 mm (2 in) diameter stainless steel guide rods (Figure 5.4) span the vertical length of the dredge carriage superstructure and sleeve bearings in the upper ladder arm assembly provide for smooth vertical motion of the cutterhead. When the cutterhead is loaded with increasing cutting forces during operation, these guide rods will be the first structural members of the dredge carriage to fail as they represent the weakest structural link in the model dredge carriage. The static analyses performed in Appendix B include the calculation of the maximum allowable bending moments. Recall that this analysis was used in Section 4.4.3 to estimate the maximum possible side winch pull force and again in Section 5.3.1 to size the tow carriage drive. Given the weight limitations expressed in Appendix A, the size of the guide rods cannot be increased for added structural rigidity. However, as the analyses used in Chapter IV and Appendix B show, the guide rods as designed are of sufficient strength to operate the dredge under the maximum predicted loading. In fact, the maximum loading can be exceeded by 26% before the yield stress is reached, and only then under specific combinations of ladder angle, ladder arm elevation, and horizontal dredge carriage position. Moreover, stainless steel materials with yield strengths up to 1.7 MPa (250 ksi) can be substituted without adding additional weight to the carriage.

The winch on top of the dredge carriage (Figure 5.10) is capable of positioning the ladder arm assembly, which is estimated to weigh approximately 9452 N (2125 lb) according to Appendix A. When the cutter head is undercutting, vertical cutting forces in the $-Z$ direction my increase the tension in the cable and the load on the winch. According to Table 4.5, the maximum vertical force on the cutterhead operating under the stated conditions is about 2108 N (474 lb) cutting at a 12.7 cm (5 in) depth with a swing speed of 35.6 cm/s (14 in/s). However, the standard cutting load of Table 4.5 can be exceeded by 26% before the dredge is at risk of failing. Therefore, a 8896 N (2000 lb) capacity winch capable of supporting a static load of 12,010 N (2700 lb) is specified.

5.4.2 Model Dredge Frame

The model dredge frame (Figure 5.10) shall be rigid enough to support the entire weight of the model dredge during removal and storage in a specially designed cradle in the work area. The frame's superstructure must support the weight of the ladder arm as well as the hoist so that the vertical guide rods are not axially loaded. A pair of 82.6 mm (3-1/4 in) diameter stainless steel horizontal guide rods (Figure 5.4) spans the width of the dredge frame, and sleeve bearings in the dredge carriage base provide for smooth horizontal motion of the cutterhead. The static load analysis performed in Appendix B includes the calculation of the maximum allowable bending moments in these members under different loading conditions. A relatively weak stainless steel material with a yield strength of 296,475 kPa (43 ksi) is used to determine the maximum allowable bending moments. If more strength is required, a higher strength steel up to 1.7 MPa (250 ksi) can be substituted. The strongest stainless steels (Series 400) have yield strengths in excess of 1.7 Mpa (250 ksi) (Gere et al 1990).

Winches on either side of the dredge frame are needed to pull the dredge carriage side-to-side to provide cutterhead translation in the +/- *Y* direction to simulate ladder swing. The side winch cable attaches to the dredge carriage in the same plane created by the two horizontal guide rods to avoid additional loading of the guides with another moment. Conversely, placing them lower with the point of attachment to the dredge carriage below the plane created by the two horizontal guide rods will help to reduce the bending moment on the horizontal guides. As stated in Table 4.7, a pair of 2.2 kW (3 hp) winches capable of pulling a 3559 N (800 lb) load at 61 cm/s (24 in/s) is required for the swing motion.

5.4.3 Dredge Frame and Dredge Carriage Instrumentation

Dredge carriage instrumentation includes a load cell in series with the ladder arm hoist cable to measure vertical reaction forces at the cutterhead. Vertical cutting forces up to 9452 N (2125 lb) in the +*Z* direction can be measured by the tension in the winch cable (overcutting). Vertical cutting forces up to 3114 N (700 lb) can be measured in the –*Z* direction via tension in the cable (undercutting). Cable extension linear position sensors (LPS) are also used to detect dredge carriage absolute horizontal position (along the *Y* axis) as well as ladder arm absolute vertical

position (along the *Z* axis). Load cells are also placed in series with the swing winch cables to measure the pull forces, giving a good approximation of horizontal cutting forces acting on the cutterhead. The feedback from the load cells prevents the drives from exceeding the maximum allowable cutterhead loading and damaging the ladder arm and dredge carriage guide rods. In addition to the feedback/control system, limit switches with hard disconnects are also recommended for the winches to prevent over travel of the ladder arm or dredge carriage.

5.5 Ladder Arm Assembly

The ladder arm assembly stands about 5.79 m (19 ft) tall and has 173 cm (68 in) of vertical travel as shown in Figures 5.4 and 5.10. At the lower end of the ladder arm is the 76.2 cm (30 in) long dredge ladder containing the suction and cutterhead. This configuration allows the ladder angle to be adjusted independently of the cutter elevation. The result is that the cutter angle can be adjusted from 0 to 90 degrees from the horizontal and cut at any elevation in the sediment pit from 3.05 to 4.27 m (10 to 14 ft) deep. Reducing the length of the ladder can reduce the amount of vertical travel required by the ladder arm to cut at any angle and at any depth of the sediment pit. Reducing the ladder length also will reduce the moment created by ladder swing. However, a longer ladder is more geometrically similar to a prototype dredge. The recommended length of 76.2 cm (30 in) is recommended as a compromise between function and similitude. It is also noted that the cutterhead can be replaced with a suctionhead or a draghead, depending on the equipment being tested.

5.5.1 Ladder Arm Equipment and Instrumentation

The upper ladder is fitted with a variable speed, variable torque, 7.5 kW (10 hp) motor to drive the 7.62 cm (3 in) diameter centrifugal pump and a 14.9 kW (20 hp) variable speed, constant power motor to drive the cutter via the 51 mm (2 in) diameter drive shaft and double universal joint. Figure 5.4 shows the configuration of the equipment contained in the upper ladder arm.

At the lower end of the ladder arm, a linear actuator will adjust the ladder angle and maintain the desired position during dredging. According to Appendix B, a maximum moment of 1898 N-m

(1400 ft-lb) is required under normal operating conditions to hold the ladder steady. The only other scenario that could load the ladder arm with a greater moment is while the tow carriage is advancing under the maximum axial load. In Section 5.3.1, a maximum allowable resistance of 4226 N (950 lb) during tow carriage advancement was computed. If this entire load acts through the ladder arm (vertical ladder), the moment at the ladder end would be about 9055 N-m (3000 ft-lb). With a 30.5 cm (12 in) lever arm, a linear motor capable of holding a 13,345 N (3000 lb) load in tension and compression is required. A hydraulic piston is not recommended due to the tendency to leak fluid. A worm gear or ball and screw type linear actuator may be suitable if the motor has an enclosure such that it can function reliably under water. An example of such a device is given in Appendix A.

Ladder arm instrumentation includes a magnetic flowmeter, nuclear densometer, pressure gauges across the pump, tachometer and dynamometer for both cutter and pump drives, and an angular position sensor to determine the ladder angle. A complete list of equipment is contained in Appendix A.

5.6 Sediment Transport, Storage, and Disposal

During a model run, slurry is to be discharged through the 7.62 cm (3 in) discharge line into a floating hopper barge behind the Dredge Carriage as shown in Figure 5.11. When the tank is used strictly for towing operations, the hopper barge can be removed and placed in the work area using the overhead crane. This concept of operation was chosen for several reasons. Most importantly, keeping the sediment contained prevents the discharge from interfering with turbidity produced by the model cutterhead or suctionhead. In the cases where model cutters are being evaluated on the basis of turbidity generation, this is an absolute necessity. Even in non-turbidity related studies, clouding the water by immediately discharging the slurry into the tank may interfere with any qualitative data being taken by persons looking through the observation windows. Disposal of the slurry at the far end of the tank does not eliminate the turbidity problem if a current is being produced via the current manifold at the far end of the towing tank.

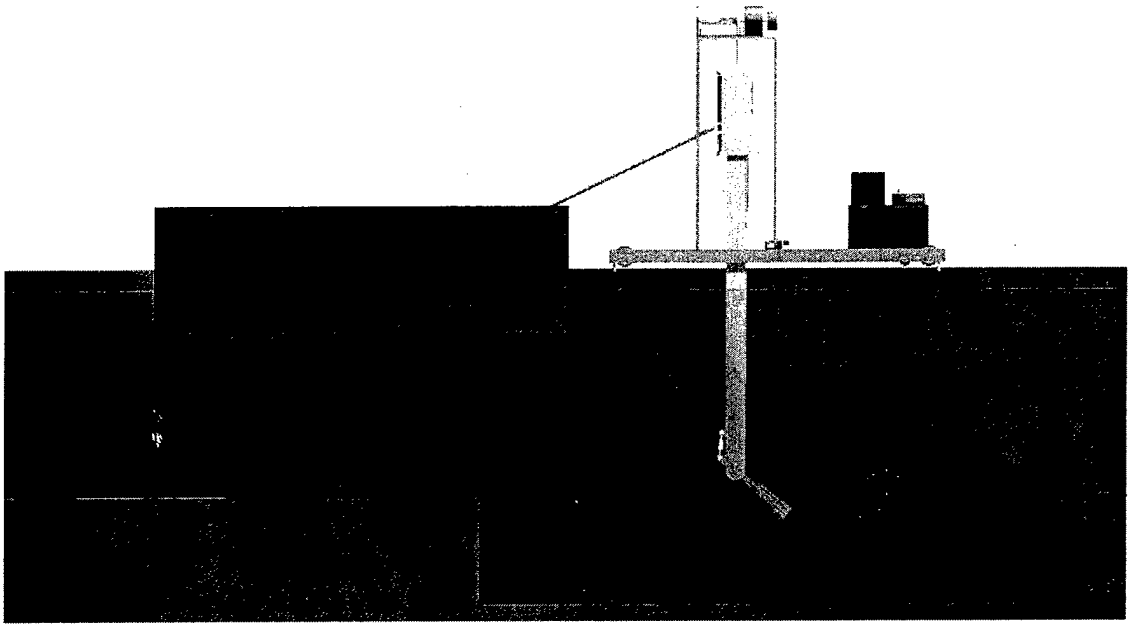

Figure 5.11: Floating Hopper Barge Behind Towing Carriage

The floating hopper concept has other advantages as well. By displacing a volume of water equal to the discharge volume, the water level in the tank remains constant during a dredging operation. The draft of a floating hopper also gives a quick and accurate estimate of total discharge volume. Lastly, a separate hopper "barge" fitted with doors underneath also allows the modeling of open water disposal while at the same time directly returning the sediment to the sediment pit.

The volumetric flow rate of the slurry depends on the geometric scale ratio and the ratio of prototype to model settling velocities in accordance with the velocity profile scaling relationship as listed in Table 4.1. The following example assumes a geometric scale of 1:10 and a prototype flow rate of 189,270 LPM (50,000 GPM) through a 76.2 cm (30 in) diameter discharge line as used previously. Modeling fine sand (d_{50} = 0.1 mm) with fine sand as a bed material requires a model flow rate of 189 LPM (500 GPM) to maintain a properly scaled velocity profile around the suction inlet according to Table 4.1. On the other end of the spectrum, modeling coarse gravel (d_{50} = 1 mm) with a fine sand bed material (d_{50} = 0.1 mm) requires a model flow rate of 129 LPM (34 GPM) to maintain a properly scaled velocity profile according to Table 4.1.

Consequently, the volume of the discharge hopper and the volumetric flow rate of the discharge limit the time allowed for a model run.

With a fixed hopper volume the model flow rate is a critical factor in determining how long a model test can run before the hopper is filled to capacity. Figure 5.12 shows the relationship between model flow rate and model run time for hopper sizes ranging from 15.3 m^3 (20 cy) to 45.9 m^3 (60 cy). Given the dimensions afforded by the tank and sediment pit geometry, the volume of the hopper barge needs to be approximately 30.6 m^3 (40 cy). This means model run time using fine sand could be anywhere from 16 minutes to several hours depending on the prototype sand and conditions being modeled. As a rule, modeling finer prototype sand results in shorter run times while modeling course gravels results in longer run times.

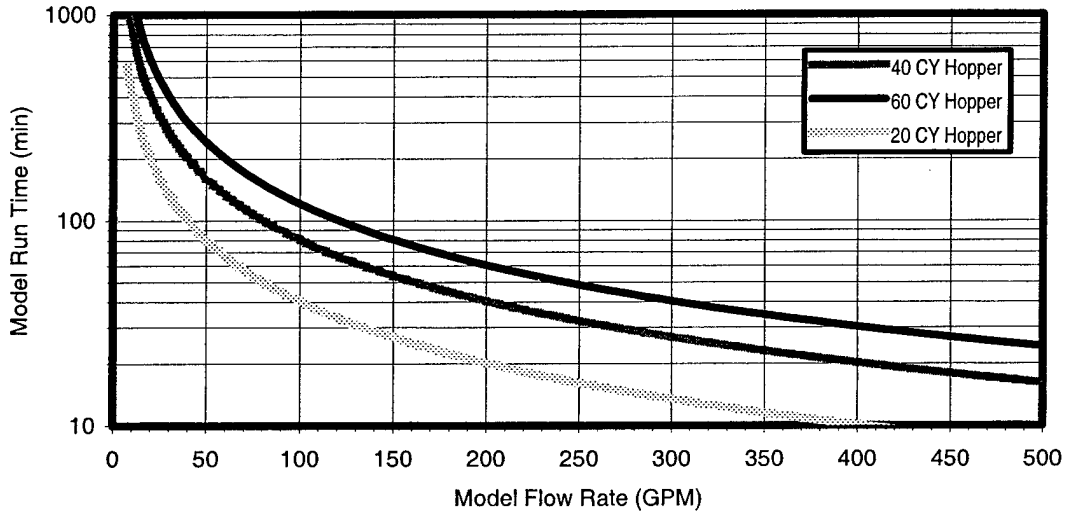

Figure 5.12: Model Run Time versus Model Flow Rate
for Different Hopper Barge Sizes

Recommended hopper dimensions are approximately 6.1 m (20 ft) long, 3.4 m (11 ft) wide, and 1.5 m (5 ft) deep with 0.3 m (1 ft) of freeboard. The hopper needs a buoyancy block attached to each end to maintain positive buoyancy when it is filled to maximum capacity. Telescoping overflow weirs are needed to allow water to drain out of the hopper in the event that maximum run times need to be exceeded. Two sets of hopper doors on the underside will allow modeling

of open water disposal. Bearings on each side of the hopper keep the hopper centered in the towing tank and minimize damage to tank walls.

5.6.1 Modeling of Open Water Disposal with Hopper Barge

When the hopper becomes filled, or a set of experiments is completed, the collected slurry needs to be returned to the sediment pit. The telescoping weirs can be adjusted to allow water to drain after settling has occurred. Once the sediment has reached its desired state, the hopper is positioned over the sediment pit and the doors opened. Not only will this return the sand to the sediment pit, but the physics of the dredged material falling through the water column can be studied as well. Figure 5.13 depicts the return of the sand to the sediment pit.

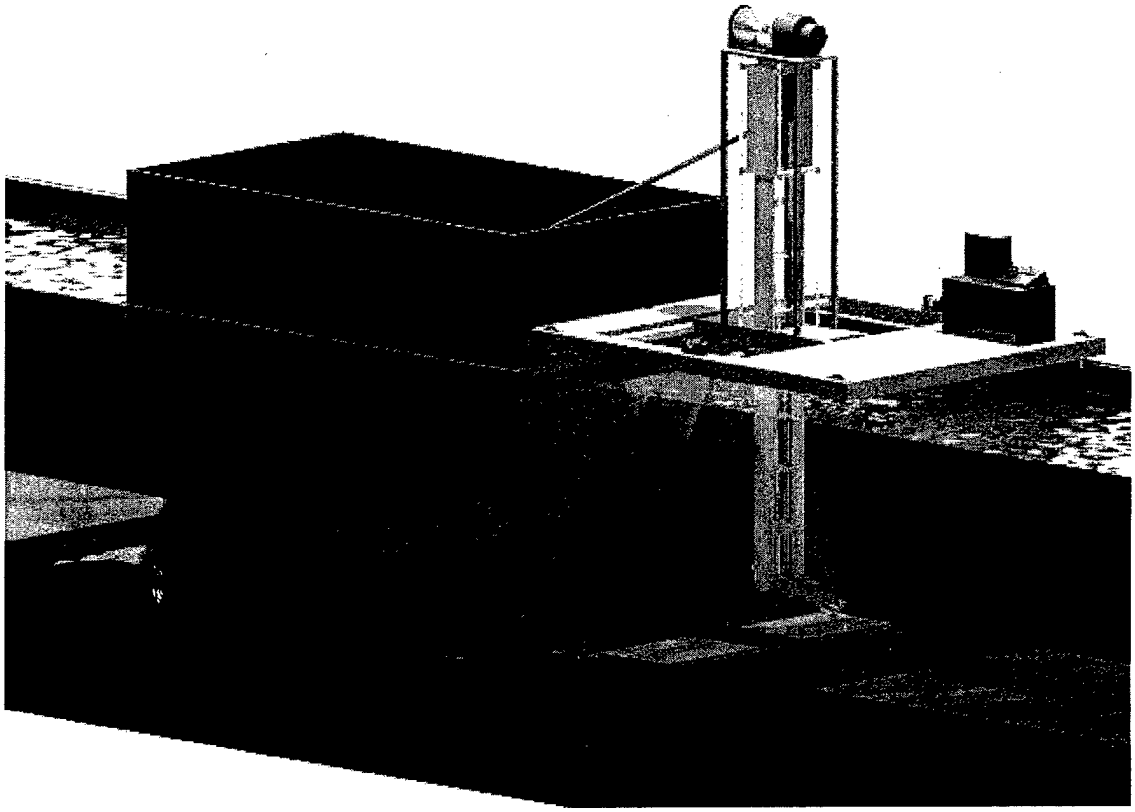

Figure 5.13: Modeling the Open Water Disposal Process

The scaling laws for modeling open water disposal have been developed and can be applied in a straightforward manner (Tetra Tech, Inc, 1988). Model to prototype length scale ratios are limited to 1:100 scale or larger for effective similarity. Smaller scales do not allow the Reynolds relationship with respect to the onset of turbulence to be satisfied. Therefore, a 4.57 m (15 ft) deep sediment pit can accurately model depths of up to 457 m (1500 ft). Since disposal usually occurs in water depths from 30 to 200 m (100 to 700 ft), geometric scale ratios on the order of 1:10 can be used. The 3.66 m (12 ft) width of the tank can limit the prototype distance in the *Y* direction depending on the prototype water depth and scale ratio used. For a prototype water depth of 30 m (100 ft), a 3:20 length scale is used and the width is limited to 24 m (80 ft). For a prototype water depth of 200 m (700 ft), a 3:140 length scale is used and the width is limited to 170 m (560 ft). If this becomes a critical issue, the scaling laws allow for a distorted length scale to be used (Tetra Tech, Inc 1988). That is, a model to prototype length scale ratio that is different along one or more axes.

Another limitation when modeling open water disposal is sediment properties. Typically, sediment material density, settling velocity, and median grain diameter are quantities that can be manipulated in the model parameters to achieve more consistent similarity between model and prototype (Tetra Tech, Inc 1988). However, the facility under consideration is being designed so that one lot of sediment material with a fixed median grain size and particle distribution is used for all model tests. This may introduce some scale effects that must be considered when modeling open water disposal with this facility. Different lots of sediment can be used, but the logistics of swapping and storing various lots of sediment, at over 46 m^3 (60 cy) each, becomes an issue.

5.6.2 Compacting/Grading the Sediment

Prior to a model dredging operation, the sediment bed material must be graded flat and compacted to the desired amount. A removable attachment on the end of the ladder can accomplish the grading. Grading can also be performed by divers or by other means if the tank were emptied prior to the model test.

Compacting the sediment can be accomplished with concrete vibrators. If the tank were empty, other mechanical means, such as an oscillating mechanical packer, could be employed. To achieve the amount of compaction used in the cutting force calculations (95%), a combination of vibration and mechanical compaction will have to be used (de Jong 2002).

5.7 Controls and Instrumentation

The carriage is fitted with an array of sensors and instruments that relay data to a Programmable Logic Controller (PLC). The PLC operates the model dredge according to any number of testing/modeling sequences that can be programmed and stored in a PC and uploaded to the PLC's internal memory for execution. The PLC forwards the acquired data to the PC for real-time output to a virtual instrument panel seen on the monitor, as well as collects and stores the data on the hard drive for further analysis. Table 5.2 shows the input data from the instrumentation and the output data to the virtual instrument panel. The PLC contains an internal clock that allows for the calculation of time-related quantities such as speed, horsepower, and efficiency.

Table 5.2: Programmable Logic Controller Input/Output Data

Inputs from Instruments	**Data Outputs to PC (Digitized by PLC)**	**Data Outputs to PC (Calculated/ Digitized by PLC)**	**Control Outputs to PLC Power relays**
Pump rpm	Pump rpm	Cutterhead Z position	Cutter Speed Control
Pump Torque	Pump Torque	Tow Carriage X Speed	Pump Speed Control
Pump Suction Pressure	Pump Suction Pressure	Dredge Carriage Y Speed	Tow Carriage X Drive
Pump Discharge Pressure	Pump Discharge Pressure	Pump Brake Horsepower	Dredge Carriage +Y
Pump Flow Rate	Pump Flow Rate	Pump Water Horsepower	Dredge Carriage - Y
Slurry Density	Slurry Density	Pump Efficiency	Dredge Arm Z Hoist
Tow Carriage X Position	Cutterhead X Position	Cutter Motor Horsepower	Ladder Angle Piston extend
Dredge Carriage Y Position	Cutterhead Y Position		Ladder Angle Piston contract
Dredge Arm Z position	Dredge Ladder Angle		
Dredge Ladder Angle	Cutterhead rpm		
Cutterhead rpm	Cutterhead Torque		
Cutterhead Torque	Cutterhead Y Force		
Cutterhead Y Force	Cutterhead Z Force		
Cutterhead Z Force	Drag Force in X Direction		
Drag Force in X Direction	Drag Force in Y Direction		
Drag Force in Y Direction	Drag Force in Z Direction		
Drag Force in Z Direction			

High current relays allow the control output to drive the motors and hydraulics required to operate the carriage. The primary advantage to automation is that experimental conditions that depend on the dredge operation (typically manual input) can be controlled for each model run. Data from each successive run can be stored in separate files for analysis. Figure 5.14 depicts the conceptual schematic of the control system.

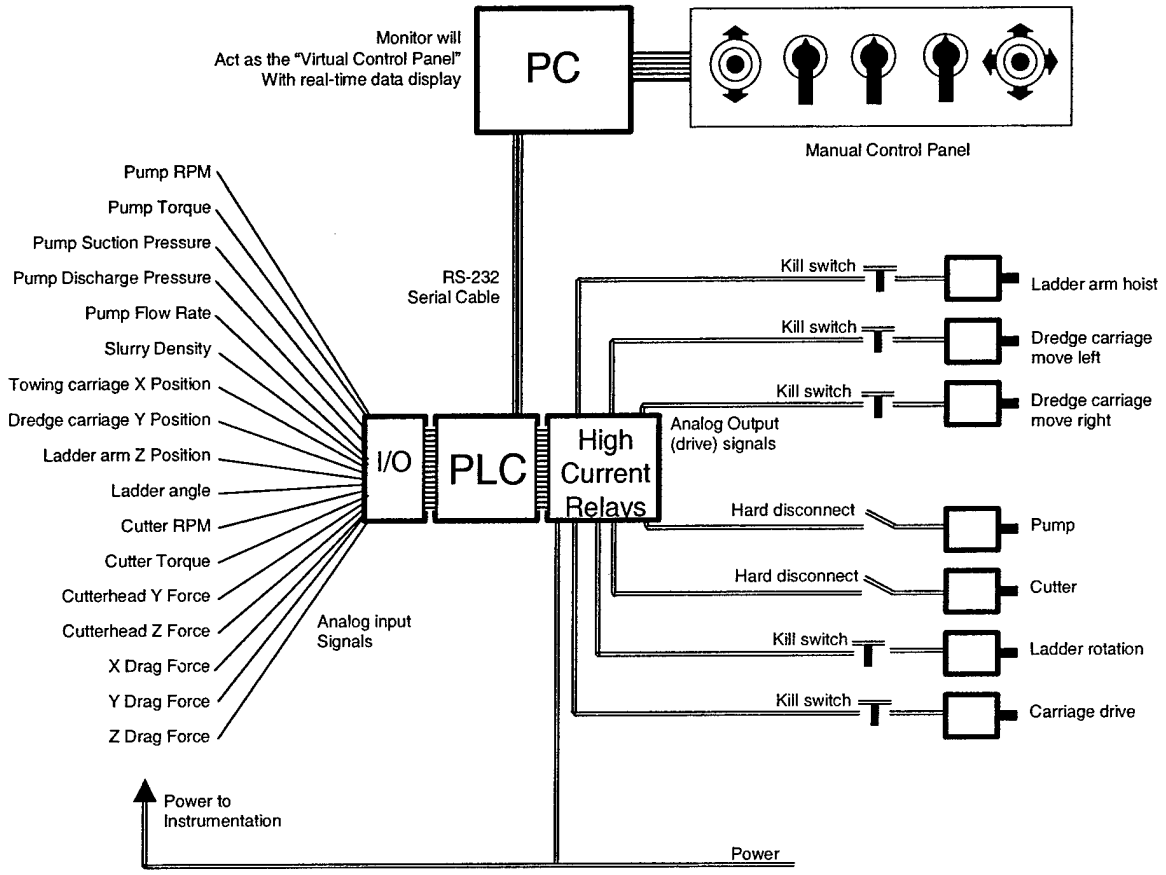

Figure 5.14: Conceptual Schematic of the PLC Control System

In the event that manual operation is required, the PLC can be programmed to run based on user input rather than a pre-programmed sequence. User input is accomplished with a control panel similar to what is shown in Figure 5.15. During manual operation, the PC monitor displays all the relevant data in any number of preprogrammed formats ranging from digital readouts to analog gauges.

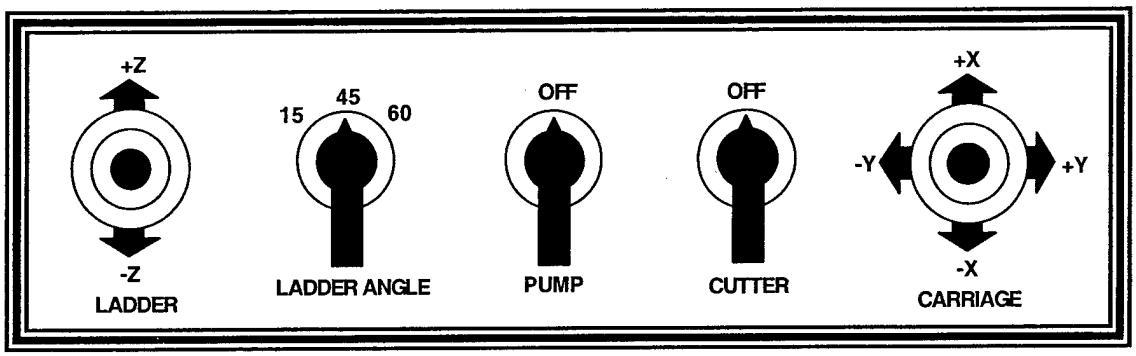

Figure 5.15: Manual Control Panel

Each program used by the PLC, whether fully automated or using some degree of manual control, has not-to-exceed parameters to ensure safe operation. This is used primarily to keep the cutter at a safe distance from tank walls. Analog limit "kill switches" for motor power are used in the event that the program fails to stop the operation if a pre-programmed set point is exceeded. Hard disconnect circuit breakers will also be available for the pump and cutter drive motors to allow give the operator manual override capacity.

CHAPTER VI

EXAMPLES OF LABORATORY MODEL STUDIES

6.1 Two Modeling Examples

The following two examples are given demonstrate the use of the proposed model dredge. While the scaling laws were helpful in sizing the model dredge drives and maximum operating parameters, their intended purpose is to correlate the model test data to the prototype. The data used are fictional since the model tests are only examples, but the exercise demonstrates how the similitude criteria are used in an actual model study.

Since all of the scale laws used to set-up a modeling experiment are derived from similitude with respect to sediment pick-up behavior, the model dredge operating parameters depend on the median grain size of the prototype dredge and the geometric scale ratio. Selecting a proper geometric scale ratio is essential to performing a successful experiment. Cutting forces, flow rates, and cutting speeds must be kept within certain ranges if the dredge is to operate efficiently. Figure 6.1 is given to aid in the selection of the geometric scale so that the resulting operating parameters can be easily computed if the prototype grain size is known. The data used to plot the charts are calculated from Equations 3.13, 3.14, and 3.15. This chart assumes that the model median grain size is 0.1 mm. If a different model sediment grain size is used, the model to prototype velocity scale must be calculated based on the relative settling velocities.

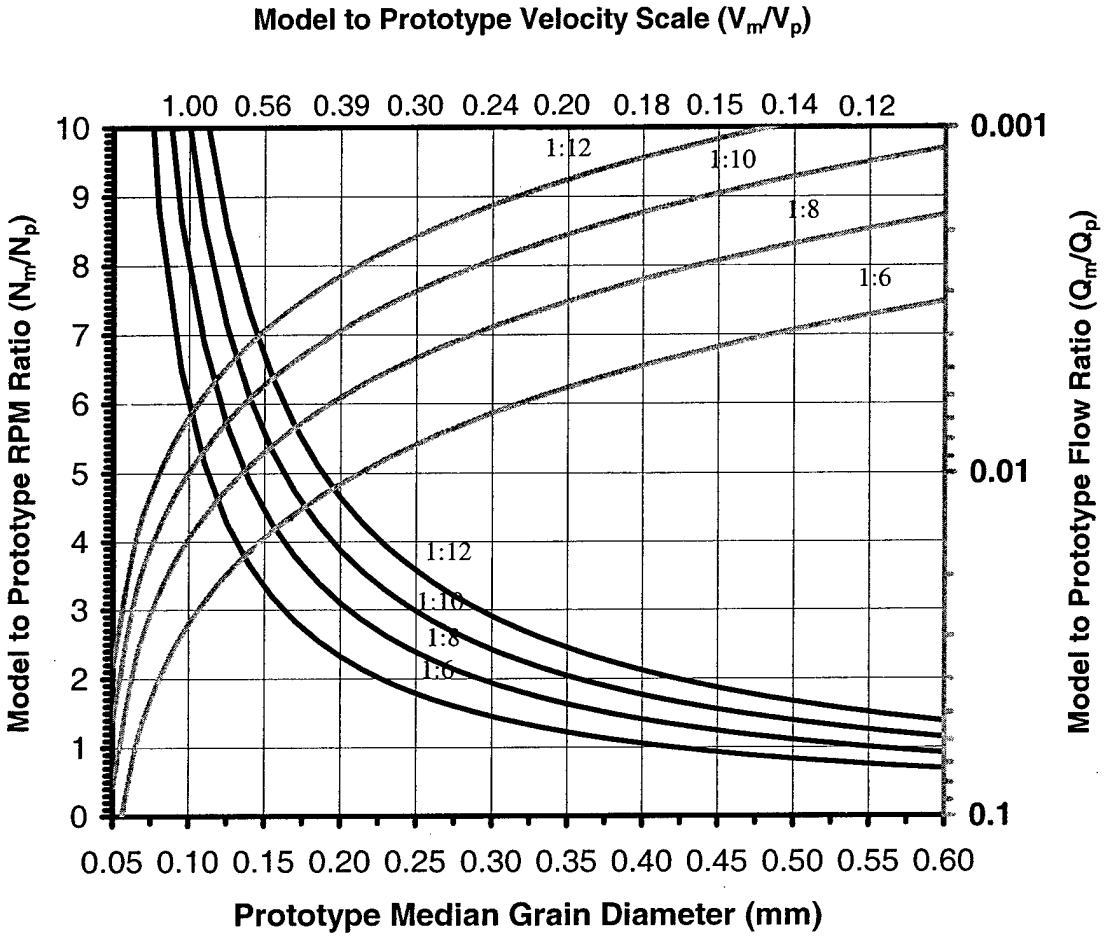

Figure 6.1: Chart For Selecting Model Dredge Operating Parameters
(Model d_{50} = 0.1 mm)

The bottom axis is the prototype median grain diameter in mm. The left axis is the model to prototype rpm ratio. The black geometric scale lines are used to determine the rpm ratio. The right axis is the model to prototype flow ratio. The gray geometric scale lines are used to determine the flow ratio. If the model grain size is 0.1 mm, the prototype grain size is the starting point along the bottom axis. If the model grain size is not 0.1 mm, the resulting velocity scale is the starting point along the top axis. Figure 6.2 is the chart as it was used to determine the model dredge operating parameters from the large prototype dredge. These operating parameters formed the basis of design for the model dredge. Only the 1:10 geometric scale lines

are shown for clarity. It can be seen how the rpm scale of 10 and the flow rate scale of 1:100 were derived from the 0.1 mm median grain size of the prototype sediment.

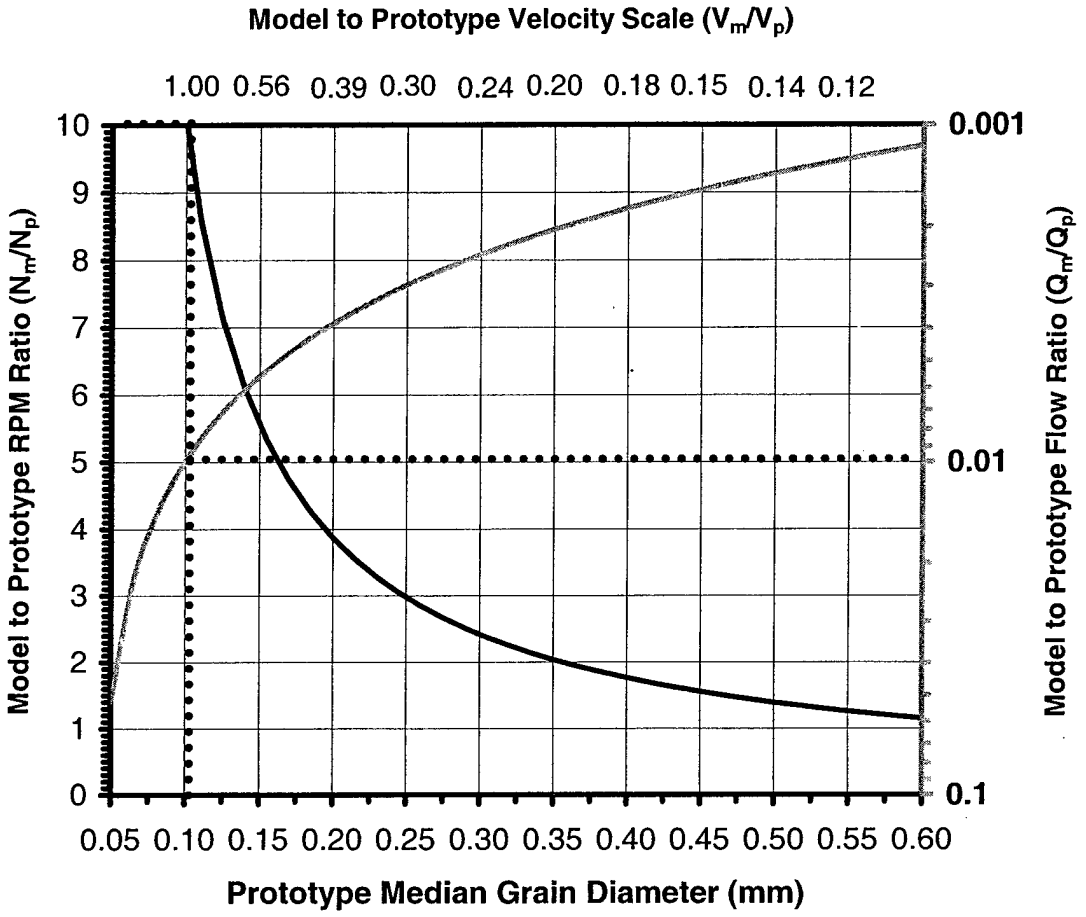

Figure 6.2: Model Dredge Basis of Design

6.1.1 Example Cutter/Suction Dredge

The first modeling example is that of a 61 cm (24 in) cutter/suction dredge. The prototype dredge employs a 183 cm (72 in) diameter by 152 cm (60 in) long cutterhead with a blade pitch of 6 and an average profile angle of 25 degrees. The prototype operates at 22,937 LPM (30,000 GPM) and pumps an average slurry specific gravity of 1.3. Prototype swing speed is about 40.6 cm/s (16 in/s) with a 2045 m^3 (2675 cy/hr) production when cutting a 91 cm (3 ft) deep cut in

12.2 m (40 ft) of water with a 45 degree ladder angle. The cutterhead rotates at 40 rpm and is cutting in medium-fine sand with an average median grain diameter of 0.2 mm. The purpose of the model test is to determine the effect of swing speed on production for a given cutterhead design. The example experiment models several different runs at prototype swing speeds ranging from 30.5 – 50.8 cm/s (12 - 20 in/s) while keeping all other parameters constant.

The dredge carriage is designed to test large dredges at scales close to 1:10 scale. This will be the first length scale chosen. Figure 6.3 shows how the chart is applied to the prototype at a 1:10 geometric scale.

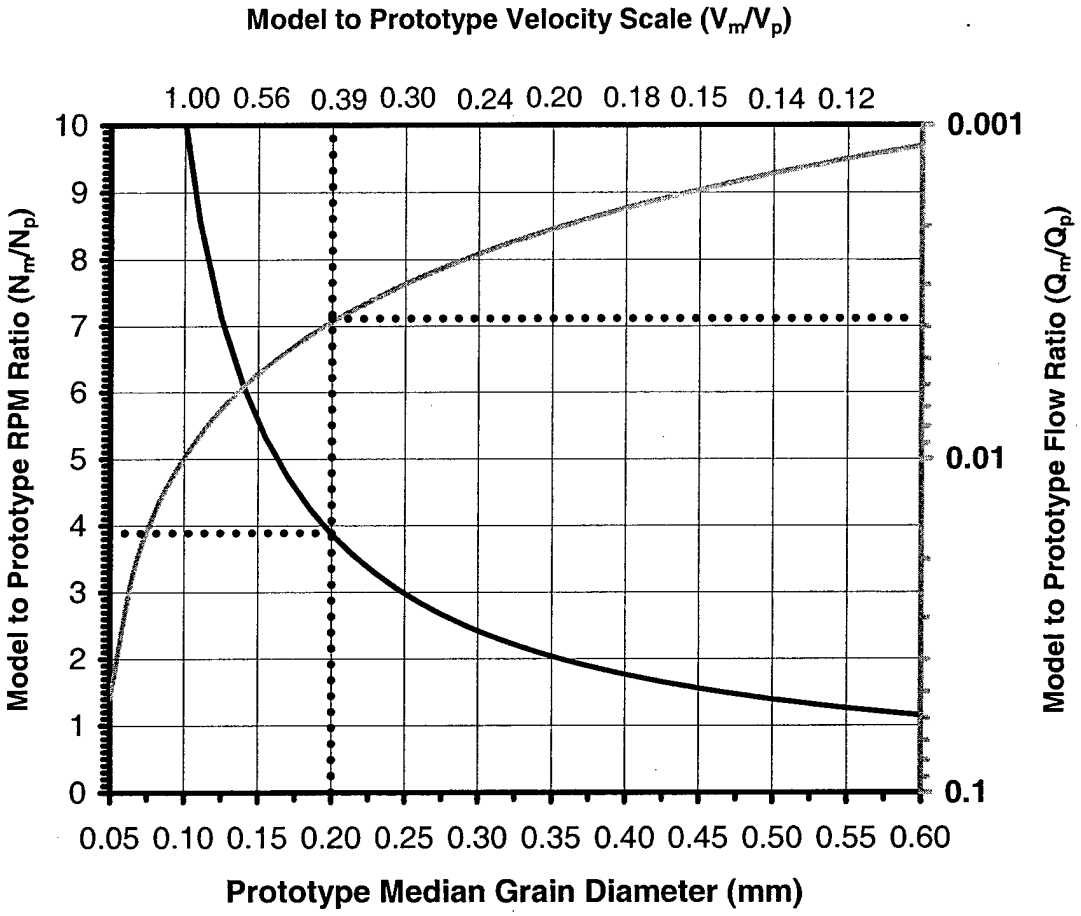

Figure 6.3: Model Dredge Operating Parameters for Cutter/Suction Dredge Example (1:10 Scale)

Table 6.1 summarizes the model and prototype operating parameters for a 1:10 geometric scale.

Table 6.1: Model and Prototype Operating Parameters for Cutter/Suction Dredge Example (1:10 Scale)

Parameter	Prototype	Model	Scale
Cutter Diameter	183 cm (72 in)	18.3 cm (7.2 in)	1:10
Water Depth	12.2 m (40 ft)	3.35 m (11 ft)	N/A*
Depth of Cut	91.4cm (36 in)	9.14 cm (3.6 in)	1:10
Sediment Diameter	0.2 mm	0.1 mm	N/A*
Settling Velocity	22.7 mm/s	8.8 mm/s	0.388
Suction	61 cm (24 in)	38 mm (2.4 in)	1:10
Flow Rate	113,562 LPM (30,000 GPM)	440 LPM (116 GPM)	0.004
Cutter rpm	40	155	3.88
Max Swing Speed	50.8 cm/s (20 in/s)	19.7 cm/s (7.76 in/s)	0.388

* These parameters do not follow any scale law, but are set by the experimental set-up.

Table 6.1 shows the model suction inlet velocity scaled according to the length scale. However, this may be unnecessary as the velocity field created by the suction inlet is not dependent on suction inlet velocity. If the resulting model dredge operating parameters are run through cutting force simulation, a maximum possible cutterhead swing velocity of 65.5 cm/s (25.8 in/s) is possible at the indicated depth of cut based on the available cutterhead power. The side winch pull force at this speed is estimated to be 6917 N (1555 lb), more than the 3556 N (800 lb) allowed by the guide rods. This also requires 4.5 kW (6 hp) of side winch power, 200% of what is available. However, according to the computed velocity scale, maximum model swing speed would not need to exceed roughly 20 cm/s (8 in/s). At this speed, only 1730 N (389 lb) of horizontal cutting force is generated by the model dredge. Only about 0.35 kW (0.50 hp) of side winch power is required to achieve this. Clearly, the model dredge, as designed, is capable of performing this experiment at 1:10 scale.

The 61 cm (24 in) dredge is considered a medium size dredge and the tendency when modeling smaller prototypes is to build the model to a larger scale so that any adverse scale effects are minimized. To see if the model dredge can do this, the geometric scale for this example will be changed to 1:6. The experimental setup will now employ a model cutterhead measuring 30.5 cm

(12 in) in diameter by 25.4 cm (10 in) long. Figure 6.4 shows how the chart is applied to the prototype at a 1:6 geometric scale.

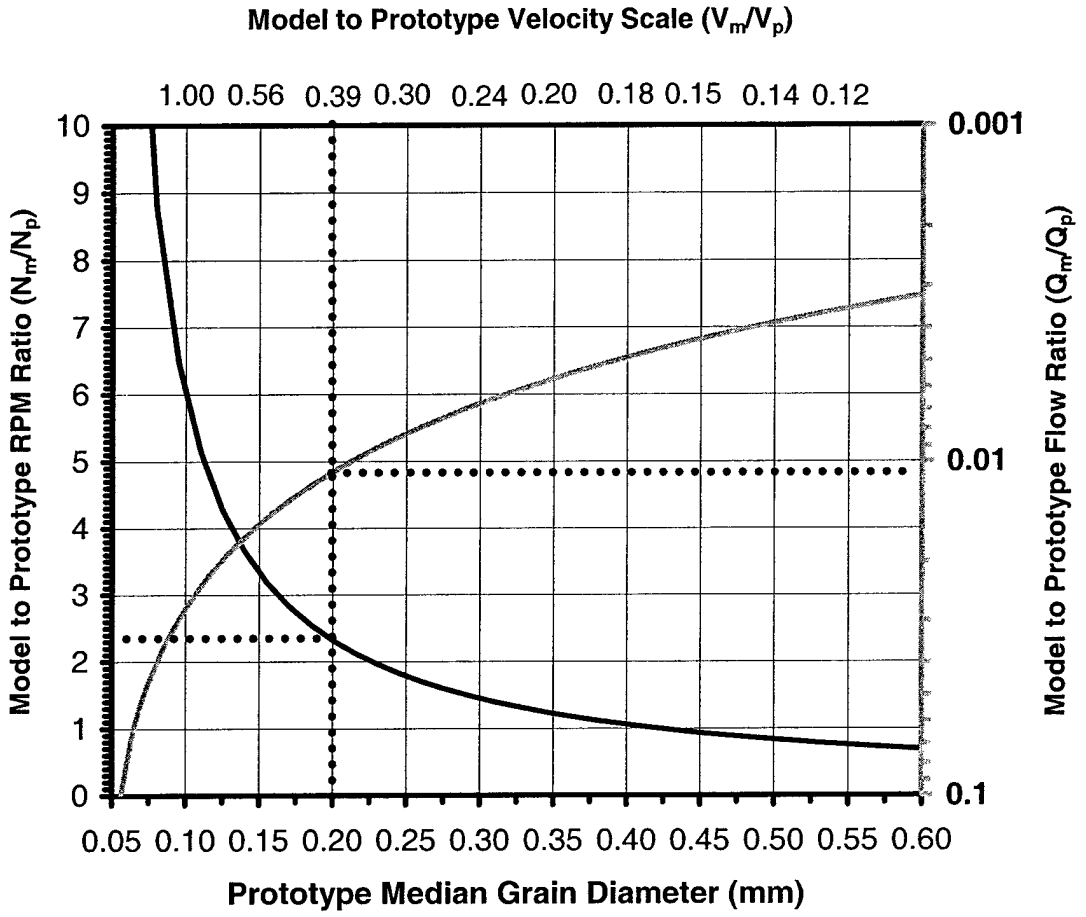

Figure 6.4: Model Dredge Operating Parameters for Cutter/Suction Dredge Example (1:6 Scale)

Table 6.2 summarizes the model and prototype operating parameters for a 1:6 geometric scale.

Table 6.2: Model and Prototype Operating Parameters for Cutter/Suction Dredge Example (1:6 Scale)

Parameter	Prototype	Model	Scale
Cutter Diameter	183 cm (72 in)	30.5 cm (12 in)	1:6
Water Depth	12.2 m (40 ft)	3.35 m (11 ft)	N/A*
Depth of Cut	91.4cm (36 in)	15.2 cm (6 in)	1:6
Sediment Diameter	0.2 mm	0.1 mm	N/A*
Settling Velocity	22.7 mm/s	8.8 mm/s	0.388
Suction	61 cm (24 in)	7.62 cm (3 in)	1:8
Flow Rate	113,562 LPM (30,000 GPM)	1223 LPM (323 GPM)	0.011
Cutter rpm	40	124	3.104
Max Swing Speed	50.8 cm/s (20 in/s)	19.7 cm/s (7.76 in/s)	0.388

* These parameters do not follow any scale law, but are set by the experimental set-up.

The scaled model quantities above satisfy the requirements for geometric, hydraulic, kinematic similitude. The exception is dynamic similitude of cutting forces with respect to cavitation. This was also true in the 1:10 scale example but will be explained in detail here. The water depths listed in Tables 6.1 and 6.2 give a cavitation coefficient of 1.659 according to Equation 3.8. According to Equations 3.9 and 3.10, the model cutterhead rpm and swing speeds would need to be 651 rpm and 147 cm/s (58 in/s) respectively. While the similitude requirement for layer geometry would be satisfied (Equation 3.20), hydraulic similitude with respect to spillage (Equation 3.14) would be compromised. This means that a disproportionate amount of slurry will be spun outside of the range of influence of the suction inlet and not be picked up. One solution would be to solve for a new cavitation coefficient that satisfies all of the similitude requirements. This gives a new cavitation coefficient of 8.71. According to Equation 3.8, this new cavitation coefficient requires a model water depth of -7.5m (-24.62 ft). This means operating the model dredge in a complete vacuum with a little more than 2.44 m (8 ft) of water depth. Since this solution is not practical and since production similarity is more important than cutting force similarity for this particular experiment, no attempt will be made to satisfy Equations 3.20 and 3.21.

Table 6.2 does not show the model suction inlet velocity being scaled according to the length scale. A 10.2 cm (4 in) diameter suction inlet is required to achieve this. However the author believes that this may be unnecessary as the velocity field created by the suction inlet is not

dependent on suction inlet velocity. It is important to note that changing the geometric scale ratio does not change the velocity scale at the top of the chart, since this is based solely on median grain diameter. However, as Table 6.2 shows, building a larger model requires a larger flow rate to increase the size of the velocity field created by the suction, and a lower cutterhead rpm so that the tangential velocity of the cutterhead blades follow the velocity scale. If the resulting model dredge operating parameters are run through cutting force simulation, a maximum possible cutterhead swing velocity of 23.6 cm/s (9.3 in/s) is possible at the indicated depth of cut based on the available cutterhead power. The side winch pull force at this speed is estimated to be 4130 N (928 lb), more than the 3556 N (800 lb) allowed by the guide rods. Only 1.0 kW (1.3 hp) of side winch power is required, less than half of the available power. However, since changing the length scale did not change the computed velocity scale, maximum model swing speed would still not exceed approximately 20 cm/s (8 in/s). At this speed, only 3505 N (788 lb) of horizontal cutting force is generated by the model dredge and there is more than enough side winch power available to pull the dredge carriage. If a high-yield stainless steel is used to fabricate the model dredge guide rods, this force would be well below safe operating levels. Less than 0.7 kW (0.84 hp) are required to pull the dredge carriage with the estimated force and velocity. Clearly, the model dredge, as designed, is capable of performing this experiment at a 1:6 geometric scale.

Recall that the purpose of the experiment is to determine the effect of swing speed on production. Model tests are conducted with the full range of swing speeds required by the velocity scale and data are collected. Higher swing speeds may result in a lower production than indicated because of spillage. Since the cutterhead rpm, swing speed, and suction inlet velocity have all been kinematically scaled to the prototype, the scale ratios for cutterhead rpm and swing speed listed in Tables 6.1 and 6.2 should provide for the quantitative interpretation of data. Other recorded quantities such as cutterhead forces, cutterhead power, pump power, slurry specific gravity, and pump head are not readily scalable up to prototype quantities until more research is done to determine the scale effects of not achieving dynamic similarity with respect to the cavitating cutting process. However, the qualitative effect of the swing speed on these quantities can still be easily observed.

6.1.2 Example Hopper Dredge

The second modeling example is that of a 76.2 cm (30 in) hopper dredge. The prototype dredge employs an 213 cm (84 in) long by 183 cm (72 in) wide draghead with 25,806 cm^2 (4000 in^2) of suction area. The prototype operates at 189,270 LPM (50,000 GPM) and pumps an average slurry specific gravity of 1.3. Prototype draghead speed is about 30.5 cm/s (12 in/s) with a 3407 m^3/hr (4456 cy/hr) production when operating in 18.3 m (60 ft) of water. The draghead is picking up medium-fine sand with an average median grain diameter of 0.15 mm. The purpose of the model test is to determine the effect of biological exclusion devices on dredge production for a given draghead design. Biological exclusion devices effectively reduce the area of suction by covering the suction inlet with a grating to keep out certain forms of marine life. The effectiveness of the devices, as well as their effect on performance needs to be determined. The model test simulates several different runs using various attachments while keeping all other parameters constant. Model tests can also be conducted in the presence of neutrally buoyant mock turtles scaled down to the appropriate size to ensure they are excluded from the suction by the attachment.

The model draghead is a perfect 1:10 scale geometric replica of the prototype measuring 21.3 cm (8.4 in) long by 18.3 cm (7.2 in) wide with 258 cm^2 (40 in^2) of suction area. Figure 6.5 is used to calculate the remaining operating parameters.

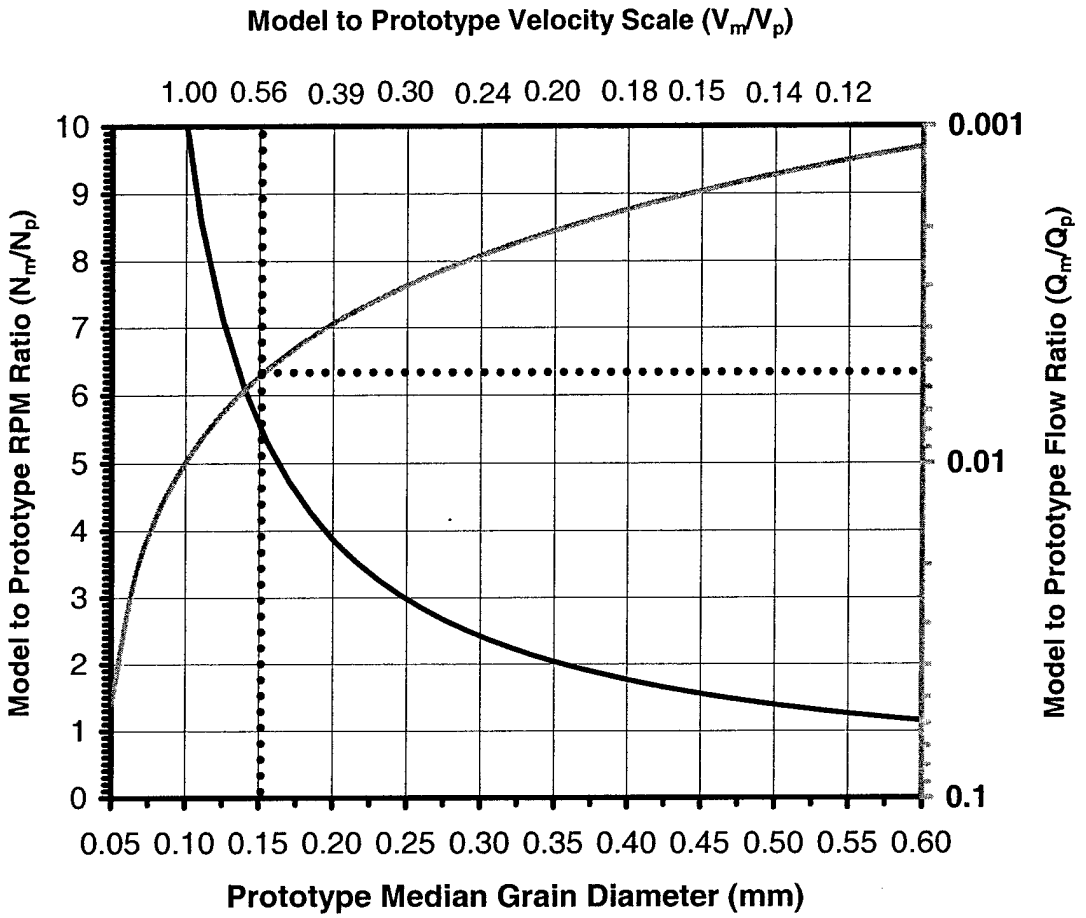

Figure 6.5: Model Dredge Operating Parameters for Hopper Dredge Example

It is important to note that when using the chart for a hopper dredge, the left axis is not needed. Table 6.3 summarizes the model and prototype operating parameters.

Table 6.3: Model and Prototype Operating Parameters for Hopper Dredge Example

Parameter	Prototype	Model	Scale
Cutter Size	213 cm (84 in) x 183 cm (72 in)	21.3 cm (8.4 in) x 18.3 cm (7.2 in)	1:10
Water Depth	18.3 m (60 ft)	3.05 m (10 ft)	N/A*
Sediment Diameter	0.15 mm	0.10 mm	N/A*
Settling Velocity	15.8 mm	8.8 mm	0.557
Suction	25,806 cm^2 (4000 in^2)	258 cm^2 (40 in^2)	1:100
Flow Rate	189,270 LPM (50,000 GPM)	1052 LPM (278 GPM)	1:180
Draghead Speed	30.5 cm/s (12 in/s)	16.9 cm/s (6.67 in/s)	0.557

* These parameters do not follow any scale law, but are set by the experimental set-up.

The scaled model quantities above satisfy the requirements for geometric, hydraulic, and kinematic similitude. The effect of cavitation on the cutting process is assumed to be negligible since the draghead removes sediment primarily by means of suction and sediment pick-up. Therefore no attempt is made to achieve dynamic similitude of cutting forces with respect to cavitation. Moreover, without a cutter digging in the sediment, the forces acting on the draghead are much less than those acting on the cutterhead. As a result, the model dredge is in no danger of failure while modeling hopper dredge operations.

Interpreting the results of such an experiment is straightforward. Model dredge production data taken without the biological exclusion device is normalized to the prototype production via a scale ratio. Model dredge production data are taken with the various devices. The recorded quantities are scaled to prototype quantities using the scale ratio. Results from such a study should give an accurate indication on exactly how such devices affect the performance of full-scale prototypes.

6.2 Conclusions

As the first example shows, the specific energy method and its corresponding cutting theory can be helpful in checking the model cutterhead loading for any given model operating parameters. The specific energy method is used to determine the maximum possible swing speed for each

required depth of cut based on the available cutterhead power of 11.7 kW (15.7 hp) and the maximum model production of 31.5 m^3 (41.2 cy). Once the required cutterhead power is computed for each swing speed and depth of cut, horizontal, vertical, and axial cutting forces can be estimated by using the cutting theory presented in Chapter IV. Table 4.5 lists the cutting forces used to design the model dredge. The cutterhead loading is then run with the static analysis for both the undercutting and overcutting conditions (-/+ vertical cutting force) for the required digging depth and ladder angle. The static analysis used to design the model dredge is included in Appendix B as a reference. Thus the operating parameters of the experiment are tested against the model dredge to ensure that maximum permissible loads are not exceeded. Since the specific energy method represents the upper limit of cutting forces for a cavitating cutting process, actual model cutting forces will likely be lower. While the PLC feedback and control system will not allow the model dredge to be operated beyond its structural limits, the model operating parameters, specifically the geometric scale, must be carefully selected so that the threat of structural failure does not limit the users' ability to conduct thorough model investigations.

According to Equations 3.20 and 3.21, the model dredge would have to operate in a vacuum in order to achieve the level of cavitation achieved by the prototype dredges. Therefore, similarity with respect to the cutting forces developed by the cutterhead is not expected to follow the dynamic scale laws. Perhaps new scale laws that compensate for the absence of cavitation in the model dredge can be developed through model testing.

Scaling down the operating parameters for a hopper dredge is fairly straightforward. Excessive cutting forces do not threaten the integrity of the model dredge and cavitation is not a factor. The size of the sediment pit, however, does limit the distance each test run can achieve. If longer test runs are required, one possible solution is to spread a few inches of sediment outside the pit along the length of the tank.

CHAPTER VII

SUMMARY AND CONCLUSIONS

7.1 Summary

This thesis investigates the model scaling relationships that have been proposed for hydraulic dredging operations. Several studies and papers are examined dating back over 60 years. The Army Corps of Engineers Waterways Experiment Station, the Hydraulics Laboratory and Dredging Technology Laboratory at the Technical University of Delft, and the Texas A&M Hydromechanics Laboratory are other facilities where the modeling of hydraulic dredging operations has been performed. Between these three institutions, only a handful of studies involving the modeling of large hydraulic dredge equipment have been published. In addition to laboratory studies, several researchers have performed dimensional analyses on selected operating parameters to obtain similitude relationships for scaling the relevant quantities. Many of these relationships have been tested, but some of them either contradict one another or cannot be physically satisfied, even in a laboratory setting. This presents many challenges to the quantitative analysis of data obtained by the scaled model testing of hydraulic dredging operations. Because of this, the results of such model studies have been traditionally been limited to only a qualitative interpretation of the data.

This thesis takes the model scaling relationships that have been developed through experimentation and dimensional analysis and applies them to the design of a model dredge apparatus. The proposed tow carriage is to ride atop the towing tank at the Texas A&M University Coastal Engineering Laboratory and includes the model dredge carriage attachment. The proposed model dredge carriage contains the model suction, cutter, ladder, and winches to perform the scaled model testing of hydraulic dredge operations. The design allows the dredge carriage to be removed from the tow carriage during towing operations so that the dredge ladder does not interfere with the model being towed. A rationale for designing the tow and dredge carriages and selecting the required equipment is also presented in this thesis. This same rationale is used to select the operating parameters for model dredge experiments.

Rather than attempt to derive new scaling laws or sort out between the various similitude relationships what scale laws should apply to the various dredging scenarios, this thesis uses the scaling relationships to set the boundaries for the key operating parameters of a model dredge. The operating parameters considered are: median grain size of the sediment, suction velocity, suction flow rate, cutterhead rpm, cutterhead swing speed, pump power, cutter drive power, and the horizontal, vertical, and axial cutting forces on the cutterhead. An operating range must be established for these quantities so that the appropriate equipment can be selected for the laboratory facility. The author believes that the operating parameters of a model dredge apparatus should not be the limiting factor when performing model studies. Therefore a useful laboratory dredge facility should have the capability to perform 1:10 scale model studies on large prototype dredges under the most extreme conditions.

To accomplish this, the scale laws are divided into geometric, kinematic, and dynamic similitude relationships, as well as Reynolds and Froude relationships. A large 76.2 cm (30 in) cutter suction dredge pumping 189,270 LPM (50,000 GPM) was used as the prototype dredge. The scale laws are applied to the prototype dredge to determine the maximum required flow rate, swing speed, and cutterhead rpm. This allows the size of the model pump motor, suction pipe, cutter drive, side winches, tow carriage drive, and sediment grain diameter to be determined. The specific energy method is used to estimate the vertical, horizontal, and axial cutting forces acting the model cutterhead. A static analysis is performed on the proposed tow and dredge carriage designs using the estimated cutting forces to ensure the structural integrity and stability of the entire assembly during operation.

Since the dredge carriage must be removable by the overhead crane, its weight is limited by the crane capacity to 2721 kg (6000 lb). Therefore, to ensure the maximum structural rigidity and stability during model dredging operations, the entire weight allowance for the dredge carriage is used. For some of the operating parameters, such as side winch power and tow carriage drive power, the maximum values are determined not by the scale laws, but rather by the structural limits of the model dredge itself. The reasons for this are based on the uncertainty of the various similitude relationships. Recall that many of the proposed scale laws have not been tested and some were only developed through dimensional analysis. Other scale laws were derived from full-scale prototype operating data, and it is uncertain as to how well these relationships hold

together on a small 7.62 cm (3 in) dredge. These uncertainties complicated the equipment selection process and require an alternate method to determine the maximum swing winch power and tow carriage drive power. Therefore, drives were selected that push the dredge carriage structure up to its failure point. During normal operation, it is not expected that the operating parameters will ever reach this limit. In fact, the feedback/control system built into the PLC can prevent this from ever happening. However, the author believes that because of the uncertainty in scaling the side winch and tow carriage advance power, as much power as the model dredge can handle should be available to the operators.

The tow and dredge carriages are equipped with a data acquisition and control system that allows for manual or automated operation. Instrumentation monitors several parameters such as pump rpm, pump torque, pump suction/discharge pressures, flow rate, slurry density, cutterhead x/y/z position, side winch pull force, vertical cutting forces, cutter rpm, cutter torque. During a towing operation, a load cell records the drag forces of the towed payload in three dimensions. These data are digitized and relayed to the Programmable Logic Controller (PLC) via the input/output modules. The PLC contains an internal clock that is used with some of the input data to calculate carriage speed, swing speed, pump brake and water horsepower, cutter horsepower, and dredge efficiency. The data are forwarded to the operators PC from the PLC via a serial cable and stored in data files on the PC's hardrive. The data can also be displayed on the PC's monitor in real time as a virtual control panel.

Control of the model dredge can be either manual or automatic with automatic being the normal mode of operation. Automation eliminates the variation between model test runs where data from several identical testing sequences are required. An operating sequence can be programmed by the PC, uploaded to the PLC and executed on command. The PLC has direct control over all of the drives and motors via a bank of high-power relays. Several different operating sequences can be stored in the PC for use at any time. In addition to the various automated programs, a program that allows the model to function based on manual input rather than the collected data can be written and stored in the PC. Such a manual program takes input from a manual control panel attached to the PC as peripheral device and uses these data to operate the dredge.

Two different examples of a modeling experiment are described. The first example is a 61 cm (24 in) cutter/suction dredge. This example shows how the model operating parameters can be adjusted by selecting different prototype median grain diameters and geometric length scales. In this example, a prototype dredge smaller than the prototype dredge selected for the design of the apparatus is used. Normally in hydrodynamic modeling, a smaller prototype dredge means that a smaller scale ratio can be used. Using a 1:6 scale rather than a 1:10 scale can reduce any scale effects and give more useful data. However, as the example shows, reducing the length scale causes the maximum achievable swing speeds to decrease and the cutting forces to increase. In both the 1:10 scale and 1:6 scale examples, the physical limits of the model dredge carriage were not exceeded. This example demonstrates the flexibility built into the model dredge and its ability to model different sized dredges at different scales. Another consideration is to ensure that operation of the model dredge carriage is not limited by the power of the drives or the structural integrity of the carriage frame. This is accomplished by taking the output from the cutting force analysis and using it run the static analysis model performed in Appendix B. This will determine the maximum loads on the key structural members and the stability of the model dredge during operation.

It seems counter-intuitive that the lower cutterhead rpms associated with smaller scale ratios give rise to higher cutting forces. However, the derivation of the cutting forces is based on the specific energy method, which assumes that to remove a cubic yard of in situ sediment at a given level of compaction based on a Standard Penetration Test, a specific amount of energy is required from the cutterhead (regardless of cutterhead rpm). Therefore, cutterhead power is directly related to the production rate. All other parameters being equal, torque on the cutterhead must increase if the rpms are reduced in order to maintain the same shaft power. The principle cutting forces (horizontal, vertical, and axial) are derived from torque. The specific energy method and the cutting theory were developed using empirical data taken from large prototype dredges. It may not accurately predict cutting forces and production for a small 7.62 cm (3 in) laboratory dredge.

The second example is a large 76.2 cm (30 in) hopper dredge. Since no cutting force or swing winch power is addressed, care is taken to properly scale the suction so that similarity with

respect to sediment pickup behavior is maintained. This is a fairly straightforward process compared to the care that is taken to ensure proper scaling of a cutterhead dredge.

7.2 Conclusions

By using the scale laws as presented in this thesis, virtually any prototype dredge can be modeled by the proposed model dredge. The limitations that determine the selection of the cutterhead rpm ratio and the cutterhead diameter ratio are the structural limits of the model dredge. That being said, some operating parameters will work better than others. For example, large prototype grain sizes necessitate a sharp reduction in model flow rate. This also requires a very small velocity scale, which affects cutter rpm and swing. Lowering the cutterhead rpms has the potential to cause higher cutting forces. However, the swing speeds usually are lowered by the same factor as the cutterhead rpms. As the example showed, the slow swing speeds tend to keep the cutting forces from becoming too great when the velocity scale and model rpms are reduced. In general, modeling finer sediment should give better results since cutting speeds are higher and the scale effects of the cavitating cutting process are reduced.

Smaller prototype dredges can allow a larger geometric scale to be used. This was shown in the example with the 1:10 and 1:6 scale cutter/suction dredge models. Larger geometric scales will required greater model flow rates and care must taken not to exceed the model dredge design value of 1893 LPM (500 GPM). Another side effect of smaller geometric scales is that larger cutterheads have lower maximum model swing speeds. This is a result of the maximum production capable from a 11.7 kW (15.7 hp) cutterhead. As a result, the velocity scale must be small enough so that the required model swing speeds are less than the maximum. If the prototype dredge operates in fine sand, then the velocity will be 1.0 and model swing speeds may exceed the maximum. In these cased, the geometric scale will have to be reduced until a workable set of model dredge operating parameters are found. As a practical matter, model cutterheads larger than 30.5 cm (12 in) in diameter should not be used so that proper clearance with the tank walls is maintained.

Once the operating parameters are selected, the cutting forces predicted by the specific energy method should be calculated for the selected parameters. The static analysis model should then

be performed using the estimated cutting forces. This will check the operating parameters to ensure that the predicted cutting forces do not overload the model dredge and cause the control system to cease operations.

The scale laws used to design the model dredge are based on hydraulic similarity between model and prototype. That is, kinematic similarity exists for the velocity fields created by the suction inlet, cutterhead rotation, and swing speed. This ensures that the sediment pick-up behavior of the model dredge will imitate the sediment pick-up behavior of the prototype dredge according the scale laws. Dynamic similarity between model and prototype with respect to the cutting forces can not be established according to the scale laws because of the cavitation coefficient. As shown by the cutter/suction modeling example in Chapter VI, the model dredge would have to operate in a vacuum or have the cutting speeds drastically increased in order to obtain the same degree of cavitation during cutting that exists in the prototype. This means that similarity with respect to the cutting forces cannot be obtained with the proposed model dredge design without compromising hydraulic similarity. If the cutting speeds (cutterhead rpm and swing speed) are increased so that similarity is obtained with respect to cavitation, then kinematic similarity with respect to sediment pick-up behavior will be lost. These limitations and the degree of the related scale effects will need to be studied after the proposed model dredge becomes operational. The relationship between suction inlet velocity and the cutterhead kinematics will also have to be explored.

The model dredge proposed in Chapter V is simply one workable concept variant. The actual model dredge build and installed in the Texas A&M University Coastal Engineering Laboratory may be slightly different from that which is proposed in this thesis. However, the scaling laws examined and how they apply to the task of designing such facilities should aid those involved in constructing such an apparatus. The fact remains that little solid data exists to verify the numerous similitude criteria proposed over the last 60 years. Several relationships have been proposed and examined in Chapter II, but many of these are either inconsistent or impossible to satisfy physically. The design methodology employed by the author seeks not to determine what criteria should be accepted and rejected. This can only be accomplished by experimentation once such facilities are operational. The methodology used in this thesis seeks to build a model

dredge capable of utilizing each of the proposed scaling laws such that the operating parameters of the individual experiments are not limited by the laboratory facilities.

The dredge modeling facility at Texas A&M University will be available for use by commercial and academic institutions for a variety of research and testing (Randall et al. 1998, deJong 2002). These facilities will be an invaluable asset to the dredging community and will serve the dredging industry for many years. Table 7.1 lists a sample of possible studies and research topics that could be conducted in the new Texas A&M Coastal Engineering Laboratory. The list is by no means all-inclusive as there is any number of topics and issues that could be explored.

Table 7.1: Possible Studies for Proposed Laboratory Facilities

Testing of proposed hydraulic dredge similitude criteria for 1:10 model scaling
Influence of suction velocity on sediment pickup
Relationship between cutter swing velocity, cutting power, and swing winch pull force
Influence of cutter swing velocity and cutting face/advance on spillage and final dredging depth
Performance of different cutterhead geometries, various length and diameter ratios, blade angles, pitch, etc.
The performance effects of environmental protection devices on dredge suction intakes
Influence of the cutter speed on spillage due to centrifugal action of the cutterhead
Performance of "reverse cone cutter" or "backfeeder" type cutterhead designs
Performance effects of cavitation on cutters and dragheads
Turbidity generation and flow visualization around cutterheads and dragheads
Investigation of capping techniques for open water disposal of contaminated sediments
Testing of hydraulic dredge instrumentation and automation
Turbidity generation of open water disposal techniques for dredged material
Testing the effectiveness of environmental protection devices such as biological exclusion devices
Performance of different hydraulic draghead types and effects of design improvements
Bank height effects on sediment flow to cutterhead
Pore water pressure variation in sediment caps
Modeling open water disposal of dredged material from a hopper, barge, or pipeline
Effectiveness of reverse slurry flow through a draghead for sediment capping
Studying the physics of dredged material behavior falling through the water column
Testing of new instruments to monitor hopper contents and overflow
Deepwater dredging research and development up to 150 ft for 1:10 scale models
Testing of new draghead instrumentation for improved cutting accuracy
Testing and development of remotely operated dredges or trenchers

REFERENCES

Army Corps of Engineers, (1947). *Model Study of Suction Head, Dredge Jadwin.* Technical Report No 2-232, U.S. Army Engineers Waterways Experiment Station, Vicksburg, MS.

Army Corps of Engineers, (2000). *Dredging: Building and Maintaining our Underwater Highways.* U.S. Army Corps of Engineers, Washington D.C.

Brahme, S.B., and Herbich, J.B. (1986). *Hydraulic Model Studies for Suction Cutterheads.* Journal of Waterway, Port, Coastal and Ocean Engineering, ASCE, Vol. 112, No. 5, pp. 590-607.

Burger, M.D. (1997). *Mixture Forming in a Cutterhead.* Proceedings of the Central Dredging Congress Dredging Days, CEDA 1997, Amsterdam, the Netherlands.

DeJong, P.S. (2002). *Personal Communication.* President, Digital Automation and Control Systems, Inc., Houston, TX.

Franco, J.J. (1967). *Model Study of Hopper Dredge Dragheads.* Technical Report No 2-755, U.S. Army Engineer Waterways Experiment Station, Vicksburg, MS.

Gere, J.M., and Timoshenko, S.P. (1990). *Mechanics of Materials,* Third Addition. PWS-Kent, Boston, MA.

Glover, T.J. (1999). *Pocket Ref, Second Edition.* Sequoia Publishing, Inc., Littleton, CO.

Herbich, J.B., and Brahme, S.B. (1983). *Literature Review and Technical Evaluation of Sediment Resuspension during Dredging.* Report No. COE-266, Ocean and Hydraulic Engineering Group, Texas A&M University, College Station, TX.

Herbich, J.B. (2000). *Handbook of Dredging Engineering,* Second Edition. McGraw-Hill, New York, NY.

Huston, J.W., and Huston, W.C. (1976). *Techniques for Reducing Turbidity with Present Dredging Procedures and Operation.* Technical Report D-76-4, U.S Army Engineer Waterways Experiment Station, Vicksburg, MS.

Joanknecht, L.W.F. (1976). *A Review of Dredge Cutterhead Modeling and Performance.* Proceedings of the Seventh World Dredging Congress, WODCON VII, San Francisco, CA, pp. 995-1016.

Johnson, B.H., McGee, R.G., and McCarley, R.W. (1989). *Modeling the Disposal of Dredge Material in a Physical Test Facility.* U.S. Army Engineer Waterways Experiment Station, Vicksburg, MS.

Miedema, S.A. (1987). *Calculation of the Cutting Forces When Cutting Water Saturated Sand.* Doctoral Dissertation at Delft University of Technology, Delft, the Netherlands.

Miedema, S.A (1989). *On the Cutting Forces in Saturated Sand of a Seagoing Cutter Suction Dredger.* Proceedings of the 12th World Dredging Congress, WODCON XII, Orlando, FL, pp. 331-352.

Miedema, S.A. (1995). *Production Estimation Based on Cutting Theories for Cutting Water Saturated Sand.* Proceedings of the 14th World Dredging Congress, WODCON XIV, Amsterdam, the Netherlands, pp. 255-275.

Mol, A. (1977a). *Flow in and around a Cutterhead: Part II, Rotating Freely in Water: Injections with Dye.* Delft Hydraulics Laboratory, Delft, the Netherlands.

Mol, A. (1977b). *Flow in and around a Cutterhead: Part III, Flow in a Cutterhead With an Artificial Breach, Injections with Pieces of Plastic.* Delft Hydraulics Laboratory, Delft, the Netherlands.

Randall, R.E., Edge, B.L., and Cox, D.T. (1998). *Laboratory Needs for Dredging and Dredged Material Disposal.* Proceedings of the 15th World Dredging Congress, WODCON XV, Las Vegas, NV, pp. 17-29.

Slotta, L.S. (1968). *Flow Visualization Techniques Used in Dredge Cutterhead Evaluation.* Proceedings of the 1968 World Dredging Congress, WODCON II, Rotterdam, the Netherlands, pp. 56-77.

Tetra Tech, Inc. (1988). *Preliminary Design for Dredged Material Placement Physical Modeling Facilities.* Tetra Tech, Inc., Arlington, VA.

Vlasblom, W.J. (1998). *Relation Between Cutting-, Sidewinch-, and Axial Forces for Cutter Suction Dredgers.* Proceedings of the 15th World Dredging Congress, WODCON XV, Las Vegas, NV, pp. 275-291.

Wilson, K.C., Addie, G.R., and Clift, R. (1997). *Slurry Transport Using Centrifugal Pumps.* Elsevier Applied Science, New York, NY.

APPENDIX A

TOW/DREDGE CARRIAGE EQUIPMENT AND SPECIFICATIONS

Tables A.1, A.2, A.3, and A.4 are sample equipment lists for the proposed tow/dredge carriage design. In some cases, several manufacturers produce similar equipment or a similar product. The items chosen represent, by example, the type and nature of the equipment needed to fulfill the stated operating requirements and do not constitute endorsements of a particular company or manufacturer. Weights listed in italics indicate an estimated weight when actual equipment weights are not available. Maximum allowable weights for custom fabricated parts are also indicated.

Table A.1: Sample Equipment List and Specifications for the Ladder

Item/Cost	Description/Manufacturer	Size	Weight
Cutterhead $250	6 blade, conical	30.5cm x 25.4cm (12 in x 10 in)	*11 kg* *25 lb*
Cutter drive shaft, lower $200	Stainless steel, solid	5.08cm x 137cm (2 in x 54 in)	22 kg 48 lb
Suction pipe, lower $75	Stainless steel	2.54cm ID x 137cm (3 in ID x 54 in)	7 kg 16 lb
Double universal joint $225	70 degree operating range Stainless steel Curtis Universal Joint Company	10.2cm x 43.2cm (4 in x 17 in)	19 kg 42 lb
Swivel joint $130	One plane of motion, stainless steel Cabris Inc., Style 30	10.2 cm (4 in) x 90	*4.5 kg* *10 lb*
Ladder frame $2000	Galvanized Steel	See Figure A.1	*<45 kg* *<100 lb*
			Total Estimated Ladder Weight = 109 kg (241 lb)

The cutterhead specified is consistent with the "model dredge" parameters used to develop the operating requirements in Chapter IV. However, a smaller or larger cutter could be used depending on the size of the prototype being modeled. If a larger diameter cutter is used, care must be taken so that no contact occurs between the cutterhead and the tank walls or sediment pit bottom. The lower suction pipe inlet should be able to accept fittings with smaller inlet diameters when needed to maintain a geometric similarity between suction inlet diameters.

The double universal joint specified only allows for a 70 degree operating range. The predicted loading on the model dredge due to the cutting forces was based on a 90 degree operating range. On a full-sized dredge, the normal range of the ladder angle is somewhere between 20 and 60 degrees with the horizontal. Never would a ladder be perfectly horizontal (0 degrees) or perfectly vertical. Therefore, a 70 degree operating range should be sufficient. However, if 90 degrees is needed, a gear system rather than a universal joint could be used.

Figure A.1 shows a conceptual drawing of the ladder frame. If constructed from 12.7 mm (0.5 in) thick steel, the weight would be approximately 38.5 kg (85 lb). This weight does not include any bearings required for the cutter drive shaft (bushings are recommended because of sub-marine operating environment). If more than 45 kg (100 lb) are needed for the entire ladder weight, care must be taken to ensure that the dredge carriage assembly does not exceed 2721 kg (6000 lb)

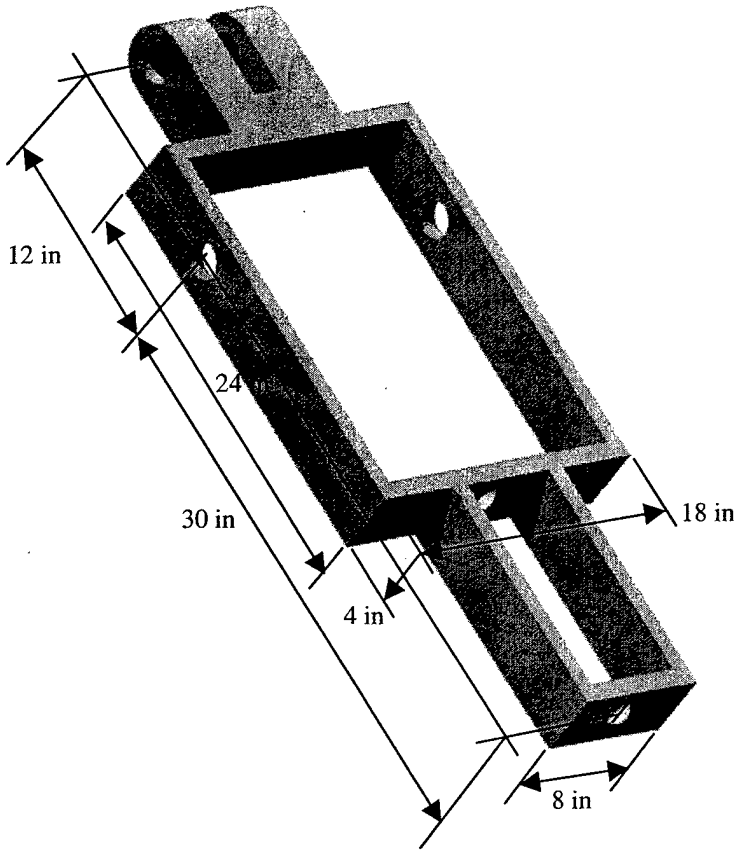

Figure A.1: Conceptual Drawing of the Ladder Frame

Table A.2: Sample Equipment List and Specification for the Ladder Arm

Item/Cost	Description/Manufacturer	Size	Weight
Rotary position sensor $150	70 degree range, potentiometer Novotechnik U.S., Inc.	Not given	N/A
Linear actuator (rod and screw type) $250	18 in travel, 1000 lb dynamic load 5000 lb static load, water tight seal Burr Engineering & Development Compact 1000 Series	66 cm (26 in) retracted 112cm (44 in) extended	*34 kg* *75 lb*
Cutter drive shaft, upper $800	Stainless steel, solid	5.1cm x 574cm (2 in x 226 in)	91 kg 201 lb
Suction pipe, upper $250	Stainless steel	7.6 cm (3 in) ID x 5.2 m (206 in)	27 kg 60 lb
Cutter drive motor $1200	20 hp, 1750 rpm, constant power, adjustable speed, fully enclosed Leeson Electric Motor Company	36 cm x 64 cm (14 in x 25 in)	146 kg 321 lb
Cutter drive gear reducer (Motor mounted) $3000	5:1 reduction, 3000 in-lbs min out max input 4000 rpm, nominal input 1600 rpm, Alpha Gear Drives, TP050-MF1-5-0X-1-XXXX-V1	18 cm x 15 cm (7 in x 6 in)	9.5 kg 21 lb
Pump drive motor $800	10 hp, 3510 rpm, variable torque, adjustable speed, fully enclosed Leeson Electric Motor Company	28 cm x 51 cm (11 in x 20 in)	76 kg 167 lb
Centrifugal pump $2100	3 in pump, 6.5 in impeller, 200 ft head, 500 GPM max at 3500 rpm Waukesha Cherry-Burrell, 2065HV	20 cm x 20 cm (8 in x 8 in)	*16 kg* *35 lb*
Discharge pipe $250	Stainless steel	7.62cm x 457cm (3 in x 180 in)	25 kg 54 lb
Nuclear densometer (provided)	Berthold Systems, Inc., NW 2100	Not given	*11 kg* *25 lb*
Dynamometer (2x) $300 total	500 rpm max, 300 ft-lb max Precision Dynamometer	Not given	*9 kg* *20 lb*
Pressure sensor (2x) $300 total	Texas Instruments	Not given	N/A
Flow meter $725	McCrometer, MF100	7.62 cm x 20 cm (3 in x 8 in)	*4.5 kg* *10 lb*
Sleeve bearings (8x) $750 total	Graphite Metallizing Corporation, Graphalloy bushing no. 117-32	508 mm (2 in) ID, 67mm (2.63 in) OD, 76 mm (3 in) long	9 kg 20 lb
Ladder arm frame $7500	Galvanized steel	See figure A.2	*<379 kg* *<875 lb*
Total Estimated Ladder Arm Weight = 854 kg (1884 lb)			
Total Estimated Ladder Arm Weight with Ladder = 964 kg (2125 lb)			

The point of attachment to the ladder arm for the linear actuator depends on the required maximum and minimum ladder angle. With a 70 degree working range of the universal joint, combinations of 20-90 degrees, 10-80, or 15-85 are possible. The cutter and pump drive motors listed are fully enclosed, three-phase, AC, with adjustable speed drives. The sleeve bearings provide smooth vertical motion of the ladder arm along the guide rods. Since vertical motion of the ladder does not occur during ladder swing, the radial sleeve bearing loads caused by ladder swing will not act while the ladder arm is in motion, which should help the performance of the bearing. Some of the instrumentation, such as the pressure sensors and the rotary position sensor, are relatively small and their mass is not known nor considered relevant to the estimation.

Figure A.2 shows a conceptual drawing of the ladder arm frame. If constructed from 13 mm (0.5 in) thick steel plate, the weight would be approximately 363 kg (800 lb). This does not include any bearings required for the cutter drive shaft (self-lubricating bushings are recommended because of sub-marine operating environment). If more than 397 kg (875 lb) are needed for the entire ladder arm weight, care must be taken to ensure that the dredge carriage assembly does not exceed 2721 kg (6000 lb). It is beneficial to construct the ladder arm assembly to be as heavy as possible to maintain sufficient downward force on the cutterhead while overcutting.

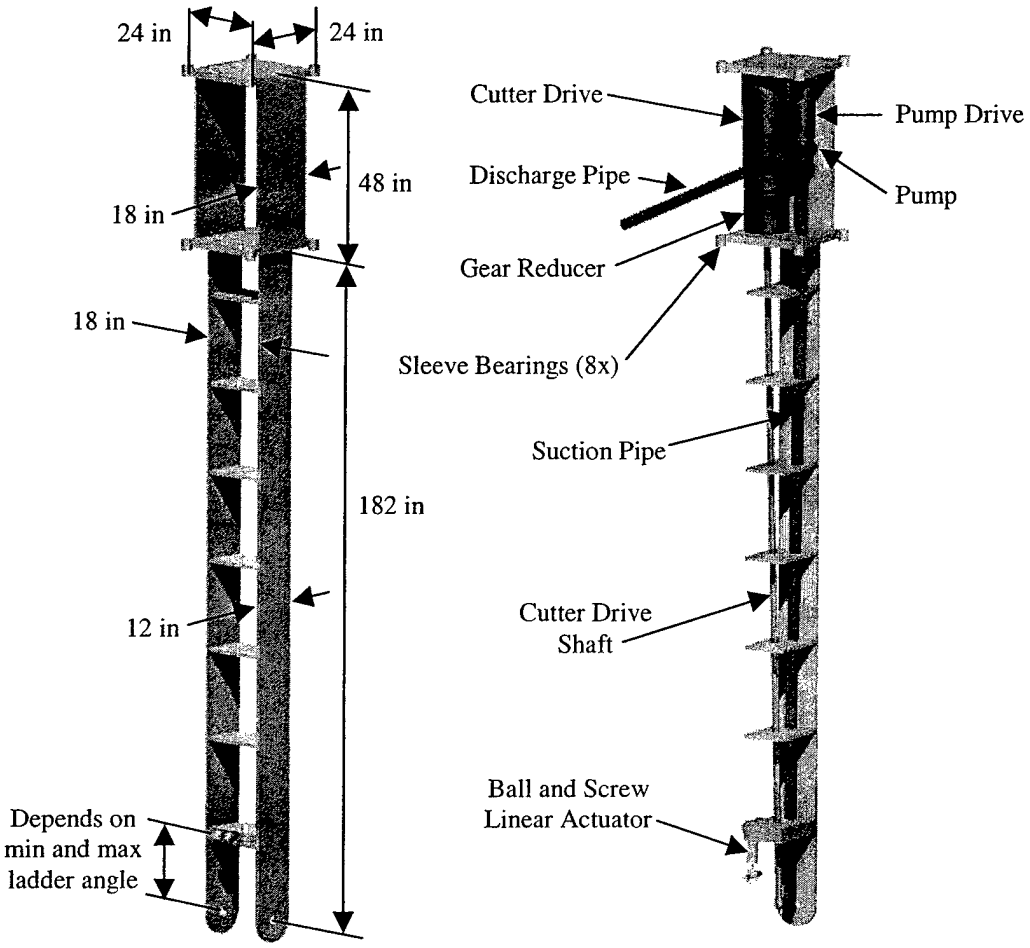

Figure A.2: Conceptual Drawing of the Ladder Arm Frame with Cutaway Rotated 90 Degrees Showing Equipment

Table A.3: Sample Equipment List and Specification for the Dredge Carriage

Item/Cost	Description/Manufacturer	Size	Weight
Motorized hoist winch $3500	2800 lb capacity Jeamar Winches, NHT 2800	89 cm x 41 cm (35 in x 16 in)	204 kg 450 lb
Vertical guide rods (4x) $1750 total	400 Series Stainless steel, Minimum yield strength = 43 ksi	5.1cm x 310cm (2 in x 122 in)	197 kg 434 lb
1D load cell $150	Range: 0 – 2125 lbs.	Not Given	N/A
Linear actuator for dredge carriage swing (rodless belt-type) (2x) $4000 including shaft	500 lb ea. capacity, max speed required = 36 in/s at 366 rpm Macron Dynamics, Single Belt Drive	335 cm (132 in)	23 kg 70 lb
Motor drive for linear actuators $500	3 hp, 3510 rpm, constant torque, adjustable speed, fully enclosed Leeson Electric Motor Company	23 cm x 41 cm (9 in x 16 in)	39 kg 85 lb
Gear reducer for linear actuators $500	3 hp, 10:1, 90 degree output shaft Leeson Electric Motor Company	20 cm x 25 cm (8 in x 10 in)	15 kg 34 lb
Horizontal guide rods (2x) $2750 total	400 Series Stainless steel, Minimum yield strength = 43 ksi	8.3 cm (3.25 in) x 366 cm (144 in)	307 kg 677 lb
Sleeve bearings (4x) $1650 total	Graphite Metallizing Corporation, Graphalloy bushing no. 453A-725222-212 Grade III	83 mm (3.25 in) ID x 102 mm (4 in) OD x (5 in) 13 cm	5.5 kg 12 lb
Dynamometer $150	366 rpm max, 43 Ft-lbs max Precision Dynamometer	Not given	*25 kg* *10 lb*
Linear Position Sensors $900 $1300	Cable extension, fully enclosed Celesco, PT9101-0075-314-X1X0 Celesco, PT9301-0150-411-X1X0	13 cm x 30 cm (5 in x 12 in)	13 kg 28 lb
Dredge carriage frame $8000	Galvanized steel	See Figure A.3	<941 kg <2075 lb
Total Estimated Dredge Carriage Weight = 1757 kg (3875 lb)			
Total Estimated Dredge Carriage Weight with Ladder Arm and Ladder = 2721 kg (6000 lb)			

The ladder arm must have approximately 183 cm (6 ft) of vertical travel. The large 2800-lb capacity winch specified can accomplish this. The speed with which the ladder arm translates in the vertical direction is not critical. A load cell is placed at the point of attachment of the winch cable to the ladder arm so that tension in the winch cable can be measured. With no vertical forces acting on the cutterhead, a tension of 964 kg (2125 lb), equal to the weight of the entire ladder arm assembly (it weighs slightly less in water), exists in the cable. Vertical forces in the +Z direction (overcutting) reduce this value while forces in the –Z direction (undercutting)

increase this value. This is how the vertical cutting forces are recorded by the data acquisition system.

A typical cutterhead dredge employs opposing side winches for ladder swing. The scale laws developed in Chapter III are used to estimate the swing winch speed and force necessary for the model dredge. Typical model dredge swing speeds are in the range of 30.5 cm/s (12 in/s) with swing winch loads less than 2224 N (500 lb). However, model swing speeds up to 91.4 cm (36 in/s) and pulling forces up to 4448 N (1000 lb) may be required for certain applications. A pair of traditional winches with free spool and brake features capable of pulling loads up to 4448 N (1000 lb) with speeds up to 91.4 cm/s (36 in/s) can weigh more than 227 kg (500 lb). This type of side winch solution is shown in Figures 5.4 and 5.10. The result is that the frame and guide rods must be weakened to reduce the overall weight. Rather than do this, an alternate solution for ladder swing is to use a pair of belt-driven linear actuators. The unit specified is capable of speeds up to 508 cm/s (200 in/s) and can move loads with a force of 2224 N (500 lb), 4448 N (1000 lb) total. The actuators, if driven by a 3 hp motor coupled with the specified gear reducer, can meet the performance requirement with a total weight (actuator + motor + gear reducer + drive shaft) of less than 91 kg (200 lb). Moreover, linear actuators have better positioning capability (+/- 0.01 inches) than a pair of opposing winches. A combination tachometer/dynamometer coupled with the drive shaft will collect data used to determine "side winch" power and pull force.

The sleeve bearings provide smooth horizontal motion of the ladder arm along the guide rods. The radial sleeve bearing loads can be severe and act while the dredge carriage is in motion. Care must be taken to ensure that the bearings used can handle the loads as shown in Appendix B. The two cable extension linear position sensors record the absolute Y and Z positions of the cutterhead. The swing speed is calculated by the PLC using the positioning data and the unit's internal clock.

Figure A.3 shows a conceptual drawing of the dredge carriage frame. If the base were constructed from 25 mm (1 in) thick steel plate, the frame from 102 mm (4 in) x 204 mm (8 in) x 5 mm (0.1875 in) and 102 mm (4 in) x 102 mm (4 in) x 5mm (0.1875 in) hollow steel tubing, and the superstructure from 51 mm (2 in) x 5 mm (0.1875 in) square steel tubing with a 13 mm

(0.5 in) thick steel top plate to support the winch, the weight would be approximately 889 kg (1960 lb). An additional 45 kg (100 lb) of structural bracing is recommended to ensure sufficient strength. If more than 941 kg (2075 lb) are needed for the dredge carriage frame, care must be taken to ensure that the entire dredge carriage assembly does not exceed 2721 kg (6000 lb). For simplicity, no additional structural bracing is shown in figure A.3. Four padeyes used by the crane to lift the dredge carriage and frame are also not shown.

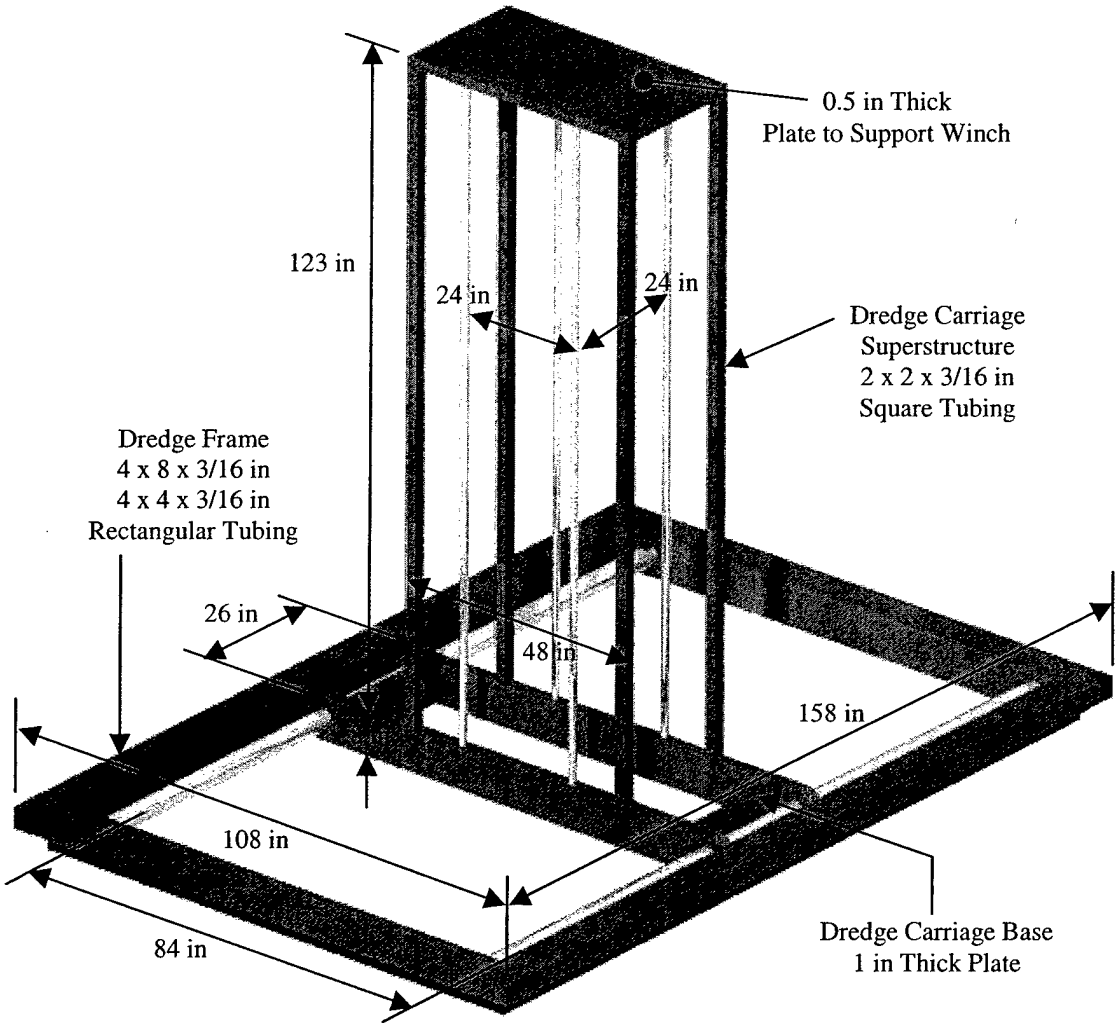

Figure A.3: Conceptual Drawing of the Dredge Carriage Frame, Guide Rods, and Superstructure

Table A.4: Sample Equipment List and Specification for the Tow Carriage

Item/Cost	Description/Manufacturer	Size	Weight
Linear Position Sensor $2000	Cable extension, fully enclosed Celesco PT9301-1700-111-X1X0	13 cm x 30 cm (5 in x 12 in)	6 kg 14 lb
Tow carriage drive motor (brake motor) $800	2 hp, 1725 rpm, constant power, adjustable speed, fully enclosed Leeson Electric Motor Company	23 cm x 48 cm (9 in x 19 in)	36 kg 80 lb
Gear reducer for tow carriage drive $650	2 hp, 20:1, 90 degree output shaft Leeson Electric Motor Company	20 cm x 25 cm (8 in x 10 in)	20 kg 44 lb
Drive shaft for carriage $300	Stainless steel	3.8cm x 396cm (1.5 in x156 in)	35 kg 78 lb
Wheels (4x) $600 total	Stainless steel hub 0.5" hard rubber rim	30 cm x 2.5 cm (12 in x 1 in)	45 kg 120 lb
PLC hardware and system integration $10,000	CompactLogix 5000 PLC, 1769 Analog I/O modules, integration of sensors and drives	N/A	*4.5 kg* *10 lb*
Standard PC $3000	Latest version	N/A	*2 kg* *5 lb*
Electrical Distribution $2500	Cables, bus, limit switches, etc…	N/A	*23 kg* *50 lb*
Dynamometer for towed payload $450	Measures forces in X,Y, Z directions	N/A	*2 kg* *5 lb*
Inside wall bearing (4x) $100 total	650 lb. max radial load stainless steel hub, hard rubber rim	76 mm 3 in	*9 kg* *20 lb*
Manual control panel $2500	See figure 5.15	N/A	*11 kg* *25 lb*
Operator	N/A	N/A	*91 kg* *200 lb*
Desk, chair $500	N/A	N/A	*91 kg* *200 lb*
Cable spool $2000	Industrial Power and Control	> 150 ft	*113 kg* *250 lb*
Tow carriage frame $12,000	Galvanized steel	See figure A.4	<1315 kg < 2900 lb
Total Estimated Tow Carriage Weight = 1814 kg (4000 lb)			
Total Estimated Tow/Dredge Carriage Weight = 4534 kg (10,000 lb)			

The tow carriage with the dredge carriage assembly removed is estimated to weigh approximately 1814 kg (4000 lb). Like the weight of the tow carriage assembly, the weight of the tow carriage by itself must be kept less than 4534 kg (6000 lb) to ensure removal using the overhead crane if necessary. However, as Table A.4 shows, the estimated weight is well below the upper limit.

Figure A.4 shows a conceptual drawing of the tow carriage frame. If constructed from 102 mm (4 in) x 204 mm (8 in) x 5 mm (0.1875 in) thick, 102 mm (4 in) x 102 mm (4 in) x 5 mm (0.1875 in) thick, 76 mm (3 in) x 204 mm (8 in) x 5 mm (0.1875 in) thick and 51 mm (2 in) x 204 mm (8 in) x 5 mm (0.1875 in) thick hollow steel tubing, with 6 mm (0.25 in) thick steel top plate over the surface to support the equipment and operator, the total weight would be approximately 1315 kg (2900 lb). However, there are an infinite number of ways to build this structure with standard steel tubing and sheet metal.

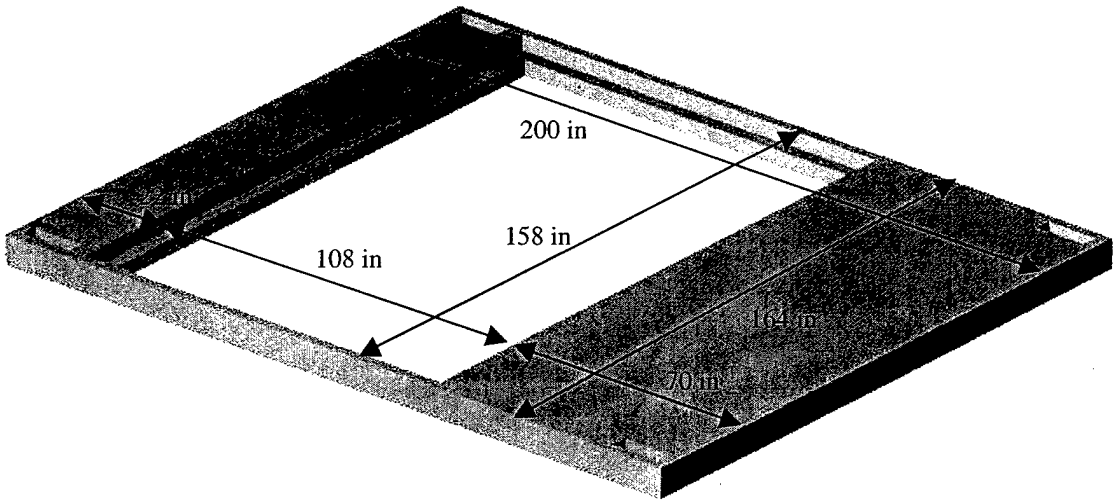

Figure A.4: Conceptual Drawing of the Tow Carriage Frame

The total estimated material costs, including fabrication of the carriage frame, are $85,000 for the model tow/dredge carriage and $15,000 for the dredge carriage cradle. Added to this are a 25% markup for engineering ($25,000), a 20% markup for testing and programming ($20,000), and a 15% markup for general administrative and overhead ($15,000). This gives a total estimated cost of approximately $160,000 to have the tow/dredge carriage built, installed, tested, integrated, and programmed.

APPENDIX B

TOW/DREDGE CARRIAGE STATIC LOAD ANALYSIS

In order to select the recommended dredge equipment and to ensure stability of the model dredge over the entire range of operating parameters, a static load analysis was performed on the structure. This analysis also determined the loads and stresses acting at key points in the frame, which aids in the detailed structural analysis of the ladder/ladder arm frame, the dredge carriage frame and superstructure, and the dredge and tow carriage frame. The maximum predicted cutterhead loading is determined in Chapter IV and Table 4.5 lists these forces. A free-body-diagram (FBD) analysis was performed based on these loads and the weight and geometry of the recommended design. Figure B.1 shows the FBD of the ladder. The distance from the ladder pivot point to the ladder center of mass is x_3. The distance from the ladder pivot point to the cutterhead center of mass is x_2.

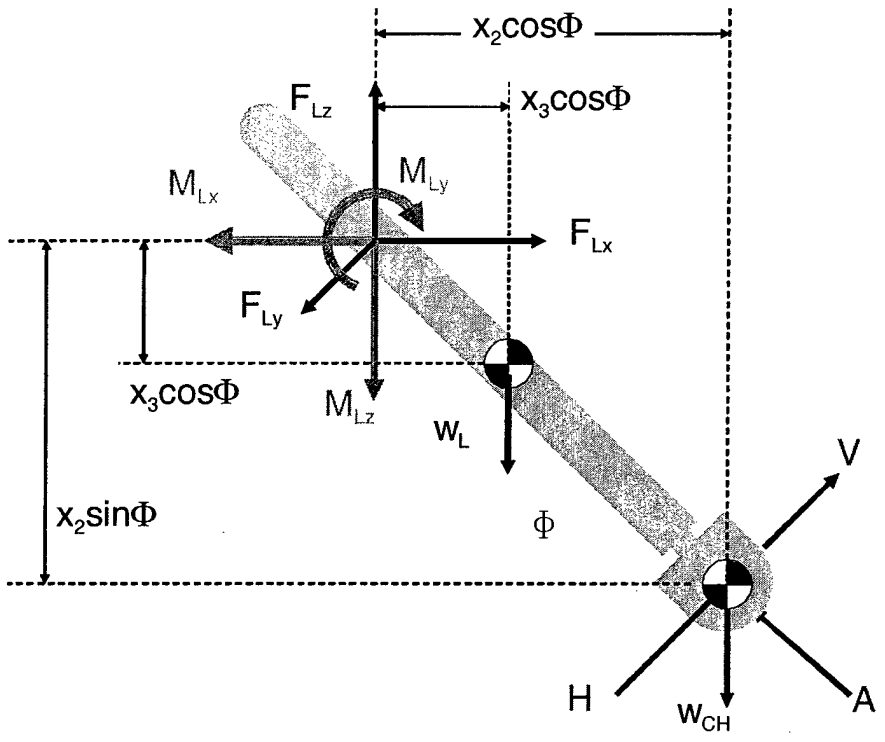

Figure B.1: Free Body Diagram of the Ladder

The horizontal, vertical, and axial cutting forces (*H, V, & A*) act on the cutter. This loading, plus the weight of the cutterhead (W_{CH}) and ladder (W_L) create a set of forces (F_{LX}, F_{LY}, & F_{LZ}) and a set of moments (M_{LX}, M_{LY}, M_{LZ}) at the ladder end. Equations B.1 through B.6 show how the moments and forces were calculated.

$$F_{LX} = -V\sin\Phi + A\cos\Phi \tag{B.1}$$

$$F_{LY} = H \tag{B.2}$$

$$F_{LZ} = W_L + W_{CH} - V\cos\Phi - A\sin\Phi \tag{B.3}$$

$$M_{LX} = Hx_2\sin\Phi \tag{B.4}$$

$$M_{LY} = Vx_2\cos\Phi - W_L x_3\cos\Phi - W_{CH}x_2\cos\Phi \tag{B.5}$$

$$M_{LZ} = Hx_2\cos\Phi \tag{B.6}$$

The ladder pivots at the end of the ladder arm through a set of two bearings approximately 12 inches apart. These bearings must be selected to withstand the forces and moments at the ladder end which are calculated in Tables B.1 through B.5 and in the data used to plot Figures B.9 through B.17. The moment about the *Y* axis (M_{LY}) is opposed by the linear actuator acting through the 12 inch lever arm. However, since the point of attachment of the linear actuator to the ladder arm cannot be determined until the maximum and minimum ladder angles are selected, this force is represented by a moment for the purposes of this analysis. The forces and moments at the ladder end are transferred to the ladder arm via the set of bearings.

Figure B.2 shows the forces and moments acting on the ladder arm. The vertical distance between the ladder arm end and the upper set of 4 sleeve bearings is z_1. The vertical distance between the upper set of 4 sleeve bearings and the lower set of 4 sleeve bearings is z_3. The horizontal distances between the vertical guide rods are x_4 and y_1. To keep Figure B.2 simple,

the reaction forces that occur at the top of the ladder arm between the sleeve bearings and the vertical guide rods forces are shown in detail in Figure B.3.

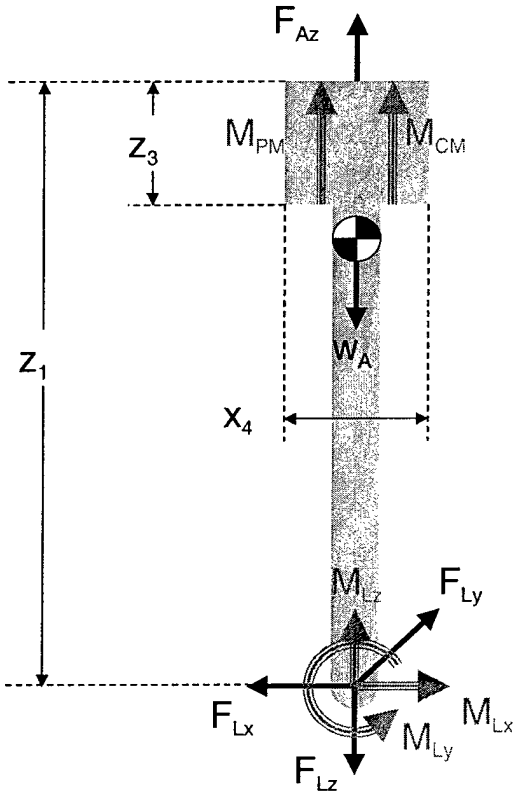

Figure B.2: Free Body Diagram of the Ladder Arm

Equation B.7 calculates the tension in the ladder arm lift cable (F_{AZ}) based on the forces acting on the end of the ladder arm and the weight of the ladder arm assembly.

$$F_{AZ} = W_A + F_{LZ} \tag{B.7}$$

The 10 hp pump motor and the 20 hp cutter motors create moments in the ladder arm (M_{PM} and M_{CM}) that should be oriented to oppose the moment created by the cutting forces (M_{LZ}) during undercutting when the moments on the vertical guide rods are highest. The forces and moments acting on the ladder arm produce 5 different sets of forces on the sleeve bearings in the upper ladder arm. Figure B.3 shows the 5 sets of forces and how they act on the bearing set. The

individual bearings represented by the 8 corners of the imaginary box are labeled 1 through 8 (number 5 not shown).

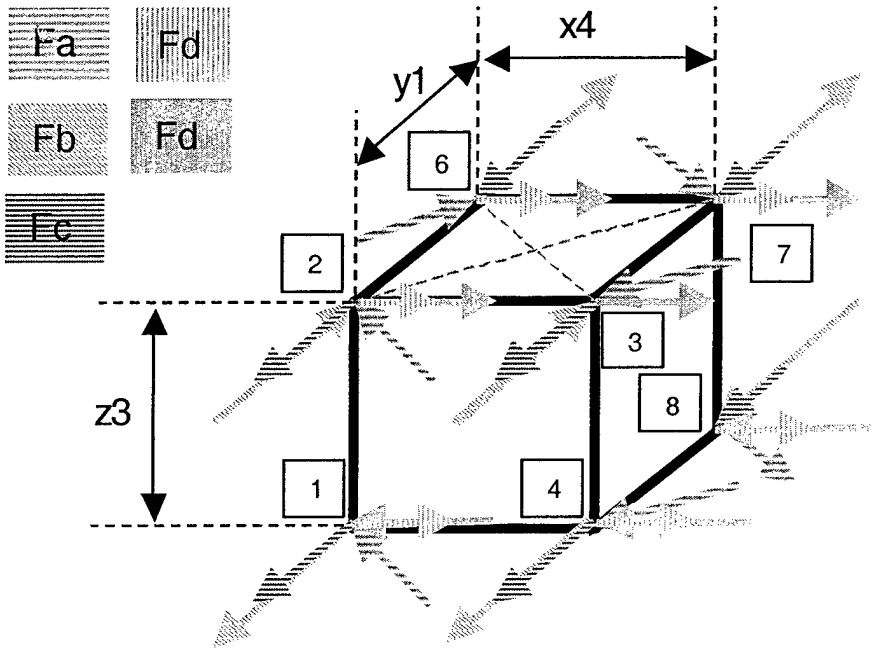

Figure B.3: Forces on the Sleeve Bearings in the Ladder Arm

The result of the moments about the Z axis (M_{LZ}, M_{CM}, and M_{PM}) is a tangential force that acts on the ladder arm sleeve bearings (F_a). While the system of 8 sleeve bearings is over constrained making the static problem indeterminate, Equation B.8 can be used to estimate F_a. This method assumes that since each bearing is equidistant from the geometric center of the ladder arm, the force acting on each of the 8 bearings produced by the moments about the Z axis will be identical.

$$F_a = \frac{M_{LZ} + M_{PM} + M_{CM}}{4\sqrt{(x_4)^2 + (y_1)^2}} \tag{B.8}$$

This force is the only one of the five forces acting on the sleeve bearings that does not act along either the X or the Y axes. Since F_a acts tangentially and the geometry of ladder arm is known,

the direction of F_a can be calculated. This allows the force to be resolved into its X and Y components to be added to the other sleeve bearing forces, F_b, F_c, F_d and F_e, which act along either the X or Y axes.

The force and moment generated by the horizontal cutting force H creates a force in each of the sleeve bearings that acts along the Y axis as seen in Figure B.3. Again, the system of sleeve bearings is over constrained and the problem is statically indeterminate. However, Equation B.9 and B.10 can be used to estimate F_b and F_c.

$$F_b = \frac{M_{LX} + F_{LY}\left(z_1 - \frac{z_3}{2}\right)}{4z_3} \tag{B.9}$$

$$F_c = \frac{F_{LY}}{8} \tag{B.10}$$

The force and moment generated by the axial and vertical cutting forces A and V respectively creates a force in each of the sleeve bearings that acts along the X axis as seen in Figure B.3. Equation B.11 and B.12 can be used to estimate these F_d and F_e.

$$F_d = \frac{F_{LX}}{8} \tag{B.11}$$

$$F_e = \frac{M_{LY} - F_{LX}\left(z_1 - \frac{z_3}{2}\right)}{4z_3} \tag{B.12}$$

The sum of these forces on each sleeve bearing is needed to determine the maximum radial loading of each bearing and the resulting bending moments created in the vertical guide rods. These forces are included in Tables B.1 through B.5, and their resulting bending moments are to plot Figures B.9 through B.17.

The forces and moments of the ladder arm are transmitted to the four vertical guide rods of the dredge carriage via the sleeve bearings and to the dredge carriage via the lift cable. Figure B.4 shows the forces and moments acting on the dredge carriage. The horizontal distances between the dredge carriage sleeve bearings are x_5 and y_2 (y_2 not shown). The vertical distance from the sleeve bearing plane and the lower set of 4 sleeve bearings in the ladder arm is z_2. This distance is also known as the ladder arm elevation and can be used, with the ladder angle Φ, to calculate the exact cutting elevation of the cutterhead.

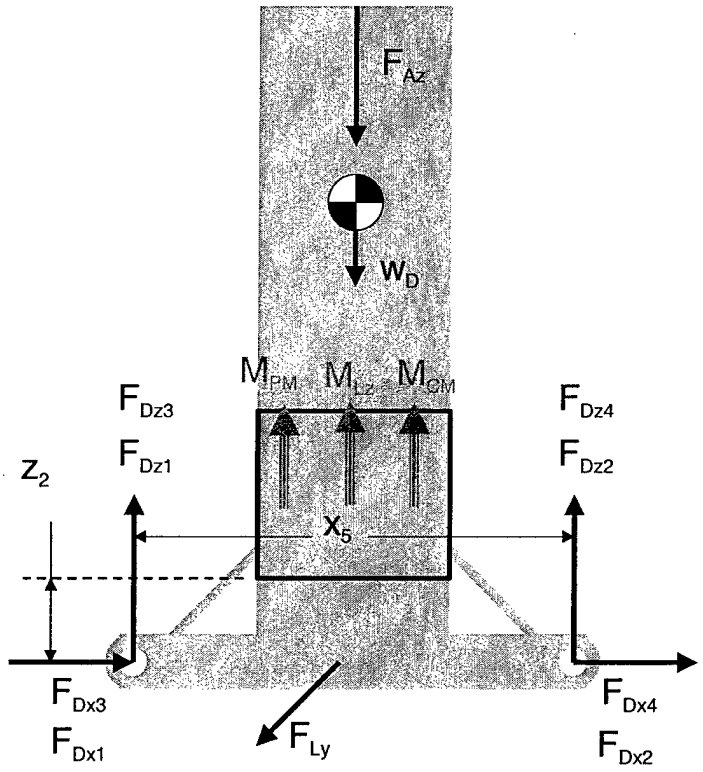

Figure B.4: Free Body Diagram of the Dredge Carriage

Since the tangential sleeve bearing force, F_a, acting through the vertical guide rods is estimated and not known exactly, this force is represented in Figure B.4 by the original moments, M_{LZ}, M_{CM}, and M_{PM}. These moments are opposed by the horizontal forces in the dredge carriage sleeve bearings, F_{DX1}, F_{DX2}, F_{DX3} and F_{DX4}. If only one horizontal guide were present, the dredge carriage would be constrained by two bearings and the bearing forces could be calculated

exactly. However, the existence of two guide rods renders the static problem indeterminate. Assuming that $F_{DX1} = F_{DX2}$ and $F_{DX3} = F_{DX4}$, the horizontal forces are estimated in accordance with Equations B.13 and B.14.

$$F_{DX1,2} = \frac{M_{LZ} + M_{CM} + M_{PM}}{-2y_2} + F_{LX} \tag{B.13}$$

$$F_{DX3,4} = \frac{M_{LZ} + M_{CM} + M_{PM}}{2y_2} + F_{LX} \tag{B.14}$$

The remaining sleeve bearing forces, F_b, F_c, F_d and F_e, act on the vertical guide rods as shown in Figure B.5. Basically, they are equal and opposite of the forces shown in Figure B.3 according to Newton's 2nd law.

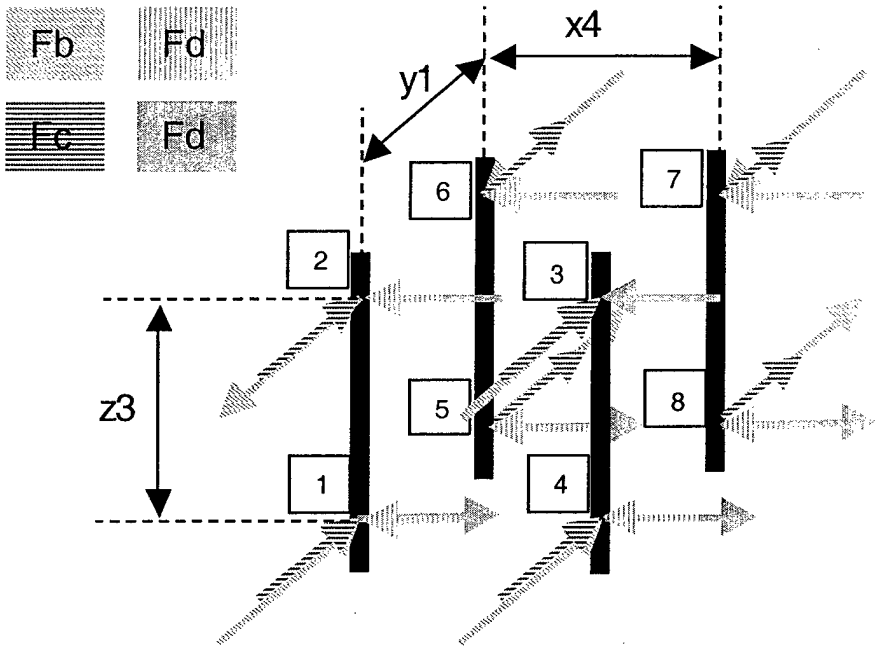

Figure B.5: Forces on the Vertical Guide Rods of the Dredge Carriage

These loads act with the tension in the lift cable, F_{AZ}, and the weight of the dredge carriage, W_D, to produce vertical forces on the dredge carriage sleeve bearings depending on the ladder arm elevation, z_2. Because the FBD of the dredge carriage is statically indeterminate, the individual vertical forces on each of the dredge carriage sleeve bearings cannot be determined. Equations B.15 and B.16 can be used to calculate the total load on the front and total load on the rear of the dredge carriage. Equations B.17 and B.18 can be used to calculate the total load on the left and total load on the right of the dredge carriage.

$$F_{DZ2} + F_{DZ4} = \frac{(W_D + F_{AZ})\left(\frac{x5}{2}\right) - 4(F_c + F_b)(z_2 + z_3) + 4(F_c - F_b)z_2}{x_5} \tag{B.15}$$

$$F_{DZ1} + F_{DZ3} = W_D + F_{AZ} - (F_{DZ2} + D_{DZ4}) \tag{B.16}$$

$$F_{DZ3} + F_{DZ4} = \frac{(W_D + F_{AZ})\left(\frac{y_2}{2}\right) + 4(F_c - F_b)(z_2 + z_3) + 4(F_c + F_b)z_2}{y_2} \tag{B.17}$$

$$F_{DZ1} + F_{DZ2} = W_D + F_{AZ} - (F_{DZ3} + D_{DZ4}) \tag{B.18}$$

The individual dredge carriage bearing loads can be estimated from the loads calculated above. For example, assume that 60% of the total load acts through the front two bearings and 40% of the total load acts through the rear two bearings. Further assume that 70% of the total load acts through the left two bearings and 30% of the total load acts through the right two bearings. The load on the front/left bearing can be estimated to be 60% x 70% = 42%. The load on the front/right bearing can be estimated to be 60% x 30% = 18%. The load on the rear/left bearing can be estimated to be 40% x 70% = 28%. Finally, the load on the rear/right bearing can be estimated to be 40% x 30% = 12%. This is reasonable since 42% + 18% + 28% + 12% equals unity. Since the total load on all four dredge carriage bearings is known, the individual loads can be estimated in this way. Tables B.1 through B.5 include this calculation.

The forces and moments of the dredge carriage are transmitted to the horizontal guide rods of the tow carriage via the dredge carriage sleeve bearings and to the tow carriage via the side winch cable. Figure B.6 shows the forces and moments acting on the tow carriage. The horizontal distance between the front and rear axles is x_6. The horizontal distance between the rear axle and the tow carriage center of mass is x_7. The horizontal distance between the rear axle and the rear horizontal guide rod is x_8. The horizontal distance between the wheels is y_3. The horizontal distance between the right wheels and the tow carriage center of mass is y_4, and the horizontal distance from the right wheels and the right sleeve bearings is y, which is continually changing between 0 and y_3 for the purposes of this analysis. In reality, the dredge carriage as designed does not travel the entire width of the tank, but leaves several inches on either side as a margin.

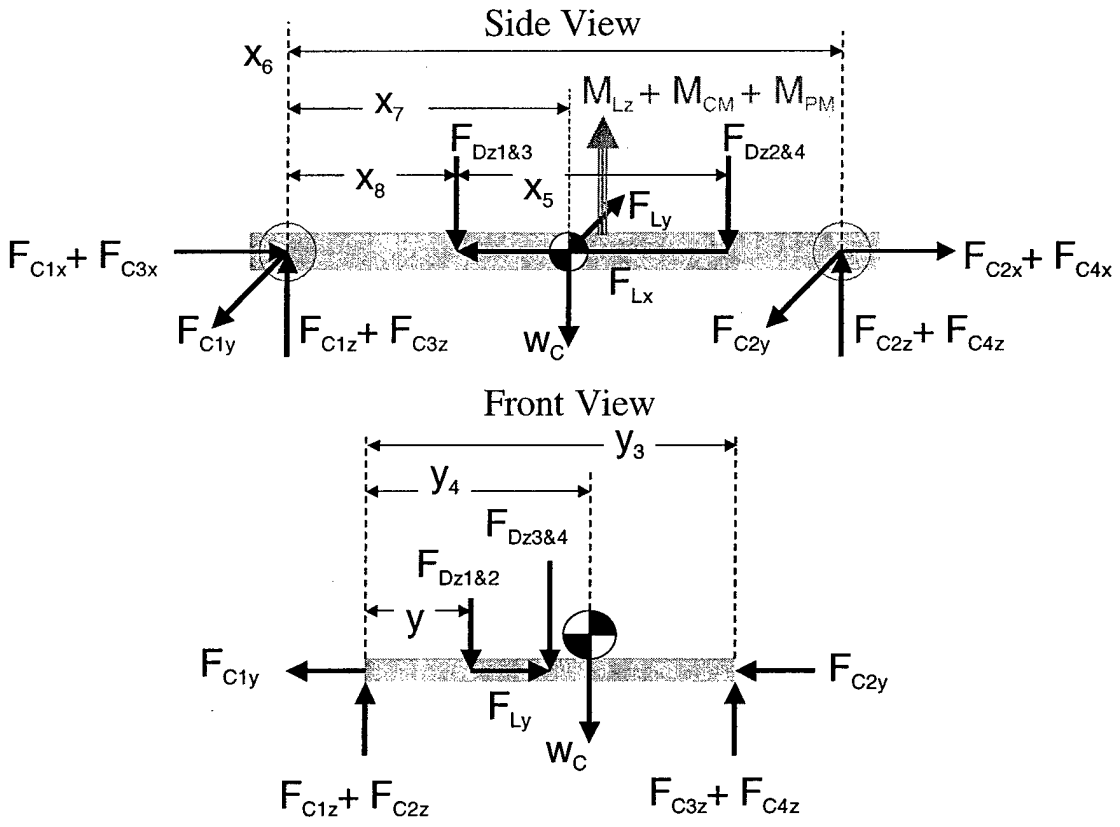

Figure B.6: Free Body Diagram of the Tow Carriage

The moments M_{LZ}, M_{CM}, and M_{PM} along with the side winch pull force, F_{LY}, are opposed by the inside bearing forces, F_{C1Y} and F_{C2Y}. Since only two of the bearings contact the inside of the tank wall at any given time, the system is not over constrained and the forces can be directly calculated. However, the calculation assumes that four wheels of the dredge carriage have no resistance to lateral motion. In reality, the tow carriage wheels will absorb some of the lateral force. However, Equations B.19 and B.20 are a conservative estimation of the maximum amount of force imposed on the inside bearings.

$$F_{C2Y} = \frac{M_{LZ} + M_{PM} + M_{CM} + \left(x_8 + \frac{x_5}{2}\right)F_{LY}}{x_6} \tag{B.19}$$

$$F_{C1Y} = F_{LY} - F_{C2Y} \tag{B.20}$$

The remaining loads transmitted to the tow carriage via the horizontal guide rods act with the weight of the tow carriage and F_{AZ} to produce loads on the four wheel bearings. Equation B.21 is used to estimate the horizontal loads assuming an equal distribution of force between the four wheels. If the brake motor is used to hold the tow carriage in place, then the horizontal loads acting along the X axis are divided between only two wheels as opposed to four.

$$F_{C1X} = F_{C2X} = F_{C3X} = F_{C4X} = \frac{F_{LX}}{4} \tag{B.21}$$

The vertical loads cannot be statically determined because the system is over constrained. However, Equations B.22 and B.23 can be used to calculate the front and rear vertical wheel loads respectively. Equations B.24 and B.25 can be used to calculate the left and right vertical wheel loads respectively.

$$F_{C2Z} + F_{C4Z} = \frac{W_C x_7 + (F_{DZ1} + F_{DZ3})x_8 + (F_{DZ2} + F_{DZ4})(x_8 + x_5)}{x_6} \tag{B.22}$$

$$F_{C1Z} + F_{C3Z} = W_C + F_{DZ1} + F_{DZ3} + F_{DZ2} + F_{DZ4} - F_{C2Z} - F_{C4Z} \tag{B.23}$$

$$F_{C3Z} + F_{C4Z} = \frac{W_C y_4 + (F_{DZ1} + F_{DZ2})y + (F_{DZ3} + F_{DZ4})(y + y_2)}{y_3} \tag{B.24}$$

$$F_{C1Z} + F_{C2Z} = W_C + F_{DZ1} + F_{DZ3} + F_{DZ2} + F_{DZ4} - F_{C3Z} - F_{C4Z} \tag{B.25}$$

Since y varies from 0 to y_3 as the dredge carriage transverses the towing tank, Equations B.24 and B.25 each have a maximum and a minimum value. The minimum values are useful in that the tow carriage becomes unstable and is in danger of tipping if this quantity approaches zero. Individual wheel bearing loads can be estimated in the same way that the individual sleeve bearing loads for the horizontal guide rods were estimated. Tables B.1 through B.5 include this data for the maximum and minimum values of y.

The cutting theory used in Chapter IV gave a set of cutterhead loading data based on the prototype dredge operating at maximum capacity. This cutterhead loading data is contained in Table 4.5. Table B.1 is the result of the static analysis for the maximum estimated cutterhead loading during overcutting and undercutting (Table 4.5 data). The ladder angle shown is 45 degrees and the ladder arm elevation shown is 1.87 m (6.12 ft) which gives a digging depth of about 3.35 m (11 ft) below the water line. Selecting different combinations of ladder angles and ladder arm elevations will change some of the values. The output of the static analysis is used to determine the maximum bearing loads, wheel loads, and bending moments in the guide rods.

Table B.1: Model Dredge Static Analysis under Maximum Predicted Cutterhead Loading

	Overcutting													
cutter horsepower	2.1	4.3	6.4	8.5	10.6	12.8	14.9	1.6	3.2	4.8	6.4	8.0	9.6	11.2
horizontal cutting force H	89.3	178.7	268.0	357.3	446.7	536.0	625.4	47.1	93.9	140.2	186.2	231.8	277.0	321.9
vertical cutting force V	9.7	19.3	29.0	38.7	48.4	58.0	67.7	48.1	96.6	145.3	194.3	243.6	293.2	343.1
axial cutting force A	5.6	11.2	16.8	22.3	27.9	33.5	39.1	4.2	8.4	12.5	16.7	20.9	25.1	29.2
moment caused by pump drive	15.00	15.00	15.00	15.00	15.00	15.00	15.00	15.00	15.00	15.00	15.00	15.00	15.00	15.00
ladder angle Φ (90-0)	45.00	45.00	45.00	45.00	45.00	45.00	45.00	45.00	45.00	45.00	45.00	45.00	45.00	45.00
elevation of dredge arm (1.5-7.17) z_2	6.12	6.12	6.12	6.12	6.12	6.12	6.12	6.12	6.12	6.12	6.12	6.12	6.12	6.12
moment caused by cutter drive	37	74	112	149	186	223	261	28	56	84	112	140	168	195
vertical cutterhead position h	-11	-11	-11	-11	-11	-11	-11	-11	-11	-11	-11	-11	-11	-11
thrust load at ladder end bearing	45	89	134	179	223	268	313	24	47	70	93	116	139	161
total radial ladder end bearing force rght side	143	321	501	682	863	1045	1226	56	148	244	341	437	532	627
total radial ladder end bearing force left side	224	397	573	748	924	1100	1275	138	228	320	412	503	595	685
dredge arm winch cable lift force F_{Az}	2114	2103	2093	2082	2071	2060	2049	2088	2051	2013	1976	1938	1900	1862
total radial ladder arm slide bearing 1 force	104	208	313	417	521	625	729	60	124	188	252	316	380	443
total radial ladder arm slide bearing 2 force	112	222	333	443	553	663	773	62	126	190	254	317	380	443
total radial ladder arm slide bearing 3 force	83	164	246	329	411	493	575	46	96	146	196	246	296	346
total radial ladder arm slide bearing 4 force	134	267	399	531	664	796	929	76	154	232	309	386	463	540
total radial ladder arm slide bearing 5 force	104	209	314	420	525	631	736	69	144	218	292	366	440	514
total radial ladder arm slide bearing 6 force	111	222	334	445	556	667	779	70	142	215	287	358	430	501
total radial ladder arm slide bearing 7 force	81	165	248	331	415	498	582	55	116	176	237	297	357	417
total radial ladder arm slide bearing 8 force	134	267	400	534	667	801	934	84	170	257	343	428	514	599
tot d-carriage slide bearing force on 1	1150	1400	1652	1907	2165	2424	2686	1054	1213	1380	1554	1737	1927	2126
tot d-carriage slide bearing force on 3	662	430	239	242	437	677	928	789	670	545	416	289	183	174
tot d-carriage slide bearing force on 2	1164	1406	1649	1889	2129	2367	2603	1012	1096	1172	1239	1296	1345	1383
tot d-carriage slide bearing force on 4	670	432	239	242	433	665	905	758	605	464	336	229	164	171
min vertical force on wheel 1	1964	1996	2029	2062	2095	2128	2160	1951	1972	1993	2013	2034	2055	2075
max vertical force on wheel 1	2526	2557	2588	2620	2651	2682	2713	2512	2529	2546	2563	2580	2597	2614
min vertical force on wheel 2	2481	2522	2562	2602	2642	2683	2723	2449	2456	2463	2470	2476	2481	2487
max vertical force on wheel 2	3192	3230	3268	3306	3344	3382	3420	3152	3150	3147	3144	3141	3137	3132
min vertical force on wheel 3	1898	1863	1828	1793	1758	1723	1688	1918	1902	1887	1872	1857	1842	1827
max vertical force on wheel 3	2460	2424	2387	2351	2314	2278	2241	2478	2459	2441	2422	2403	2384	2366
min vertical force on wheel 4	2398	2353	2308	2263	2218	2173	2128	2406	2370	2333	2296	2260	2224	2188
max vertical force on wheel 4	3109	3062	3014	2967	2920	2872	2825	3110	3063	3017	2971	2925	2880	2834
total radial force on front bearing	-4	-7	-11	-14	-17	-20	-23	-3	-5	-8	-10	-12	-14	-17
total radial force on rear bearing	49	97	145	192	240	288	336	27	52	78	103	128	153	178
weight of Ladder w_L	100	100	100	100	100	100	100	100	100	100	100	100	100	100
weight of cutterhead w_{CH}	25	25	25	25	25	25	25	25	25	25	25	25	25	25
weight of dredge arm w_A	2000	2000	2000	2000	2000	2000	2000	2000	2000	2000	2000	2000	2000	2000
weight of dredge carriage W_D	1523	1523	1523	1523	1523	1523	1523	1523	1523	1523	1523	1523	1523	1523
weight of towing carriage w_C	6377	6377	6377	6377	6377	6377	6377	6377	6377	6377	6377	6377	6377	6377
length of ladder X_2	3.00	3.00	3.00	3.00	3.00	3.00	3.00	3.00	3.00	3.00	3.00	3.00	3.00	3.00
distance to leverage point X_1	1.00	1.00	1.00	1.00	1.00	1.00	1.00	1.00	1.00	1.00	1.00	1.00	1.00	1.00
distance to ladder centroid X_3	1.00	1.00	1.00	1.00	1.00	1.00	1.00	1.00	1.00	1.00	1.00	1.00	1.00	1.00
distance between ladder end bearings	1.50	1.50	1.50	1.50	1.50	1.50	1.50	1.50	1.50	1.50	1.50	1.50	1.50	1.50
length of dredge arm z_1	19.00	19.00	19.00	19.00	19.00	19.00	19.00	19.00	19.00	19.00	19.00	19.00	19.00	19.00
distance to lower slide bearing set z_3	4.00	4.00	4.00	4.00	4.00	4.00	4.00	4.00	4.00	4.00	4.00	4.00	4.00	4.00
horizontal dist between d-arm bearngs x_4	2.00	2.00	2.00	2.00	2.00	2.00	2.00	2.00	2.00	2.00	2.00	2.00	2.00	2.00
horizontal dist between d-arm bearngs y_1	2.00	2.00	2.00	2.00	2.00	2.00	2.00	2.00	2.00	2.00	2.00	2.00	2.00	2.00
dist between d-carriage slide bearings x_5	7.00	7.00	7.00	7.00	7.00	7.00	7.00	7.00	7.00	7.00	7.00	7.00	7.00	7.00
height of dredge carriage z_5	10.58	10.58	10.58	10.58	10.58	10.58	10.58	10.58	10.58	10.58	10.58	10.58	10.58	10.58
dist between d-carriage slide bearings y_2	2.00	2.00	2.00	2.00	2.00	2.00	2.00	2.00	2.00	2.00	2.00	2.00	2.00	2.00
dist from t-c wheel to d-carrge bearing X_8	2.00	2.00	2.00	2.00	2.00	2.00	2.00	2.00	2.00	2.00	2.00	2.00	2.00	2.00
dist from t-carriage wheel to centroid X_7	10.00	10.00	10.00	10.00	10.00	10.00	10.00	10.00	10.00	10.00	10.00	10.00	10.00	10.00
distance between carriage wheels X_6	15.00	15.00	15.00	15.00	15.00	15.00	15.00	15.00	15.00	15.00	15.00	15.00	15.00	15.00
width of towing carriage Y_3	12.83	12.83	12.83	12.83	12.83	12.83	12.83	12.83	12.83	12.83	12.83	12.83	12.83	12.83
dist from wheel to carriag centroid Y_4	6.42	6.42	6.42	6.42	6.42	6.42	6.42	6.42	6.42	6.42	6.42	6.42	6.42	6.42
vertical force at ladder end F_{Lz}	114	103	93	82	71	60	49	88	51	13	-24	-62	-100	-138
horizontal force at ladder end F_{Lx}	-3	-6	-9	-12	-14	-17	-20	-31	-62	-94	-126	-157	-190	-222
horizontal moment at ladder end M_{Lx}	190	379	569	758	948	1137	1327	100	199	297	395	492	588	683
vertical moment at ladder end M_{Lz}	190	379	569	758	948	1137	1327	100	199	297	395	492	588	683
moment due to lader rotation device M_{Lv}	-103	-83	-62	-42	-21	-1	20	-22	81	184	288	393	498	604
Fa =	21.4	41.4	61.4	81.5	101.5	121.6	141.6	12.6	23.9	35.0	46.1	57.1	68.1	78.9
Fb =	106.8	213.5	320.3	427.1	533.8	640.6	747.4	56.3	112.2	167.6	222.5	277.0	331.1	384.7
Fc =	11.2	22.3	33.5	44.7	55.8	67.0	78.2	5.9	11.7	17.5	23.3	29.0	34.6	40.2
Fd =	-0.4	-0.7	-1.1	-1.4	-1.8	-2.2	-2.5	-3.9	-7.8	-11.7	-15.7	-19.7	-23.7	-27.7
Fe =	-3.4	1.0	5.3	9.7	14.0	18.4	22.7	31.7	71.3	111.3	151.5	191.9	232.6	273.6
angle between r_a and F_{bc} in radians =	0.79	0.79	0.79	0.79	0.79	0.79	0.79	0.79	0.79	0.79	0.79	0.79	0.79	0.79
vert force on both left d-c slide brng $F_{Dz1\&2}$	2310	2796	3282	3768	4254	4740	5226	2065	2303	2540	2774	3006	3235	3463
vert force on both right d-c slide brng $F_{Dz3\&4}$	1327	830	334	-163	-660	-1157	-1654	1546	1271	997	725	455	188	-78
vert force on both front d-c slide brng $F_{Dz2\&4}$	1830	1818	1806	1794	1782	1770	1758	1769	1696	1623	1549	1475	1400	1324
vert force on both rear d-c slide brng $F_{Dz1\&3}$	1808	1809	1810	1811	1812	1814	1815	1842	1878	1914	1950	1986	2023	2060
vert force on d-c slide bearing 1	1148	1395	1643	1893	2145	2399	2655	1053	1210	1374	1546	1725	1912	2108
vert force on d-c slide bearing 2	660	414	167	-82	-333	-585	-840	789	668	539	404	261	111	-48
vert force on d-c slide bearing 3	1162	1401	1639	1875	2109	2341	2571	1012	1093	1165	1228	1281	1323	1355
vert force on d-c slide bearing 4	668	416	167	-81	-327	-571	-814	758	603	457	321	194	77	-31
horiz force each d-carriage bearing $F_{Dx1,2}$	-61	-119	-176	-233	-291	-348	-406	-43	-83	-123	-162	-201	-240	-279
horiz force each d-carriage bearing $F_{Dx3,4}$	60	116	172	228	284	340	395	28	52	76	99	122	145	168
vertical force on front wheels $F_{C2z} + F_{C4z}$	5590	5583	5576	5569	5562	5555	5548	5558	5519	5480	5441	5401	5361	5321
vertical force on rear wheels $F_{C1z} + F_{C3z}$	4424	4420	4417	4413	4409	4405	4402	4430	4431	4433	4435	4437	4439	4441
min vert force on right wheels $F_{C1z} + F_{C2z}$	4445	4518	4591	4664	4737	4810	4883	4400	4428	4456	4483	4510	4536	4562
max vert force on right wheels $F_{C1z} + F_{C2z}$	5718	5787	5856	5926	5995	6064	6134	5664	5679	5693	5707	5721	5734	5747
min vert force on left wheels $F_{C3z} + F_{C4z}$	4297	4216	4136	4056	3976	3896	3816	4324	4272	4220	4168	4117	4066	4015
max vert force on left wheels $F_{C3z} + F_{C4z}$	5569	5486	5402	5318	5234	5150	5066	5588	5523	5458	5393	5328	5264	5200

Table B.1: Continued

cutter horsepower	12.8	14.4	1.1	2.1	3.2	4.3	5.3	6.4	7.4	8.5	9.6	10.6	11.7	12.8
horizontal reaction force at cutter H	366.3	410.4	28.3	57.0	85.9	115.1	144.6	174.5	204.6	235.0	265.7	296.7	328.0	359.7
vertical reaction force at cutter V	393.4	443.9	34.9	69.6	104.2	138.6	172.8	206.9	240.8	274.6	308.2	341.6	374.9	408.0
axial reaction force at cutter A	33.4	37.6	2.8	5.6	8.4	11.2	14.0	16.8	19.6	22.5	25.3	28.1	31.0	33.8
moment caused by pump drive	15.00	15.00	15.00	15.00	15.00	15.00	15.00	15.00	15.00	15.00	15.00	15.00	15.00	15.00
ladder angle Φ (90-0)	45.00	45.00	45.00	45.00	45.00	45.00	45.00	45.00	45.00	45.00	45.00	45.00	45.00	45.00
elevation of dredge arm (1.5-7.17) z_2	6.12	6.12	6.12	6.12	6.12	6.12	6.12	6.12	6.12	6.12	6.12	6.12	6.12	6.12
moment caused by cutter drive	223	251	19	37	56	74	93	112	130	149	168	186	205	223
vertical cutterhead position h	-11	-11	-11	-11	-11	-11	-11	-11	-11	-11	-11	-11	-11	-11
thrust load at ladder end bearing	183	205	14	28	43	58	72	87	102	117	133	148	164	180
total radial ladder end bearing force rght side	721	815	30	73	132	193	256	319	382	447	512	577	644	710
total radial ladder end bearing force left side	775	865	103	156	212	270	329	389	450	511	574	636	700	764
dredge arm winch cable lift force F_{Az}	1823	1785	2098	2072	2045	2019	1993	1967	1941	1915	1889	1864	1838	1813
total radial ladder arm slide bearing 1 force	507	570	36	78	121	163	206	248	291	334	378	421	465	509
total radial ladder arm slide bearing 2 force	506	568	38	79	120	162	204	246	288	331	374	417	460	504
total radial ladder arm slide bearing 3 force	395	445	27	60	93	126	160	193	227	261	295	329	363	397
total radial ladder arm slide bearing 4 force	616	692	47	97	147	198	249	300	352	404	456	509	561	614
total radial ladder arm slide bearing 5 force	587	660	43	92	141	191	240	290	340	389	439	490	540	591
total radial ladder arm slide bearing 6 force	572	643	43	90	137	185	233	280	329	377	425	474	523	572
total radial ladder arm slide bearing 7 force	477	537	34	74	114	155	195	236	276	317	358	399	440	481
total radial ladder arm slide bearing 8 force	684	768	52	108	165	221	278	335	393	451	509	567	625	684
tot d-carriage slide bearing force on 1	2334	2550	996	1093	1194	1301	1412	1527	1648	1774	1904	2040	2181	2327
tot d-carriage slide bearing force on 3	287	444	837	768	694	616	535	450	363	277	200	157	185	269
tot d-carriage slide bearing force on 2	1412	1431	972	1021	1068	1113	1156	1196	1233	1268	1300	1329	1354	1377
tot d-carriage slide bearing force on 4	229	301	818	718	621	528	439	356	280	214	168	154	175	217
min vertical force on wheel 1	2096	2117	1944	1957	1970	1983	1996	2010	2024	2038	2052	2066	2080	2095
max vertical force on wheel 1	2631	2649	2505	2515	2526	2537	2548	2559	2570	2582	2593	2605	2617	2629
min vertical force on wheel 2	2491	2496	2444	2447	2450	2453	2457	2460	2464	2467	2471	2475	2479	2483
max vertical force on wheel 2	3127	3122	3150	3146	3142	3139	3135	3132	3129	3126	3124	3121	3119	3117
min vertical force on wheel 3	1812	1797	1924	1915	1906	1897	1887	1878	1868	1857	1847	1837	1826	1815
max vertical force on wheel 3	2347	2328	2486	2474	2463	2451	2439	2427	2414	2402	2389	2376	2363	2349
min vertical force on wheel 4	2153	2118	2419	2395	2371	2347	2322	2298	2274	2249	2225	2201	2176	2152
max vertical force on wheel 4	2789	2744	3125	3094	3063	3032	3001	2970	2939	2908	2877	2847	2816	2785
total radial force on front bearing	-19	-21	-2	-4	-5	-7	-8	-10	-11	-13	-14	-16	-17	-19
total radial force on rear bearing	202	226	17	32	48	64	81	97	114	130	147	164	181	199
weight of Ladder w_L	100	100	100	100	100	100	100	100	100	100	100	100	100	100
weight of cutterhead w_{CH}	25	25	25	25	25	25	25	25	25	25	25	25	25	25
weight of dredge arm w_A	2000	2000	2000	2000	2000	2000	2000	2000	2000	2000	2000	2000	2000	2000
weight of dredge carriage W_D	1523	1523	1523	1523	1523	1523	1523	1523	1523	1523	1523	1523	1523	1523
weight of towing carriage w_C	6377	6377	6377	6377	6377	6377	6377	6377	6377	6377	6377	6377	6377	6377
length of ladder X_2	3.00	3.00	3.00	3.00	3.00	3.00	3.00	3.00	3.00	3.00	3.00	3.00	3.00	3.00
distance to leverage point X_1	1.00	1.00	1.00	1.00	1.00	1.00	1.00	1.00	1.00	1.00	1.00	1.00	1.00	1.00
distance to ladder centroid X_3	1.00	1.00	1.00	1.00	1.00	1.00	1.00	1.00	1.00	1.00	1.00	1.00	1.00	1.00
distance between ladder end bearings	1.50	1.50	1.50	1.50	1.50	1.50	1.50	1.50	1.50	1.50	1.50	1.50	1.50	1.50
length of dredge arm z_1	19.00	19.00	19.00	19.00	19.00	19.00	19.00	19.00	19.00	19.00	19.00	19.00	19.00	19.00
distance to lower slide bearing set z_3	4.00	4.00	4.00	4.00	4.00	4.00	4.00	4.00	4.00	4.00	4.00	4.00	4.00	4.00
horizontal dist between d-arm bearngs x_4	2.00	2.00	2.00	2.00	2.00	2.00	2.00	2.00	2.00	2.00	2.00	2.00	2.00	2.00
horizontal dist between d-arm bearngs y_1	2.00	2.00	2.00	2.00	2.00	2.00	2.00	2.00	2.00	2.00	2.00	2.00	2.00	2.00
dist between d-carriage slide bearings x_5	7.00	7.00	7.00	7.00	7.00	7.00	7.00	7.00	7.00	7.00	7.00	7.00	7.00	7.00
height of dredge carriage z_5	10.58	10.58	10.58	10.58	10.58	10.58	10.58	10.58	10.58	10.58	10.58	10.58	10.58	10.58
dist between d-carriage slide bearings y_2	2.00	2.00	2.00	2.00	2.00	2.00	2.00	2.00	2.00	2.00	2.00	2.00	2.00	2.00
dist from t-c wheel to d-carrge bearing X_8	2.00	2.00	2.00	2.00	2.00	2.00	2.00	2.00	2.00	2.00	2.00	2.00	2.00	2.00
dist from t-carriage wheel to centroid X_7	10.00	10.00	10.00	10.00	10.00	10.00	10.00	10.00	10.00	10.00	10.00	10.00	10.00	10.00
distance between carriage wheels X_6	15.00	15.00	15.00	15.00	15.00	15.00	15.00	15.00	15.00	15.00	15.00	15.00	15.00	15.00
width of towing carriage Y_3	12.83	12.83	12.83	12.83	12.83	12.83	12.83	12.83	12.83	12.83	12.83	12.83	12.83	12.83
dist from wheel to carriag centroid Y_4	6.42	6.42	6.42	6.42	6.42	6.42	6.42	6.42	6.42	6.42	6.42	6.42	6.42	6.42
vertical force at ladder end F_{Lz}	-177	-215	98	72	45	19	-7	-33	-59	-85	-111	-136	-162	-187
horizontal force at ladder end F_{Lx}	-255	-287	-23	-45	-68	-90	-112	-134	-156	-178	-200	-222	-243	-265
horizontal moment at ladder end M_{Lx}	777	871	60	121	182	244	307	370	434	498	564	629	696	763
vertical moment at ladder end M_{Lz}	777	871	60	121	182	244	307	370	434	498	564	629	696	763
moment due to lader rotation device M_{Lv}	711	818	-50	24	97	170	243	315	387	459	530	601	671	742
Fa =	89.7	100.5	8.3	15.3	22.4	29.5	36.7	43.9	51.2	58.5	65.9	73.4	80.9	88.5
Fb =	437.8	490.4	33.9	68.1	102.7	137.6	172.9	208.5	244.5	280.8	317.5	354.6	392.0	429.8
Fc =	45.8	51.3	3.5	7.1	10.7	14.4	18.1	21.8	25.6	29.4	33.2	37.1	41.0	45.0
Fd =	-31.8	-35.9	-2.8	-5.7	-8.5	-11.3	-14.0	-16.8	-19.6	-22.3	-25.0	-27.7	-30.4	-33.1
Fe =	314.9	356.4	21.0	49.6	78.0	106.4	134.5	162.5	190.4	218.1	245.7	273.1	300.4	327.5
angle between F_a and $F_{b/c}$ in radians =	0.79	0.79	0.79	0.79	0.79	0.79	0.79	0.79	0.79	0.79	0.79	0.79	0.79	0.79
vert force on both left d-c slide brng $F_{Dz1\&2}$	3688	3911	1967	2111	2257	2404	2554	2705	2857	3012	3168	3325	3485	3646
vert force on both right d-c slide brng $F_{Dz3\&4}$	-342	-603	1655	1484	1312	1138	962	785	607	426	245	61	-124	-311
vert force on both front d-c slide brng $F_{Dz2\&4}$	1249	1172	1789	1737	1684	1632	1581	1529	1478	1427	1377	1326	1276	1226
vert force on both rear d-c slide brng $F_{Dz1\&3}$	2098	2135	1832	1858	1884	1910	1935	1960	1986	2011	2036	2060	2085	2109
vert force on d-c slide bearing 1	2312	2525	995	1091	1192	1296	1405	1519	1638	1761	1890	2023	2162	2306
vert force on d-c slide bearing 2	-214	-390	837	767	693	613	530	441	348	249	146	37	-77	-196
vert force on d-c slide bearing 3	1376	1386	972	1020	1065	1108	1148	1185	1219	1250	1278	1302	1323	1340
vert force on d-c slide bearing 4	-128	-214	817	717	619	524	433	344	259	177	99	24	-47	-114
horiz force each d-carriage bearing $F_{Dx1,2}$	-317	-356	-29	-55	-80	-106	-132	-158	-184	-210	-237	-263	-290	-316
horiz force each d-carriage bearing $F_{Dx3,4}$	190	212	18	32	46	61	76	91	106	121	137	152	168	184
vertical force on front wheels $F_{C2z} + F_{C4z}$	5280	5239	5569	5541	5513	5485	5458	5430	5403	5376	5349	5322	5295	5268
vertical force on rear wheels $F_{C1z} + F_{C3z}$	4443	4445	4429	4431	4432	4434	4435	4436	4438	4439	4440	4442	4443	4444
min vert force on right wheels $F_{C1z} + F_{C2z}$	4588	4613	4387	4403	4419	4436	4453	4470	4487	4505	4523	4541	4560	4579
max vert force on right wheels $F_{C1z} + F_{C2z}$	5759	5770	5655	5661	5668	5676	5683	5691	5699	5708	5717	5726	5736	5746
min vert force on left wheels $F_{C3z} + F_{C4z}$	3964	3914	4344	4311	4277	4244	4210	4176	4141	4107	4072	4037	4002	3967
max vert force on left wheels $F_{C3z} + F_{C4z}$	5136	5072	5611	5569	5526	5483	5440	5397	5354	5310	5266	5222	5178	5134

Table B.1: Continued

cutter horsepower	13.8	14.9	0.5	1.1	1.6	2.1	3.2	3.7	4.3	4.8	5.3	5.8	6.4	6.9
horizontal reaction force at cutter H	391.6	423.9	18.9	37.9	56.9	76.1	114.8	134.2	153.8	173.5	193.2	213.1	233.0	253.1
vertical reaction force at cutter V	440.9	473.7	12.2	24.3	36.2	48.1	71.4	82.9	94.3	105.6	116.7	127.8	138.7	149.6
axial reaction force at cutter A	36.6	39.5	1.4	2.8	4.2	5.6	8.4	9.8	11.2	12.6	14.0	15.4	16.9	18.3
moment caused by pump drive	15.00	15.00	15.00	15.00	15.00	15.00	15.00	15.00	15.00	15.00	15.00	15.00	15.00	15.00
ladder angle Φ (90-0)	45.00	45.00	45.00	45.00	45.00	45.00	45.00	45.00	45.00	45.00	45.00	45.00	45.00	45.00
elevation of dredge arm (1.5-7.17) z_2	6.12	6.12	6.12	6.12	6.12	6.12	6.12	6.12	6.12	6.12	6.12	6.12	6.12	6.12
moment caused by cutter drive	242	261	9	19	28	37	56	65	74	84	93	102	112	121
vertical cutterhead position h	-11	-11	-11	-11	-11	-11	-11	-11	-11	-11	-11	-11	-11	-11
thrust load at ladder end bearing	196	212	9	19	28	38	57	67	77	87	97	107	117	127
total radial ladder end bearing force rght side	778	846	39	46	76	113	190	229	269	309	350	390	431	472
total radial ladder end bearing force left side	828	893	90	123	158	195	270	308	346	385	424	463	502	542
dredge arm winch cable lift force F_{Az}	1787	1762	2115	2106	2096	2087	2069	2059	2050	2041	2033	2024	2015	2006
total radial ladder arm slide bearing 1 force	553	597	21	43	66	90	136	160	184	207	231	255	279	303
total radial ladder arm slide bearing 2 force	548	592	24	48	72	96	144	169	194	218	243	268	293	318
total radial ladder arm slide bearing 3 force	431	466	16	33	51	69	106	124	143	161	180	198	217	236
total radial ladder arm slide bearing 4 force	668	721	29	57	86	116	175	204	234	264	294	324	354	385
total radial ladder arm slide bearing 5 force	641	692	22	48	73	99	151	177	204	230	256	282	309	335
total radial ladder arm slide bearing 6 force	622	672	25	51	77	103	156	182	209	236	262	289	316	343
total radial ladder arm slide bearing 7 force	522	564	17	37	58	79	121	142	163	184	205	226	248	269
total radial ladder arm slide bearing 8 force	743	802	30	61	92	123	187	218	250	282	314	346	378	411
tot d-carriage slide bearing force on 1	2479	2637	959	1017	1075	1135	1258	1320	1384	1449	1515	1582	1650	1719
tot d-carriage slide bearing force on 3	379	502	856	807	758	708	606	553	501	448	395	344	294	248
tot d-carriage slide bearing force on 2	1397	1413	964	1007	1050	1092	1176	1218	1259	1300	1341	1381	1421	1461
tot d-carriage slide bearing force on 4	268	321	860	800	740	681	567	511	457	404	353	306	262	224
min vertical force on wheel 1	2110	2125	1939	1946	1954	1962	1978	1986	1994	2002	2010	2018	2026	2034
max vertical force on wheel 1	2642	2654	2502	2508	2515	2522	2536	2543	2550	2557	2565	2572	2579	2586
min vertical force on wheel 2	2488	2492	2446	2452	2457	2463	2474	2480	2486	2492	2498	2504	2510	2516
max vertical force on wheel 2	3115	3113	3157	3160	3163	3166	3173	3176	3180	3183	3187	3191	3195	3199
min vertical force on wheel 3	1804	1793	1926	1920	1913	1906	1892	1885	1878	1871	1864	1857	1850	1842
max vertical force on wheel 3	2336	2322	2489	2482	2474	2466	2451	2443	2435	2427	2419	2411	2403	2395
min vertical force on wheel 4	2127	2103	2431	2418	2406	2393	2367	2355	2342	2329	2317	2304	2291	2279
max vertical force on wheel 4	2754	2723	3141	3126	3111	3096	3066	3051	3036	3021	3006	2991	2976	2962
total radial force on front bearing	-20	-22	-2	-3	-3	-4	-6	-6	-7	-8	-9	-10	-10	-11
total radial force on rear bearing	216	234	11	21	32	42	63	74	84	95	105	116	127	138
weight of Ladder w_L	100	100	100	100	100	100	100	100	100	100	100	100	100	100
weight of cutterhead w_{CH}	25	25	25	25	25	25	25	25	25	25	25	25	25	25
weight of dredge arm w_A	2000	2000	2000	2000	2000	2000	2000	2000	2000	2000	2000	2000	2000	2000
weight of dredge carriage W_D	1523	1523	1523	1523	1523	1523	1523	1523	1523	1523	1523	1523	1523	1523
weight of towing carriage w_C	6377	6377	6377	6377	6377	6377	6377	6377	6377	6377	6377	6377	6377	6377
length of ladder X_2	3.00	3.00	3.00	3.00	3.00	3.00	3.00	3.00	3.00	3.00	3.00	3.00	3.00	3.00
distance to leverage point X_1	1.00	1.00	1.00	1.00	1.00	1.00	1.00	1.00	1.00	1.00	1.00	1.00	1.00	1.00
distance to ladder centroid X_3	1.00	1.00	1.00	1.00	1.00	1.00	1.00	1.00	1.00	1.00	1.00	1.00	1.00	1.00
distance between ladder end bearings	1.50	1.50	1.50	1.50	1.50	1.50	1.50	1.50	1.50	1.50	1.50	1.50	1.50	1.50
length of dredge arm z_1	19.00	19.00	19.00	19.00	19.00	19.00	19.00	19.00	19.00	19.00	19.00	19.00	19.00	19.00
distance to lower slide bearing set z_3	4.00	4.00	4.00	4.00	4.00	4.00	4.00	4.00	4.00	4.00	4.00	4.00	4.00	4.00
horizontal dist between d-arm bearngs x_4	2.00	2.00	2.00	2.00	2.00	2.00	2.00	2.00	2.00	2.00	2.00	2.00	2.00	2.00
horizontal dist between d-arm bearngs y_1	2.00	2.00	2.00	2.00	2.00	2.00	2.00	2.00	2.00	2.00	2.00	2.00	2.00	2.00
dist between d-carriage slide bearings x_5	7.00	7.00	7.00	7.00	7.00	7.00	7.00	7.00	7.00	7.00	7.00	7.00	7.00	7.00
height of dredge carriage z_5	10.58	10.58	10.58	10.58	10.58	10.58	10.58	10.58	10.58	10.58	10.58	10.58	10.58	10.58
dist between d-carriage slide bearings y_2	2.00	2.00	2.00	2.00	2.00	2.00	2.00	2.00	2.00	2.00	2.00	2.00	2.00	2.00
dist from t-c wheel to d-carrge bearing X_8	2.00	2.00	2.00	2.00	2.00	2.00	2.00	2.00	2.00	2.00	2.00	2.00	2.00	2.00
dist from t-carriage wheel to centroid X_7	10.00	10.00	10.00	10.00	10.00	10.00	10.00	10.00	10.00	10.00	10.00	10.00	10.00	10.00
distance between carriage wheels X_6	15.00	15.00	15.00	15.00	15.00	15.00	15.00	15.00	15.00	15.00	15.00	15.00	15.00	15.00
width of towing carriage Y_3	12.83	12.83	12.83	12.83	12.83	12.83	12.83	12.83	12.83	12.83	12.83	12.83	12.83	12.83
dist from wheel to carriag centroid Y_4	6.42	6.42	6.42	6.42	6.42	6.42	6.42	6.42	6.42	6.42	6.42	6.42	6.42	6.42
vertical force at ladder end F_{Lz}	-213	-238	115	106	96	87	69	59	50	41	33	24	15	6
horizontal force at ladder end F_{Lx}	-286	-307	-8	-15	-23	-30	-45	-52	-59	-66	-73	-79	-86	-93
horizontal moment at ladder end M_{Lx}	831	899	40	80	121	161	243	285	326	368	410	452	494	537
vertical moment at ladder end M_{Lz}	831	899	40	80	121	161	243	285	326	368	410	452	494	537
moment due to lader rotation device M_{Lv}	812	881	-98	-72	-47	-22	28	52	76	100	124	147	171	194
Fa =	96.1	103.8	5.7	10.1	14.5	18.9	27.8	32.3	36.7	41.3	45.8	50.3	54.9	59.5
Fb =	468.0	506.5	22.6	45.2	68.0	91.0	137.2	160.4	183.8	207.3	230.9	254.7	278.5	302.5
Fc =	49.0	53.0	2.4	4.7	7.1	9.5	14.3	16.8	19.2	21.7	24.2	26.6	29.1	31.6
Fd =	-35.7	-38.4	-1.0	-1.9	-2.8	-3.8	-5.6	-6.5	-7.3	-8.2	-9.1	-9.9	-10.8	-11.6
Fe =	354.5	381.3	2.0	11.6	21.1	30.6	49.1	58.2	67.2	76.1	84.9	93.6	102.2	110.7
angle between F_a and F_{bc} in radians =	0.79	0.79	0.79	0.79	0.79	0.79	0.79	0.79	0.79	0.79	0.79	0.79	0.79	0.79
vert force on both left d-c slide brng $F_{Dz1\&2}$	3809	3974	1923	2023	2123	2224	2427	2530	2633	2736	2841	2946	3051	3157
vert force on both right d-c slide brng $F_{Dz3\&4}$	-499	-689	1715	1606	1497	1386	1164	1053	941	828	715	601	487	372
vert force on both front d-c slide brng $F_{Dz2\&4}$	1177	1127	1823	1805	1788	1770	1735	1718	1701	1685	1668	1652	1635	1619
vert force on both rear d-c slide brng $F_{Dz1\&3}$	2134	2158	1815	1823	1832	1840	1856	1864	1872	1880	1888	1895	1903	1910
vert force on d-c slide bearing 1	2455	2611	959	1016	1074	1133	1254	1316	1379	1443	1508	1574	1641	1708
vert force on d-c slide bearing 2	-322	-453	856	807	757	707	602	548	493	437	379	321	262	202
vert force on d-c slide bearing 3	1354	1364	964	1006	1049	1090	1173	1213	1253	1293	1333	1372	1410	1448
vert force on d-c slide bearing 4	-177	-236	860	799	739	680	563	505	448	391	335	280	225	171
horiz force each d-carriage bearing $F_{Dx1,2}$	-343	-370	-18	-32	-47	-61	-90	-104	-119	-133	-148	-162	-177	-191
horiz force each d-carriage bearing $F_{Dx3,4}$	200	217	14	25	35	46	67	78	89	100	111	122	134	145
vertical force on front wheels $F_{C2z} + F_{C4z}$	5242	5215	5587	5578	5568	5559	5540	5531	5522	5513	5504	5495	5486	5478
vertical force on rear wheels $F_{C1z} + F_{C3z}$	4446	4447	4428	4428	4428	4428	4429	4429	4429	4429	4429	4429	4429	4429
min vert force on right wheels $F_{C1z} + F_{C2z}$	4598	4617	4385	4398	4411	4425	4452	4465	4479	4493	4507	4521	4536	4550
max vert force on right wheels $F_{C1z} + F_{C2z}$	5756	5767	5658	5668	5678	5688	5709	5719	5730	5741	5752	5763	5774	5785
min vert force on left wheels $F_{C3z} + F_{C4z}$	3931	3895	4357	4338	4319	4299	4260	4240	4221	4201	4181	4161	4141	4121
max vert force on left wheels $F_{C3z} + F_{C4z}$	5090	5045	5631	5608	5585	5562	5517	5494	5471	5448	5425	5402	5379	5356

Table B.1: Continued

cutter horsepower	7.4	8.0	8.5	9.0	9.6	10.1	10.6	11.2	11.7	12.2	12.8	13.3	13.8	14.4
horizontal reaction force at cutter H	273.2	293.5	313.8	334.2	354.7	375.3	396.0	416.7	437.6	458.6	479.6	500.7	521.9	543.2
vertical reaction force at cutter V	160.3	170.9	181.4	191.8	202.1	212.3	222.4	232.4	242.3	252.1	261.8	271.4	280.9	290.3
axial reaction force at cutter A	19.7	21.1	22.5	23.9	25.4	26.8	28.2	29.7	31.1	32.5	34.0	35.4	36.8	38.3
moment caused by pump drive	15.00	15.00	15.00	15.00	15.00	15.00	15.00	15.00	15.00	15.00	15.00	15.00	15.00	15.00
ladder angle Φ (90-0)	45.00	45.00	45.00	45.00	45.00	45.00	45.00	45.00	45.00	45.00	45.00	45.00	45.00	45.00
elevation of dredge arm (1.5-7.17) z_2	6.12	6.12	6.12	6.12	6.12	6.12	6.12	6.12	6.12	6.12	6.12	6.12	6.12	6.12
moment caused by cutter drive	130	140	149	158	168	177	186	195	205	214	223	233	242	251
vertical cutterhead position h	-11	-11	-11	-11	-11	-11	-11	-11	-11	-11	-11	-11	-11	-11
thrust load at ladder end bearing	137	147	157	167	177	188	198	208	219	229	240	250	261	272
total radial ladder end bearing force rght side	513	555	596	638	680	722	765	807	850	893	936	979	1023	1066
total radial ladder end bearing force left side	582	622	662	703	743	784	825	866	907	949	990	1032	1074	1116
dredge arm winch cable lift force F_{Az}	1998	1989	1981	1972	1964	1956	1948	1940	1932	1924	1916	1908	1900	1893
total radial ladder arm slide bearing 1 force	327	351	375	400	424	449	473	498	522	547	572	597	622	647
total radial ladder arm slide bearing 2 force	343	368	394	419	445	470	496	522	548	574	600	626	652	679
total radial ladder arm slide bearing 3 force	255	273	292	311	330	350	369	388	407	427	446	465	485	505
total radial ladder arm slide bearing 4 force	415	446	476	507	538	569	600	631	662	694	725	757	788	820
total radial ladder arm slide bearing 5 force	362	388	415	441	468	495	521	548	575	602	629	656	683	710
total radial ladder arm slide bearing 6 force	370	397	425	452	479	507	534	562	589	617	645	673	701	729
total radial ladder arm slide bearing 7 force	290	311	333	354	376	397	418	440	462	483	505	526	548	570
total radial ladder arm slide bearing 8 force	443	475	508	540	573	606	639	672	705	738	771	804	838	871
tot d-carriage slide bearing force on 1	1789	1860	1932	2005	2078	2153	2229	2305	2383	2461	2541	2621	2702	2784
tot d-carriage slide bearing force on 3	210	185	180	197	233	281	337	398	462	528	597	667	739	813
tot d-carriage slide bearing force on 2	1500	1539	1578	1617	1655	1692	1730	1767	1803	1839	1875	1911	1946	1981
tot d-carriage slide bearing force on 4	195	180	180	195	222	257	297	340	384	429	475	521	567	613
min vertical force on wheel 1	2042	2051	2059	2067	2076	2084	2093	2101	2110	2118	2127	2135	2144	2153
max vertical force on wheel 1	2594	2601	2609	2616	2624	2631	2639	2646	2654	2662	2670	2678	2685	2693
min vertical force on wheel 2	2522	2528	2535	2541	2548	2554	2561	2568	2574	2581	2588	2595	2602	2609
max vertical force on wheel 2	3203	3207	3211	3216	3220	3225	3229	3234	3239	3244	3249	3254	3259	3264
min vertical force on wheel 3	1835	1828	1820	1812	1805	1797	1789	1782	1774	1766	1758	1750	1742	1734
max vertical force on wheel 3	2386	2378	2370	2361	2353	2344	2336	2327	2318	2310	2301	2292	2283	2274
min vertical force on wheel 4	2266	2253	2241	2228	2215	2203	2190	2177	2165	2152	2139	2127	2114	2101
max vertical force on wheel 4	2947	2932	2917	2903	2888	2873	2858	2844	2829	2815	2800	2785	2771	2756
total radial force on front bearing	-12	-13	-13	-14	-15	-16	-17	-17	-18	-19	-20	-21	-21	-22
total radial force on rear bearing	149	159	170	181	192	203	215	226	237	248	260	271	282	294
weight of Ladder w_L	100	100	100	100	100	100	100	100	100	100	100	100	100	100
weight of cutterhead w_{CH}	25	25	25	25	25	25	25	25	25	25	25	25	25	25
weight of dredge arm w_A	2000	2000	2000	2000	2000	2000	2000	2000	2000	2000	2000	2000	2000	2000
weight of dredge carriage W_D	1523	1523	1523	1523	1523	1523	1523	1523	1523	1523	1523	1523	1523	1523
weight of towing carriage w_C	6377	6377	6377	6377	6377	6377	6377	6377	6377	6377	6377	6377	6377	6377
length of ladder X_2	3.00	3.00	3.00	3.00	3.00	3.00	3.00	3.00	3.00	3.00	3.00	3.00	3.00	3.00
distance to leverage point X_1	1.00	1.00	1.00	1.00	1.00	1.00	1.00	1.00	1.00	1.00	1.00	1.00	1.00	1.00
distance to ladder centroid X_3	1.00	1.00	1.00	1.00	1.00	1.00	1.00	1.00	1.00	1.00	1.00	1.00	1.00	1.00
distance between ladder end bearings	1.50	1.50	1.50	1.50	1.50	1.50	1.50	1.50	1.50	1.50	1.50	1.50	1.50	1.50
length of dredge arm z_1	19.00	19.00	19.00	19.00	19.00	19.00	19.00	19.00	19.00	19.00	19.00	19.00	19.00	19.00
distance to lower slide bearing set z_3	4.00	4.00	4.00	4.00	4.00	4.00	4.00	4.00	4.00	4.00	4.00	4.00	4.00	4.00
horizontal dist between d-arm bearngs x_4	2.00	2.00	2.00	2.00	2.00	2.00	2.00	2.00	2.00	2.00	2.00	2.00	2.00	2.00
horizontal dist between d-arm bearngs y_1	2.00	2.00	2.00	2.00	2.00	2.00	2.00	2.00	2.00	2.00	2.00	2.00	2.00	2.00
dist between d-carriage slide bearings x_5	7.00	7.00	7.00	7.00	7.00	7.00	7.00	7.00	7.00	7.00	7.00	7.00	7.00	7.00
height of dredge carriage z_5	10.58	10.58	10.58	10.58	10.58	10.58	10.58	10.58	10.58	10.58	10.58	10.58	10.58	10.58
dist between d-carriage slide bearings y_2	2.00	2.00	2.00	2.00	2.00	2.00	2.00	2.00	2.00	2.00	2.00	2.00	2.00	2.00
dist from t-c wheel to d-carrge bearing X_8	2.00	2.00	2.00	2.00	2.00	2.00	2.00	2.00	2.00	2.00	2.00	2.00	2.00	2.00
dist from t-carriage wheel to centroid X_7	10.00	10.00	10.00	10.00	10.00	10.00	10.00	10.00	10.00	10.00	10.00	10.00	10.00	10.00
distance between carriage wheels X_6	15.00	15.00	15.00	15.00	15.00	15.00	15.00	15.00	15.00	15.00	15.00	15.00	15.00	15.00
width of towing carriage Y_3	12.83	12.83	12.83	12.83	12.83	12.83	12.83	12.83	12.83	12.83	12.83	12.83	12.83	12.83
dist from wheel to carriag centroid Y_4	6.42	6.42	6.42	6.42	6.42	6.42	6.42	6.42	6.42	6.42	6.42	6.42	6.42	6.42
vertical force at ladder end F_{Lz}	-2	-11	-19	-28	-36	-44	-52	-60	-68	-76	-84	-92	-100	-107
horizontal force at ladder end F_{Lx}	-99	-106	-112	-119	-125	-131	-137	-143	-149	-155	-161	-167	-173	-178
horizontal moment at ladder end M_{Lx}	580	623	666	709	752	796	840	884	928	973	1017	1062	1107	1152
vertical moment at ladder end M_{Lz}	580	623	666	709	752	796	840	884	928	973	1017	1062	1107	1152
moment due to lader rotation device M_{Lv}	216	239	261	283	305	327	348	369	390	411	432	452	472	492
Fa =	64.1	68.7	73.3	78.0	82.6	87.3	92.0	96.7	101.5	106.2	111.0	115.8	120.6	125.4
Fb =	326.5	350.7	375.0	399.4	423.9	448.5	473.2	498.0	523.0	548.0	573.1	598.4	623.7	649.2
Fc =	34.2	36.7	39.2	41.8	44.3	46.9	49.5	52.1	54.7	57.3	59.9	62.6	65.2	67.9
Fd =	-12.4	-13.2	-14.0	-14.8	-15.6	-16.4	-17.2	-17.9	-18.7	-19.4	-20.1	-20.9	-21.6	-22.3
Fe =	119.1	127.5	135.7	143.8	151.9	159.8	167.7	175.4	183.1	190.7	198.2	205.6	212.9	220.1
angle between F_a and $F_{b/c}$ in radians =	0.79	0.79	0.79	0.79	0.79	0.79	0.79	0.79	0.79	0.79	0.79	0.79	0.79	0.79
vert force on both left d-c slide brng $F_{Dz1\&2}$	3263	3370	3478	3586	3695	3804	3914	4024	4134	4246	4357	4470	4582	4696
vert force on both right d-c slide brng $F_{Dz3\&4}$	257	142	26	-91	-208	-325	-443	-561	-680	-799	-919	-1039	-1159	-1280
vert force on both front d-c slide brng $F_{Dz2\&4}$	1603	1588	1572	1557	1541	1526	1511	1497	1482	1468	1453	1439	1425	1411
vert force on both rear d-c slide brng $F_{Dz1\&3}$	1917	1925	1932	1939	1946	1953	1959	1966	1973	1979	1985	1992	1998	2004
vert force on d-c slide bearing 1	1777	1847	1917	1989	2061	2135	2209	2285	2361	2438	2516	2595	2675	2755
vert force on d-c slide bearing 2	140	78	14	-50	-116	-182	-250	-319	-388	-459	-530	-603	-677	-751
vert force on d-c slide bearing 3	1486	1523	1560	1597	1633	1669	1704	1739	1774	1808	1842	1875	1908	1940
vert force on d-c slide bearing 4	117	64	12	-40	-92	-143	-193	-243	-292	-340	-388	-436	-483	-529
horiz force each d-carriage bearing $F_{Dx1,2}$	-206	-221	-235	-250	-265	-280	-295	-309	-324	-339	-354	-369	-384	-399
horiz force each d-carriage bearing $F_{Dx3,4}$	156	168	179	191	202	214	226	238	250	262	274	286	298	310
vertical force on front wheels $F_{C2z} + F_{C4z}$	5469	5461	5452	5444	5436	5427	5419	5411	5404	5396	5388	5380	5373	5365
vertical force on rear wheels $F_{C1z} + F_{C3z}$	4429	4429	4429	4429	4429	4428	4428	4428	4428	4428	4428	4428	4427	4427
min vert force on right wheels $F_{C1z} + F_{C2z}$	4565	4579	4594	4609	4624	4639	4654	4669	4684	4699	4715	4731	4746	4762
max vert force on right wheels $F_{C1z} + F_{C2z}$	5797	5808	5820	5832	5844	5856	5868	5881	5893	5906	5918	5931	5944	5957
min vert force on left wheels $F_{C3z} + F_{C4z}$	4101	4081	4061	4041	4020	4000	3980	3959	3939	3918	3897	3877	3856	3835
max vert force on left wheels $F_{C3z} + F_{C4z}$	5333	5310	5287	5264	5241	5217	5194	5171	5148	5124	5101	5078	5054	5031

Table B.1: Continued

	Undercutting													
cutter horsepower	14.9	15.4	2.1	4.3	6.4	8.5	10.6	12.8	14.9	1.6	3.2	4.8	8.0	9.6
horizontal reaction force at cutter H	564.6	586.0	89.3	178.7	268.0	357.3	446.7	536.0	625.4	47.1	93.9	140.2	231.8	277.0
vertical reaction force at cutter V	299.6	308.8	-9.7	-19.3	-29.0	-38.7	-48.4	-58.0	-67.7	-48.1	-96.6	-145.3	-243.6	-293.2
axial reaction force at cutter A	39.7	41.2	5.6	11.2	16.8	22.3	27.9	33.5	39.1	4.2	8.4	12.5	20.9	25.1
moment caused by pump drive	15.00	15.00	-15.00	-15.00	-15.00	-15.00	-15.00	-15.00	-15.00	-15.00	-15.00	-15.00	-15.00	-15.00
ladder angle Φ (90-0)	45.00	45.00	45.00	45.00	45.00	45.00	45.00	45.00	45.00	45.00	45.00	45.00	45.00	45.00
elevation of dredge arm (1.5-7.17) z_2	6.12	6.12	6.12	6.12	6.12	6.12	6.12	6.12	6.12	6.12	6.12	6.12	6.12	6.12
moment caused by cutter drive	261	270	-37	-74	-112	-149	-186	-223	-261	-28	-56	-84	-140	-168
vertical cutterhead position h	-11	-11	-11	-11	-11	-11	-11	-11	-11	-11	-11	-11	-11	-11
thrust load at ladder end bearing	282	293	45	89	134	179	223	268	313	24	47	70	116	139
total radial ladder end bearing force rght side	1110	1154	146	323	504	685	866	1047	1229	86	174	269	461	556
total radial ladder end bearing force left side	1158	1201	225	400	575	750	926	1102	1278	152	246	339	524	616
dredge arm winch cable lift force F_{Az}	1885	1878	2128	2131	2134	2137	2139	2142	2145	2156	2187	2219	2282	2315
total radial ladder arm slide bearing 1 force	672	697	113	224	335	446	557	668	779	85	164	244	402	481
total radial ladder arm slide bearing 2 force	705	732	108	215	322	429	536	643	751	75	146	217	358	428
total radial ladder arm slide bearing 3 force	524	544	91	180	268	357	445	534	623	70	135	199	328	392
total radial ladder arm slide bearing 4 force	852	884	130	260	389	519	648	778	908	90	176	262	433	518
total radial ladder arm slide bearing 5 force	737	765	110	218	327	435	544	652	761	80	153	227	373	446
total radial ladder arm slide bearing 6 force	757	785	105	210	315	420	525	630	735	70	136	202	332	397
total radial ladder arm slide bearing 7 force	592	613	88	174	260	346	432	518	604	65	124	182	299	357
total radial ladder arm slide bearing 8 force	905	938	127	255	382	510	637	765	892	85	166	246	406	486
tot d-carriage slide bearing force on 1	2867	2951	1137	1367	1594	1816	2034	2247	2456	1004	1096	1178	1315	1370
tot d-carriage slide bearing force on 3	887	963	656	418	208	172	357	575	796	757	621	496	291	223
tot d-carriage slide bearing force on 2	2016	2050	1181	1446	1715	1990	2269	2552	2840	1095	1276	1465	1864	2074
tot d-carriage slide bearing force on 4	659	705	681	441	219	174	386	641	906	825	722	614	391	285
min vertical force on wheel 1	2162	2170	1962	1993	2024	2054	2085	2116	2146	1943	1955	1967	1989	2000
max vertical force on wheel 1	2701	2709	2525	2556	2586	2616	2647	2677	2707	2509	2523	2536	2562	2575
min vertical force on wheel 2	2616	2623	2487	2534	2581	2627	2674	2721	2769	2479	2517	2556	2633	2671
max vertical force on wheel 2	3269	3275	3202	3250	3298	3346	3395	3443	3492	3201	3248	3296	3391	3439
min vertical force on wheel 3	1726	1718	1897	1860	1824	1788	1752	1716	1680	1910	1887	1864	1820	1798
max vertical force on wheel 3	2265	2256	2460	2423	2386	2350	2313	2277	2240	2476	2455	2434	2393	2373
min vertical force on wheel 4	2089	2076	2404	2365	2326	2286	2247	2207	2167	2437	2429	2423	2409	2402
max vertical force on wheel 4	2742	2727	3119	3081	3043	3005	2967	2929	2890	3158	3160	3163	3168	3170
total radial force on front bearing	-23	-24	3	5	6	8	10	12	13	2	4	5	8	10
total radial force on rear bearing	305	317	42	85	128	171	214	256	299	21	43	65	107	129
weight of Ladder w_L	100	100	100	100	100	100	100	100	100	100	100	100	100	100
weight of cutterhead w_{CH}	25	25	25	25	25	25	25	25	25	25	25	25	25	25
weight of dredge arm w_A	2000	2000	2000	2000	2000	2000	2000	2000	2000	2000	2000	2000	2000	2000
weight of dredge carriage W_D	1523	1523	1523	1523	1523	1523	1523	1523	1523	1523	1523	1523	1523	1523
weight of towing carriage w_C	6377	6377	6377	6377	6377	6377	6377	6377	6377	6377	6377	6377	6377	6377
length of ladder X_2	3.00	3.00	3.00	3.00	3.00	3.00	3.00	3.00	3.00	3.00	3.00	3.00	3.00	3.00
distance to leverage point X_1	1.00	1.00	1.00	1.00	1.00	1.00	1.00	1.00	1.00	1.00	1.00	1.00	1.00	1.00
distance to ladder centroid X_3	1.00	1.00	1.00	1.00	1.00	1.00	1.00	1.00	1.00	1.00	1.00	1.00	1.00	1.00
distance between ladder end bearings	1.50	1.50	1.50	1.50	1.50	1.50	1.50	1.50	1.50	1.50	1.50	1.50	1.50	1.50
length of dredge arm z_1	19.00	19.00	19.00	19.00	19.00	19.00	19.00	19.00	19.00	19.00	19.00	19.00	19.00	19.00
distance to lower slide bearing set z_3	4.00	4.00	4.00	4.00	4.00	4.00	4.00	4.00	4.00	4.00	4.00	4.00	4.00	4.00
horizontal dist between d-arm bearngs x_4	2.00	2.00	2.00	2.00	2.00	2.00	2.00	2.00	2.00	2.00	2.00	2.00	2.00	2.00
horizontal dist between d-arm bearngs y_1	2.00	2.00	2.00	2.00	2.00	2.00	2.00	2.00	2.00	2.00	2.00	2.00	2.00	2.00
dist between d-carriage slide bearings x_5	7.00	7.00	7.00	7.00	7.00	7.00	7.00	7.00	7.00	7.00	7.00	7.00	7.00	7.00
height of dredge carriage z_5	10.58	10.58	10.58	10.58	10.58	10.58	10.58	10.58	10.58	10.58	10.58	10.58	10.58	10.58
dist between d-carriage slide bearings y_2	2.00	2.00	2.00	2.00	2.00	2.00	2.00	2.00	2.00	2.00	2.00	2.00	2.00	2.00
dist from t-c wheel to d-carrge bearing X_8	2.00	2.00	2.00	2.00	2.00	2.00	2.00	2.00	2.00	2.00	2.00	2.00	2.00	2.00
dist from t-carriage wheel to centroid X_7	10.00	10.00	10.00	10.00	10.00	10.00	10.00	10.00	10.00	10.00	10.00	10.00	10.00	10.00
distance between carriage wheels X_6	15.00	15.00	15.00	15.00	15.00	15.00	15.00	15.00	15.00	15.00	15.00	15.00	15.00	15.00
width of towing carriage Y_3	12.83	12.83	12.83	12.83	12.83	12.83	12.83	12.83	12.83	12.83	12.83	12.83	12.83	12.83
dist from wheel to carriag centroid Y_4	6.42	6.42	6.42	6.42	6.42	6.42	6.42	6.42	6.42	6.42	6.42	6.42	6.42	6.42
vertical force at ladder end F_{Lz}	-115	-122	128	131	134	137	139	142	145	156	187	219	282	315
horizontal force at ladder end F_{Lx}	-184	-189	11	22	32	43	54	65	76	37	74	112	187	225
horizontal moment at ladder end M_{Lx}	1198	1243	190	379	569	758	948	1137	1327	100	199	297	492	588
vertical moment at ladder end M_{Lz}	1198	1243	190	379	569	758	948	1137	1327	100	199	297	492	588
moment due to lader rotation device M_{Lv}	512	531	-144	-165	-185	-206	-226	-247	-267	-226	-329	-432	-641	-746
Fa =	130.2	135.1	12.1	25.6	39.1	52.5	66.0	79.4	92.9	5.0	11.3	17.6	29.8	35.8
Fb =	674.7	700.3	106.8	213.5	320.3	427.1	533.8	640.6	747.4	56.3	112.2	167.6	277.0	331.1
Fc =	70.6	73.3	11.2	22.3	33.5	44.7	55.8	67.0	78.2	5.9	11.7	17.5	29.0	34.6
Fd =	-23.0	-23.7	1.3	2.7	4.0	5.4	6.7	8.1	9.4	4.6	9.3	14.0	23.4	28.1
Fe =	227.3	234.3	-20.5	-33.2	-46.0	-58.7	-71.4	-84.2	-96.9	-53.4	-99.4	-145.6	-238.8	-285.8
angle between F_a and $F_{b/c}$ in radians =	0.79	0.79	0.79	0.79	0.79	0.79	0.79	0.79	0.79	0.79	0.79	0.79	0.79	0.79
vert force on both left d-c slide brng $F_{Dz1\&2}$	4809	4924	2317	2810	3303	3795	4288	4781	5274	2099	2371	2642	3178	3443
vert force on both right d-c slide brng $F_{Dz3\&4}$	-1401	-1523	1334	844	354	-136	-626	-1116	-1606	1580	1339	1100	628	395
vert force on both front d-c slide brng $F_{Dz2\&4}$	1398	1384	1860	1878	1896	1914	1932	1950	1968	1919	1996	2074	2232	2311
vert force on both rear d-c slide brng $F_{Dz1\&3}$	2010	2016	1791	1776	1761	1746	1730	1715	1700	1760	1714	1668	1574	1527
vert force on d-c slide bearing 1	2837	2919	1137	1366	1590	1810	2026	2237	2444	1004	1096	1178	1314	1370
vert force on d-c slide bearing 2	-827	-903	654	410	171	-65	-296	-522	-744	756	619	490	260	157
vert force on d-c slide bearing 3	1973	2004	1180	1444	1712	1985	2262	2544	2830	1095	1276	1465	1864	2073
vert force on d-c slide bearing 4	-575	-620	680	434	184	-71	-330	-594	-862	824	720	610	368	238
horiz force each d-carriage bearing $F_{Dx1,2}$	-414	-429	-32	-67	-102	-138	-173	-209	-244	-5	-14	-22	-38	-45
horiz force each d-carriage bearing $F_{Dx3,4}$	322	335	37	78	119	159	200	241	282	24	51	78	131	158
vertical force on front wheels $F_{C2z} + F_{C4z}$	5358	5351	5606	5615	5624	5632	5641	5650	5659	5637	5678	5718	5800	5841
vertical force on rear wheels $F_{C1z} + F_{C3z}$	4427	4427	4422	4416	4410	4404	4398	4392	4386	4419	4410	4401	4382	4373
min vert force on right wheels $F_{C1z} + F_{C2z}$	4778	4794	4449	4527	4604	4682	4759	4837	4914	4422	4472	4522	4622	4671
max vert force on right wheels $F_{C1z} + F_{C2z}$	5970	5984	5727	5805	5884	5963	6041	6120	6198	5710	5771	5832	5953	6014
min vert force on left wheels $F_{C3z} + F_{C4z}$	3815	3794	4301	4225	4150	4074	3998	3923	3847	4346	4316	4287	4229	4201
max vert force on left wheels $F_{C3z} + F_{C4z}$	5007	4984	5579	5504	5429	5355	5280	5205	5131	5634	5615	5596	5561	5544

Table B.1: Continued

cutter horsepower	11.2	12.8	14.4	1.1	2.1	3.2	4.3	5.3	6.4	7.4	8.5	9.6	10.6	11.7
horizontal reaction force at cutter H	321.9	366.3	410.4	28.3	57.0	85.9	115.1	144.6	174.5	204.6	235.0	265.7	296.7	328.0
vertical reaction force at cutter V	-343.1	-393.4	-443.9	-34.9	-69.6	-104.2	-138.6	-172.8	-206.9	-240.8	-274.6	-308.2	-341.6	-374.9
axial reaction force at cutter A	29.2	33.4	37.6	2.8	5.6	8.4	11.2	14.0	16.8	19.6	22.5	25.3	28.1	31.0
moment caused by pump drive	-15.00	-15.00	-15.00	-15.00	-15.00	-15.00	-15.00	-15.00	-15.00	-15.00	-15.00	-15.00	-15.00	-15.00
ladder angle Φ (90-0)	45.00	45.00	45.00	45.00	45.00	45.00	45.00	45.00	45.00	45.00	45.00	45.00	45.00	45.00
elevation of dredge arm (1.5-7.17) z_2	6.12	6.12	6.12	6.12	6.12	6.12	6.12	6.12	6.12	6.12	6.12	6.12	6.12	6.12
moment caused by cutter drive	-195	-223	-251	-19	-37	-56	-74	-93	-112	-130	-149	-168	-186	-205
vertical cutterhead position h	-11	-11	-11	-11	-11	-11	-11	-11	-11	-11	-11	-11	-11	-11
thrust load at ladder end bearing	161	183	205	14	28	43	58	72	87	102	117	133	148	164
total radial ladder end bearing force rght side	651	745	839	63	107	163	223	284	346	409	473	538	603	669
total radial ladder end bearing force left side	707	797	887	117	174	233	292	352	412	473	535	597	660	723
dredge arm winch cable lift force F_{Az}	2347	2380	2412	2148	2170	2193	2215	2237	2259	2281	2303	2325	2347	2368
total radial ladder arm slide bearing 1 force	559	638	716	58	110	163	215	268	321	374	427	481	534	588
total radial ladder arm slide bearing 2 force	498	568	638	50	97	143	189	236	283	330	378	426	473	521
total radial ladder arm slide bearing 3 force	456	520	583	48	91	134	176	219	262	306	349	392	436	480
total radial ladder arm slide bearing 4 force	602	687	771	60	116	172	229	285	342	399	457	514	572	630
total radial ladder arm slide bearing 5 force	519	592	664	55	104	152	201	250	299	348	398	447	497	546
total radial ladder arm slide bearing 6 force	462	526	590	48	90	133	176	219	263	306	350	394	438	483
total radial ladder arm slide bearing 7 force	415	473	531	46	84	123	162	201	240	279	319	358	398	437
total radial ladder arm slide bearing 8 force	565	645	723	58	110	162	215	268	322	375	429	483	537	592
tot d-carriage slide bearing force on 1	1417	1456	1487	962	1018	1071	1121	1169	1214	1256	1295	1332	1367	1398
tot d-carriage slide bearing force on 3	194	211	257	811	723	638	558	481	409	343	285	239	208	198
tot d-carriage slide bearing force on 2	2290	2512	2740	1029	1142	1259	1381	1507	1637	1772	1911	2054	2201	2353
tot d-carriage slide bearing force on 4	210	214	302	868	811	750	685	616	544	470	394	320	254	210
min vertical force on wheel 1	2010	2020	2030	1938	1945	1952	1958	1966	1973	1980	1987	1994	2001	2009
max vertical force on wheel 1	2587	2599	2610	2503	2511	2520	2528	2536	2545	2553	2561	2570	2578	2587
min vertical force on wheel 2	2710	2748	2787	2466	2491	2516	2541	2567	2592	2618	2644	2670	2697	2723
max vertical force on wheel 2	3487	3536	3584	3185	3217	3248	3280	3312	3344	3376	3409	3441	3474	3507
min vertical force on wheel 3	1777	1756	1735	1918	1904	1889	1875	1860	1845	1831	1816	1801	1787	1772
max vertical force on wheel 3	2354	2335	2316	2484	2471	2457	2444	2431	2417	2404	2391	2377	2364	2350
min vertical force on wheel 4	2396	2389	2383	2441	2439	2436	2433	2429	2425	2421	2417	2412	2407	2402
max vertical force on wheel 4	3173	3176	3180	3161	3164	3168	3171	3174	3177	3179	3182	3183	3185	3186
total radial force on front bearing	11	13	14	2	3	4	5	6	7	8	9	10	11	12
total radial force on rear bearing	150	170	191	12	25	39	53	66	80	94	108	123	137	152
weight of Ladder w_L	100	100	100	100	100	100	100	100	100	100	100	100	100	100
weight of cutterhead w_{CH}	25	25	25	25	25	25	25	25	25	25	25	25	25	25
weight of dredge arm w_A	2000	2000	2000	2000	2000	2000	2000	2000	2000	2000	2000	2000	2000	2000
weight of dredge carriage W_D	1523	1523	1523	1523	1523	1523	1523	1523	1523	1523	1523	1523	1523	1523
weight of towing carriage w_C	6377	6377	6377	6377	6377	6377	6377	6377	6377	6377	6377	6377	6377	6377
length of ladder X_2	3.00	3.00	3.00	3.00	3.00	3.00	3.00	3.00	3.00	3.00	3.00	3.00	3.00	3.00
distance to leverage point X_1	1.00	1.00	1.00	1.00	1.00	1.00	1.00	1.00	1.00	1.00	1.00	1.00	1.00	1.00
distance to ladder centroid X_3	1.00	1.00	1.00	1.00	1.00	1.00	1.00	1.00	1.00	1.00	1.00	1.00	1.00	1.00
distance between ladder end bearings	1.50	1.50	1.50	1.50	1.50	1.50	1.50	1.50	1.50	1.50	1.50	1.50	1.50	1.50
length of dredge arm z_1	19.00	19.00	19.00	19.00	19.00	19.00	19.00	19.00	19.00	19.00	19.00	19.00	19.00	19.00
distance to lower slide bearing set z_3	4.00	4.00	4.00	4.00	4.00	4.00	4.00	4.00	4.00	4.00	4.00	4.00	4.00	4.00
horizontal dist between d-arm bearngs x_4	2.00	2.00	2.00	2.00	2.00	2.00	2.00	2.00	2.00	2.00	2.00	2.00	2.00	2.00
horizontal dist between d-arm bearngs y_1	2.00	2.00	2.00	2.00	2.00	2.00	2.00	2.00	2.00	2.00	2.00	2.00	2.00	2.00
dist between d-carriage slide bearings x_5	7.00	7.00	7.00	7.00	7.00	7.00	7.00	7.00	7.00	7.00	7.00	7.00	7.00	7.00
height of dredge carriage z_5	10.58	10.58	10.58	10.58	10.58	10.58	10.58	10.58	10.58	10.58	10.58	10.58	10.58	10.58
dist between d-carriage slide bearings y_2	2.00	2.00	2.00	2.00	2.00	2.00	2.00	2.00	2.00	2.00	2.00	2.00	2.00	2.00
dist from t-c wheel to d-carrge bearing X_8	2.00	2.00	2.00	2.00	2.00	2.00	2.00	2.00	2.00	2.00	2.00	2.00	2.00	2.00
dist from t-carriage wheel to centroid X_7	10.00	10.00	10.00	10.00	10.00	10.00	10.00	10.00	10.00	10.00	10.00	10.00	10.00	10.00
distance between carriage wheels X_6	15.00	15.00	15.00	15.00	15.00	15.00	15.00	15.00	15.00	15.00	15.00	15.00	15.00	15.00
width of towing carriage Y_3	12.83	12.83	12.83	12.83	12.83	12.83	12.83	12.83	12.83	12.83	12.83	12.83	12.83	12.83
dist from wheel to carriag centroid Y_4	6.42	6.42	6.42	6.42	6.42	6.42	6.42	6.42	6.42	6.42	6.42	6.42	6.42	6.42
vertical force at ladder end F_{Lz}	347	380	412	148	170	193	215	237	259	281	303	325	347	368
horizontal force at ladder end F_{Lx}	263	302	340	27	53	80	106	132	158	184	210	236	261	287
horizontal moment at ladder end M_{Lx}	683	777	871	60	121	182	244	307	370	434	498	564	629	696
vertical moment at ladder end M_{Lz}	683	777	871	60	121	182	244	307	370	434	498	564	629	696
moment due to lader rotation device M_{Lv}	-852	-958	-1065	-198	-271	-345	-418	-490	-563	-635	-706	-777	-848	-919
Fa =	41.8	47.6	53.4	2.3	6.1	9.8	13.7	17.6	21.5	25.5	29.6	33.7	37.9	42.1
Fb =	384.7	437.8	490.4	33.9	68.1	102.7	137.6	172.9	208.5	244.5	280.8	317.5	354.6	392.0
Fc =	40.2	45.8	51.3	3.5	7.1	10.7	14.4	18.1	21.8	25.6	29.4	33.2	37.1	41.0
Fd =	32.9	37.7	42.6	3.3	6.6	10.0	13.2	16.5	19.8	23.0	26.3	29.5	32.7	35.9
Fe =	-333.0	-380.5	-428.3	-40.7	-73.5	-106.1	-138.6	-171.0	-203.2	-235.3	-267.3	-299.1	-330.8	-362.3
angle between F_a and $F_{b/c}$ in radians =	0.79	0.79	0.79	0.79	0.79	0.79	0.79	0.79	0.79	0.79	0.79	0.79	0.79	0.79
vert force on both left d-c slide brng $F_{Dz1\&2}$	3705	3966	4225	1991	2160	2330	2502	2676	2851	3027	3206	3386	3567	3750
vert force on both right d-c slide brng $F_{Dz3\&4}$	165	-64	-290	1679	1533	1385	1236	1085	932	777	621	463	303	141
vert force on both front d-c slide brng $F_{Dz2\&4}$	2391	2471	2552	1897	1953	2008	2063	2118	2172	2226	2280	2334	2388	2441
vert force on both rear d-c slide brng $F_{Dz1\&3}$	1479	1432	1384	1773	1740	1708	1675	1643	1610	1578	1546	1514	1482	1450
vert force on d-c slide bearing 1	1416	1455	1485	962	1018	1071	1121	1169	1214	1256	1295	1332	1366	1398
vert force on d-c slide bearing 2	63	-23	-102	811	722	637	554	474	397	322	251	182	116	53
vert force on d-c slide bearing 3	2289	2511	2740	1029	1142	1259	1381	1507	1637	1772	1911	2054	2201	2352
vert force on d-c slide bearing 4	102	-40	-188	868	811	749	682	611	535	455	370	281	187	89
horiz force each d-carriage bearing $F_{Dx1.2}$	-52	-59	-66	0	-4	-8	-12	-17	-21	-26	-31	-36	-42	-47
horiz force each d-carriage bearing $F_{Dx3.4}$	184	210	236	13	30	48	65	83	100	118	136	154	172	191
vertical force on front wheels $F_{C2z} + F_{C4z}$	5883	5925	5967	5626	5655	5684	5713	5741	5769	5798	5826	5854	5882	5909
vertical force on rear wheels $F_{C1z} + F_{C3z}$	4364	4355	4345	4421	4415	4409	4403	4396	4390	4384	4378	4371	4365	4359
min vert force on right wheels $F_{C1z} + F_{C2z}$	4720	4769	4817	4403	4435	4467	4500	4532	4565	4598	4631	4665	4698	4732
max vert force on right wheels $F_{C1z} + F_{C2z}$	6074	6134	6194	5688	5728	5768	5808	5848	5889	5929	5970	6011	6052	6094
min vert force on left wheels $F_{C3z} + F_{C4z}$	4173	4145	4118	4360	4343	4325	4307	4289	4271	4252	4233	4214	4194	4174
max vert force on left wheels $F_{C3z} + F_{C4z}$	5527	5511	5495	5644	5635	5625	5615	5605	5594	5583	5572	5561	5549	5536

Table B.1: Continued

cutter horsepower	12.8	13.8	14.9	0.5	1.1	1.6	2.1	2.7	3.2	3.7	4.3	4.8	5.3	5.8
horizontal reaction force at cutter H	359.7	391.6	423.9	18.9	37.9	56.9	76.1	95.4	114.8	134.2	153.8	173.5	193.2	213.1
vertical reaction force at cutter V	-408.0	-440.9	-473.7	-12.2	-24.3	-36.2	-48.1	-59.8	-71.4	-82.9	-94.3	-105.6	-116.7	-127.8
axial reaction force at cutter A	33.8	36.6	39.5	1.4	2.8	4.2	5.6	7.0	8.4	9.8	11.2	12.6	14.0	15.4
moment caused by pump drive	-15.00	-15.00	-15.00	-15.00	-15.00	-15.00	-15.00	-15.00	-15.00	-15.00	-15.00	-15.00	-15.00	-15.00
ladder angle Φ (90-0)	45.00	45.00	45.00	45.00	45.00	45.00	45.00	45.00	45.00	45.00	45.00	45.00	45.00	45.00
elevation of dredge arm (1.5-7.17) z_2	6.12	6.12	6.12	6.12	6.12	6.12	6.12	6.12	6.12	6.12	6.12	6.12	6.12	6.12
moment caused by cutter drive	-223	-242	-261	-9	-19	-28	-37	-47	-56	-65	-74	-84	-93	-102
vertical cutterhead position h	-11	-11	-11	-11	-11	-11	-11	-11	-11	-11	-11	-11	-11	-11
thrust load at ladder end bearing	180	196	212	9	19	28	38	48	57	67	77	87	97	107
total radial ladder end bearing force rght side	735	802	870	51	65	95	130	167	206	245	284	324	364	404
total radial ladder end bearing force left side	787	851	916	96	131	168	205	243	281	319	358	397	436	475
dredge arm winch cable lift force F_{Az}	2390	2411	2432	2133	2140	2148	2155	2162	2170	2177	2184	2191	2198	2204
total radial ladder arm slide bearing 1 force	642	696	750	32	60	87	115	142	170	197	225	253	281	309
total radial ladder arm slide bearing 2 force	570	618	667	29	54	79	105	130	156	182	208	234	260	286
total radial ladder arm slide bearing 3 force	524	568	612	27	49	71	94	116	138	161	183	205	228	250
total radial ladder arm slide bearing 4 force	689	747	806	34	64	95	126	157	188	219	250	282	313	345
total radial ladder arm slide bearing 5 force	596	646	696	31	56	82	107	133	159	185	210	236	262	288
total radial ladder arm slide bearing 6 force	527	572	617	27	51	74	98	122	146	170	195	219	243	268
total radial ladder arm slide bearing 7 force	477	517	557	26	46	66	86	106	127	147	168	188	209	229
total radial ladder arm slide bearing 8 force	646	701	756	33	61	90	119	149	178	208	237	267	297	327
tot d-carriage slide bearing force on 1	1428	1454	1479	948	992	1036	1080	1122	1165	1206	1248	1289	1329	1369
tot d-carriage slide bearing force on 3	209	237	275	846	790	735	680	627	574	522	472	423	375	330
tot d-carriage slide bearing force on 2	2509	2668	2833	984	1047	1112	1178	1245	1314	1383	1453	1524	1596	1670
tot d-carriage slide bearing force on 4	210	258	339	878	834	788	742	695	647	597	548	497	446	395
min vertical force on wheel 1	2016	2024	2031	1937	1942	1948	1954	1959	1965	1971	1977	1983	1989	1995
max vertical force on wheel 1	2595	2604	2613	2501	2507	2513	2519	2525	2531	2538	2544	2550	2556	2563
min vertical force on wheel 2	2750	2777	2804	2454	2467	2480	2493	2506	2519	2533	2546	2559	2572	2586
max vertical force on wheel 2	3540	3573	3606	3169	3184	3199	3215	3230	3245	3261	3276	3291	3307	3322
min vertical force on wheel 3	1757	1743	1728	1924	1916	1907	1898	1890	1881	1872	1864	1855	1846	1838
max vertical force on wheel 3	2337	2323	2309	2489	2480	2472	2464	2456	2447	2439	2431	2422	2414	2406
min vertical force on wheel 4	2397	2391	2385	2439	2433	2428	2423	2417	2412	2406	2400	2394	2388	2382
max vertical force on wheel 4	3187	3188	3188	3154	3151	3148	3144	3141	3138	3134	3130	3127	3123	3119
total radial force on front bearing	13	14	15	1	2	2	3	3	4	4	5	5	6	6
total radial force on rear bearing	167	182	197	8	17	26	35	44	54	63	72	82	91	100
weight of Ladder w_L	100	100	100	100	100	100	100	100	100	100	100	100	100	100
weight of cutterhead w_{CH}	25	25	25	25	25	25	25	25	25	25	25	25	25	25
weight of dredge arm w_A	2000	2000	2000	2000	2000	2000	2000	2000	2000	2000	2000	2000	2000	2000
weight of dredge carriage W_D	1523	1523	1523	1523	1523	1523	1523	1523	1523	1523	1523	1523	1523	1523
weight of towing carriage w_C	6377	6377	6377	6377	6377	6377	6377	6377	6377	6377	6377	6377	6377	6377
length of ladder X_2	3.00	3.00	3.00	3.00	3.00	3.00	3.00	3.00	3.00	3.00	3.00	3.00	3.00	3.00
distance to leverage point X_1	1.00	1.00	1.00	1.00	1.00	1.00	1.00	1.00	1.00	1.00	1.00	1.00	1.00	1.00
distance to ladder centroid X_3	1.00	1.00	1.00	1.00	1.00	1.00	1.00	1.00	1.00	1.00	1.00	1.00	1.00	1.00
distance between ladder end bearings	1.50	1.50	1.50	1.50	1.50	1.50	1.50	1.50	1.50	1.50	1.50	1.50	1.50	1.50
length of dredge arm z_1	19.00	19.00	19.00	19.00	19.00	19.00	19.00	19.00	19.00	19.00	19.00	19.00	19.00	19.00
distance to lower slide bearing set z_3	4.00	4.00	4.00	4.00	4.00	4.00	4.00	4.00	4.00	4.00	4.00	4.00	4.00	4.00
horizontal dist between d-arm bearngs x_4	2.00	2.00	2.00	2.00	2.00	2.00	2.00	2.00	2.00	2.00	2.00	2.00	2.00	2.00
horizontal dist between d-arm bearngs y_1	2.00	2.00	2.00	2.00	2.00	2.00	2.00	2.00	2.00	2.00	2.00	2.00	2.00	2.00
dist between d-carriage slide bearings x_5	7.00	7.00	7.00	7.00	7.00	7.00	7.00	7.00	7.00	7.00	7.00	7.00	7.00	7.00
height of dredge carriage z_5	10.58	10.58	10.58	10.58	10.58	10.58	10.58	10.58	10.58	10.58	10.58	10.58	10.58	10.58
dist between d-carriage slide bearings y_2	2.00	2.00	2.00	2.00	2.00	2.00	2.00	2.00	2.00	2.00	2.00	2.00	2.00	2.00
dist from t-c wheel to d-carrge bearing X_6	2.00	2.00	2.00	2.00	2.00	2.00	2.00	2.00	2.00	2.00	2.00	2.00	2.00	2.00
dist from t-carriage wheel to centroid X_7	10.00	10.00	10.00	10.00	10.00	10.00	10.00	10.00	10.00	10.00	10.00	10.00	10.00	10.00
distance between carriage wheels X_8	15.00	15.00	15.00	15.00	15.00	15.00	15.00	15.00	15.00	15.00	15.00	15.00	15.00	15.00
width of towing carriage Y_3	12.83	12.83	12.83	12.83	12.83	12.83	12.83	12.83	12.83	12.83	12.83	12.83	12.83	12.83
dist from wheel to carriag centroid Y_4	6.42	6.42	6.42	6.42	6.42	6.42	6.42	6.42	6.42	6.42	6.42	6.42	6.42	6.42
vertical force at ladder end F_{Lz}	390	411	432	133	140	148	155	162	170	177	184	191	198	204
horizontal force at ladder end F_{Lx}	312	338	363	10	19	29	38	47	56	66	75	84	92	101
horizontal moment at ladder end M_{Lx}	763	831	899	40	80	121	161	202	243	285	326	368	410	452
vertical moment at ladder end M_{Lz}	763	831	899	40	80	121	161	202	243	285	326	368	410	452
moment due to lader rotation device M_{Lv}	-989	-1059	-1129	-150	-175	-201	-226	-251	-275	-300	-324	-348	-371	-395
Fa =	46.4	50.7	55.1	1.4	4.1	6.9	9.7	12.4	15.3	18.1	20.9	23.8	26.7	29.6
Fb =	429.8	468.0	506.5	22.6	45.2	68.0	91.0	114.0	137.2	160.4	183.8	207.3	230.9	254.7
Fc =	45.0	49.0	53.0	2.4	4.7	7.1	9.5	11.9	14.3	16.8	19.2	21.7	24.2	26.6
Fd =	39.0	42.2	45.4	1.2	2.4	3.6	4.7	5.9	7.1	8.2	9.3	10.4	11.6	12.7
Fe =	-393.7	-425.0	-456.1	-19.6	-31.3	-42.9	-54.4	-65.8	-77.2	-88.4	-99.5	-110.5	-121.4	-132.3
angle between F_a and $F_{b/c}$ in radians =	0.79	0.79	0.79	0.79	0.79	0.79	0.79	0.79	0.79	0.79	0.79	0.79	0.79	0.79
vert force on both left d-c slide brng $F_{Dz1\&2}$	3935	4121	4309	1932	2040	2149	2258	2367	2478	2588	2699	2811	2923	3036
vert force on both right d-c slide brng $F_{Dz3\&4}$	-22	-187	-354	1724	1623	1522	1420	1318	1215	1111	1007	903	797	692
vert force on both front d-c slide brng $F_{Dz2\&4}$	2494	2547	2599	1861	1881	1900	1919	1938	1957	1976	1994	2013	2031	2049
vert force on both rear d-c slide brng $F_{Dz1\&3}$	1419	1387	1356	1794	1782	1770	1759	1747	1735	1724	1712	1701	1690	1679
vert force on d-c slide bearing 1	1427	1453	1477	948	992	1036	1080	1122	1164	1206	1247	1288	1328	1367
vert force on d-c slide bearing 2	-8	-66	-121	846	790	734	679	625	571	518	465	413	362	311
vert force on d-c slide bearing 3	2508	2668	2832	984	1047	1112	1178	1245	1313	1382	1452	1523	1595	1669
vert force on d-c slide bearing 4	-14	-121	-233	878	834	788	741	693	644	594	542	489	435	380
horiz force each d-carriage bearing $F_{Dx1,2}$	-53	-59	-65	-2	-7	-12	-18	-23	-29	-35	-41	-46	-52	-58
horiz force each d-carriage bearing $F_{Dx3,4}$	209	228	247	6	16	27	37	47	57	68	78	88	99	109
vertical force on front wheels $F_{C2z} + F_{C4z}$	5937	5964	5992	5607	5618	5628	5637	5647	5657	5667	5676	5686	5695	5704
vertical force on rear wheels $F_{C1z} + F_{C3z}$	4353	4347	4340	4425	4423	4420	4418	4415	4413	4410	4408	4405	4403	4400
min vert force on right wheels $F_{C1z} + F_{C2z}$	4766	4800	4835	4390	4409	4428	4447	4466	4485	4504	4523	4542	4561	4580
max vert force on right wheels $F_{C1z} + F_{C2z}$	6135	6177	6219	5670	5691	5712	5734	5755	5777	5798	5820	5841	5863	5885
min vert force on left wheels $F_{C3z} + F_{C4z}$	4154	4134	4113	4363	4349	4335	4321	4307	4293	4278	4264	4249	4235	4220
max vert force on left wheels $F_{C3z} + F_{C4z}$	5523	5510	5497	5642	5631	5620	5608	5597	5585	5573	5561	5549	5537	5524

Table B.1: Continued

cutter horsepower	6.4	6.9	7.4	8.0	9.0	9.6	10.1	10.6	11.2	11.7	12.2	12.8	13.3	13.8
horizontal reaction force at cutter H	233.0	253.1	273.2	293.5	334.2	354.7	375.3	396.0	416.7	437.6	458.6	479.6	500.7	521.9
vertical reaction force at cutter V	-138.7	-149.6	-160.3	-170.9	-191.8	-202.1	-212.3	-222.4	-232.4	-242.3	-252.1	-261.8	-271.4	-280.9
axial reaction force at cutter A	16.9	18.3	19.7	21.1	23.9	25.4	26.8	28.2	29.7	31.1	32.5	34.0	35.4	36.8
moment caused by pump drive	-15.00	-15.00	-15.00	-15.00	-15.00	-15.00	-15.00	-15.00	-15.00	-15.00	-15.00	-15.00	-15.00	-15.00
ladder angle Φ (90-0)	45.00	45.00	45.00	45.00	45.00	45.00	45.00	45.00	45.00	45.00	45.00	45.00	45.00	45.00
elevation of dredge arm (1.5-7.17) z_2	6.12	6.12	6.12	6.12	6.12	6.12	6.12	6.12	6.12	6.12	6.12	6.12	6.12	6.12
moment caused by cutter drive	-112	-121	-130	-140	-158	-168	-177	-186	-195	-205	-214	-223	-233	-242
vertical cutterhead position h	-11	-11	-11	-11	-11	-11	-11	-11	-11	-11	-11	-11	-11	-11
thrust load at ladder end bearing	117	127	137	147	167	177	188	198	208	219	229	240	250	261
total radial ladder end bearing force rght side	445	486	527	568	651	693	735	778	820	863	905	948	991	1035
total radial ladder end bearing force left side	515	554	594	634	714	755	796	837	878	919	960	1002	1044	1085
dredge arm winch cable lift force F_{Az}	2211	2218	2224	2231	2244	2250	2256	2262	2268	2274	2280	2286	2292	2298
total radial ladder arm slide bearing 1 force	337	365	393	421	477	505	534	562	590	619	647	676	704	733
total radial ladder arm slide bearing 2 force	312	338	365	391	444	470	497	524	550	577	604	631	658	685
total radial ladder arm slide bearing 3 force	273	295	318	341	386	409	432	454	477	500	523	546	569	592
total radial ladder arm slide bearing 4 force	376	408	440	472	535	568	600	632	664	697	729	762	794	827
total radial ladder arm slide bearing 5 force	315	341	367	393	446	472	499	526	552	579	606	633	659	686
total radial ladder arm slide bearing 6 force	292	317	342	367	416	441	466	492	517	542	568	593	619	644
total radial ladder arm slide bearing 7 force	250	271	292	312	354	375	396	417	438	459	481	502	523	544
total radial ladder arm slide bearing 8 force	357	387	417	447	508	538	569	600	631	661	692	723	755	786
tot d-carriage slide bearing force on 1	1408	1447	1485	1523	1598	1634	1670	1706	1741	1776	1811	1845	1878	1912
tot d-carriage slide bearing force on 3	287	248	215	189	173	185	207	236	271	308	346	386	427	468
tot d-carriage slide bearing force on 2	1744	1819	1895	1972	2129	2209	2290	2371	2454	2538	2622	2707	2793	2880
tot d-carriage slide bearing force on 4	345	296	251	212	174	186	218	263	316	375	437	502	568	637
min vertical force on wheel 1	2000	2006	2012	2018	2031	2037	2043	2049	2055	2061	2068	2074	2080	2087
max vertical force on wheel 1	2569	2575	2581	2588	2601	2607	2613	2620	2626	2633	2639	2646	2652	2659
min vertical force on wheel 2	2599	2612	2626	2639	2666	2680	2693	2707	2720	2734	2748	2761	2775	2789
max vertical force on wheel 2	3337	3353	3368	3384	3414	3430	3445	3461	3476	3492	3507	3523	3538	3554
min vertical force on wheel 3	1829	1820	1811	1803	1785	1776	1767	1759	1750	1741	1732	1723	1714	1706
max vertical force on wheel 3	2397	2389	2380	2372	2355	2346	2338	2329	2321	2312	2304	2295	2286	2278
min vertical force on wheel 4	2376	2370	2363	2357	2344	2337	2330	2323	2316	2309	2302	2294	2287	2280
max vertical force on wheel 4	3114	3110	3106	3101	3092	3087	3082	3077	3072	3067	3061	3056	3050	3044
total radial force on front bearing	7	7	7	8	9	9	10	10	11	11	12	12	12	13
total radial force on rear bearing	110	120	129	139	158	168	178	188	198	208	218	228	238	248
weight of Ladder w_L	100	100	100	100	100	100	100	100	100	100	100	100	100	100
weight of cutterhead w_{CH}	25	25	25	25	25	25	25	25	25	25	25	25	25	25
weight of dredge arm w_A	2000	2000	2000	2000	2000	2000	2000	2000	2000	2000	2000	2000	2000	2000
weight of dredge carriage W_D	1523	1523	1523	1523	1523	1523	1523	1523	1523	1523	1523	1523	1523	1523
weight of towing carriage w_C	6377	6377	6377	6377	6377	6377	6377	6377	6377	6377	6377	6377	6377	6377
length of ladder X_2	3.00	3.00	3.00	3.00	3.00	3.00	3.00	3.00	3.00	3.00	3.00	3.00	3.00	3.00
distance to leverage point X_1	1.00	1.00	1.00	1.00	1.00	1.00	1.00	1.00	1.00	1.00	1.00	1.00	1.00	1.00
distance to ladder centroid X_3	1.00	1.00	1.00	1.00	1.00	1.00	1.00	1.00	1.00	1.00	1.00	1.00	1.00	1.00
distance between ladder end bearings	1.50	1.50	1.50	1.50	1.50	1.50	1.50	1.50	1.50	1.50	1.50	1.50	1.50	1.50
length of dredge arm z_1	19.00	19.00	19.00	19.00	19.00	19.00	19.00	19.00	19.00	19.00	19.00	19.00	19.00	19.00
distance to lower slide bearing set z_3	4.00	4.00	4.00	4.00	4.00	4.00	4.00	4.00	4.00	4.00	4.00	4.00	4.00	4.00
horizontal dist between d-arm bearngs x_4	2.00	2.00	2.00	2.00	2.00	2.00	2.00	2.00	2.00	2.00	2.00	2.00	2.00	2.00
horizontal dist between d-arm bearngs y_1	2.00	2.00	2.00	2.00	2.00	2.00	2.00	2.00	2.00	2.00	2.00	2.00	2.00	2.00
dist between d-carriage slide bearings x_5	7.00	7.00	7.00	7.00	7.00	7.00	7.00	7.00	7.00	7.00	7.00	7.00	7.00	7.00
height of dredge carriage z_5	10.58	10.58	10.58	10.58	10.58	10.58	10.58	10.58	10.58	10.58	10.58	10.58	10.58	10.58
dist between d-carriage slide bearings y_2	2.00	2.00	2.00	2.00	2.00	2.00	2.00	2.00	2.00	2.00	2.00	2.00	2.00	2.00
dist from t-c wheel to d-carrge bearing X_8	2.00	2.00	2.00	2.00	2.00	2.00	2.00	2.00	2.00	2.00	2.00	2.00	2.00	2.00
dist from t-carriage wheel to centroid X_7	10.00	10.00	10.00	10.00	10.00	10.00	10.00	10.00	10.00	10.00	10.00	10.00	10.00	10.00
distance between carriage wheels X_6	15.00	15.00	15.00	15.00	15.00	15.00	15.00	15.00	15.00	15.00	15.00	15.00	15.00	15.00
width of towing carriage Y_3	12.83	12.83	12.83	12.83	12.83	12.83	12.83	12.83	12.83	12.83	12.83	12.83	12.83	12.83
dist from wheel to carriag centroid Y_4	6.42	6.42	6.42	6.42	6.42	6.42	6.42	6.42	6.42	6.42	6.42	6.42	6.42	6.42
vertical force at ladder end F_{Lz}	211	218	224	231	244	250	256	262	268	274	280	286	292	298
horizontal force at ladder end F_{Lx}	110	119	127	136	153	161	169	177	185	193	201	209	217	225
horizontal moment at ladder end M_{Lx}	494	537	580	623	709	752	796	840	884	928	973	1017	1062	1107
vertical moment at ladder end M_{Lz}	494	537	580	623	709	752	796	840	884	928	973	1017	1062	1107
moment due to lader rotation device M_{Lv}	-418	-441	-464	-486	-531	-553	-574	-596	-617	-638	-659	-679	-699	-720
Fa =	32.5	35.4	38.4	41.4	47.4	50.4	53.4	56.5	59.5	62.6	65.7	68.9	72.0	75.1
Fb =	278.5	302.5	326.5	350.7	399.4	423.9	448.5	473.2	498.0	523.0	548.0	573.1	598.4	623.7
Fc =	29.1	31.6	34.2	36.7	41.8	44.3	46.9	49.5	52.1	54.7	57.3	59.9	62.6	65.2
Fd =	13.8	14.8	15.9	17.0	19.1	20.1	21.1	22.2	23.2	24.2	25.2	26.1	27.1	28.1
Fe =	-143.0	-153.6	-164.2	-174.6	-195.3	-205.4	-215.5	-225.5	-235.4	-245.3	-255.0	-264.6	-274.2	-283.7
angle between F_a and $F_{b/c}$ in radians =	0.79	0.79	0.79	0.79	0.79	0.79	0.79	0.79	0.79	0.79	0.79	0.79	0.79	0.79
vert force on both left d-c slide brng $F_{Dz1\&2}$	3149	3263	3377	3491	3722	3838	3954	4071	4188	4306	4424	4543	4662	4781
vert force on both right d-c slide brng $F_{Dz3\&4}$	585	478	371	263	45	-65	-175	-285	-397	-508	-621	-733	-847	-961
vert force on both front d-c slide brng $F_{Dz2\&4}$	2066	2084	2101	2119	2153	2169	2186	2203	2219	2235	2251	2267	2283	2298
vert force on both rear d-c slide brng $F_{Dz1\&3}$	1668	1657	1646	1635	1614	1603	1593	1583	1572	1562	1552	1542	1532	1522
vert force on d-c slide bearing 1	1406	1445	1483	1521	1595	1631	1667	1702	1737	1772	1806	1839	1872	1905
vert force on d-c slide bearing 2	261	212	163	114	19	-27	-74	-119	-165	-209	-253	-297	-340	-383
vert force on d-c slide bearing 3	1743	1818	1893	1970	2127	2207	2287	2369	2451	2534	2618	2703	2789	2876
vert force on d-c slide bearing 4	324	266	208	148	26	-37	-101	-166	-232	-299	-367	-437	-507	-578
horiz force each d-carriage bearing $F_{Dx1,2}$	-64	-71	-77	-83	-96	-102	-109	-115	-122	-129	-136	-142	-149	-156
horiz force each d-carriage bearing $F_{Dx3,4}$	119	130	140	151	172	183	193	204	215	225	236	247	258	269
vertical force on front wheels $F_{C2z} + F_{C4z}$	5714	5723	5732	5741	5758	5767	5775	5784	5792	5801	5809	5817	5825	5833
vertical force on rear wheels $F_{C1z} + F_{C3z}$	4398	4395	4393	4390	4386	4383	4381	4378	4376	4374	4371	4369	4367	4364
min vert force on right wheels $F_{C1z} + F_{C2z}$	4600	4619	4638	4658	4697	4716	4736	4756	4776	4795	4815	4835	4855	4875
max vert force on right wheels $F_{C1z} + F_{C2z}$	5906	5928	5950	5971	6015	6037	6059	6081	6102	6124	6146	6168	6190	6212
min vert force on left wheels $F_{C3z} + F_{C4z}$	4205	4190	4175	4159	4129	4113	4097	4082	4066	4050	4034	4018	4002	3985
max vert force on left wheels $F_{C3z} + F_{C4z}$	5512	5499	5486	5473	5447	5434	5420	5406	5393	5379	5365	5351	5337	5322

Table B.1: Continued

cutter horsepower	14.4	14.9	15.4
horizontal reaction force at cutter H	543.2	564.6	586.0
vertical reaction force at cutter V	-290.3	-299.6	-308.8
axial reaction force at cutter A	38.3	39.7	41.2
moment caused by pump drive	-15.00	-15.00	-15.00
ladder angle Φ (90-0)	45.00	45.00	45.00
elevation of dredge arm (1.5-7.17) z_2	6.12	6.12	6.12
moment caused by cutter drive	-251	-261	-270
vertical cutterhead position h	-11	-11	-11
thrust load at ladder end bearing	272	282	293
total radial ladder end bearing force rght side	1078	1122	1165
total radial ladder end bearing force left side	1127	1170	1212
dredge arm winch cable lift force F_{Az}	2303	2309	2314
total radial ladder arm slide bearing 1 force	762	791	819
total radial ladder arm slide bearing 2 force	712	739	767
total radial ladder arm slide bearing 3 force	615	638	662
total radial ladder arm slide bearing 4 force	860	893	926
total radial ladder arm slide bearing 5 force	713	740	768
total radial ladder arm slide bearing 6 force	670	696	722
total radial ladder arm slide bearing 7 force	566	587	609
total radial ladder arm slide bearing 8 force	817	849	880
tot d-carriage slide bearing force on 1	1945	1977	2009
tot d-carriage slide bearing force on 3	509	550	591
tot d-carriage slide bearing force on 2	2968	3056	3146
tot d-carriage slide bearing force on 4	707	779	852
min vertical force on wheel 1	2093	2099	2106
max vertical force on wheel 1	2665	2672	2679
min vertical force on wheel 2	2803	2816	2830
max vertical force on wheel 2	3569	3585	3600
min vertical force on wheel 3	1697	1688	1679
max vertical force on wheel 3	2269	2261	2252
min vertical force on wheel 4	2272	2264	2257
max vertical force on wheel 4	3039	3033	3027
total radial force on front bearing	13	14	14
total radial force on rear bearing	258	268	279
weight of Ladder w_L	100	100	100
weight of cutterhead w_{CH}	25	25	25
weight of dredge arm w_A	2000	2000	2000
weight of dredge carriage W_D	1523	1523	1523
weight of towing carriage w_C	6377	6377	6377
length of ladder X_2	3.00	3.00	3.00
distance to leverage point X_1	1.00	1.00	1.00
distance to ladder centroid X_3	1.00	1.00	1.00
distance between ladder end bearings	1.50	1.50	1.50
length of dredge arm z_1	19.00	19.00	19.00
distance to lower slide bearing set z_3	4.00	4.00	4.00
horizontal dist between d-arm bearngs x_4	2.00	2.00	2.00
horizontal dist between d-arm bearngs y_1	2.00	2.00	2.00
dist between d-carriage slide bearings x_5	7.00	7.00	7.00
height of dredge carriage z_5	10.58	10.58	10.58
dist between d-carriage slide bearings y_2	2.00	2.00	2.00
dist from t-c wheel to d-carrge bearing X_8	2.00	2.00	2.00
dist from t-carriage wheel to centroid X_7	10.00	10.00	10.00
distance between carriage wheels X_6	15.00	15.00	15.00
width of towing carriage Y_3	12.83	12.83	12.83
dist from wheel to carriag centroid Y_4	6.42	6.42	6.42
vertical force at ladder end F_{Lz}	303	309	314
horizontal force at ladder end F_{Lx}	232	240	247
horizontal moment at ladder end M_{Lx}	1152	1198	1243
vertical moment at ladder end M_{Lz}	1152	1198	1243
moment due to lader rotation device M_{Lv}	-740	-759	-779
Fa =	78.3	81.5	84.7
Fb =	649.2	674.7	700.3
Fc =	67.9	70.6	73.3
Fd =	29.0	30.0	30.9
Fe =	-293.1	-302.4	-311.6
angle between F_a and $F_{b/c}$ in radians =	0.79	0.79	0.79
vert force on both left d-c slide brng $F_{Dz1\&2}$	4901	5021	5142
vert force on both right d-c slide brng $F_{Dz3\&4}$	-1075	-1190	-1305
vert force on both front d-c slide brng $F_{Dz2\&4}$	2313	2329	2344
vert force on both rear d-c slide brng $F_{Dz1\&3}$	1513	1503	1493
vert force on d-c slide bearing 1	1938	1970	2001
vert force on d-c slide bearing 2	-425	-467	-508
vert force on d-c slide bearing 3	2963	3052	3141
vert force on d-c slide bearing 4	-650	-723	-797
horiz force each d-carriage bearing $F_{Dx1,2}$	-163	-171	-178
horiz force each d-carriage bearing $F_{Dx3,4}$	280	290	301
vertical force on front wheels $F_{C2z} + F_{C4z}$	5841	5849	5857
vertical force on rear wheels $F_{C1z} + F_{C3z}$	4362	4360	4358
min vert force on right wheels $F_{C1z} + F_{C2z}$	4895	4916	4936
max vert force on right wheels $F_{C1z} + F_{C2z}$	6234	6256	6279
min vert force on left wheels $F_{C3z} + F_{C4z}$	3969	3952	3936
max vert force on left wheels $F_{C3z} + F_{C4z}$	5308	5293	5279

The static load analysis presented in Appendix B shows that, for the estimated weights listed in Tables A.1 through A.4, a side winch force in excess of 17,837 N (4010 lb) could cause the net force on one side of the dredge to go to zero if no vertical or axial cutting forces acted on the cutterhead and the ladder angle was 90 degrees relative to the seabed cutting at a maximum depth of 4.27 m (14 ft). Table B.2 shows the amount of horizontal force required to tip the dredge with no other forces acting on the cutter. In this case, the minimum normal force on two of the four wheels becomes negative and the carriage becomes unstable and is in danger of tipping. The maximum vertical cutting force possible when overcutting is 9452 N (2125 lb). This is due to the weight and function of the proposed model dredge design that is presented in Chapter V. Table A.2 shows that the ladder arm weighs 9452 N (2125 lb) and is suspended from the dredge carriage by a cable (Figure 5.4). Any vertical cutting force in excess of 9452 N (2125 lb) resulting from overcutting (+Z direction) simply lifts the cutter and adds slack in the lift cable. Any vertical cutting force resulting from undercutting (-Z direction) acts to pull the carriage down more tightly onto the rails and works against tipping the dredge. If a maximum vertical cutting force in the +Z direction of 9452 N (2125 lb) is applied, then a pull force of only 15,026 N (3378 lb) will cause the carriage to overturn (ladder angle 90 degrees, depth of cut 4.27 m or 14 feet). Table B.3 is the amount of horizontal force required to tip the dredge with the maximum vertical cutting force during overcutting. Therefore, the side winch force must not exceed 15,026 N (3378 lb) at the risk of overturning the carriage. This is more than 5 times greater than the maximum average horizontal cutting force predicted by the calculations in Table 4.5. For both of these tables, the combination of ladder angle and ladder arm elevation that was found to produce the greatest instability was 90 degrees and 1.22 m (4 ft) respectively. This combination produces the maximum digging depth of 4.27 m (14 ft) below the water line.

Table B.2: Maximum Pull Force Required to Overturn Tow Carriage

weight of Ladder w_L	100.00	100.00	100.00
weight of cutterhead w_{CH}	25.00	25.00	25.00
length of ladder X_2	3.00	3.00	3.00
distance to leverage point X_1	1.00	1.00	1.00
distance to ladder centroid X_3	1.00	1.00	1.00
horizontal reaction force at cutter H	4009.00	4010.00	4011.00
vertical reaction force at cutter V	0.00	0.00	0.00
axial reaction force at cutter A	0.00	0.00	0.00
ladder angle Φ (90-0)	90.00	90.00	90.00
distance between ladder end bearings	1.50	1.50	1.50
vertical force at ladder end F_{Lz}	125.00	125.00	125.00
horizontal force at ladder end F_{Lx}	0.00	0.00	0.00
horiz force at ladder end F_{Ly}	4009.00	4010.00	4011.00
horizontal moment at ladder end M_{Lx}	12027.00	12030.00	12033.00
vertical moment at ladder end M_{Lz}	0.00	0.00	0.00
moment due to lader rotation device M_{Ly}	0.00	0.00	0.00
total bearing force rght side at ladder enc	7955.50	7957.50	7959.50
total bearing force left side at ladder enc	8080.50	8082.50	8084.50
Moment due to Pump motor	15.00	15.00	15.00
Moment due to Cutter Drive	275.00	275.00	275.00
length of dredge arm z_1	19.00	19.00	19.00
distance to lower slide bearing set z_3	4.00	4.00	4.00
horizontal dist between d-arm bearngs x_4	2.00	2.00	2.00
weight of dredge arm w_A	2000.00	2000.00	2000.00
horizontal dist between d-arm bearngs y_1	2.00	2.00	2.00
Fa =	25.6326	25.6326	25.6326
Fb =	5011.2500	5012.5000	5013.7500
Fc =	501.1250	501.2500	501.3750
Fd =	0.0000	0.0000	0.0000
Fe =	0.0000	0.0000	0.0000
angle between F_a and $F_{b/c}$ in radians =	0.7854	0.7854	0.7854
dredge arm lift force F_{Az}	2125.00	2125.00	2125.00
total horiz slide bearing force at point 1	**5494.28**	**5495.65**	**5497.03**
total horiz slide bearing force at point 2	**4528.29**	**4529.41**	**4530.54**
total horiz slide bearing force at point 3	**4492.04**	**4493.16**	**4494.29**
total horiz slide bearing force at point 4	**5530.53**	**5531.90**	**5533.28**
total horiz slide bearing force at point 5	**5494.28**	**5495.65**	**5497.03**
total horiz slide bearing force at point 6	**4528.29**	**4529.41**	**4530.54**
total horiz slide bearing force at point 7	**4492.04**	**4493.16**	**4494.29**
total horiz slide bearing force at point 8	**5530.53**	**5531.90**	**5533.28**
dist between d-carriage slide bearings x_5	7.00	7.00	7.00
weight of dredge carriage W_D	1523.00	1523.00	1523.00
height of dredge carriage z_5	10.58	10.58	10.58
elevation of dredge arm (1.5-7.17) z_2	4.00	4.00	4.00
dist between d-carriage slide bearings y_2	2.00	2.00	2.00
vert force on both right d-c slide brng $F_{Dz1\&2}$	29887.00	29894.00	29901.00
vert force on both left d-c slide brng $F_{Dz3\&4}$	-26239.00	-26246.00	-26253.00
vert force on both front d-c slide brng $F_{Dz2\&4}$	1824.00	1824.00	1824.00
vert force on both rear d-c slide brng $F_{Dz1\&3}$	1824.00	1824.00	1824.00
horiz force on each left d-c bearing $F_{Dx1,2}$	-72.50	-72.50	-72.50
horiz force on each right d-c bearing $F_{Dx3,4}$	72.50	72.50	72.50
tot d-carriage slide bearing force on 1	**14943.68**	**14947.18**	**14950.68**
tot d-carriage slide bearing force on 2	**14943.68**	**14947.18**	**14950.68**
tot d-carriage slide bearing force on 3	**13119.70**	**13123.20**	**13126.70**
tot d-carriage slide bearing force on 4	**13119.70**	**13123.20**	**13126.70**
dist from t-c wheel to d-carrge bearing X_8	2.00	2.00	2.00
dist from t-carriage wheel to centroid X_7	10.00	10.00	10.00
distance between carriage wheels X_6	15.00	15.00	15.00
weight of towing carriage w_C	6377.00	6377.00	6377.00
width of towing carriage Y_3	12.83	12.83	12.83
dist from wheel to carriag centroid Y_4	6.42	6.42	6.42
vertical dredge position h	-14.00	-14.00	-14.00
vertical force on front wheels $F_{C2z} + F_{C4z}$	5588.93	5588.93	5588.93
vertical force on rear wheels $F_{C1z} + F_{C3z}$	4436.07	4436.07	4436.07
min vert force on right wheels $F_{C1z} + F_{C2z}$	8746.28	8747.37	8748.46
max vert force on right wheels $F_{C1z} + F_{C2z}$	10022.93	10024.03	10025.12
min vert force on left wheels $F_{C3z} + F_{C4z}$	2.07	0.97	-0.12
max vert force on left wheels $F_{C3z} + F_{C4z}$	1278.72	1277.63	1276.54
min vertical force on wheel 1	**3870.23**	**3870.71**	**3871.20**
max vertical force on wheel 1	4435.15	4435.64	4436.12
min vertical force on wheel 2	**4876.05**	**4876.65**	**4877.26**
max vertical force on wheel 2	5587.78	5588.39	5589.00
min vertical force on wheel 3	**0.91**	**0.43**	**-0.05**
max vertical force on wheel 3	565.84	565.35	564.87
min vertical force on wheel 4	**1.15**	**0.54**	**-0.07**
max vertical force on wheel 4	712.89	712.28	711.67
horizontal force on rear bearing F_{C1v}	2519.70	2520.33	2520.97
horizontal force on front bearing F_{C2v}	1489.30	1489.67	1490.03

Table B.3: Minimum Pull Force Required to Overturn Tow Carriage

weight of Ladder w_L	100.00	100.00	100.00
weight of cutterhead w_{CH}	25.00	25.00	25.00
length of ladder X_2	3.00	3.00	3.00
distance to leverage point X_1	1.00	1.00	1.00
distance to ladder centroid X_3	1.00	1.00	1.00
horizontal reaction force at cutter H	3377.00	3378.00	3379.00
vertical reaction force at cutter V	0.00	0.00	0.00
axial reaction force at cutter A	2125.00	2125.00	2125.00
ladder angle Φ (90-0)	90.00	90.00	90.00
distance between ladder end bearings	1.50	1.50	1.50
vertical force at ladder end F_{Lz}	-2000.00	-2000.00	-2000.00
horizontal force at ladder end F_{Lx}	0.00	0.00	0.00
horiz force at ladder end F_{Ly}	3377.00	3378.00	3379.00
horizontal moment at ladder end M_{Lx}	10131.00	10134.00	10137.00
vertical moment at ladder end M_{Lz}	0.00	0.00	0.00
moment due to lader rotation device M_{Ly}	0.00	0.00	0.00
total bearing force rght side at ladder enc	7754.00	7756.00	7758.00
total bearing force left side at ladder enc	5754.00	5756.00	5758.00
Moment due to Pump motor	15.00	15.00	15.00
Moment due to Cutter Drive	275.00	275.00	275.00
length of dredge arm z_1	19.00	19.00	19.00
distance to lower slide bearing set z_3	4.00	4.00	4.00
horizontal dist between d-arm bearngs x_4	2.00	2.00	2.00
weight of dredge arm w_A	2000.00	2000.00	2000.00
horizontal dist between d-arm bearngs y_1	2.00	2.00	2.00
Fa =	25.6326	25.6326	25.6326
Fb =	4221.2500	4222.5000	4223.7500
Fc =	422.1250	422.2500	422.3750
Fd =	0.0000	0.0000	0.0000
Fe =	0.0000	0.0000	0.0000
angle between F_a and $F_{b/c}$ in radians =	0.7854	0.7854	0.7854
dredge arm lift force F_{Az}	0.00	0.00	0.00
total horiz slide bearing force at point 1	**4625.29**	**4626.66**	**4628.04**
total horiz slide bearing force at point 2	**3817.29**	**3818.42**	**3819.54**
total horiz slide bearing force at point 3	**3781.04**	**3782.17**	**3783.29**
total horiz slide bearing force at point 4	**4661.54**	**4662.91**	**4664.29**
total horiz slide bearing force at point 5	**4625.29**	**4626.66**	**4628.04**
total horiz slide bearing force at point 6	**3817.29**	**3818.42**	**3819.54**
total horiz slide bearing force at point 7	**3781.04**	**3782.17**	**3783.29**
total horiz slide bearing force at point 8	**4661.54**	**4662.91**	**4664.29**
dist between d-carriage slide bearings x_5	7.00	7.00	7.00
weight of dredge carriage W_D	1523.00	1523.00	1523.00
height of dredge carriage z_5	10.58	10.58	10.58
elevation of dredge arm (1.5-7.17) z_2	4.00	4.00	4.00
dist between d-carriage slide bearings y_2	2.00	2.00	2.00
vert force on both right d-c slide brng $F_{Dz1\&2}$	24400.50	24407.50	24414.50
vert force on both left d-c slide brng $F_{Dz3\&4}$	-22877.50	-22884.50	-22891.50
vert force on both front d-c slide brng $F_{Dz2\&4}$	761.50	761.50	761.50
vert force on both rear d-c slide brng $F_{Dz1\&3}$	761.50	761.50	761.50
horiz force on each left d-c bearing $F_{Dx1,2}$	-72.50	-72.50	-72.50
horiz force on each right d-c bearing $F_{Dx3,4}$	72.50	72.50	72.50
tot d-carriage slide bearing force on 1	**12200.47**	**12203.97**	**12207.47**
tot d-carriage slide bearing force on 2	**12200.47**	**12203.97**	**12207.47**
tot d-carriage slide bearing force on 3	**11438.98**	**11442.48**	**11445.98**
tot d-carriage slide bearing force on 4	**11438.98**	**11442.48**	**11445.98**
dist from t-c wheel to d-carrge bearing X_8	2.00	2.00	2.00
dist from t-carriage wheel to centroid X_7	10.00	10.00	10.00
distance between carriage wheels X_6	15.00	15.00	15.00
weight of towing carriage w_C	6377.00	6377.00	6377.00
width of towing carriage Y_3	12.83	12.83	12.83
dist from wheel to carriag centroid Y_4	6.42	6.42	6.42
vertical dredge position h	-14.00	-14.00	-14.00
vertical force on front wheels $F_{C2z} + F_{C4z}$	4809.77	4809.77	4809.77
vertical force on rear wheels $F_{C1z} + F_{C3z}$	3090.23	3090.23	3090.23
min vert force on right wheels $F_{C1z} + F_{C2z}$	7365.98	7367.07	7368.16
max vert force on right wheels $F_{C1z} + F_{C2z}$	7898.97	7900.06	7901.15
min vert force on left wheels $F_{C3z} + F_{C4z}$	**1.03**	**-0.06**	**-1.15**
max vert force on left wheels $F_{C3z} + F_{C4z}$	534.02	532.93	531.84
min vertical force on wheel 1	**2881.34**	**2881.77**	**2882.19**
max vertical force on wheel 1	3089.83	3090.26	3090.68
min vertical force on wheel 2	**4484.64**	**4485.30**	**4485.97**
max vertical force on wheel 2	4809.14	4809.80	4810.47
min vertical force on wheel 3	**0.40**	**-0.02**	**-0.45**
max vertical force on wheel 3	208.89	208.47	208.04
min vertical force on wheel 4	**0.63**	**-0.04**	**-0.70**
max vertical force on wheel 4	325.13	324.47	323.80
horizontal force on rear bearing F_{C1v}	2119.43	2120.07	2120.70
horizontal force on front bearing F_{C2v}	1257.57	1257.93	1258.30

Figures B.9 through B.17 require a special application of the static load analysis. Every structure has its weakest member. In the case of the tow/dredge carriage, the weakest members are the vertical and horizontal guide rods. The static analysis can reasonably estimate the total radial loads on the 8 ladder arm sleeve bearings as well as the 4 dredge carriage sleeve bearings. In the case of the 8 ladder arm sleeve bearings that slide along the vertical guide rods, the total force can be decoupled into a force along each of the *X* and *Y* axes. In the case of the 4 dredge carriage bearings that slide along the horizontal guide rods, the total force can be decoupled into a force along each of the *X* and *Z* axes. These forces create a bending moments in the guide rods that produce stresses. These stresses need to be calculated in order to determine the maximum allowable cutting forces. However, the static analysis of each of the rods is indeterminate since the rods are over constrained. In both cases, the result is four forces acting on a single beam at two different locations along two different orthogonal planes. Figure B.7 illustrates the statistically indeterminate beam problem.

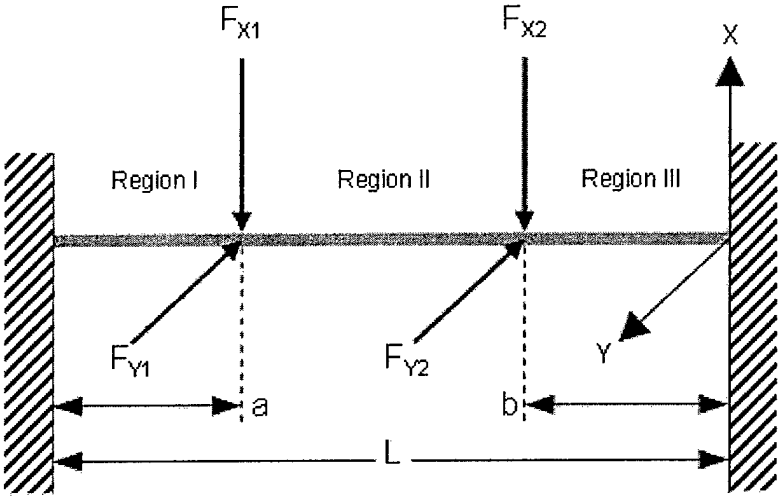

Figure B.7: Statically Indeterminate Beam Problem for Guide Rods

The beam in Figure B.7 can be split into two distinct problems by finding the bending moment for each set of forces along an axis. For round beams, the maximum combined bending moment can be expresses as the square root of the sum of the two orthogonal bending moments squared. Figure B.8 illustrates the simplified problem.

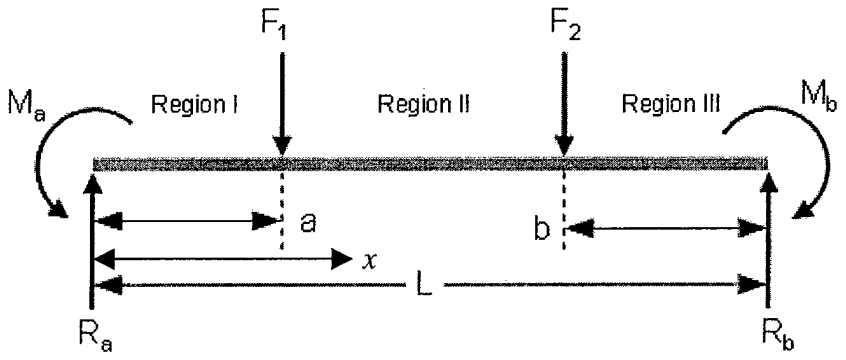

Figure B.8: Simplified Beam Problem for Guide Rods

The Forces F_1 and F_2 create reaction forces R_a and R_b and moments M_a and M_b at either end of the beam. Each of the three regions has a different expression for the bending moment in terms of x. Equations B.26 through B.28 are the bending moment equations for regions I, II, and III respectively.

$$M_I = R_a x - M_a \tag{B.26}$$

$$M_{II} = R_a x - M_a - F_1(x-a) \tag{B.27}$$

$$M_{III} = R_b L - R_b x - M_b \tag{B.28}$$

Integrating the moment equation once gives the slope of the beam at x. Integrating the moment equation twice gives the deflection of the beam at x. Since each end is fixed, there is no deflection and no slope at $x = 0$ and $x = L$. Moreover, since the beam is continuous, the deflection and slope are identical for adjacent regions at $x = a$ and $x = (L-b)$. By integrating the differential equations of the deflection curve and using the boundary conditions to determine the constants of integration, equations for the reaction forces and moments can be derived. Equations B.29 through B.32 are the solutions to the problem as seen in Figure B.8.

$$R_a = F_2\left[\frac{3b^2}{L^2} - \frac{2b^3}{L^3}\right] + F_1\left[1 - \frac{3a^2}{L^2} + \frac{2a^3}{L^3}\right] \tag{B.29}$$

$$R_b = F_2\left[1-\frac{3b^2}{L^2}+\frac{2b^3}{L^3}\right]+F_1\left[\frac{3a^2}{L^2}-\frac{2a^3}{L^3}\right] \tag{B.30}$$

$$M_a = F_2\left[\frac{b^2}{L}-\frac{b^3}{L^2}\right]+F_1\left[\frac{a^3}{L^2}-\frac{2a^2}{L}+a\right] \tag{B.31}$$

$$M_b = F_2\left[\frac{b^3}{L^2}-\frac{2b^2}{L}+b\right]+F_1\left[\frac{a^2}{L}-\frac{a^3}{L^2}\right] \tag{B.32}$$

Once the reaction forces and moments are found, they can be substituted back into Equations B.26 through B.28 to find the moment along the entire length of the beam. The maximum bending moments occur at the nodes $x = 0$, $x = a$, $x = b$, and $x = L$. By substituting this into the bending moment equations, the four maximum bending moments can be expressed by Equations B.33 through B.36.

$$M_{Max1} = M_a \tag{B.33}$$

$$M_{Max2} = R_a a \tag{B.34}$$

$$M_{Max3} = R_b b \tag{B.35}$$

$$M_{Max4} = M_b \tag{B.36}$$

This procedure must be done on both pairs of forces acting on each beam. Since the beam is round and prismatic and the bending moments are orthogonal, the resulting bending moment can be calculated according to Equation B.37. Equation B.38 is used to calculate the maximum bending stress in the guide rods.

$$M_{total} = \sqrt{(M_X)^2 + (M_Y)^2} \tag{B.37}$$

$$\sigma = \frac{M_{total} r}{I} \text{ where } I = \frac{\pi r^4}{4} \tag{B.38}$$

Even a relatively weak stainless steel can have a yield stress of 296,475 kPa (43 ksi) with stronger materials yielding in excess of 1.7 MPa (250 ksi) (Gere et al. 1990). To ensure that an additional margin of safety is built into the model dredge, a stainless steel of 296,475 kPa (43 ksi) is used to determine the maximum bending moments for the purposes of this analysis. Using Equation B.38, the 51 mm (2 in) diameter vertical guide rods have a maximum allowable bending moment of approximately 118 N-m (2,800 ft-lb). The 83 mm (3.25 in) diameter horizontal guide rods have a maximum allowable bending moment of approximately 509 N-m (12,075 ft-lb).

In the analysis of the vertical guide rods, the bending moment in each rod is treated independently of the other three rods. When the guide rods are loaded by the cutting forces, they are not always loaded evenly. Under heavy loading, the bending moments in each of the rods are different by a fairly significant amount. When yielding occurred in the simulations, it was always in only one of the guide rods while the other three were well below the yielding point. Since the four guide rods are interconnected by a rigid structure at each of the four locations where the maximum bending moments occur, the greater deflection in the more heavily loaded rods would be constrained by the lesser deflection of the lesser loaded rods. This would have the effect of distributing the radial bearing forces more evenly onto the guide rods and would add strength and rigidity to the structure by delaying the yielding of the more heavily loaded rods. An analysis that included this level of detail would be overkill on this application, but the simplified approach does add an unknown, but probably significant, additional factor of safety to the proposed design.

Figure B.9 is the bending moment in the four vertical guide rods as a function of the maximum predicted cutterhead loading data. The cutting force data listed in Table 4.5 is used as input to the static analysis model and the maximum bending moment in the four vertical guide rods is

calculated and plotted. Each of the four vertical guide rods is shown in a different shade. Maximum allowable bending moment in the 51 mm (2 in) diameter rods is 118 N-m (2,800 ft-lb). The combination of ladder angle and ladder arm elevation that was found to produce the greatest bending moment for the given loading was 32 degrees and 0.79 m (2.59 ft) respectively.

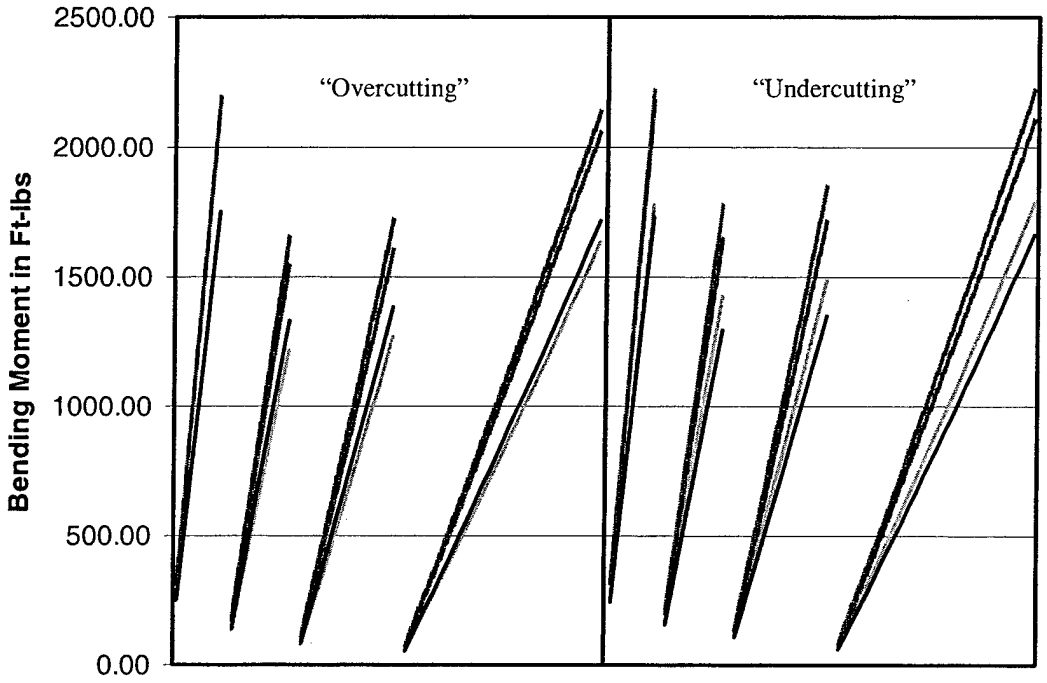

Figure B.9: Bending Moment in the Vertical Guide Rods
under the Maximum Predicted Cutterhead Loading

If the standard loading of Table 4.5 is increased by 26%, the stress in the vertical guide rods reaches the yield point. Figure B.10 is the bending moment in the vertical guide rods with 126% of the maximum predicted cutterhead loading. The maximum allowable bending moment is shown as the dotted horizontal line

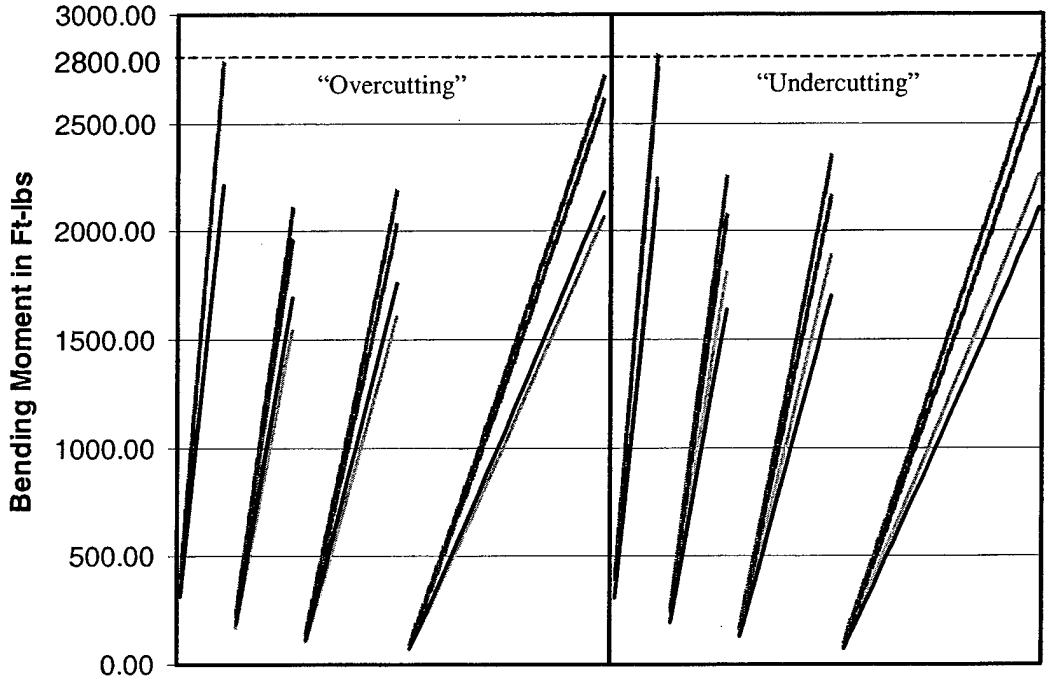

Figure B.10: Bending Moment in the Vertical Guide Rods
under 126% Maximum Predicted Cutterhead Loading

The maximum predicted cutterhead loading can be exceeded by 26% before the vertical guide rods are in danger of yielding under the most severe combination of ladder angle and ladder arm elevation. However, when the vertical guide rods are fully loaded under this scenario, the horizontal cutting force is not at its maximum value due to the combined loading of horizontal, vertical, and axial cutting forces. There may be a situation where the dredge needs to be pulled at its maximum possible pull force and no other loading on the cutterhead is considered. Given this scenario, a maximum pull force of 3559 N (800 lb), with the ladder angle at 31 degrees and the digging depth at 4.27 m (14 ft), can be obtained before the vertical guide rods are in danger of yielding. Figure B.11 shows the maximum pull force with no other forces acting on the cutterhead. The maximum allowable bending moment is shown as the dotted horizontal line and the forces and geometry used to induce the bending moments are listed in the Figure. Each of the lines represents one of the vertical guide rods. The four lines are grouped into two pairs of two, indicating two pairs of identical loading on the vertical guide rods

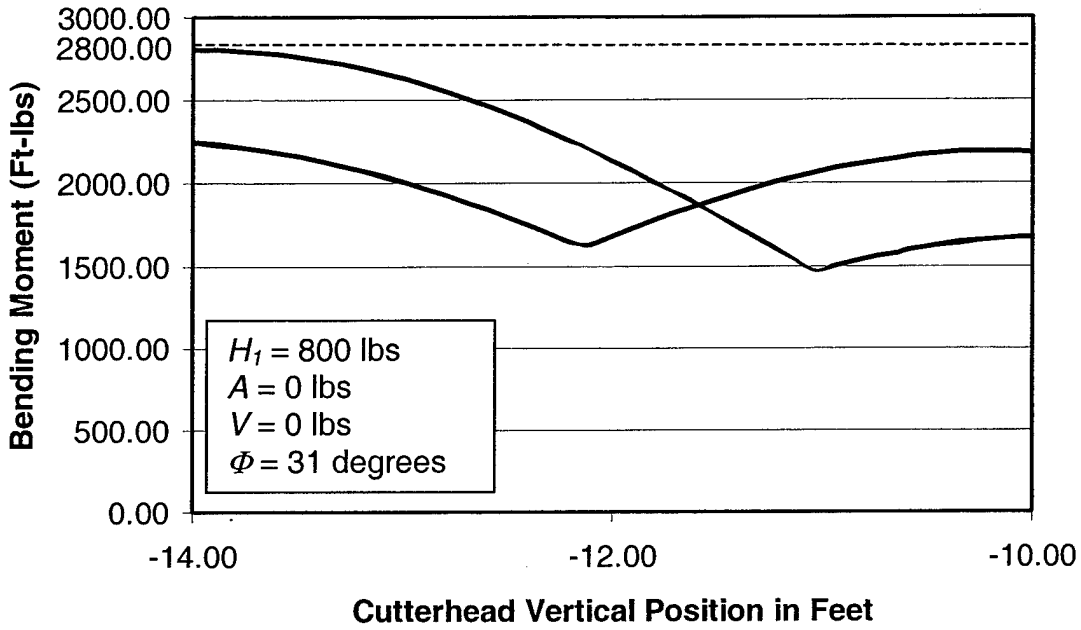

Figure B.11: Maximum Bending Moment in Vertical Guides
for a Maximum Allowable Pull Force, H_1

The static load analysis presented in Appendix B also shows that for the cutting forces listed in Table 4.5, the maximum bending moment in the horizontal guide rods is well below the structural limit. Figure B.12 is the bending moment in the two horizontal guide rods as a function of the maximum predicted cutterhead loading data as listed in Table 4.5. The cutting force data listed in Table 4.5 is used as input to the static analysis model and the maximum bending moment in the two guide rods is calculated and plotted. Each of the two horizontal guide rods is shown in a different shade. Maximum allowable bending moment in the 83 mm (3.25 in) diameter rods is 509 N-m (12,075 ft-lb). The combination of ladder angle, ladder arm elevation, and dredge carriage position that was found to produce the greatest bending moment for the given loading was 55 degrees, 1.06 m (3.46 ft), and 1.55 m (5.10 ft) respectively.

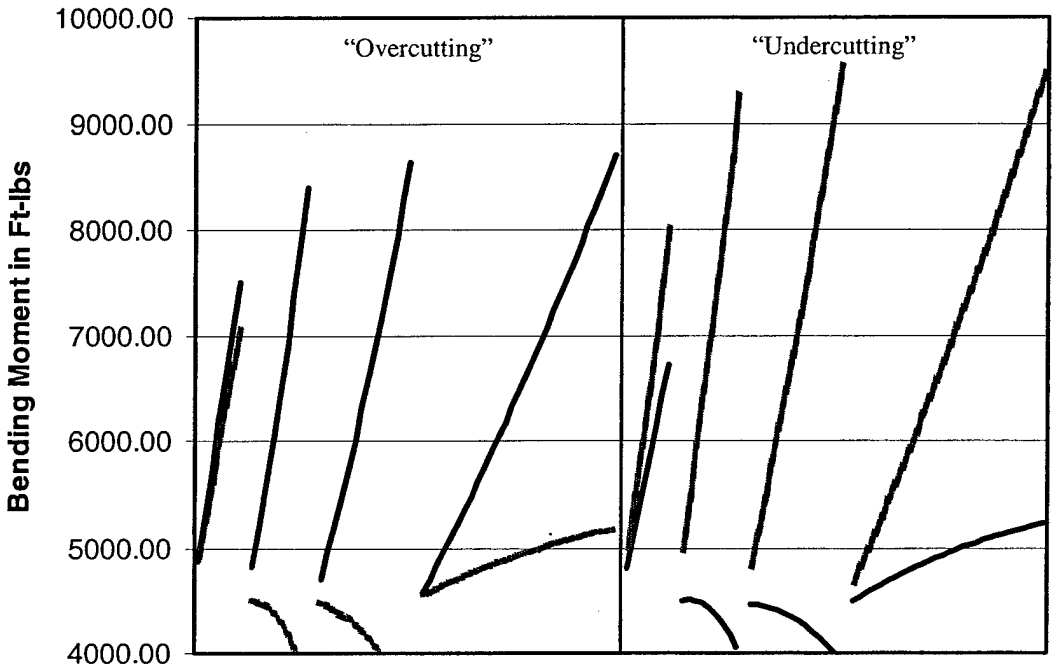

Figure B.12: Bending Moment in the Horizontal Guide Rods
under the Maximum Predicted Cutterhead Loading

When the standard loading of Table 4.5 is increased by a factor of 42%, the stress in the horizontal guide rods reaches the yield point. Figure B.13 is the bending moment in the horizontal guide rods with 142% of the maximum predicted cutterhead loading. The maximum allowable bending moment is shown as the dotted horizontal line.

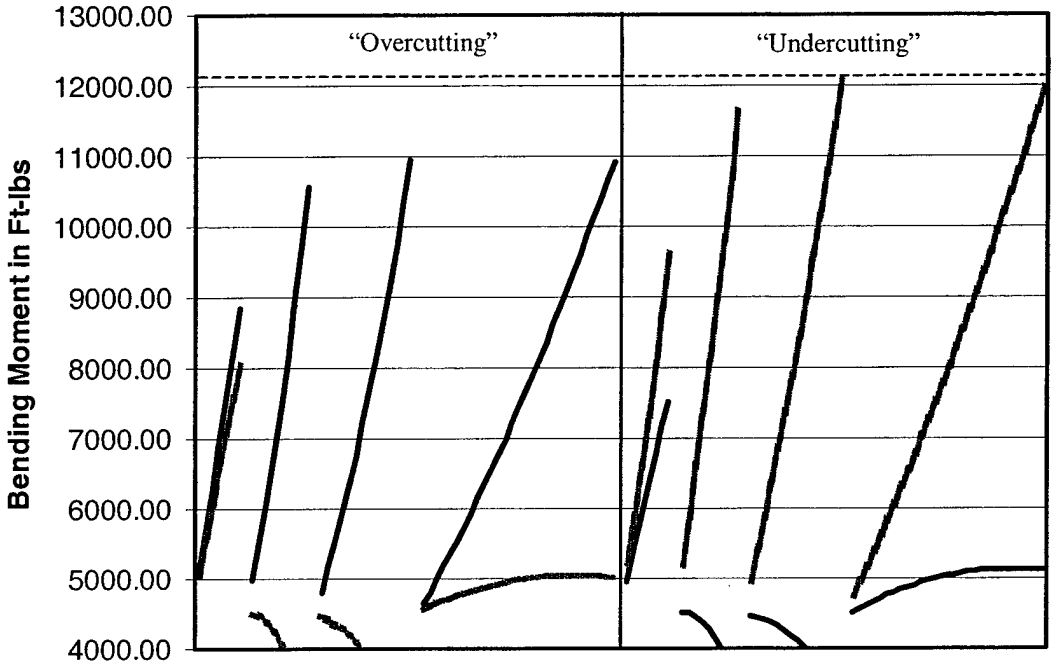

Figure B.13: Bending Moment in the Vertical Guide Rods
under 142% Maximum Predicted Cutterhead Loading

The maximum predicted cutterhead loading can be exceeded by 42% before the horizontal guide rods are in danger of yielding under the most severe combination of ladder angle, ladder arm elevation, and dredge carriage position. Just as was considered for the vertical guide rod loading, there may be a situation where the dredge needs to be pulled at its maximum possible pull force and no other loading on the cutterhead is considered. Given this scenario, a maximum pull force of 6721 N (1511 lb), with the ladder angle at 10 degrees and the digging depth at 4.27 m (14 ft) can be reached before the horizontal guide rods are in danger of yielding. Figure B.14 shows the maximum pull force with no other forces acting on the cutterhead. The maximum allowable bending moment is shown as the dotted horizontal line and the forces and geometry used to induce the bending moments are listed in the Figure. Each of the lines represents one of the horizontal guide rods.

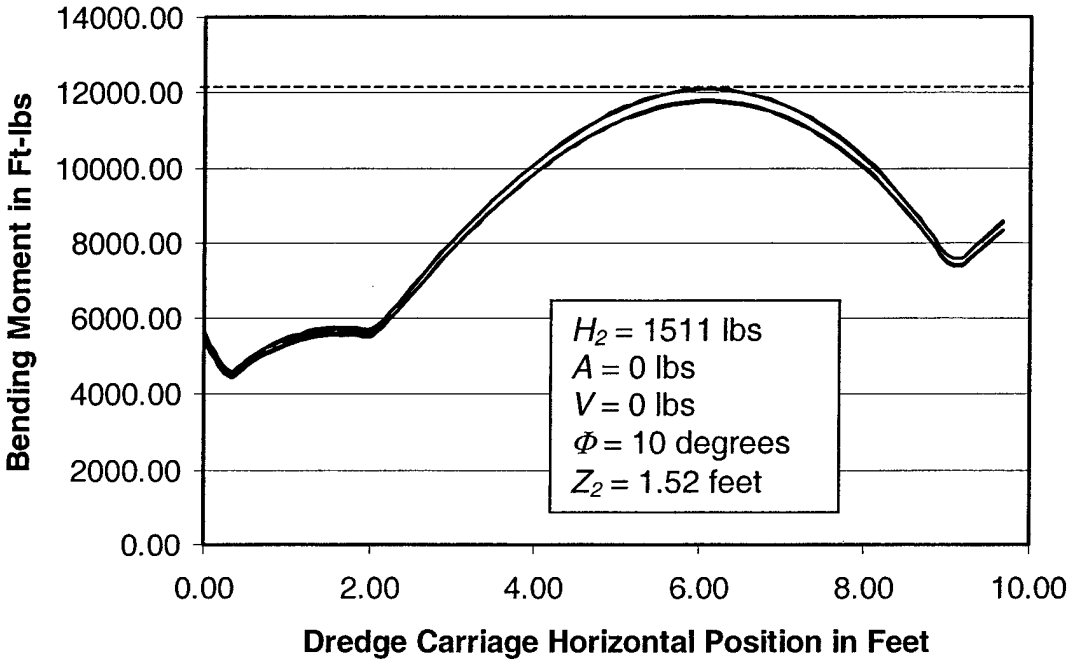

Figure B.14: Maximum Bending Moment in Horizontal Guides
for a Maximum Allowable Pull Force, H_2

Maximum pull force and side winch power depends on whether the structural integrity of the vertical or horizontal guide rods is the limiting factor. Figure B.15 shows that each of the 4 vertical guide rods will fail if the maximum pull force is allowed to be 6721 N (1511 lb). The maximum allowable bending moment is shown as the dotted horizontal line and the forces and geometry used to induce the bending moments are listed in the Figure. Each of the lines represents one of the vertical guide rods. The four lines are grouped into two pairs of two, indicating two pairs of identical loading on the vertical guide rods

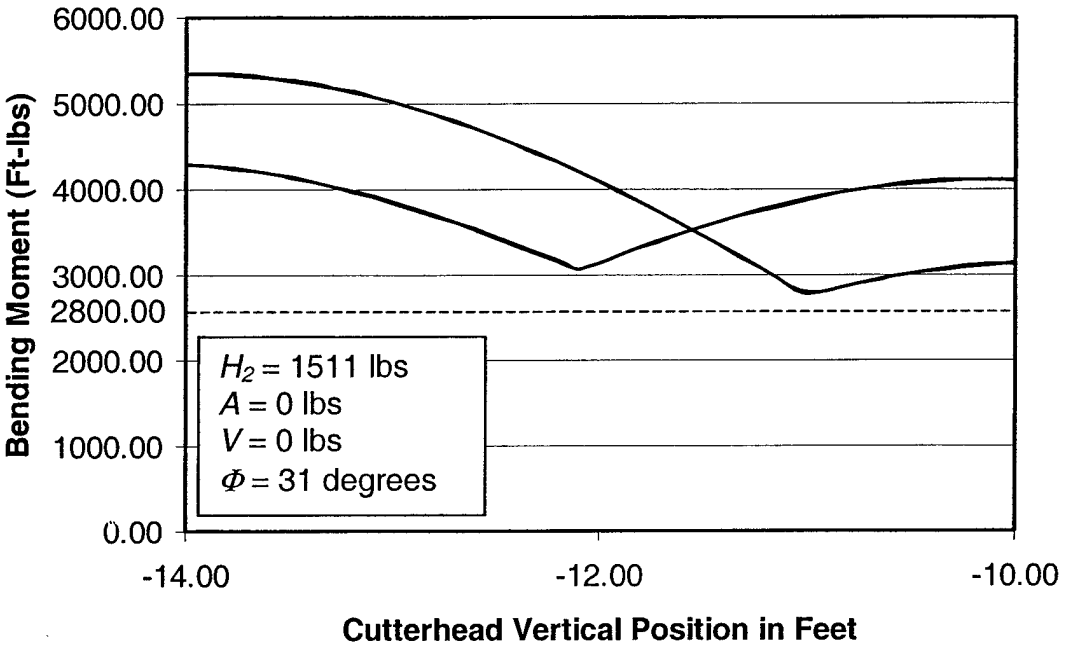

Figure B.15: Maximum Bending Moment in Vertical Guides
for the Maximum Allowable Pull Force, H_2

A maximum axial cutting force of 4226 N (950 lb) will cause the bending stress in the vertical guide rods to reach their yield strength for a horizontal ladder and a 3.81 m (12.5 ft) digging depth. Figure B.16 shows the bending moments in the vertical guide rods at maximum axial loading. The maximum allowable bending moment is shown as the dotted horizontal line and the forces and geometry used to induce the bending moments are listed in the Figure. Each of the lines represents one of the vertical guide rods.

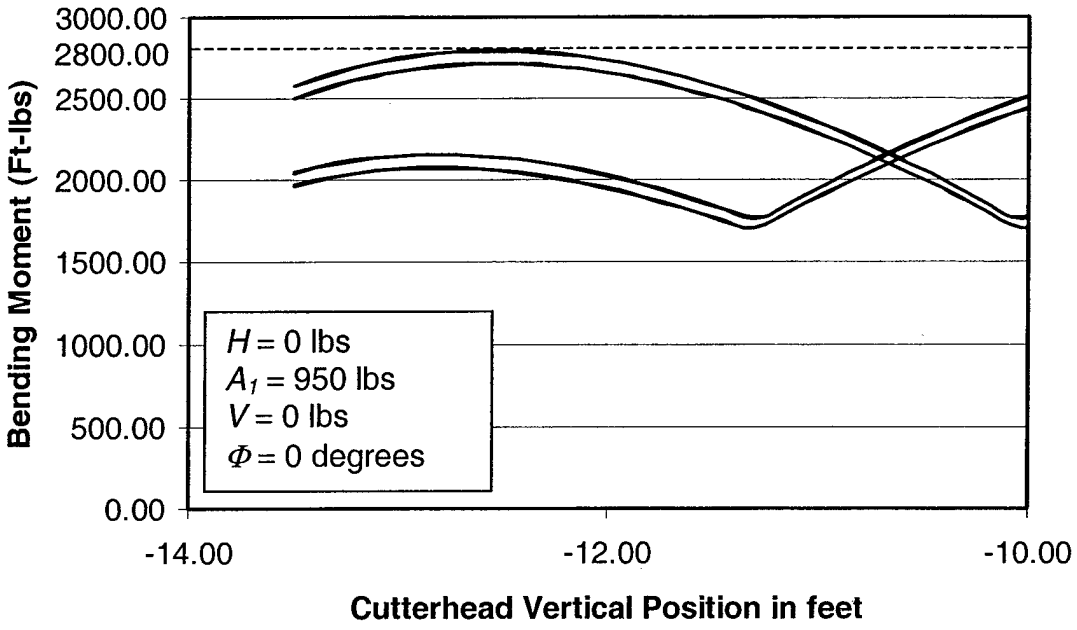

Figure B.16: Maximum Bending Moment in Vertical Guides
for a Maximum Allowable Axial Force, A_1

A maximum axial cutting force of 6628 N (1490 lb) will cause the bending stress in the vertical guide rods to reach their yield strength for a horizontal ladder and a 4.11 m (13.5 ft) digging depth. Figure B.17 shows the bending moments in the horizontal guide rods at maximum axial loading. The maximum allowable bending moment is shown as the dotted horizontal line and the forces and geometry used to induce the bending moments are listed in the Figure. Each of the lines represents one of the horizontal guide rods.

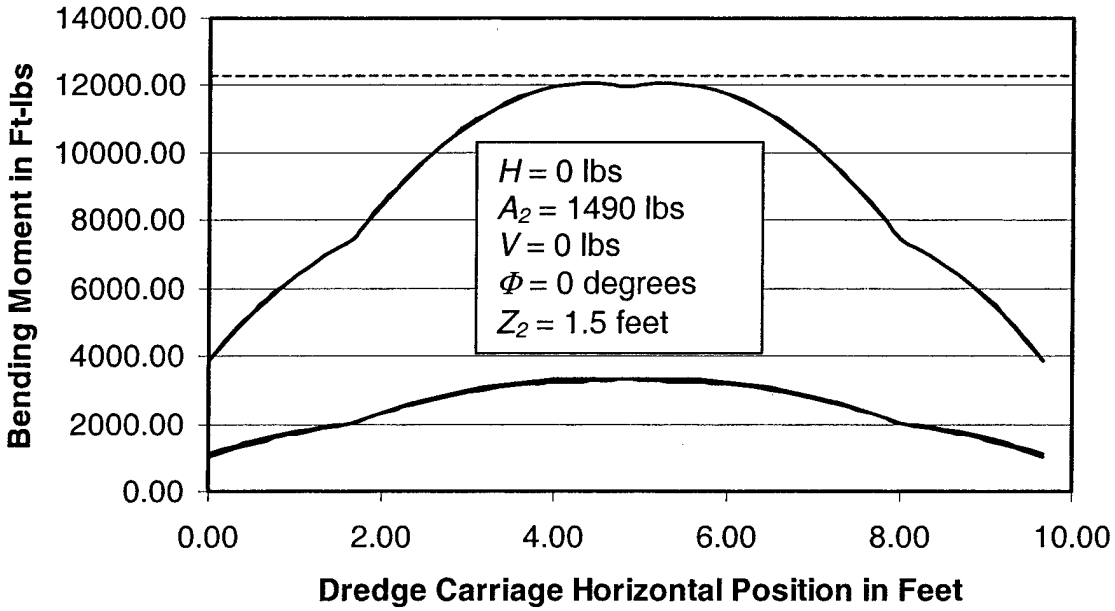

Figure B.17: Maximum Bending Moment in Horizontal Guides
for a Maximum Allowable Axial Force, A_2

Since an axial force of this magnitude would certain cause a failure in the vertical guide rods, the maximum axial loading from Figure B.16 will be used. The normal force acting on the front wheels with no cutterhead loading is 24,910 N (5600 lb) as shown in Table B.4. The normal force acting on the front wheels under this maximum load is 28,718 N (6456 lb) as shown in Table B.5. These are used in Chapter V to estimate the power needed for the tow carriage drive.

Table B.4: Tow Carriage Weight Distribution with No Cutterhead Loading

weight of Ladder w_L	100.00
weight of cutterhead w_{CH}	25.00
length of ladder X_2	3.00
distance to leverage point X_1	1.00
distance to ladder centroid X_3	1.00
horizontal reaction force at cutter H	0.00
vertical reaction force at cutter V	0.00
axial reaction force at cutter A	0.00
ladder angle Φ (90-0)	0.00
distance between ladder end bearings	1.50
vertical force at ladder end F_{Lz}	125.00
horizontal force at ladder end F_{Lx}	0.00
horiz force at ladder end F_{Lv}	0.00
horizontal moment at ladder end M_{Lx}	0.00
vertical moment at ladder end M_{Lz}	0.00
moment due to lader rotation device M_{Lv}	-175.00
total bearing force rght side at ladder enc	62.50
total bearing force left side at ladder enc	62.50
Moment due to Pump motor	15.00
Moment due to Cutter Drive	275.00
length of dredge arm z_1	19.00
distance to lower slide bearing set z_3	4.00
horizontal dist between d-arm bearngs x_4	2.00
weight of dredge arm w_A	2000.00
horizontal dist between d-arm bearngs y_1	2.00
Fa =	25.6326
Fb =	0.0000
Fc =	0.0000
Fd =	0.0000
Fe =	-10.9375
angle between F_a and $F_{b/c}$ in radians =	0.7854
dredge arm lift force F_{Az}	2125.00
total horiz slide bearing force at point 1	**34.25**
total horiz slide bearing force at point 2	**34.25**
total horiz slide bearing force at point 3	**34.25**
total horiz slide bearing force at point 4	**34.25**
total horiz slide bearing force at point 5	**19.50**
total horiz slide bearing force at point 6	**19.50**
total horiz slide bearing force at point 7	**19.50**
total horiz slide bearing force at point 8	**19.50**
dist between d-carriage slide bearings x_5	7.00
weight of dredge carriage W_D	1523.00
height of dredge carriage z_5	10.58
elevation of dredge arm (1.5-7.17) z_2	7.17
dist between d-carriage slide bearings y_2	2.00
vert force on both right d-c slide brng $F_{Dz1\&2}$	1824.00
vert force on both left d-c slide brng $F_{Dz3\&4}$	1824.00
vert force on both front d-c slide brng $F_{Dz2\&4}$	1849.00
vert force on both rear d-c slide brng $F_{Dz1\&3}$	1799.00
horiz force on each left d-c bearing $F_{Dx1,2}$	-72.50
horiz force on each right d-c bearing $F_{Dx3,4}$	72.50
tot d-carriage slide bearing force on 1	**902.42**
tot d-carriage slide bearing force on 2	**927.34**
tot d-carriage slide bearing force on 3	**902.42**
tot d-carriage slide bearing force on 4	**927.34**
dist from t-c wheel to d-carrge bearing X_8	2.00
dist from t-carriage wheel to centroid X_7	10.00
distance between carriage wheels X_6	15.00
weight of towing carriage w_C	6377.00
width of towing carriage Y_3	12.83
dist from wheel to carriag centroid Y_4	6.42
vertical dredge position h	-7.83
vertical force on front wheels $F_{C2z} + F_{C4z}$	5600.60
vertical force on rear wheels $F_{C1z} + F_{C3z}$	4424.40
min vert force on right wheels $F_{C1z} + F_{C2z}$	4371.69
max vert force on right wheels $F_{C1z} + F_{C2z}$	5648.34
min vert force on left wheels $F_{C3z} + F_{C4z}$	4376.66
max vert force on left wheels $F_{C3z} + F_{C4z}$	5653.31
min vertical force on wheel 1	**1929.39**
max vertical force on wheel 1	2492.82
min vertical force on wheel 2	**2442.30**
max vertical force on wheel 2	3155.52
min vertical force on wheel 3	**1931.58**
max vertical force on wheel 3	2495.01
min vertical force on wheel 4	**2445.08**
max vertical force on wheel 4	3158.30
horizontal force on rear bearing F_{C1v}	-19.33
horizontal force on front bearing F_{C2y}	19.33

Table B.5: Tow Carriage Weight Distribution with Axial Cutterhead Loading

weight of Ladder w_L	100.00	100.00
weight of cutterhead w_{CH}	25.00	25.00
length of ladder X_2	3.00	3.00
distance to leverage point X_1	1.00	1.00
distance to ladder centroid X_3	1.00	1.00
horizontal reaction force at cutter H	0.00	0.00
vertical reaction force at cutter V	0.00	0.00
axial reaction force at cutter A	625.00	950.00
ladder angle Φ (90-0)	0.00	0.00
distance between ladder end bearings	1.50	1.50
vertical force at ladder end F_{Lz}	125.00	125.00
horizontal force at ladder end F_{Lx}	625.00	950.00
horiz force at ladder end F_{Ly}	0.00	0.00
horizontal moment at ladder end M_{Lx}	0.00	0.00
vertical moment at ladder end M_{Lz}	0.00	0.00
moment due to lader rotation device M_{Ly}	-175.00	-175.00
total bearing force rght side at ladder enc	318.69	479.09
total bearing force left side at ladder enc	318.69	479.09
Moment due to Pump motor	15.00	15.00
Moment due to Cutter Drive	275.00	275.00
length of dredge arm z_1	19.00	19.00
distance to lower slide bearing set z_3	4.00	4.00
horizontal dist between d-arm bearngs x_4	2.00	2.00
weight of dredge arm w_A	2000.00	2000.00
horizontal dist between d-arm bearngs y_1	2.00	2.00
Fa =	25.6326	25.6326
Fb =	0.0000	0.0000
Fc =	0.0000	0.0000
Fd =	78.1250	118.7500
Fe =	-675.0000	-1020.3125
angle between F_a and $F_{b/c}$ in radians =	0.7854	0.7854
dredge arm lift force F_{Az}	2125.00	2125.00
total horiz slide bearing force at point 1	**771.46**	**1157.33**
total horiz slide bearing force at point 2	**615.27**	**919.87**
total horiz slide bearing force at point 3	**615.27**	**919.87**
total horiz slide bearing force at point 4	**771.46**	**1157.33**
total horiz slide bearing force at point 5	**735.22**	**1121.08**
total horiz slide bearing force at point 6	**579.03**	**883.62**
total horiz slide bearing force at point 7	**579.03**	**883.62**
total horiz slide bearing force at point 8	**735.22**	**1121.08**
dist between d-carriage slide bearings x_5	7.00	7.00
weight of dredge carriage W_D	1523.00	1523.00
height of dredge carriage z_5	10.58	10.58
elevation of dredge arm (1.5-7.17) z_2	1.50	1.50
dist between d-carriage slide bearings y_2	2.00	2.00
vert force on both right d-c slide brng $F_{Dz1\&2}$	1824.00	1824.00
vert force on both left d-c slide brng $F_{Dz3\&4}$	1824.00	1824.00
vert force on both front d-c slide brng $F_{Dz2\&4}$	3054.36	3681.14
vert force on both rear d-c slide brng $F_{Dz1\&3}$	593.64	-33.14
horiz force on each left d-c bearing $F_{Dx1,2}$	83.75	165.00
horiz force on each right d-c bearing $F_{Dx3,4}$	228.75	310.00
tot d-carriage slide bearing force on 1	**308.41**	**165.83**
tot d-carriage slide bearing force on 2	**1529.47**	**1847.95**
tot d-carriage slide bearing force on 3	**374.74**	**310.44**
tot d-carriage slide bearing force on 4	**1544.22**	**1866.49**
dist from t-c wheel to d-carrge bearing X_8	2.00	2.00
dist from t-carriage wheel to centroid X_7	10.00	10.00
distance between carriage wheels X_6	15.00	15.00
weight of towing carriage w_C	6377.00	6377.00
width of towing carriage Y_3	12.83	12.83
dist from wheel to carriag centroid Y_4	6.42	6.42
vertical dredge position h	-13.50	-13.50
vertical force on front wheels $F_{C2z} + F_{C4z}$	6163.10	6455.60
vertical force on rear wheels $F_{C1z} + F_{C3z}$	3861.90	3569.40
min vert force on right wheels $F_{C1z} + F_{C2z}$	4371.69	4371.69
max vert force on right wheels $F_{C1z} + F_{C2z}$	5648.34	5648.34
min vert force on left wheels $F_{C3z} + F_{C4z}$	4376.66	4376.66
max vert force on left wheels $F_{C3z} + F_{C4z}$	5653.31	5653.31
min vertical force on wheel 1	**1684.09**	**1556.54**
max vertical force on wheel 1	2175.89	2011.09
min vertical force on wheel 2	**2687.59**	**2815.15**
max vertical force on wheel 2	3472.45	3637.25
min vertical force on wheel 3	**1686.01**	**1558.31**
max vertical force on wheel 3	2177.81	2012.86
min vertical force on wheel 4	**2690.65**	**2818.35**
max vertical force on wheel 4	3475.51	3640.45
horizontal force on rear bearing F_{C1v}	-19.33	-19.33
horizontal force on front bearing F_{C2v}	19.33	19.33

VITA

Gordon Jason Glover was born April 17, 1973 in Corpus Christi, Texas. He received a Bachelor of Science degree in mechanical engineering from The University of Texas at Austin in May of 1996. After being commissioned as a United States Naval Officer in the Civil Engineer Corps, Ensign Glover worked at the Pacific Naval Facilities Engineering Division as a Resident Officer in Charge of Construction for the Pearl Harbor area. In January of 1999, Lieutenant Junior Grade (jg) Glover was assigned as a Staff Civil Engineer for the Commander in Chief, United States Pacific Fleet at Pearl Harbor. Since being accepted into the Navy's Ocean Facilities Program, Lt. Glover's first assignment was to Texas A&M University in the Fall of 2001 for the completion of a Master of Science degree in ocean engineering. Mr. Glover received the "Best Student Paper" award for a paper presented at WEDA XXII in June 2002. He also was awarded the Murden Scholarship for the 2002-2003 academic year.

After graduating from Texas A&M in December 2002, Lt. Glover will serve in the U.S. Navy as the Executive Officer, Underwater Construction Team 1 based in Little Creek, Virginia. Mr. Glover is a registered Professional Engineer (P.E.-Mechanical) in the State of California.

Permanent Address:
201 Southern
Corpus Christi, TX 78411
(361) 881-9455

SCALING OF MODEL HYDRAULIC DREDGES

G. J. Glover[1]
R. E. Randall[2]

ABSTRACT

The deepening and maintenance of the world's ports and navigable waterways has been an integral part of the world economy for centuries. In recent years, cutterhead and draghead hydraulic suction dredges have performed a majority of the dredging work. The ongoing design and testing of hydraulic dredges is important for maintaining efficient dredging operations within the limits set by increasing environmental regulations.

The high cost of building and operating a hydraulic dredge makes field testing of full-scale prototypes very expensive and time consuming. And thus, the need for laboratory model testing of hydraulic dredging operations.

The usefulness of any hydraulic model depends on the degree of geometric, kinematic, and dynamic similarity between the model and its prototype. The primary challenge in establishing useful similitude criteria for model dredge studies is proper kinematic scaling of the suction inlet velocity, average particle settling velocity, dredge swing velocity, and cutter rotational speed. Despite the inherent challenges, model studies of hydraulic dredge equipment have proven useful for obtaining qualitative results.

The purpose of this paper is to investigate scaling relationships for hydraulic dredge model studies and to develop a rationale for scaling the model dredge operating parameters based on previous model studies.

INTRODUCTION

The design of hydraulic dredges has traditionally been by trial-and-error with testing of full-scale prototypes (Brahme and Herbich 1986). The high cost of operating a hydraulic dredge makes field testing of full-scale prototypes very expensive. Moreover, it is very difficult to filter out and/or control environmental effects such as current, wind, bed topography, sediment properties, and surface waves so that experimental results can be properly evaluated for the effects that are being studied. Evaluating turbidity generation of full-scale prototypes has been done, but with great cost and difficulty (Huston 1976). Complete flow visualization in the vicinity of the cutterhead or draghead is practically impossible due to the limited visibility of most navigable waterways. In the past, researchers have resorted to dangerous techniques such as sending divers to make physical observations of flows in the vicinity of a rotating full-scale cutterhead (Slotta

[1] Glover, G.J., LT, CEC, USN, Graduate Student, Ocean Engineering Program, Civil Engineering Department, Texas A&M University, College Station, Texas, 77843. E-mail address: gglov432@earthlink.net.
[2] Randall, R.E., Professor, Ocean Engineering Program, Civil Engineering Department, Texas A&M University, College Station, Texas, 77843. E-mail address: r-randall@tamu.edu.

1968). Results obtained from prototype tests are subject to errors that could render them inconclusive and unreliable (Franco 1967). For these reasons, scaled model testing of hydraulic dredging equipment can save time and money in the design process.

The usefulness of any hydraulic model depends on the degree of geometric, kinematic, and dynamic similarity between the model and its prototype (Franco 1967). It is generally accepted that all of these relationships cannot be accurately scaled with the same model using a consistent set of scale laws (Joanknecht 1976, Slotta 1968). For example, Froude scaling requires model velocities to decrease and Reynolds scaling requires model velocities to increase. Moreover, how to scale the median grain diameter of the bed material and how the ensuing reduction in particle settling velocity affects the model has been an issue from the earliest studies (Army Corps of Engineers 1947, Franco 1967). However, research suggests that meaningful hydraulic model studies can still be conducted if the limits of the model are clearly understood. During the last 60 years, there have been a handful of studies and model experiments published that have attempted to establish valid similitude relationships for hydraulic suction dredge models.

PREVIOUS HYDRAULIC MODEL STUDIES

Model Dredge Studies

From 1942 to 1944 the Army Corps of Engineers Waterways Experiment Station conducted a model study of the suction head for the dredge Jadwin (Army Corps of Engineers 1947). The purpose of this study was to investigate the performance characteristics of a newly designed dustpan-type suction head by testing different 1:10 scale models. Data from the model tests were used to determine how changes in the suction head design parameters would affect solids output, soil removal rate, and efficiency. Consequently, no attempt was made to use the model test data to quantitatively predict prototype performance.

While the objectives of these tests were not to establish a set of similitude criteria between the model and the prototype, several useful observations were made during the study. Most importantly, the grain diameter of the sand that was used for the bed material was not linearly scaled to the model leading the researchers to conclude: "...exact similarity was not established for those tests in which the suction head operated in the sand bed. Thus, the results of the latter tests are only qualitative in nature, and cannot be translated to absolute prototype terms; this notwithstanding, the results of these tests may be used as a satisfactory basis for comparison between the relative efficiencies and performances of the various designs tested (Army Corps of Engineers 1947)."

From 1959 to 1963, the Army Corps of Engineers Waterways Experiment Station conducted another hydraulic model investigation to improve the design of dredge dragheads (Franco 1967). Like the previous hydraulic model study, the purpose of this study was to make qualitative observations on model performance under various operating conditions in order to improve performance of the full-scale prototype. Once again, the median grain diameter of the bed material used was full-scale for the model tests. As a result of the sand not being proportionately

scaled to the model, it was determined that a linear 1:6 scale for the drag-head model and suction line was the smallest possible without adverse scale effects. Ideally, a set of useful similitude relationships for dredge modeling should be scalable on the order of 1:10 geometric scale ratio without any adverse scale effects.

In this case, physical limitations of the testing facilities prevented the water depth, suction line length, pump elevation above the water level, and median grain size of bed material from being appropriately scaled. As a result, data collected from the model runs could not be directly used to calculate the analogous quantities for the prototype. Attempts to correct the model data for the differences in similarity related to the median grain diameter of the bed material were unsuccessful. As a result, the adjusted model data did not accurately reflect the data eventually obtained from the prototype. The study concludes: "Because of the limitations and dissimilarities between model and prototype mentioned above, the results of this study cannot be considered strictly quantitative when applied to the prototype. However, the results do provide reasonable indications of the comparative effectiveness of the various dragheads and modifications (Franco 1967)."

Neither of these studies at the Waterways Experiment Station provide a quantitative scaling rationale for interpreting model data. Later studies made attempts to provide scaling laws by dimensional analysis and verify them experimentally. These scaling laws can be characterized by similarity with respect to a Reynolds or Froude relationship, similarity with respect to sediment pick-up behavior, and similarity with respect to the cavitation that occurs during the cutting process.

Flow Visualization Studies

Results of a cutterhead flow visualization study using scaled models were presented at the 1968 World Dredging Conference (Slotta 1968). The purpose of this model study was to examine the flow in and around the cutterhead under different operating conditions and how the flow affects turbidity and solids production. The experiments were performed with a 1:15 scale cutterhead using clear water in a Plexiglas tank. Hydrogen bubbles created by electrolysis provided visualization of the streamlines that were recorded onto film for further observation and analysis. In this study, the test conditions attempted to satisfy the similitude criteria for the Reynolds number (Equation 1), the Froude number (Equation 2), a kinematic scale of velocities (Equation 3), and the specific speed of the rotating cutterhead (Equation 4). It should be noted that if the model and prototype suction inlet pipe diameters follow the geometric scale, Equation 4 reduces to Equation 3. Equations 3 and 4 are based on similarity with respect to sediment pick-up behavior.

$$\left[\frac{U_{suction} D_{cutter}}{\nu}\right]_{model} = \left[\frac{U_{suction} D_{cutter}}{\nu}\right]_{prototype} \quad (1)$$

Where $U_{suction}$ = suction inlet velocity, D_{cutter} = cutterhead diameter, ν = fluid viscosity.

$$\left[\frac{(U_{suction})^2}{gD_{cutter}}\right]_{model} = \left[\frac{(U_{suction})^2}{gD_{cutter}}\right]_{prototype}$$ Where g = gravitational acceleration (2)

$$\left[\frac{\omega_{cutter} D_{cutter}}{U_{suction}}\right]_{model} := \left[\frac{\omega_{cutter} D_{cutter}}{U_{suction}}\right]_{prototype}$$ Where wcutter = cutterhead angular velocty (3)

$$\left[\frac{\omega_{cutter}\sqrt{Q_{Suction}}}{(H_{velocity})^{3/4}}\right]_{model} = \left[\frac{\omega_{cutter}\sqrt{Q_{suction}}}{(H_{velocity})^{3/4}}\right]_{prototype}$$ (4)

Where $H_{velocity} = \frac{(U_{suction})^2}{2g}$ and $Q_{suction}$ = volumetric flow rate of suction inlet

These relationships were developed by a dimensional analysis on the cutterhead and suction pipe parameters. Equations 1 and 2 showed a poor correlation to the experimental data while Equations 3 and 4 were found to accurately correlate the data for suction velocity, cutterhead speed, and volumetric flow rate. Since the tests were done without any swing or haulage velocity, this quantity was omitted from the dimensional analysis. Moreover, no attempt was made to scale cutting forces, production, or cutter power, only the fluid behavior. The following was concluded: "A rationale for projecting the results from model tests is at present not available, except on a qualitative basis. Dimensional analysis offers a guide to experimentation and forms a rational basis for proper analysis of results...(Slotta 1968)."

Model Cutterhead Studies

Results of another suction cutterhead model study were presented at the 1976 World Dredging Conference (Joanknecht 1976). The cutterheads used in this study were 1:3 and 1:4 scales, and the sand used had a median grain diameter of 0.2 mm. In this study, the dominant parameter for overall dynamic and kinematic similarity was assumed to be the Froude number. However, rather than using the intake velocities at the suction inlet and the cutterhead diameters as was the common practice, the Froude relationship (Equation 5) was applied using the particle settling velocities ($V_{settling}$) and the median grain diameter (d_{50}) of the model and prototype bed materials.

$$\left[\frac{V_{settling}}{\sqrt{gd_{50}}}\right]_{model} = \left[\frac{V_{settling}}{\sqrt{gd_{50}}}\right]_{prototype}$$ (5)

Since the same bed material was used for both model and prototype in these experiments, this condition was automatically satisfied. However, given that settling velocity is strictly a function of grain diameter for a given material density, it would be difficult to satisfy this relationship

using sand if the model median grain diameter differed from the prototype median grain diameter. For example, if particle size were to be scaled at a 1:10 ratio, particle density would have to be increased by an order of magnitude to satisfy this parameter.

Froude scaling was also used to develop the kinematic similitude relationships for cutterhead swing velocity (Equation 6) and cutterhead rpm (Equation 7). The relationships were developed on the basis of scaling the forces only, without concern for any similarity of the production, sediment pick-up behavior, or cavitation in the sediment voids caused by the cutter.

$$\left[\frac{V_{swing}}{\sqrt{gD_{cutter}}}\right]_{\text{model}} = \left[\frac{V_{swing}}{\sqrt{gD_{cutter}}}\right]_{\text{prototype}} \qquad \text{Where } V_{swing} = \text{cutterhead swing velocity} \qquad (6)$$

$$\left[N_{cutter}\sqrt{\frac{D_{cutter}}{g}}\right]_{\text{model}} = \left[N_{cutter}\sqrt{\frac{D_{cutter}}{g}}\right]_{\text{prototype}} \qquad \text{Where } N_{cutter} = \text{cutterhead RPM} \qquad (7)$$

Kinematic similarity for fluid/particle interaction was achieved by keeping the ratio of particle settling velocity to the velocity at the suction pipe inlet identical for both model and prototype (Equation 8).

$$\left[\frac{V_{settling}}{U_{suction}}\right]_{\text{model}} = \left[\frac{V_{settling}}{U_{suction}}\right]_{\text{prototype}} \qquad (8)$$

This relationship attempts to ensure proper scaling of the velocity field relative to the settling velocity of the bed material so that similarity with respect to sediment pick-up behavior is achieved. Since the same bed material was used for both model tests, the suction velocity was also made to be identical for both model tests.

Providing that Equations 5 through 8 are satisfied, other similitude relationships based on the Froude relationship were developed that showed a favorable correlation to test data between the two models for volumetric flow rate (Equation 9), cutting force (Equation 10), and shaft torque (Equation 11). Noting that the two models tested were 1:3 scale and 1:4 scale, their relative scale to each other would only be 3:4. For these similitude relationships to be useful, they would need to be tested for scale ratios on the order of 1:5 to 1:10 so that any possible scale effects can be more easily seen.

$$\left[\frac{Q_{suction}}{(D_{cutter})^{5/2}}\right]_{\text{model}} = \left[\frac{Q_{suction}}{(D_{cutter})^{5/2}}\right]_{\text{prototype}} \qquad (9)$$

$$\left[\frac{F_{cutting}}{(D_{cutter})^3}\right]_{\text{model}} = \left[\frac{F_{cutting}}{(D_{cutter})^3}\right]_{\text{prototype}} \qquad \text{Where } F_{cutting} = \text{cutting force} \qquad (10)$$

$$\left[\frac{\Gamma_{shaft}}{(D_{cutterhead})^4}\right]_{\text{model}} = \left[\frac{\Gamma_{shaft}}{(D_{cutterhead})^4}\right]_{\text{prototype}} \qquad \text{Where } \Gamma_{shaft} = \text{shaft torque} \qquad (11)$$

Other studies have shown that the kinematic scale of suction and cutterhead velocities by Slotta (1968) (Equation 3) is useful in scaling the flow in and around the cutterhead (Burger 1997). The purpose of the cutterhead is twofold, to excavate the sediment from the seabed, and to form a slurry that is captured by and moves into the velocity field created by the suction. The rotation of the cutterhead also creates a velocity field that interacts with the velocity field created by the suction. This may cause some of the material that would have been captured by the pump suction velocity field, had the cutterhead been stationary, to "spill" outside of the range of influence of the suction. This portion of the slurry mixture, known as spillage, creates turbidity in the water as these particles either slowly settle to the bottom or remain suspended.

If the spillage of slurry outside the cutterhead between model and prototype is to be similar, then Equation 3 can be used to normalize the cutterhead angular velocity to the magnitude of the suction velocity (Burger 1997). Model tests have shown there is a threshold for the cutterhead rpm above which spillage occurs (Mol 1977a, Mol 1977b). The kinematic scale of velocities for geometrically similar models can be used to determine that point. Thus, if similarity with respect to sediment pick-up behavior (spillage) is to be achieved, Equation 3 must be satisfied.

Flow Field Studies and Sediment Pick-up Behavior

Brahme and Herbich (1986) described a series of studies conducted in the Texas A&M University Hydromechanics Laboratory to examine the velocity flow field around the suction inlet and the influence of the velocity field on sediment pick-up behavior. A dimensionless parameter (Equation 12) was developed while creating dimensionless velocity field plots around suction inlets of various orientations. It was found that by using these dimensionless plots, the velocity (V) at any point in the field could be determined with reasonable accuracy if the volumetric flow rate (Q) and the radial distance (R) of the point from the suction inlet are known. This was found to hold true regardless of the geometric scale of the velocity field.

$$\frac{Q_{suction}}{R^2 V} = \text{Dimensionless velocity field} \qquad (12)$$

One very important observation is the fact that the magnitude of the velocity field was not found to depend on intake velocity or intake diameter if the volumetric flow rate through the suction pipe was held constant. In fact, the magnitude of the velocity field was found to depend solely on volumetric flow rate through the suction pipe, regardless of pipe geometry or intake velocity.

Joanknect (1976) established the importance of properly scaling the velocity field at the suction inlet to the settling velocity of the bed material (Joanknect 1976). However, the studies with dimensionless velocity field plots showed that the magnitude of the velocity field was found to be more a function of the volumetric flow rate through the suction pipe than the suction inlet velocity (Brahme and Herbich 1986). More importantly, outside the immediate vicinity of the suction inlet, suction pipe velocity and diameter have a negligible effect on the velocity field. Since the velocity in the immediate vicinity of the suction inlet is several orders of magnitude greater than the particle settling velocity, proper scaling of the velocity field for the purposes of sediment pick-up similitude is only critical at distances from the suction inlet where field velocities are similar to particle settling velocities. Therefore, proper scaling of the velocity field shape and magnitude created by the suction pipe is dependent only on the volumetric flow rate through the suction pipe. As a result, accurate velocity field scaling can be achieved for any given median grain diameter, geometric scale ratio, and pipe diameter simply by scaling the volumetric model flow rate in accordance with Equation 13.

$$\left[\frac{Q_{suction}}{(D_{cutter})^2 V_{settling}}\right]_{model} = \left[\frac{Q_{suction}}{(D_{cutter})^2 V_{settling}}\right]_{prototype} \tag{13}$$

The dimensionless parameter developed by Brahme and Herbich (1986) to plot dimensionless velocity fields for different intakes can be used to non-dimensionalize the velocity field around any suction inlet. By replacing the sediment pick up range with the cutterhead diameter and the field velocity with the settling velocity, the velocity field is "normalized" to the geometric scale of the dredge and the settling velocity of the sediment. Unlike Equation 8, this relationship takes into consideration geometric scaling of the velocity field as well as scaling the velocity field magnitude relative to the particle settling velocity. Moreover, stronger or weaker prototype velocity fields, larger or smaller prototype cutterheads, and different prototype sediment sizes can be modeled without changing the model suction pipe geometry or the model bed material. Only the model volumetric flow rate need be adjusted. Accurate scaling of the velocity field shape and magnitude for sediment pick-up is critical when modeling hydraulic dredges for the purpose of studying turbidity and the effects of re-suspension, as well as sediment pick-up and solids production.

It is important to note the relationship between Equation 13 and Equation 8. While the magnitude of the velocity field created by the suction is not dependent on the velocity at the suction inlet as expressed by Equation 13, Equation 8 is still a valid relationship under the right circumstances. If the prototype and model suction inlet diameters do not follow the geometric scale ratio, then certainly Equation 8 will not be valid as model suction inlet velocity will be determined by model suction inlet diameter. However, if the prototype and model suction inlet diameters do follow the geometric scale ratio, then Equation 13 reduces to Equation 8. Therefore, Equation 8 is simply a special case of the dimensionless velocity field parameter in which the prototype and model suction inlet diameters exactly follow the geometric scale ratio.

Cavitation and Cutterhead Dynamics

According to Miedema (1987) the cutting process is characterized by two quantities: the geometry of the layer being cut and whether a cavitating or non-cavitation cutting process is occurring. Moreover, if cavitation does occur during cutting in both model and prototype, then the angle of the cutterhead blade at the start of cavitation (φ_c) must also be similar between model and prototype.

When the rotating cutterhead is being translated over the seabed via the swing motion of the ladder, each blade takes a specified path through the sediment based on the swing speed, the cutterhead rpm (N_{cutter}), the pitch of the blades or teeth (p), and the profile angle (κ) (Miedema 1987). The path of each cutting edge through the sediment cuts individual layers with a thickness (t_{layer}) as a function of the angular position of the blade (φ) as defined by Equation 14. Figure 1 illustrates the relationship of the layer thickness to the other parameters.

$$t_{layer} = \frac{V_{swing}\,60}{N_{cutter}\,p}\cos(\varphi)\cos(\kappa) \tag{14}$$

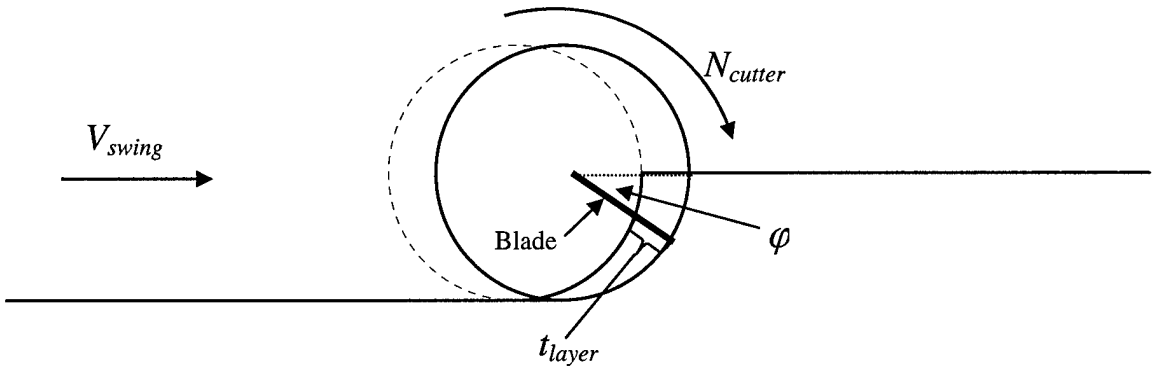

Figure 1: The Layer Thickness in Relation to Cutterhead Geometry and Kinematics

The model layer thickness must follow the same geometric scale ratio applied to the rest of the model. This is accomplished when the ratio of cutterhead blade velocity to swing speed is identical for model and prototype according to Equation 15.

$$\left[\frac{N_{cutter}D_{cutter}}{V_{swing}}\right]_{model} = \left[\frac{N_{cutter}D_{cutter}}{V_{swing}}\right]_{prototype} \tag{15}$$

The effect of cavitation in the sediment during cutting has a significant impact on the cutting forces developed by the cutter (Miedema 1989). If no cavitation occurs during the cutting process, the cutting forces increase as the cutting velocity increases. As the cutting velocity continues to increase, the pressure in the voids of the sediment continues to decrease. When the pore pressure in the sediment drops below the vapor pressure of the water during the cutting

process, cavitation occurs. Once cavitation has begun, continuing to increase the cutting velocity does not drop the pore pressure any further and the cutting forces become primarily a function only of digging depth rather than cutting velocity. The effects of inertia, gravity, cohesion and adhesion still affect the cutting forces developed as the cutting velocity increases, but they are relatively insignificant.

If and when cavitation occurs is a function of the digging depth, the cutterhead rpm, and the layer thickness as well as the sediment properties and blade angle. Equation 16 shows the condition that has to be met for cavitation to occur (Miedema 1995),

$$\left(\frac{d_1}{c_1}\right)\left(\frac{k_m}{e}\right)\frac{z+33}{V_{cutter}t_{layer}}<1 \qquad \text{Where } V_{cutter} \text{ is equal to } N_{cutter}\pi D_{cutter}/60 \tag{16}$$

The ratio of d_1/c_1 is a function of the given blade angle and the ratio k_m/e is a function of the sediment mechanical properties. Since the layer thickness is a function of the blade position as it moves through the sediment for any given swing speed and cutterhead rpm (Equation 14), cavitation usually occurs at a certain cutting angle as each blade progresses through the layer. Figure 2 illustrates the relationship between the cavitation transition angle (φ_c) and the other operating parameters.

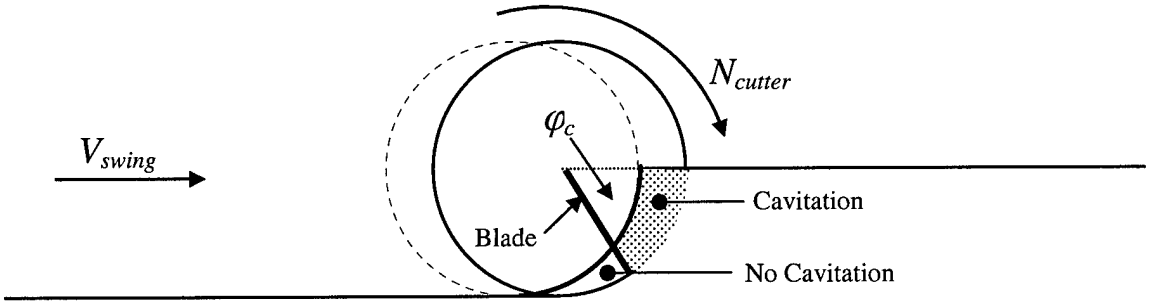

Figure 2: The Cavitation Transition Angle

The onset of cavitation in the prototype occurs when the absolute pore pressure reaches the limit described by Equation 17 (Miedema 1987). This will also occur in the model dredge according to Equation 18 (Miedema 1987). The ratio of the prototype to model cavitation pressures ($p_{cavitaton}$) is known as the cavitation scale factor, or hydrostatic pressure factor λ_c, and is defined by Equation 19 (Miedema 1987). It is important to note that Equation 19 assumes that the model soil mechanics (i.e. volume strain, e, and average permeability, k_m) are identical to the prototype soil mechanics. This may not always be the case in actual scale model testing.

$$\left[p_{cavitation}\right]_{\text{prototype}} = \left[\rho_{water}\, g(z+33)\right]_{\text{prototype}} \qquad \text{Where } \rho_{water} = \text{density of water} \tag{17}$$

$$\left[p_{cavitation}\right]_{\text{model}} = \left[\rho_{water}\, g(z+33)\right]_{\text{model}} \qquad \text{Where } z = \text{digging depth} \tag{18}$$

$$\frac{z_{\text{prototype}}+33}{z_{\text{model}}+33}=\lambda_c \tag{19}$$

To achieve similarity between model and prototype with respect to the degree of cavitation during the cutting process, the prototype/model pore pressure ratio must be equal to the cavitation scale factor. Since the pore pressure for the non-cavitating case is proportional to the product of the layer thickness and the cutterhead rpm, this leads to another rationale for scaling the model cutterhead rpm according to Equation 20.

$$\left(N_{cutter}\right)_{\text{model}}=\left(N_{cutter}\right)_{\text{prototype}}\left[\frac{\left(D_{cutter}\right)_{\text{prototype}}}{\left(D_{cutter}\right)_{\text{model}}}\right]^2\frac{1}{\lambda_c} \tag{20}$$

To achieve similarity between model and prototype with respect to the geometry of cavitation during the cutting process, the cavitation transition angle as shown in Figure 2 needs to be identical between model and prototype. This involves solving Equations 14 and 16 in terms of the angular position of the blade, φ, and setting the two quantities equal to each other. This leads to another rationale for scaling the model cutterhead swing speed according to Equation 21.

$$\left(V_{swing}\right)_{\text{model}}=\left(V_{swing}\right)_{\text{prototype}}\left[\frac{\left(D_{cutter}\right)_{\text{prototype}}}{\left(D_{cutter}\right)_{\text{model}}}\right]\frac{1}{\lambda_c} \tag{21}$$

SCALING LAWS FOR MODELING HYDRAULIC DREDGING OPERATIONS

According to previous hydraulic dredge model studies, scaling laws can be divided into three categories. One is based on similarity with respect to sediment pick-up behavior, one is based on similarity with respect to the Froude or Reynolds number, and one is based on similarity with respect to cavitation during the cutting process. These criteria cannot all be satisfied with one set of model operating parameters. Laboratory data collected by Slotta (1968), Joanknect (1976), Brahme and Herbich (1986), and Burger (1997), suggest that similarity with respect to sediment pick-up is the most important similitude criterion when modeling hydraulic dredges. The scale laws based on similarity with respect to cavitation require very high model cutting speeds in order to be satisfied. Excessive cutterhead swing and rotational velocities will create disproportionately high velocity fields that will overpower the velocity field created by the suction inlet. This will compromise similarity of the model with respect to sediment pick-up behavior. At kinematically scaled cutting speeds, negative digging depths, or a model dredge operating in a vacuum, are required. Since this is not practically possible in a laboratory facility, there will be scale effects in the model cutting forces when similarity is based on sediment pick-up behavior.

Sediment Pick-up Behavior

If a model dredge is to be successful, the model suction must be properly scaled such that the sediment pick-up behavior is similar to the prototype suction. The flow of water through the suction inlet creates a velocity field around the inlet. Before any amount of sediment can be drawn towards the suction inlet via the velocity field, it must first be excavated by the cutter. Assuming that the model cutter has been geometrically, kinematically, and dynamically scaled to the prototype, then the model cutter is removing a geometrically similar volume of material as the prototype. Given this, the model suction needs to pick up a geometrically similar volume of material as the prototype suction. Consider the following example illustrated in Figure 3: suction A and suction B are both geometrically similar suction inlets with a 1:2 geometric scale ratio. Each suction inlet has a flow rate (Q) that creates a velocity field around the inlet with a similar geometry and magnitude. The lines of constant velocity potential are shown. The heavy line represents the range (R) at which the magnitude of the velocity field (V) is equal to the median grain diameter settling velocity.

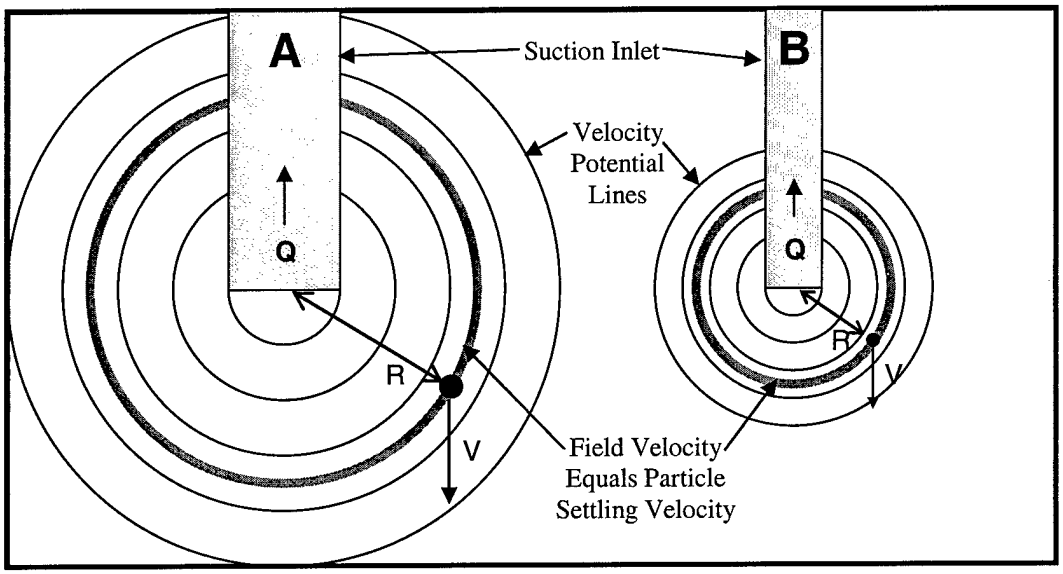

Figure 3: Velocity Field Similitude Example

Theoretically, all particles within the heavy line are captured by the velocity field and drawn towards the suction inlet. Conversely, all particles outside the heavy line will either settle out or remain in suspension. For suction A and suction B to be geometrically similar with respect to sediment pick-up, the range for A must be twice that of B, in accordance with the 1:2 geometric scale ratio. The range (R) of the heavy line is a function of both velocity field magnitude and particle settling velocity. For instance, for a given median grain size, the range will move closer or further from the inlet as the magnitude of the velocity field is changed. Higher field velocities will pick up more material (move the range out), and lower field velocities will pick up less material (move the range in). Likewise, for a given velocity field magnitude, the range will move closer or further from the inlet as the particle settling velocity is changed. Higher settling

velocities will cause less material to be picked up (move the range in) and lower settling velocities will cause more material to be picked up (move the range out).

The rotating cutterhead also creates a velocity field around the suction inlet (Burger 1997), as do the cutterhead swing and any currents passing through the area. These velocity fields also have an impact on sediment pick-up behavior. As a result, they too must be similarly scaled if similarity with respect to sediment pick-up is to be maintained between model and prototype. To summarize, for two dredges of different scale to achieve similarity with regard to sediment pick up behavior, the velocity fields must be all scaled in accordance with the geometric scale ratio and normalized to the sediment settling velocity.

Normalizing the Velocity Fields to the Particle Settling Velocity

Equation 13, which is used to scale the velocity field created by the model suction to the prototype, is already expressed in terms of $V_{settling}$. It should be noted that the scale laws developed by Slotta (1968) and Burger (1997) scale the model cutterhead rotation to the model suction inlet velocity (Equation 3). However, Brahme and Herbich (1986) proved that velocity field scaling was dependent on the volumetric flow rate through the suction and not the velocity at the suction inlet. Therefore, since scaling the velocity field created by the suction inlet to the velocity at the suction inlet is a special case of the dimensionless velocity field parameter, Equation 3 must assume that the model and prototype suction inlet diameters follow the geometric scale, which may not always be the case. In order to avoid confusion, Equation 3 can be rewritten in terms of the volumetric flow rate. If Equation 13 is satisfied, Equation 3 can again be rewritten in terms of the particle settling velocity. Equation 22 is a more general application of the scale laws by Slotta (1968) and Burger (1997) in light of the dimensionless velocity field parameter developed by Brahme and Herbich (1986).

$$\left[\frac{N_{cutter} D_{cutter}}{V_{settling}}\right]_{\text{prototype}} = \left[\frac{N_{cutter} D_{cutter}}{V_{settling}}\right]_{\text{model}} \tag{22}$$

The distinction between the velocity field created by the suction and the suction inlet velocity may seem trivial. However, the difference becomes clear if one considers two identical suction pipes with identical flow rates. Each suction creates an identical velocity field around each suction inlet. Each suction also creates an identical suction inlet velocity. Placing a fitting over one of the suction inlets to reduce the suction inlet diameter will change the velocity at the suction inlet. However, the velocity field created by the suction will not change, being dependent on the volumetric flow rate only. Therefore, Equation 8 is considered a special case of Equation 13 that assumes the suction inlet diameters follow the geometric scale ratio.

Following this same rationale for cutterhead swing as for cutterhead rpm, the swing speed of the cutterhead also creates a velocity field relative to the cutterhead that interacts with the velocity fields created by the suction and cutterhead rotation. Equation 15 can be rewritten in terms of Equation 22 as shown in Equation 23.

$$\left[\frac{V_{swing}}{V_{settling}}\right]_{\text{prototype}} = \left[\frac{V_{swing}}{V_{settling}}\right]_{\text{model}} \tag{23}$$

Therefore, if the model and prototype settling velocities are known, Equations 13, 22, and 23 can be used to scale the model flow rate, swing speed, and cutterhead rpm.

Other Challenges for Sediment Scaling

Even if perfect kinematic and geometric scaling of the velocity field around a model cutterhead can be achieved, there are several other factors that require experimentation to determine. For instance, the effect of geometrically scaling the median grain diameter of the model bed material on cutterhead dynamics has not been tested. It appears that proper geometric scaling of the model bed material in this way is practically impossible to achieve without adversely affecting the settling velocity of the model sediment particles and creating unintended scale effects with increased material density. Perhaps proper scaling of the sediment material entails more than simply geometric scaling of the median grain diameters and dynamic scaling of the particle settling velocities. Bed sediment compactness, void ratio, material density, and cohesive/adhesive properties will all contribute to dynamic scaling of the cutting forces.

THE TEXAS A&M UNIVERSITY COASTAL ENGINEERING LABORATORY

This paper takes the model scaling relationships that have been developed through experimentation and dimensional analysis and develops rational for hydraulic dredge model studies. This rational serves as the basis for the design of the proposed hydraulic dredge modeling facilities at the Texas A&M University Coastal Engineering Laboratory. The model dredge apparatus contains a suction pipe, cutter, ladder, and winches to perform the scaled model testing of hydraulic dredge operations. The ladder arm translates vertically and horizontally in the Z and Y direction. The tow carriage advances the entire apparatus in the X direction. The ladder rotates from 20 to 90 degrees from the horizontal. Figure 4 shows the dredge carriage riding atop the towing tank.

The tow and dredge carriages are equipped with a data acquisition and control system that allows for manual or automated operation. Instrumentation monitors several parameters such as pump rpm, pump torque, pump suction/discharge pressures, flow rate, slurry density, cutterhead x/y/z position, side winch pull force, vertical cutting forces, cutter rpm, cutter torque. During a towing operation, a load cell records the drag forces of the towed payload in three dimensions. These data are digitized and relayed to the Programmable Logic Controller (PLC) via the input/output modules. The PLC contains an internal clock that is used with some of the input data to calculate carriage speed, swing speed, pump brake and water horsepower, cutter horsepower, and dredge efficiency. The data are forwarded to the operators PC from the PLC via a serial cable and stored in data files on the PC's hardrive. The data can also be displayed on the PC's monitor in real time as a virtual control panel.

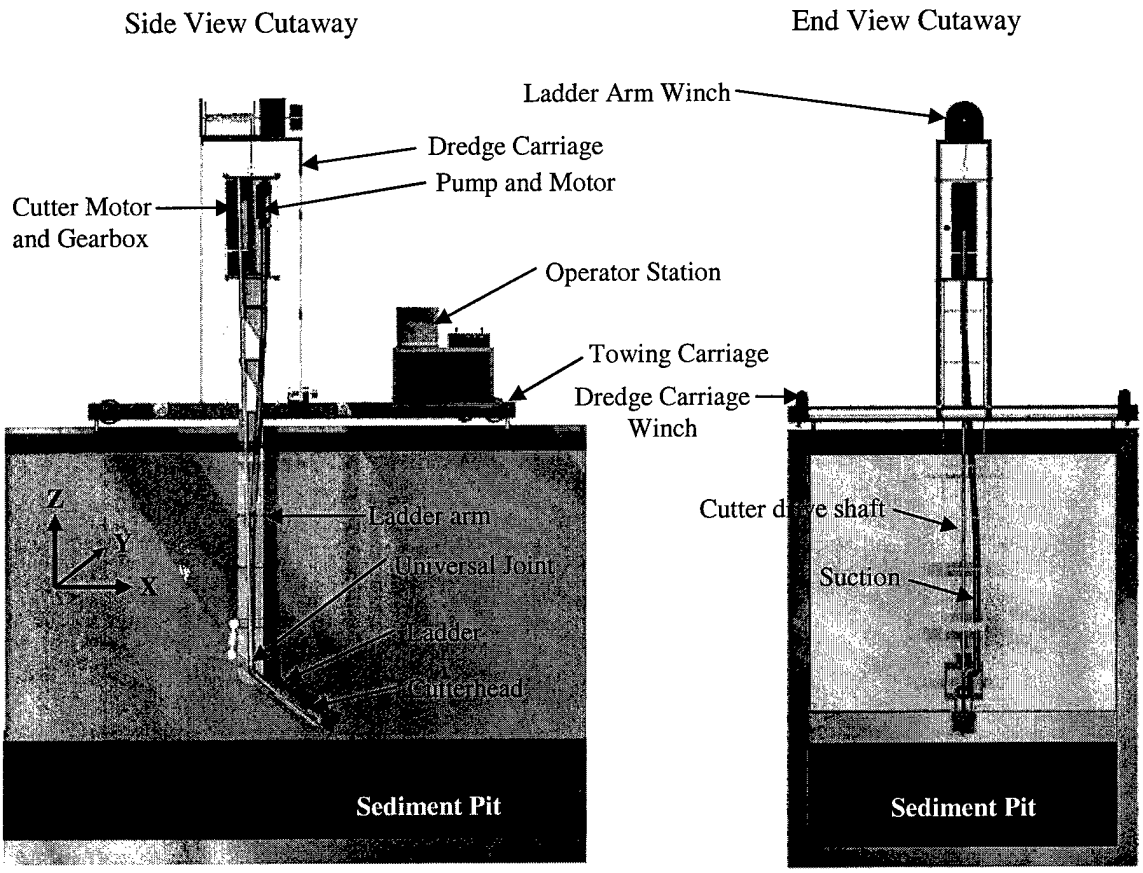

Figure 4: Towing Carriage with Dredge Carriage Sitting atop Towing Tank

Control of the model dredge can be either manual or automatic with automatic being the normal mode of operation. Automation eliminates the variation between model test runs where data from several identical testing sequences are required. An operating sequence can be programmed by the PC, uploaded to the PLC and executed on command. The PLC has direct control over all of the drives and motors via a bank of high-power relays. Several different operating sequences can be stored in the PC for use at any time. In addition to the various automated programs, a program that allows the model to function based on manual input rather than the collected data can be written and stored in the PC. Such a manual program takes input from a manual control panel attached to the PC as peripheral device and uses these data to operate the dredge.

EXAMPLE CUTTER/SUCTION DREDGE LABORATORY MODEL STUDY

The purpose of the example is to demonstrate how the similitude criteria are used in an actual model study. The modeling example is that of a 61 cm (24 in) cutter/suction dredge. The prototype dredge employs a 183 cm (72 in) diameter by 152 cm (60 in) long cutterhead with a blade pitch of 6 and an average profile angle of 25 degrees. The prototype operates at 22,937 LPM (30,000 GPM) and pumps an average slurry specific gravity of 1.3. Prototype swing speed

is about 40.6 cm/s (16 in/s) with a 2045 m^3 (2675 cy/hr) production when cutting a 91 cm (3 ft) deep cut in 12.2 m (40 ft) of water with a 45 degree ladder angle. The cutterhead rotates at 40 rpm and is cutting in medium-fine sand with an average median grain diameter of 0.2 mm. The purpose of the model test is to determine the effect of swing speed on production for a given cutterhead design. The example experiment models several different runs at prototype swing speeds ranging from 30.5 to 50.8 cm/s (12 to 20 in/s) while keeping all other parameters constant.

Since all of the scale laws used to set-up a modeling experiment are derived from similitude with respect to sediment pick-up behavior, the model dredge operating parameters depend on the median grain size of the prototype dredge and the geometric scale ratio. Selecting a proper geometric scale ratio is essential to performing a successful experiment. Cutting forces, flow rates, and cutting speeds must be kept within certain ranges if the dredge is to operate efficiently. Figure 5 is given to aid in the selection of the geometric scale so that the resulting operating parameters can be easily computed if the prototype grain size is known. The data used to plot the charts are calculated from Equations 13, 22, and 23. This chart assumes that the model median grain size is 0.1 mm. If a different model sediment grain size is used, the model to prototype velocity scale must be calculated based on the relative settling velocities.

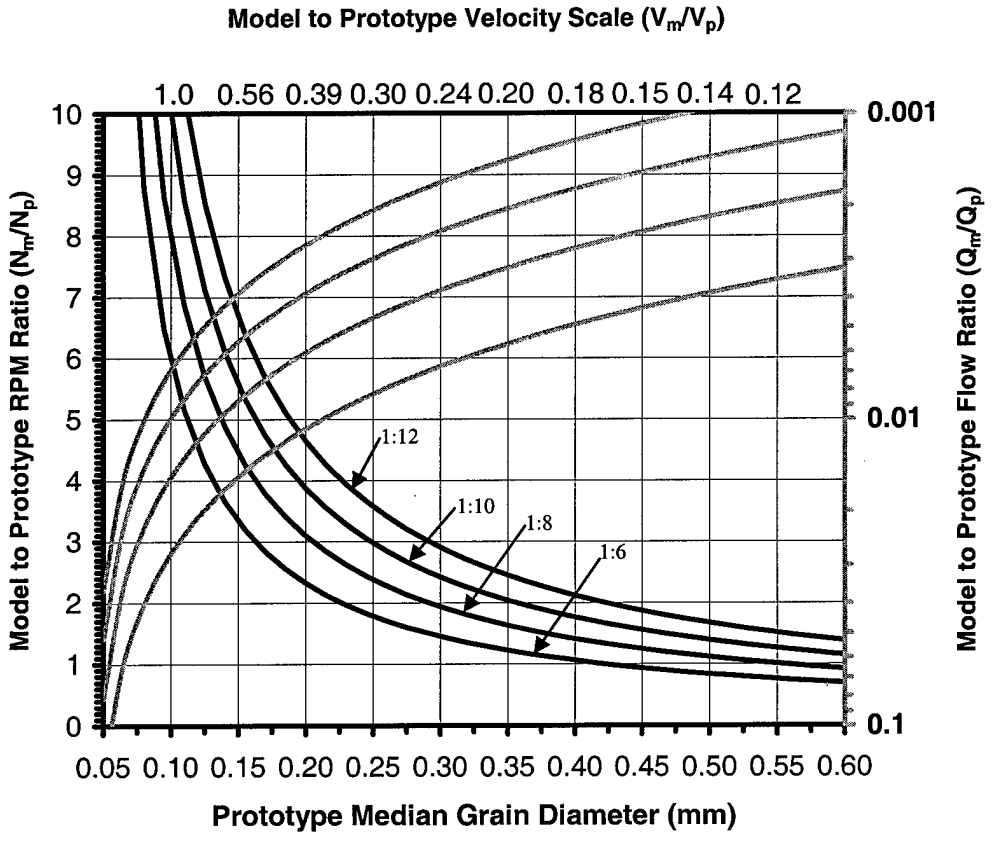

Figure 5: Chart For Selecting Model Dredge Operating Parameters
(Model d_{50} = 0.1 mm)

The bottom axis is the prototype median grain diameter in mm. The left axis is the model to prototype rpm ratio. The black geometric scale lines are used to determine the rpm ratio. The right axis is the model to prototype flow ratio. The gray geometric scale lines are used to determine the flow ratio. If the model grain size is 0.1 mm, the prototype grain size is the starting point along the bottom axis. If the model grain size is not 0.1 mm, the resulting velocity scale is the starting point along the top axis.

The proposed model dredge carriage at the Texas A&M Coastal Engineering Laboratory (Glover 2002) is designed to test large dredges at scales close to 1:10 scale. This will be the first length scale chosen. Table 1 summarizes the model and prototype operating parameters for a 1:10 geometric scale. Equations 13, 22, 23, and the length scale are used to scale the parameters.

Table 1: Model and Prototype Operating Parameters for Cutter/Suction Dredge Example (1:10 Scale)

Parameter	Prototype	Model	Scale
Cutter Diameter	183 cm (72 in)	18.3 cm (7.2 in)	1:10
Water Depth	12.2 m (40 ft)	3.35 m (11 ft)	N/A
Depth of Cut	91.4cm (36 in)	9.14 cm (3.6 in)	1:10
Sediment Diameter	0.2 mm	0.1 mm	N/A
Settling Velocity	22.7 mm/s	8.8 mm/s	0.388
Suction Diameter	61 cm (24 in)	38 mm (2.4 in)	1:10
Suction Flow Rate	113,562 LPM (30,000 GPM)	440 LPM (116 GPM)	0.004
Cutter RPM	40	155	3.88
Max Swing Speed	50.8 cm/s (20 in/s)	19.7 cm/s (7.76 in/s)	0.388

The model dredge water depth is a function of the laboratory facility and does not follow any scaling rationale. Since dredging in a vacuum would be required to satisfy the similitude criteria with respect to cavitation of the cutterhead, no attempt is made to specify a water depth. Therefore, the depth of the tank is used. The model dredge sediment median grain diameter is 0.1 mm. This allows coarser prototype material to be modeled by adjusting the model flow rate according to Equation 15.

Table 1 shows the model suction inlet velocity scaled according to the length scale. However, this may be unnecessary as the velocity field created by the suction inlet is not dependent on suction inlet velocity. If the resulting model dredge operating parameters are run through a cutting force simulation, a maximum possible cutterhead swing velocity of 65.5 cm/s (25.8 in/s) is possible at the indicated depth of cut based on the available cutterhead power. The side winch pull force at this speed is estimated to be 6917 N (1555 lb), more than the 3556 N (800 lb) allowed by model dredge. This also requires 4.5 kW (6 hp) of model side winch power, 200% of what is available. However, according to the computed velocity scale, maximum model swing speed would not need to exceed roughly 20 cm/s (8 in/s). At this speed, only 1730 N (389 lb) of

horizontal cutting force is generated by the model dredge. Only about 0.35 kW (0.50 hp) of side winch power is required to achieve this. Therefore, this experiment, with the operating parameters shown, could be performed in the facilities.

The 61 cm (24 in) dredge is considered a medium size dredge and the tendency when modeling smaller prototypes is to build the model to a larger scale so that any adverse scale effects are minimized. To see if the model dredge facilities can do this, the geometric scale for this example will be changed to 1:6. The experimental setup will now employ a model cutterhead measuring 30.5 cm (12 in) in diameter by 25.4 cm (10 in) long. Table 2 summarizes the model and prototype operating parameters for a 1:6 geometric scale.

Table 2: Model and Prototype Operating Parameters for Cutter/Suction Dredge Example (1:6 Scale)

Parameter	Prototype	Model	Scale
Cutter Diameter	183 cm (72 in)	30.5 cm (12 in)	1:6
Water Depth	12.2 m (40 ft)	3.35 m (11 ft)	N/A
Depth of Cut	91.4cm (36 in)	15.2 cm (6 in)	1:6
Sediment Diameter	0.2 mm	0.1 mm	N/A
Settling Velocity	22.7 mm/s	8.8 mm/s	0.388
Suction Diameter	61 cm (24 in)	7.62 cm (3 in)	1:8
Suction Flow Rate	113,562 LPM (30,000 GPM)	1223 LPM (323 GPM)	0.011
Cutter RPM	40	124	3.104
Max Swing Speed	50.8 cm/s (20 in/s)	19.7 cm/s (7.76 in/s)	0.388

The scaled model quantities above satisfy the requirements for geometric, hydraulic, kinematic similitude. Table 2 does not show the model suction inlet velocity being scaled according to the length scale. A 10.2 cm (4 in) diameter suction inlet is required to achieve this. However, this is unnecessary as the velocity field created by the suction inlet is not dependent on suction inlet velocity but on the volumetric flow rate. It is important to note that changing the geometric scale ratio does not change the velocity scale, since this is based solely on median grain diameter. However, as Table 2 shows, building a larger model requires a larger flow rate to increase the size of the velocity field created by the suction, and a lower cutterhead rpm so that the tangential velocity of the cutterhead blades follow the velocity scale. If the resulting model dredge operating parameters are run through a cutting force simulation, a maximum possible cutterhead swing velocity of 23.6 cm/s (9.3 in/s) is possible at the indicated depth of cut based on the available cutterhead power. The side winch pull force at this speed is estimated to be 4130 N (928 lb), more than the 3556 N (800 lb) allowed by the model dredge. Only 1.0 kW (1.3 hp) of side winch power is required, less than half of the available power. However, since changing the length scale did not change the computed velocity scale, maximum model swing speed would still not exceed approximately 20 cm/s (8 in/s). At this speed, only 3505 N (788 lb) of horizontal cutting force is generated by the model dredge and there is more than enough side winch power

available to pull the dredge carriage. Less than 0.7 kW (0.84 hp) are required to pull the dredge carriage with the estimated force and velocity. Therefore, this experiment, with the operating parameters shown, could be performed in the facilities at a 1:6 geometric scale.

Recall that the purpose of the experiment is to determine the effect of swing speed on production. Model tests are conducted with the full range of swing speeds required by the velocity scale and data are collected. Higher swing speeds may result in a lower production than indicated because of spillage. Since the cutterhead rpm, swing speed, and suction inlet velocity have all been kinematically scaled to the prototype, the scale ratios for cutterhead rpm and swing speed listed in Tables 1 and 2 should provide for the quantitative interpretation of data. Other recorded quantities such as cutterhead forces, cutterhead power, pump power, slurry specific gravity, and pump head are not readily scalable up to prototype quantities until more research is done to determine the scale effects of not achieving dynamic similarity with respect to the cavitating cutting process. However, the qualitative effect of the swing speed on these quantities can still be easily observed.

Specific Energy Method

As the example shows, the specific energy method and its corresponding cutting theory can be helpful in checking the model cutterhead loading for any given model operating parameters. The specific energy method is used to determine the maximum possible swing speed for each required depth of cut based on the available model cutterhead power of 11.7 kW (15.7 hp) and the maximum model production of 31.5 m^3 (41.2 cy). Once the required cutterhead power is computed for each swing speed and depth of cut, horizontal, vertical, and axial cutting forces can be estimated by using the cutting theory (Vlasblom 1998). The operating parameters of the experiment are then tested against the model dredge to ensure that maximum permissible loads are not exceeded. Since the specific energy method represents the upper limit of cutting forces for a cavitating cutting process, actual model cutting forces will likely be lower. While the model dredge feedback and control system will not allow the apparatus to be operated beyond its structural limits, the model operating parameters, specifically the geometric scale, must be carefully selected so that the threat of structural failure does not limit the users' ability to conduct thorough model investigations.

According to Equations 20 and 21, the model dredge would have to operate in a vacuum in order to achieve the level of cavitation achieved by the prototype dredges. Therefore, similarity with respect to the cutting forces developed by the cutterhead is not expected to follow the dynamic scale laws. Perhaps new scale laws that compensate for the absence of cavitation in the model dredge can be developed through model testing.

CONCLUSIONS

This paper investigates the model scaling relationships that have been proposed for hydraulic dredging operations. Several studies and papers are examined dating back over 60 years. In all of this time, only a handful of studies involving the modeling of large hydraulic dredge

equipment have been published. In addition to laboratory studies, several researchers have performed dimensional analyses on selected operating parameters to obtain similitude relationships for scaling the relevant quantities. Many of these relationships have been tested, but some of them either contradict one another or cannot be physically satisfied, even in a laboratory setting. This presents many challenges to the quantitative analysis of data obtained by the scaled model testing of hydraulic dredging operations. Because of this, the results of such model studies have traditionally been limited to only a qualitative interpretation of the data.

By using the scale laws as presented in this paper, virtually any prototype dredge can be modeled by the model dredge facilities. The limitations that determine the selection of the cutterhead rpm ratio and the cutterhead diameter ratio are the structural limits of the model dredge. That being said, some operating parameters will work better than others. For example, large prototype grain sizes necessitate a sharp reduction in model flow rate. This also requires a very small velocity scale, which affects cutter rpm and swing speed. Lowering the cutterhead rpms has the potential to cause higher cutting forces. However, the swing speeds usually are lowered by the same factor as the cutterhead rpms. As the example showed, the slow swing speeds tend to keep the cutting forces from becoming too great when the velocity scale and model rpms are reduced. In general, modeling finer sediment should give better results since cutting speeds are higher and the scale effects of the cavitating cutting process are reduced.

Smaller prototype dredges can allow a larger geometric scale to be used. This was shown in the example with the 1:10 and 1:6 scale cutter/suction dredge models. Larger geometric scales will required greater model flow rates and care must taken not to exceed the model dredge design value of 1893 LPM (500 GPM). Another side effect of smaller geometric scales is that larger cutterheads have lower maximum model swing speeds. This is a result of the maximum production capable from a 11.7 kW (15.7 hp) cutterhead. As a result, the velocity scale must be small enough so that the required model swing speeds are less than the maximum. If the prototype dredge operates in fine sand, then the velocity scale will be unity and model swing speeds may exceed the maximum. In these cases, the geometric scale will have to be reduced until a workable set of model dredge operating parameters are found. As a practical matter, model cutterheads larger than 30.5 cm (12 in) in diameter should not be used so that proper clearance with the tank walls is maintained.

Once the operating parameters are selected, the cutting forces predicted by the specific energy method should be calculated for the selected parameters. This will check the operating parameters to ensure that the predicted cutting forces do not overload the model dredge and cause the control system to cease operations.

The scale laws used to design the model dredge are based on hydraulic similarity between model and prototype. That is, kinematic similarity exists for the velocity fields created by the suction inlet, cutterhead rotation, and swing speed. This ensures that the sediment pick-up behavior of the model dredge will imitate the sediment pick-up behavior of the prototype dredge according the scale laws. Dynamic similarity between model and prototype with respect to the cutting forces cannot be established according to the scale laws because of the cavitation coefficient. As

shown by the modeling example, the model dredge would have to operate in a vacuum or have the cutting speeds drastically increased in order to obtain the same degree of cavitation during cutting that exists in the prototype. This means that similarity with respect to the cutting forces cannot be obtained with the proposed model dredge design without compromising hydraulic similarity. If the cutting speeds (cutterhead rpm and swing speed) are increased so that similarity is obtained with respect to cavitation, then kinematic similarity with respect to sediment pick-up behavior will be lost. These limitations and the degree of the related scale effects will need to be studied.

The dredge modeling facility at Texas A&M University will be available for use by commercial and academic institutions for a variety of research and testing (Randall et al. 1998). These facilities will be an invaluable asset to the dredging community and will serve the dredging industry for many years.

NOMENCLATURE

c_1	= Cutting Force Coefficient (non-cavitating)	-
d_1	= Cutting Force Coefficient (cavitating)	-
d_{50}	= Mean grain diameter	mm
D_{cutter}	= Diameter of cutterhead	in
e	= Volume Strain	%
ϕ_c	= Cavitation Transition Angle	rad
$F_{cutting}$	= Cutterhead forces	lb
Fr	= Froude Number	-
g	= Gravitational constant	ft/s^2
Γ_{cutter}	= Cutterhead torque	ft-lb (in-lb)
$H_{velocity}$	= Velocity head	ft
φ	= Angular Position of Cutterhead Blade	rad
κ	= Cutterhead Profile Angle	rad
k_m	= Average Permeability	ft/s
λ_c	= Hydrostatic Pressure Factor	-
ν	= Kinematic viscosity	ft^2/s
N_{cutter}	= Cutterhead rotational speed (rpm)	rpm
$p_{cavitation}$	= Cavitation Pore Pressure	psi
Re	= Reynolds Number	-
ρ_{water}	= Water Density	lb/ft^3
t_{layer}	= Layer Thickness	in
$U_{suction}$	= Average suction pipe flow velocity	ft/s
$V_{settling}$	= Settling velocity	mm/s
V_{swing}	= Cutterhead swing velocity	in/s (ft/min)
ω_{cutter}	= Cutterhead angular velocity	rad/s
$Q_{suction}$	= Volumetric flow rate through suction/discharge pipe	GPM (ft^3/s)
z	= Water Depth	ft

REFERENCES

Army Corps of Engineers, (1947). *Model Study of Suction Head, Dredge Jadwin.* Technical Report No 2-232, U.S. Army Engineers Waterways Experiment Station, Vicksburg, MS.

Army Corps of Engineers, (2000). *Dredging: Building and Maintaining our Underwater Highways.* U.S. Army Corps of Engineers, Washington D.C.

Brahme, S.B., and Herbich, J.B. (1986). *Hydraulic Model Studies for Suction Cutterheads.* Journal of Waterway, Port, Coastal and Ocean Engineering, ASCE, Vol. 112, No. 5, pp. 590-607.

Burger, M.D. (1997). *Mixture Forming in a Cutterhead.* Proceedings of the Central Dredging Congress Dredging Days, CEDA 1997, Amsterdam, the Netherlands.

Franco, J.J. (1967). *Model Study of Hopper Dredge Dragheads.* Technical Report No 2-755, U.S. Army Engineer Waterways Experiment Station, Vicksburg, MS.

Glover, G.J. (2002). *Laboratory Modeling of Hydraulic Dredges and Design of Dredge Carriage for laboratory Facility.* Masters Thesis at Texas A&M University, College Station, TX.

Herbich, J.B., and Brahme, S.B. (1983). *Literature Review and Technical Evaluation of Sediment Resuspension during Dredging.* Report No. COE-266, Ocean and Hydraulic Engineering Group, Texas A&M University, College Station, TX.

Huston, J.W., and Huston, W.C. (1976). *Techniques for Reducing Turbidity with Present Dredging Procedures and Operation.* Technical Report D-76-4, U.S Army Engineer Waterways Experiment Station, Vicksburg, MS.

Joanknecht, L.W.F. (1976). *A Review of Dredge Cutterhead Modeling and Performance.* Proceedings of the Seventh World Dredging Congress, WODCON VII, San Francisco, CA, pp. 995-1016.

Miedema, S.A. (1987). *Calculation of the Cutting Forces When Cutting Water Saturated Sand.* Doctoral Dissertation at Delft University of Technology, Delft, the Netherlands.

Miedema, S.A (1989). *On the Cutting Forces in Saturated Sand of a Seagoing Cutter Suction Dredger.* Proceedings of the 12th World Dredging Congress, WODCON XII, Orlando, FL, pp. 331-352.

Miedema, S.A. (1995). *Production Estimation Based on Cutting Theories for Cutting Water Saturated Sand.* Proceedings of the 14th World Dredging Congress, WODCON XIV, Amsterdam, the Netherlands, pp. 255-275.

Mol, A. (1977a). *Flow in and around a Cutterhead: Part II, Rotating Freely in Water: Injections with Dye.* Delft Hydraulics Laboratory, Delft, the Netherlands.

Mol, A. (1977b). *Flow in and around a Cutterhead: Part III, Flow in a Cutterhead With an Artificial Breach, Injections with Pieces of Plastic.* Delft Hydraulics Laboratory, Delft, the Netherlands.

Randall, R.E., Edge, B.L., and Cox, D.T. (1998). *Laboratory Needs for Dredging and Dredged Material Disposal.* Proceedings of the 15th World Dredging Congress, WODCON XV, Las Vegas, NV, pp. 17-29.

Slotta, L.S. (1968). *Flow Visualization Techniques Used in Dredge Cutterhead Evaluation.* Proceedings of the 1968 World Dredging Congress, WODCON II, Rotterdam, the Netherlands, pp. 56-77.

Vlasblom, W.J. (1998). *Relation Between Cutting-, Sidewinch-, and Axial Forces for Cutter Suction Dredgers.* Proceedings of the 15th World Dredging Congress, WODCON XV, Las Vegas, NV, pp. 275-291.